Modulation of tumor invasion through the alteration of the cell identity in pediatric Diffuse Midline Gliomas

Hoa Nguyen

université PARIS-SACLAY

Modulation of tumor invasion through the alteration of the cell identity in pediatric Diffuse Midline Gliomas

Modulation de l'invasion tumorale par l'altération de l'identité cellulaire dans les gliomes pédiatriques infiltrants de la ligne médiane

Thèse de doctorat de l'université Paris-Saclay

École doctorale n° 582, Cancérologie : Biologie, Médecine, Santé (CBMS)
Spécialité de doctorat : Aspects moléculaire et cellulaire de la biologie
Graduate School : Sciences de la vie et santé
Référent : Faculté de médecine

Thèse préparée dans l'unité de recherche **Prédicteurs moléculaires et nouvelles cibles en oncologie (Université Paris Saclay, INSERM)**, sous la direction de **David CASTEL**, CRCN, INSERM

Thèse soutenue à Paris-Saclay, le 29 avril 2024, par

Hoa NGUYEN

Composition du Jury

Kevin BECCARIA Professeur des universités, Université Paris-Cité	Président
Jean-Philippe HUGNOT Professeur des Universités, Université de Montpellier	Rapporteur & Examinateur
Emmanuelle HUILLARD CRCN, CNRS	Rapporteur & Examinatrice
Nadia ELKHATIB CRCN, CNRS	Examinatrice

THÈSE DE DOCTORAT

NNT : 2024UPASL026

université PARIS-SACLAY | ÉCOLE DOCTORALE Cancérologie : biologie - médecine - santé (CBMS)

Titre : Modulation de l'invasion tumorale par l'altération de l'identité cellulaire dans les gliomes pédiatriques infiltrants de la ligne médiane

Mots clés : Gliomes infiltrants de la ligne médiane, tumeurs cérébrales pédiatriques, invasion tumorale, identité cellulaire, *NKX2-2*

Résumé : Les gliomes diffus de la ligne médiane (DMG) sont des tumeurs incurables prenant leur origine dans ligne la médiane du cerveau et qui infiltrent le système nerveux central. Des travaux publiés suggèrent que les progéniteurs des oligodendrocytes (OPC), une population cellulaire présentant un fort potentiel de migration pendant le développement cérébral, sont les cellules d'origine des DMG. Cependant, à ce jour, aucun lien direct entre l'identité cellulaire des cellules de DMG et leur comportement invasif n'a été établi. Mon travail de doctorat est le premier à valider la corrélation entre l'expression du facteur de transcription NKX2-2 et l'invasivité des cellules de DMG.

La répression de NKX2-2 dans les cellules de DMG en utilisant des shARN entraîne une transition d'une identité d'OPC à une identité de neuroblastes, associée à une diminution de leur potentiel invasif et prolifératif. Ces résultats suggèrent que NKX2-2 module l'invasion en altérant les voies de signalisations liées à CDH11, les RHO-GTPases et la voie WNT non-canonique. De plus, le processus d'invasion régulée par NKX2-2 pourrait également impliquer les interactions synaptiques entre neurone et gliome et l'interconnexion entre les cellules de gliomes. Au total, NKX2-2 et ses gènes cibles pourraient représenter des cibles intéressantes pour réduire l'invasion des DMG et améliorer la prise en charge des patients.

Title: Modulation of tumor invasion through the alteration of the cell identity in pediatric Diffuse Midline Gliomas, reprograming

Keywords: Diffuse Midline Gliomas, pediatric brain tumors, tumor invasion, cell identity, *NKX2-2*

Abstract: Diffuse midline gliomas (DMG) are incurable tumors originating from midline structures that infiltrate throughout the brain. Evidence suggests that oligodendrocyte progenitor cells (OPC), a highly migratory cell population during brain development, serve as the cell-of-origin for DMG. However, to date, there has been no direct study investigating the link between the cell identity of DMG cells and their invasive behavior. My PhD work is the first to validate the positive correlation between expression of NKX2-2, a master transcription factor, and the invasiveness of DMG cells.

Knocking down NKX2-2 using an shRNA approach resulted in the transition from OPC-like to neuroblast identity in highly invasive DMG cells, with a less invasive and less proliferative profile.It suggests that NKX2-2 modulates invasion via CDH11 and through RHO GTPases signaling pathways and the noncanonical WNT pathway. Moreover, the invasion process regulated by NKX2-2 may also involve neuron-glioma synaptic interaction and the interconnection between glioma cells. Taken together, NKX2-2 and its downstream genes could represent interesting targets for reducing DMG invasion and improving survival rates in patients.

Les gliomes diffus de la ligne médiane (DMG) sont des tumeurs incurables prenant leur origine dans ligne la médiane du cerveau et qui infiltrent l'intégralité du système nerveux central. Malgré des avancées significatives dans la compréhension des aspects moléculaires et épigénétiques de leur oncogenèse, le pronostic des patients atteints de DMG ne s'est pas significativement amélioré au cours des cinquante dernières années. Des analyses transcriptomiques suggèrent que les cellules progénitrices d'oligodendrocytes (OPC), une population cellulaire hautement migratoire pendant le développement précoce du cerveau, pourraient constituer les cellules d'origine pour les DMG, et de par leur nature hautement motile expliquer le caractère invasif des DMG. Une étude récente du laboratoire a démontré une corrélation entre le pronostic et le développement de métastases. Cependant, à ce jour, aucune étude n'a directement examiné le lien entre l'identité cellulaire des cellules cancéreuses DMG et leur comportement invasif. Pour combler cette lacune, j'ai validé durant mon travail de thèse la corrélation positive entre l'expression du facteur de transcription NKX2-2 et l'invasivité des cellules DMG. L'extinction de NKX2-2 en utilisant des shARN entraine une transition d'une identité d'OPC à une identité de neuroblastes, associée à une diminution de leur potentiel invasif et prolifératif. L'analyse des données de transcriptomique en bulk de modèles de DMG cultivés en 3D et de CUT&Tag suggère que NKX2-2 joue un rôle d'activateur de CDH11 et que l'extinction de NKX2-2 pourrait réduite l'invasion des cellules de DMG via une cascade impliquante CDH11. De plus, NKX2-2 semble réguler l'expression la voie des RHO-GTPases et la voie WNT non canonique, toutes deux liées à la motilité cellulaire et à l'invasion. Les gènes cibles de NKX2-2 dans ces deux voies de signalisation comprennent WNT7A, ARHGEF4/28, ARHGAP24 et FZD3. De plus, les données montrent que NKX2-2 pourrait également être impliqué dans la régulation des interactions synaptiques neurone-gliome et l'interconnexion des cellules de gliome. Au total, NKX2-2 et ses gènes cibles pourraient représenter des cibles intéressantes pour réduire l'invasion des DMG et améliorer la prise en charge des patients.

ACKNOWLEDGEMENTS

First and foremost, I would like to sincerely thank all the members of the jury, Jean-Philippe Hugnot, Emmanuelle Huillard, Nadia ElKhatib, and Kevin Beccaria, for taking the time to evaluate this project. Specifically, a big thank you to Emmanuelle Huillard and Jean-Philippe Hugnot for accepting the role of rapporteurs and encouraging me to finish the manuscript despite the short review time.

Then, I would like to thank my follow-up committee jury, Guillaume Montagnac, Pierre Savagner, and Maite Verreault. Without their validation, there would not have been a third and fourth year for me to start this project with a completely new candidate gene.

Thank you to the École Doctorale, and here I must stress the enormous patience and empathy that Léa Poisot has shown me, whether dealing with the titre de séjour or all the procrastination I have had in the last 6 months. Without your support, I do not know if it would have been possible for me to have a defense.

No money, hard life. The same goes for PhD students. I would like to thank two organizations, CRIS Cancer and FRM, who supported me financially so that I could be here in France and work on this project for four continuous years.

And now, all my heart is with my team, where I have spent four years with so many ups and downs, laughter, tears, success, and failure. It has been such a long, special, and emotional journey.

I would like to express my heartfelt gratitude to Jacques, David, and Marie-Anne. Thank you for accepting me, at that time, a master student who knew nothing about neuro-oncology, who could not even speak a full French sentence, into this lab. Thank you for bearing with me through the follow-up meetings and guiding me all the way during these four years. Especially David, I will never forget that you helped me so much during my first few months in Paris, whether it was about financial support or administrative support. I always appreciate that. Thank you for teaching me your impressive experimental skills and so many smart tips in the lab, for imparting all your knowledge about DMG/DIPG, epigenetics, and how to work in a scientific way with a critical mindset. Thank you very much for not giving up on me these last few months and always wishing me good luck in your emails.

My dearest mentor, Marco, you absolutely saved my PhD plan with the hint about NKX2-2. You never said no, never said less whenever I showed up with a question. You are the greatest and most reliable mentor that I have met in my life.

Manon, Emilie, Ludivine, Coralie, and Samia – I know that I caused a lot of struggles for you when I first arrived in the lab because you had to speak English full-time to me. It was not easy. But all of you were so patient and nice whenever we did training together or you were always ready to help whenever I encountered any trouble in the lab. Most of the techniques that I first learned during my internship; it was all with you. Thank

you so much for that. And Manon, my desk neighbor for quite a long time, you were such a sweetheart to always care about me whenever I needed, anytime and about anything. I was lucky to sit next to you.

Chloé, Virginie, Lucie, Maxime G, Saima, Lilia – the PhD student team. Only PhD students understand PhD students. And I have to say, talking to you sometimes was one of the best ways for me to regain confidence and continue working on this project. Thank you for showing enormous support and lots of laughter to help me through my difficult times, whether with work or with my personal stuff. Working in the lab with you has never been boring.

Clem, Yassine, Thomas – the source of humor and kindness for me. I miss sitting in the office and just hearing you guys chatting with each other, sometimes sharing such bizarre but funny things and pulling me out of my clumsy mood and chasing the tiredness away. Yassine and Thomas, thank you for teaching me all the bioinformatic things and for doing all the analysis that builds up such an important piece of my work now. Claudia, it is always a pleasure to discuss experiments and ideas with you; you are always full of energy, and your passion for your work also impresses me a lot.

Melis – my dear friend. There are too many things that I want to share with you again. Without you (and Tiphaine) being with me, talking to me during the suffocating times in the past, my life would have totally changed now. I do not know how to express my appreciation for that.

Maxime D, Irma – you joined the lab after me, but I wish we could have known each other earlier or that I could have had more time working in the lab with you. We have shared more than we thought we could have. And I want you to know that I enjoyed those moments.

Tudor, Cyril, Philippe, Yann, Julie, and Amelie – all the staff at different platforms at IGR who have trained and helped me to be able to do so many important experiments. Without them, I bet I would have had a real struggling time.

Tal, Majorie, Bintou, Hela, Khawla, Valentine, Stéphanie, Bilal, Adam – It was nice to know you from the lab. Most of the time, we were so busy with our ongoing experiments, but every time we could have a break, it was a good time. And I enjoyed it.

Marie, Antonin, Romain, Nolwenn, Paul, Sarra, Sarah – we did not talk much when I was at the lab, but I remember when each of you gave me a sincere wish for my life after the PhD. Thank you.

Mathias and Saci – all the problems with the Incucyte allowed me to, I hope, become a good user of this machine, and I am happy when everything was worth it in the end.

My dear words to three sisters that I met in France, sister Thai Hoa, sister Diep, and sister Nhi. Every time I miss Vietnam, I talked to you. And from you, I have learned so much about work, but more importantly, about life and family. I sincerely thank you for all of that.

Thank you Agathe, Marie-Anne, Nicolas, Emna, Naoual, Widad, and Catherine. You might not know why I am saying thank you to you, but I would like to say that every little action, word, or help from you, from time to time, has helped me to facilitate my work or just simply made me feel welcome. And I do remember all of that.

Thank you, J and family, for making my journey in France so unique and exciting with all the excellent food and amazing adventures.

Yanina, Maryam, Kristýna – my dearest girls who gave me a real hug whenever I needed it, without me even having to ask. You were always there for me with endless support. I miss the good old times when we gathered in the kitchen and felt safe and free. Those are my most beautiful memories with our campus house.

Thanh, Bích – we have not met each other for almost 5 years, but yet, our hearts and minds were never far away from each other. You girls are never strangers to me no matter where we are in this large world. Having known you in this life is my luckiness.

Lara, Aqsa, Trang, the two Nicolas, Iryna, Lisha, Gabi, Dilbar, Dat, Dung, Jiou, Romaric, Lucas, Mohamed, Maxime, MIDF and CIUP team, Giang, Melissa, Scott – Each of you has added more colors to my stay in France, bringing me joy in different ways. Cảm ơn gia đình chị Nhi, không chỉ là chủ nhà trọ tuyệt vời nhất mà còn quan tâm, giúp đỡ em như người thân trong những năm qua.

王OK和李天责，在我PhD生涯最艰难的几个月里，你们的音乐陪伴我度过了无数个日夜。我非常高兴能够认识你们美妙的音乐、声音、思想和灵魂。

My relatives from my father's and my mother's family: I might not have been able to end up here, in Paris, without their support and courage. I am really, really, really lucky to have such an amazing big family like this.

Sayang: the man who has to suffer from my craziest 6 months in my life, the man who makes me feel loved every day, the one who accepts anything from me without judging. Thank you for being a shoulder for me to lean on and for always believing in me.

Gửi Bố, Mẹ và Kẹo yêu quý, cảm ơn Gia Đình vẫn luôn tin tưởng và cổ vũ con trong những năm tháng này, từ bước đầu tiên con chập chững biết đi tới bước đường ngày hôm nay con đi, vượt đại dương qua tận chân trời khác. Cảm ơn cả nhà đã luôn khiến con cảm nhận được tình yêu thương vô bờ, để con biết con mãi có một mái ấm để được ôm ấp và dỗ dành, để con mạnh dạn bước đi xa hơn và khám phá thật nhiều điều trong thế giới rộng lớn này. Tất cả những gì con đạt được ngày hôm nay, đều nhờ công dưỡng dục của Bố Mẹ và sự yêu thương không ngừng nghỉ của cả nhà. Con yêu cả nhà.

TABLES OF CONTENTS

TABLES OF FIGURES

LIST OF TABLES

ABBREVIATIONS

2',3'-cyclic nucleotide 3'-phosphohydrolase
CNPase, 49
activin A receptor type I
ACVR1, 26
basic helix-loop-helix
bHLH, 40
bone morphogenetic proteins
BMP, 27
cancer stem cells
CSC, 51
Central nervous system
CNS, 14
Cleavage Under Targets and Tagmentation
CUT&Tag, 109
Death-associated protein
DAXX, 20
Differential Expression Genes
DEG, 73
Diffuse Intrinsic Pontine Gliomas
DIPG, 16
Diffuse Midline Gliomas
DMG, 14
DNMT3A
DNA Methyltransferase 3 Alpha, 148
Enhancer of Zeste Homologs Inhibitory Protein
EZHIP, 16
Ephrin-A5
EFNA5, 147
extracellular matrix
ECM, 32
False Discovery Rate
FDR, 98
FGFR1
Fibroblast growth factor receptor 1, 16
G protein-coupled receptor
GPCR, 98
G protein–coupled receptor 124
GPR124, 60
galactocerebroside
GalC, 49
Gene Ontology
GO, 98
gene set enrichment analysis
GSEA, 53
gestational week
gw, 48
glial progenitor cells
GPC, 35
glioblastoma multiforme
GBM, 53
glioma stem-like cells
GSC, 78
Histone H3 lysine27-to-methionine
H3K27M, 15
IDH
Isocitrate dehydrogenase, 15
Immunohistochemistry
IHC, 23
induced NSC
iNSC, 52
intermediate neural/oligodendrocyte progenitor cells
nIPC or oIPC, 37
knock-down
KD, 80
lateral ganglionic eminence
LGE, 59
magnetic resonance imaging
MRI, 18
MEK
Mitogen-activated protein kinase kinase, 62
multiplicity of infection
MOI, 82
myelin basic protein
MBP, 49

INTRODUCTION

Part I: Overview about Diffuse Midline Gliomas (DMG)

1. Background of pediatric DMG

Data on the incidence of pediatric cancer indicates that central nervous system (CNS) tumors rank as the second most common cancer type in children aged 0-14, following leukemia (Force et al., 2019; Steliarova-Foucher et al., 2017). The worldwide incidence rate for CNS tumors was 28.2 per million over the entire decade of 2001-2010 (Steliarova-Foucher et al., 2017), while a separate report stated that the rate was 35 per million in Europe between 2000-2007 (Gatta et al., 2017).

Among CNS tumors, brain tumors are the main type, and represent the most lethal and aggressive cancers in the pediatric and adolescent population (Cohen, 2022; Rahman et al., 2023). These tumors display diverse locations and histological characteristics, with gliomas constituting the most complex subgroup. Gliomas are brain tumors that originate from glial cells found in the brain and nervous system. Notably, it was not until the fifth World Health Organization (WHO) classification of CNS tumors in 2021 (WHO-CNS5) that the term "pediatric-type" was introduced to address the distinct complexity and pathology of gliomas in children compared to adults (Louis et al., 2021; WHO Classification of Tumours Editorial Board, 2021).

Unlike low-grade gliomas, which have a 10-year overall survival rate of up to 90%, pediatric high-grade gliomas (pHGG) are less common but portend a dismal prognosis despite numerous clinical trials (Da-Veiga et al., 2022; Hoffman et al., 2018; Jones et al., 2012; Wang et al., 2021). Multiple studies have demonstrated that pHGG do not stem from pediatric low-grade gliomas (pLGG), as they harbor distinct molecular profiles compared to their adult counterparts (Cohen, 2022; Ryall et al., 2020a). The WHO CNS5 classification of CNS tumors categorize pHGG into four subgroups: Infant-type hemispheric gliomas, diffuse hemispheric glioma H3 G34-mutant, diffuse midline

glioma (DMG) H3K27M-altered, and diffuse pediatric-type high-grade glioma with histone H3-WT (wild-type) and IDH-WT. Among these subgroups, DMG are recognized as extremely aggressive and are associated with a poor prognosis (Grill and Bhangoo, 2007; Jansen et al., 2015; Vuong et al., 2022; WHO Classification of Tumours Editorial Board, 2021).

1.1. A glance at clinical features of DMG

Diffuse midline gliomas were first incorporated into the WHO classification of CNS tumors in 2016, without age restrictions, despite their predominant occurrence in children. This represented a significant advancement, marking the first instance where a single mutation was utilized to define a distinct tumor entity (along with IDH-mutant gliomas). Initially, DMG were defined as tumors that met the following criteria: (1) gliomas bearing the H3K27M (Histone H3 lysine27-to-methionine) mutation typically found in midline structures of the brain, including common locations such as the pons, thalamus, midbrain, and spinal cord; (2) the presence of mitotic activity, microvascular proliferation, and necrosis; (3) infiltration of tumor cells into adjacent and distant brain regions; and (4) a poor prognosis, with less than 10% of patients surviving beyond 2 years . There was debate at that time about whether additional features should be considered in the definition (Louis et al., 2016, 2018).

Initially, the term “H3K27-mutant” was used to describe gliomas with mutations affecting the H3K27 residue of histone H3, it became apparent that not all cases of diffuse midline glioma exhibited these specific mutations. Instead, there emerged a recognition of other mechanisms leading to alterations in H3K27 trimethylation, such as overexpression of EZHIP (Enhancer of Zeste Homologs Inhibitory Protein). Moreover, clinical reports demonstrated that many other tumors can also carry the H3K27M mutation, and some patients could survive for more than 10 years (Hochart et al., 2015; Louis et al., 2018; Zhang et al., 2013). Furthermore, it was proposed by Castel et al. in 2020 that DMG without the H3K27M mutation but overexpressing EZHIP should be considered as a distinct subgroup (Castel et al., 2020). Patients belonging to this

subgroup tend to be older at the time of diagnosis and exhibit similar overall survival rates compared to those with H3.1-K27M mutations (Castel et al., 2020). Finally, in 2021, with the release of the latest WHO CNS5 classification, the term "H3K27-altered" was adopted to encompass a broader spectrum of genetic and epigenetic alterations affecting the H3K27 methylation status. This modification provides a more inclusive and precise classification of these tumors. In a recent study, Auffret et al. proposed identifying a new subtype of DMG H3K27-altered tumors that harbor *BRAF*^{V600E} or *FGFR1* mutations (Auffret et al., 2024). This classification is based on their unique features, including predominantly thalamic localization, atypical radiological and histopathological profiles characterized by calcification and/or a solid tumor component, and a comparatively longer overall survival when contrasted with other DMG (Auffret et al., 2024).

DMG now represent approximately 20% of pediatric CNS tumors and also include Diffuse Intrinsic Pontine Gliomas (DIPG), which are DMG that arise in the pontine area and account for 75-80% of brainstem tumors.

1.1.1. Epidemiology

The incidence rate of DIPG exhibits significant variability across different countries and regions. In the United States (USA), there are approximately 150-300 cases of DIPG annually, whereas Europe reports an estimated 240-355 patients per year, despite the population of the USA being less than half that of European countries. Notably, France records around 50 DIPG cases annually, while the Netherlands reports approximately 9 cases (Jansen et al., 2015; Mellema; Veldhuijzen van Zanten et al., 2015; Warren, 2012). Albeit rare, DMG/DIPG of the deadliest tumor, with an overall survival rate of less than 1 year. Despite significant advances in understanding the biological landscape of DMG/DIPG, the survival rate has remained unchanged for decades, with fewer than 10% of cases surviving for up to 2 years (Jovanovich et al., 2023; Mackay et al., 2017). A study by Lobon-Iglesias et al. involving 142 DIPG patients revealed two peaks in the age distribution, with the more predominant peak at 5.6 years and a second peak at 12

years (Lobon-Iglesias et al., 2018a) (Fig. 1). Independent studies conducted in the USA, the Netherlands, and China have corroborated these typical onset peaks between 6-9 and 12 years in childhood, indicating that DMG/DIPG predominantly affects children but can also occur in adolescents and young adults (Liu et al., 2022a; Monje et al., 2011; Veldhuijzen van Zanten et al., 2015; Zheng et al., 2022). Interestingly, the anatomical location of these tumors differs significantly between children and adults, with the brainstem being the most frequent site in children and the thalamus in adults (Zheng et al., 2022). While data consistency varies among studies, overall, there does not appear to be a gender-associated trend among DMG/DIPG patients (Karremann et al., 2018; Vuong et al., 2022; Zheng et al., 2022) (Fig. 1).

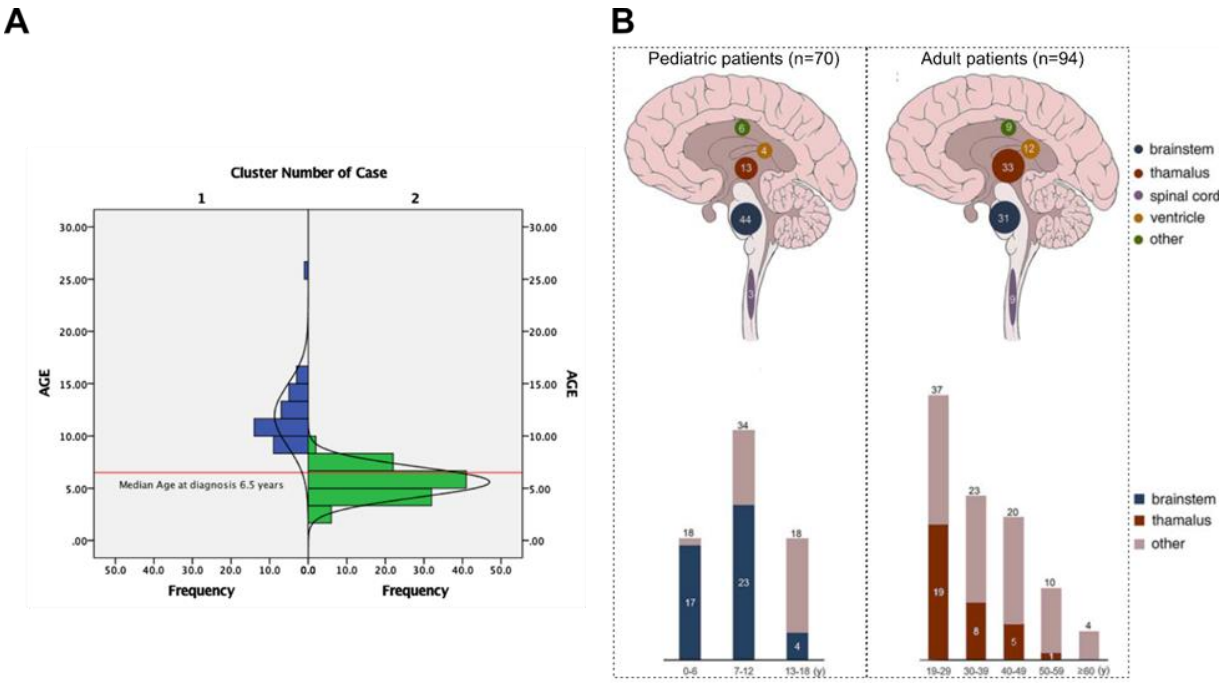

Figure 1: Age distribution and anatomical location of H3K27M DMG/DIPG

A- Two peaks of the age distribution of DMG/DIPG defined by K-means clustering approach: one at 5.6 years (n = 103) and one at 12 years (n = 39) (Lobon-Iglesias et al., 2018).

B- Anatomical location and age distribution of H3K27M DMG/DIPG in children and adult cohorts (Zheng et al., 2022).

However, recent revisions in tumor classification within the past few years have necessitated a reevaluation of data published prior to 2021 to establish standardized

criteria for diagnosis and disease assessment. Consequently, epidemiological information concerning DMG/DIPG remains fragmented and has yet to achieve global coverage, with the most concentrated data originating from the USA and Europe.

1.1.2. Diagnosis and biopsies of DMG/DIPG

Diagnosis of DMG/DIPG tumors historically relied on the histology of tissue samples and cell morphology, posing challenges due to the wide variability in morphologies and grades, not only among patients but even within samples from the same patient (Buczkowicz et al., 2014; Hoffman et al., 2016). Presently, medical professionals integrate information from symptoms, histology, and magnetic resonance imaging (MRI) techniques for DMG/DIPG diagnosis. Lesions infiltrating brainstem structures are frequently observed with a hyperintense signal on T2 and a hypointense signal on T1, often displaying minimal contrast enhancement on conventional MRI (Fig. 2). In the case of DIPG, more than 50% of the pons structure is typically affected.

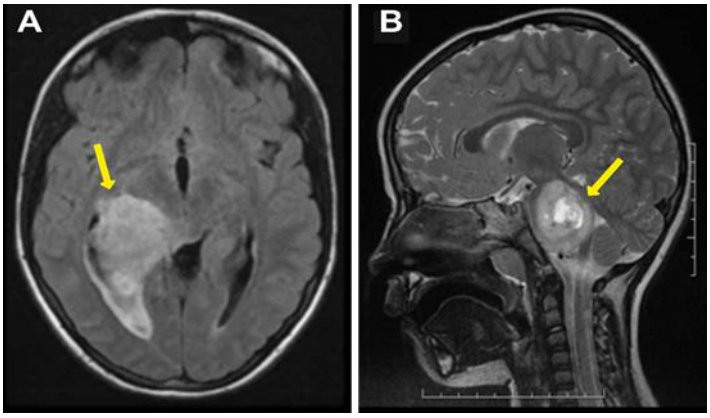

Figure 2: MRI images of patients with DMG/DIPG tumors

Yellow arrows point indicate tumors in A- thalamus (Tauziède-Espariat et al., 2022); B- pons (Necker–Enfants Malades Hospital).

Tissue biopsy was a topic of debate in DMG/DIPG due to its delicate location at midline, particularly within the brainstem structure, leading to a high risk of damaging adjacent brain structures during surgical intervention. However, stereotactic biopsy has been a routine practice for DMG/DIPG patients in France since 2003 (Puget et al., 2015; Roujeau et al., 2007). According to a meta-analysis conducted by Hamisch et al. on 735

patients with pediatric brainstem tumors (pedBSTs), stereotactic biopsy is a safe diagnostic method with a low prevalence of procedure-related complications (overall morbidity 6.7%, permanent morbidity 0.6%, and mortality 0.6%) (Hamisch et al., 2017). Moreover, in 96.1% of cases, an appropriate tissue sample is obtained, which is essential for histological diagnosis and molecular characterization of these tumors. Currently, performing systematic stereotactic biopsies is common practice in many countries, especially at all centers in France. This advancement has significantly facilitated the genetic and epigenetic studies on treatment-naïve samples, which was not feasible with autopsies. A novel approach is emerging, involving the development of models derived from biopsies and the integration of clinical data with laboratory research. However, there is still a considerable journey ahead to establish this approach as a systematic practice.

2. Genomic landscape of DMG/DIPG

For many years, pHGG were considered as adult gliomas occurring in children until recent genomic studies discovered their distinct (epi)genetic alteration (Paugh et al., 2010). The two latest WHO classification gave the recognition to the critical role of the unique epigenetic reprogramming, precisely the mutation of encoding genes of histone H3 variants, in the oncogenesis of DMG/DIPG. Several independent genomic studies have shown that about 75-90% of DMG/DIPG tumors harbor the H3K27M mutation (Schwartzentruber et al., 2012; Wu et al., 2012). This part will take a summarize frequent genomic alterations found in DMG/DIPG.

1.1.3. Histone H3 mutation – a crucial DMG/DIPG hallmark

In humans, there exist different histone H3 variants: H3.1/H3.2 that correspond to canonical H3, and the H3.3 variant. The two most studied histone variants in DMG/DIPG are H3.1 and H3.3, with approximately 80% of patients exclusively carrying mutations in either *H3C2/H3C3*, two of the many genes encoding H3.1, or *H3-3A*, one of the two genes encoding the H3.3 variant (Khuong-Quang et al., 2012; Schwartzentruber et al., 2012; Wu et al., 2012). Canonical H3 variants are more abundant in heterochromatin,

particularly in silent gene regions recognized by DNA methylation, trimethylation of lysine 27 on histone H3 (H3K27me3) or H3K9me2/3. H3.1 exhibits an S-phase expression peak and contributes the majority of histones during replication. In contrast, the non-canonical H3.3 variant is expressed throughout the cell cycle. Histone H3.3 is enriched in pericentric heterochromatin, euchromatin, *i.e.* in actively transcribed gene regions, and in telomeres of embryonic stem cells (Fig. 3) (Boros et al., 2014; Stroud et al., 2012; Szenker et al., 2011). The deposition of H3.1 and H3.3 variants involves specific histone chaperones, such as CAF-1 and HIRA for H3.1, or the DAXX/ATRX complex for H3.3 (Sitbon et al., 2017; Tagami et al., 2004).

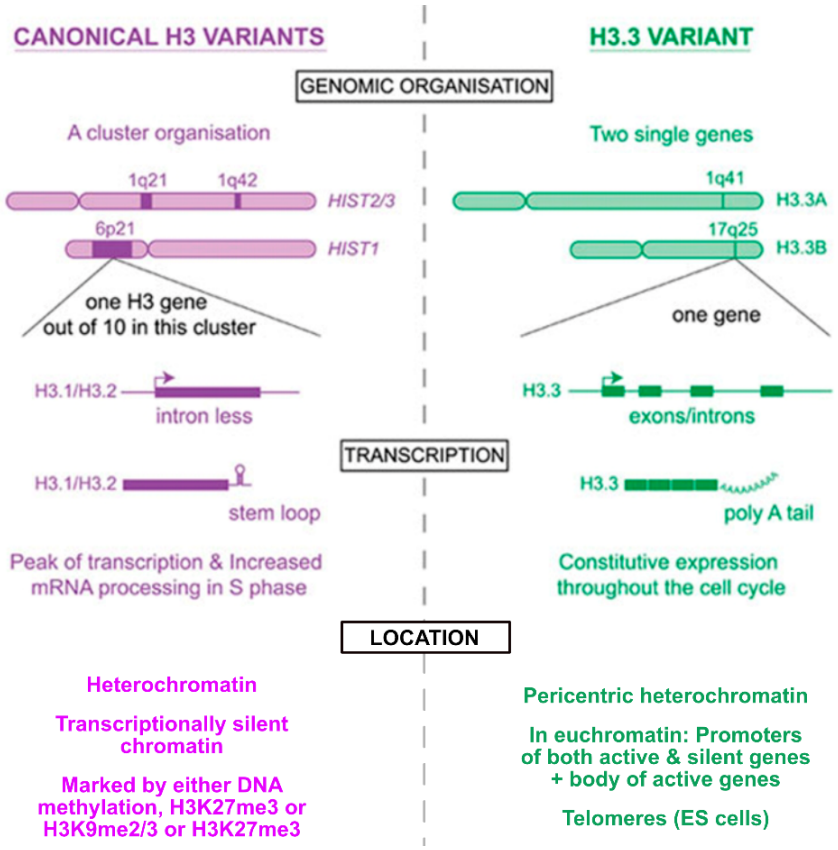

Figure 3: Canonical and non-canonical variants of histone H3
Figure adapted from (Stroud et al., 2012; Szenker et al., 2011).

In 2012, two independent research groups announced the discovery in pediatric glioblastoma and DIPG of a mutation of histone 3 leading to the substitution from lysine to methionine at position 27 -referred to as H3K27M mutation (Schwartzentruber et al., 2012; Wu et al., 2012). This mutation was not reported in any

cancer before and it shed light on the particular oncogenesis of these tumors. Subsequent work provided insights into the unique epigenetic reprogramming induced by H3 mutations and highlighted their pivotal role in gliomagenesis. Notably, even though the H3K27M histone mutation accounts for a very small percentage (3-18%) of the total histones, it is sufficient to prevent global di/trimethylation at position K27 on every H3 molecule, whether wild-type or mutated (Krug et al., 2021; Lewis et al., 2013). Interestingly, besides causing this global loss of H3K27me3 (Fig. 4A), the H3K27M mutation also leads to focal gains or maintenance of H3K27me3 at specific locus where genes remained repressed (Bender et al., 2013; Chan et al., 2013).

Initially, it was believed that the H3K27M mutated histone could outcompete the WT histone due to its stronger affinity for EZH2 (Chan et al., 2013; Lewis et al., 2013). Consequently, the H3K27M mutated histone dominantly inhibits Polycomb repressive complexes 2 (PRC2) function through the EZH2 catalytic subunit, leading to global loss of H3K27me3. This proposition was supported by immunoprecipitation results, which indicated significant enrichment of PRC2 at nucleosomes containing the mutated histone (Bender et al., 2013) (Fig. 4B-1). Additionally, other studies focused on poised enhancers or weak promoters in H3K27M cells, revealing the colocalization of EZH2 and H3K27M mutant proteins at these loci. The presence of H3K27M mutant proteins induced a conformational change in the PRC2 complex, enhancing PRC2 avidity and prolonging its residence time at poised enhancers, thereby reducing the amount of PCR2 at sites with strong affinity (Fang et al., 2018; Justin et al., 2016) (Fig. 4B-2). However, Stafford et al. subsequently demonstrated that the interaction between PRC2 and H3K27M is transient, followed by substantial release of PRC2 from histone 3. Despite not affecting the recruitment of PRC2, the effect of H3K27me3 loss persisted long afterward, indicating that H3K27M might inactivate PRC2 and thus inhibiting its ability to spread H3K27me3 repressive marks (Fig. 4B-3) (Harutyunyan et al., 2019; Stafford et al., 2018; Zhang and Zhang, 2019).

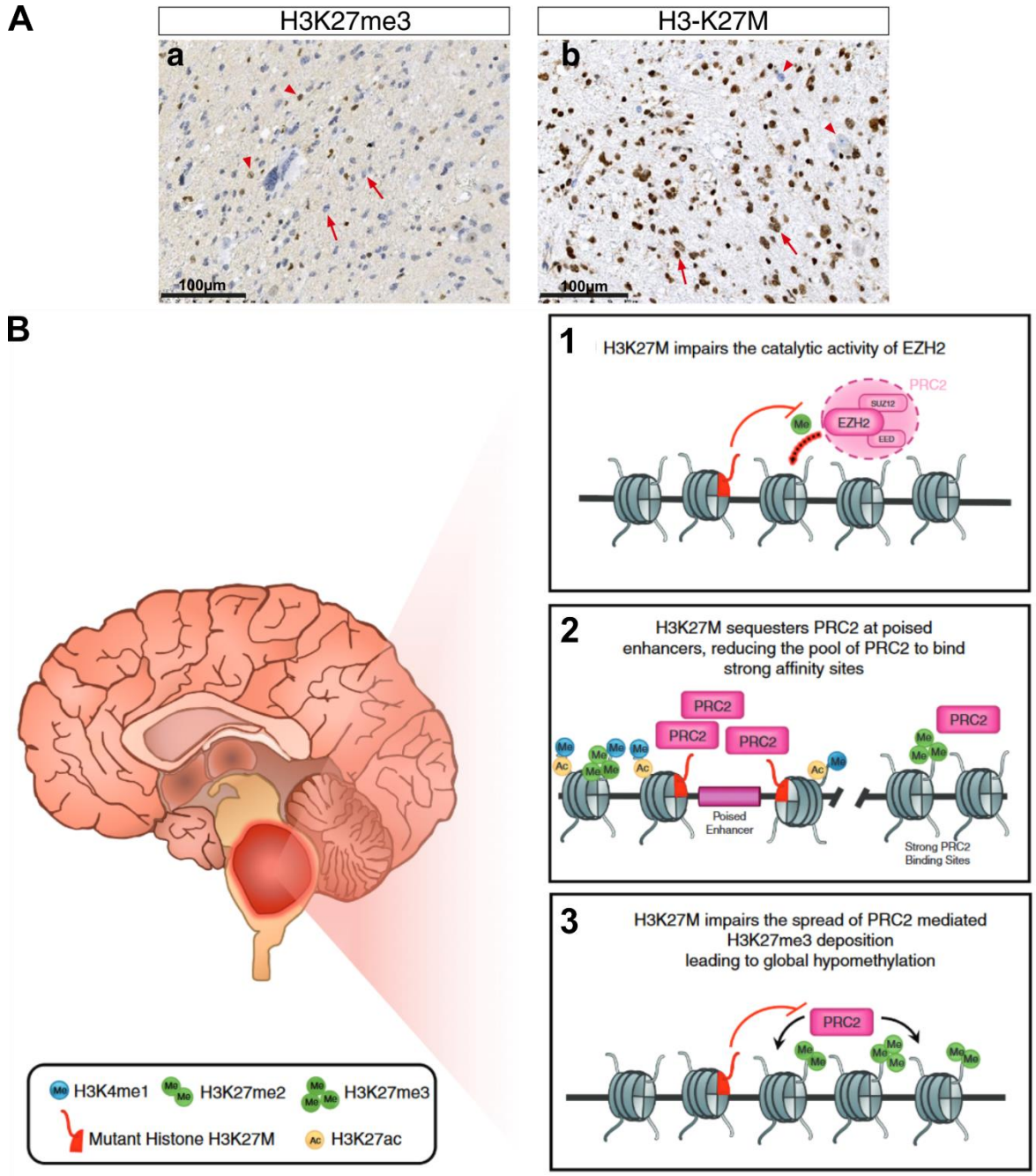

Figure 4 : H3K27M mutation drives H3K27me3 global loss in DIPG

A- Immunohistochemistry (IHC) of the tumor sample showed an overall loss of H3K27me3 in the cancer cell nuclei (arrow), but it was expressed normally in normal cells (triangle). H3K27M-mutated proteins were observed in almost all cancer cells (arrow) (Castel et al., 2015).

B- Different modes in which H3K27M disrupts PRC2 function and induces global H3K27 hypomethylation: 1- The H3K27M mutant histone hinders (curved bracket) EZH2's catalytic activity, impeding the deposition of the H3K27me3 mark (red arrow); 2- PRC2 is sequestered at poised enhancers through its interaction with H3K27M, limiting the available PRC2 pool for binding to its sites

with high affinity; 3- H3K27M disrupts (curved bracket) the spreading of the H3K27me3 mark by PRC2 (black arrows), resulting in global hypomethylation (Mendez et al., 2020).

Through the gene expression microarray analysis of stereotactic DIPG biopsy at diagnosis, our lab categorized DIPG into two subgroups: H3.1 (*H3C2/H3C3*) and H3.3 (*H3-3A*), each exhibiting distinct phenotypes (Castel et al., 2015). These H3.3 and H3.1 mutations are widely recognized as the two main subgroups with differing behaviors. Patients with H3.1 mutations are typically older and exhibit less aggressive characteristics, often responding better to radiotherapy. Conversely, H3.3 mutant tumors display a contrary behavior (Castel, 2015; Jones, 2016). Survival analyses using 22 H3.1-K27M and 55 H3.3-K27M patients, indicated that the former group has a better overall survival rate (Castel et al., Acta Neuropathol, 2015) (Table 1).

Characteristic	*H3.1-K27M* tumors	*H3.3-K27M* tumors
Age of set	Younger age of onset (5.1 years)	Older age of onset (7.4 years)
Location	Pontine tumors	Midline tumors
Frequent associated alterations	*ACVR1* mutation Chr2 gain	*PDGFRA* amplification *TP53* mutation
Phenotype	Astroglial Mesenchymal GBM	Oligodendroglial Proneural GBM
Metastases	Less disseminated	More prone to metastatis
Signature	Neoangiogenic marker Hypoxia and oedema	Altered ECM adhesion
Response to RT	Better	Poor
Survival rate	Longer survival	Short survival

Table 1: Distinctive characteristics between H3.1K27M and H3.3K27M DMG patients (Castel et al, Acta Neuropathol, 2015)

The differing locations of H3.1K27M and H3.3K27M tumors within the brain, coupled with their distinct partner mutations and gene expression profiles, suggest distinct cell-of-origin, a mutated stem cell or a committed progenitor cell which has potential to become a cancer stem cell (this will be discussed further in Chapter 2), and oncogenic mechanisms thereby complicating the task of unraveling the effects of H3.1K27M and H3.3K27M on chromatin (Castel et al., 2015; Jessa et al., 2022a).

EZHIP

About 10-15% of DMG patients have H3-WT tumors, yet they exhibit a global loss of H3K27me3 (Fig. 5A). These tumors were recently showed to overexpress EZHIP (Castel et al., 2020). EZHIP mimics the H3K27M mutation by carrying a conserved C-terminal peptide that replicates the amino acid sequence of the H3K27M oncohistone. This allows EZHIP to bind to the active site of allosterically activated PRC2 and change its conformation, thereby inhibiting the spreading of methylation (Jain et al., 2020) (Fig. 5B). Interestingly, patients with H3-WT DMG exhibit similar overall survival compared to H3.1K27M patients and longer survival rates than those with H3.3K27M DMG (Castel et al., 2020). Tumors in DMG patients lacking H3K27M alterations but overexpressing EZHIP are now considered a distinct subtype of DMG according to the latest WHO Classification of CNS Tumors (Louis et al., 2016).

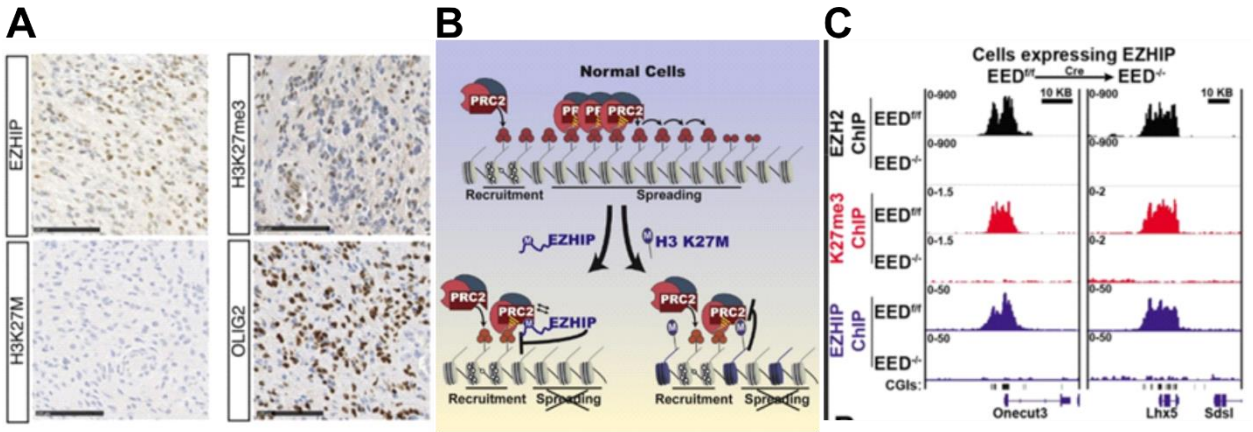

Figure 5: EZHIP mimics the H3K27M mutation in H3-WT DMG

A- Representative IHC of H3-WT DMG tumor showing a loss of H3K27me3 (Castel et al., 2020).

B- Illustration of EZHIP mimicking H3K27M interacting with allosterically activated PRC2 (Jain et al., 2020).

C- ChIP-seq data showing that EZHIP and EZH2 colocalized with residual H3K27me3 at CpG islands in EZHIP-expressing cells (Jain et al., 2020).

1.1.4. Other frequent mutations in DMG/DIPG

DMG exhibit a low tumor mutational burden, and apart from H3K27M, the most frequently detected somatic mutations or alterations involve *ACVR1*, *TP53*, *PPM1D*, *PDGFRA* (Duchatel et al., 2019; Findlay et al., 2022; Mackay et al., 2017; Taylor et al.,

2014a) (Fig. 6, Table 2).

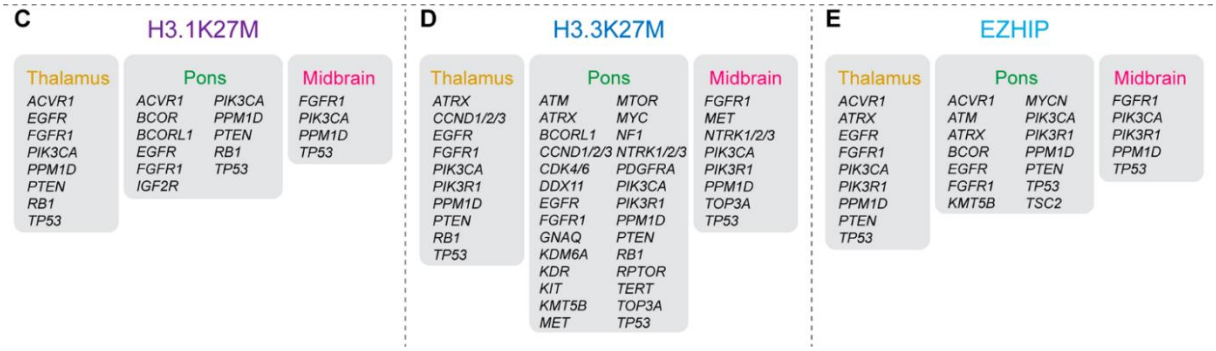

Figure 6: Summary of identified recurrent somatic mutations in DMG

List of mutations in H3.1K27M, H3.3K27M and EZHIP DMG H3-altered according to tumors location (Findlay et al., 2022).

Tumor type	Subtypes	Frequent molecular alterations
Diffuse midline glioma, H3K27-altered	Diffuse midline glioma, H3.3K27-mutant	H3.3K27M mutation, often co-ocurring with *TP53* / *PPM1D* mutation and *PDGFRA* alteration
	Diffuse midline glioma, H3.1 or H3.2K27-mutant	H3.1 or H3.2 K27M mutation, often co-occuring with *PIK3CA* , *PIK3R1* or *PTEN* mutations and *ACVR1* mutation
	Diffuse midline glioma, H3-wildtype with *EZHIP* overexpression	*EZHIP* overexpression
	Diffuse midline glioma, H3K27M and *EGFR* - mutant	*EGFR* mutation, often co-occuring with *TP53* mutation
	Diffuse midline glioma, H3K27-altered with MAPK-activating co-driver mutations	H3.3K27M mutation, co-occurring with BRAFV600E or *FGFR1* -mutant

Table 2: Subclassification of DMG H3K27-altered

Subclassification according to WHO Classification of Pediatric Tumors and suggestion of new subtype. Table modified from (Auffret et al., 2024; Pfister et al., 2022)

ACVR1

ACVR1 encodes activin A receptor type I, and its four common somatic mutations (R206H, G328E/V/W, G356D, R258G) have been found in 21% to 32% of DMG/DIPG tumors and in 85% of H3.1K27M DMG/DIPG tumors (Buczkowicz et al., 2014; Findlay et al., 2022; Fontebasso et al., 2013; Mackay et al., 2017; Taylor et al., 2014a; Wu et al., 2014). *ACVR1* mutations have been demonstrated to upregulate the genes encoding

DNA-binding protein inhibitors ID1 and ID2 by inducing phosphorylation of SMAD proteins through a ligand-independent mechanism. This indicates that ACVR1 mutations can activate the bone morphogenetic proteins (BMP) signaling pathway in the absence of ligands and facilitate cell cycle progression (Fig. 7) (Zadeh and Aldape, 2014).

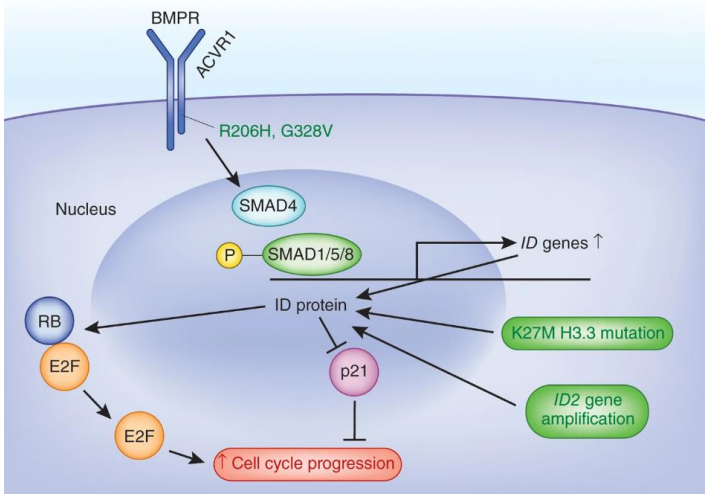

Figure 7: ACVR1 mutations signaling pathway

ACVR1 mutations activate phosphorylation and translocation of SMAD and result in upregulation of BMP downstream genes (Zadeh and Aldape, 2014).

Interestingly, the ACVR1 mutations identified in DIPG closely resembled those found in fibrodysplasia ossificans progressive, a connective tissue disorder. However, none of the FOP patients developed DIPG, indicating that an *ACVR1* mutation alone is insufficient for gliomagenesis (Taylor et al., 2014b).

The combination of H3.1K27M and $ACVR1^{G328V}$, along with $PIK3CA^{H1047R}$, led to the spontaneous development of gliomas in the brainstem and thalamus in mouse model (Fortin et al., 2020). In another study, co-expressing of $ACVR1^{R206H}$ or $ACVR1^{G328V}$ with H3.1K27M and p53 deletion leaded to the development of glioma-like lesions, yet it is inadequate for complete gliomagenesis. However, when combined with PDGFA signaling, this combination significantly elevated tumor incidence and dramatically decreased mouse survival (Hoeman et al., 2019).

TP53 or PPM1D mutation

TP53, a tumor suppressor gene, encodes the p53 protein, which plays a crucial role in regulating the G1/S checkpoint during the cell cycle. *TP53* mutations are found in up to 70-80% of H3K27M DMG tumors (Tomita et al., 2022). Meanwhile, approximately 80% of $TP53^{WT}$ DMG tumors have *PPM1D* mutations, which encode WT p53-induced phosphatase 1D (WIP1), serves to inactivate TP53 and to stop the DNA damage response pathway, potentially leading to tumorigenesis (Kleiblova et al., 2013; Zhang et al., 2014). iPSCs models have demonstrated that TP53 loss can sustain the survival and development of H3K27M cells, contributing to gliomagenesis (Haag et al., 2021).

A study in our lab revealed that *TP53* mutation is a driver of primary radio resistance in DIPG. Indeed $TP53^{WT}$ patients showed a better clinical and radiological response to radiation compared to *TP53*-mutated patients (Fig. 8) (Werbrouck et al., 2019). Similar to *TP53* mutation, *PPM1D* mutation has been reported in DIPG to lead to radio resistance by inactivating DNA damage response (Akamandisa et al., 2019; Wang et al., 2020). Meanwhile, $TP53^{WT}/PPM1D^{MUT}$ was shown to be sensitive to TP53 pathway reactivator (Xu et al., 2021).

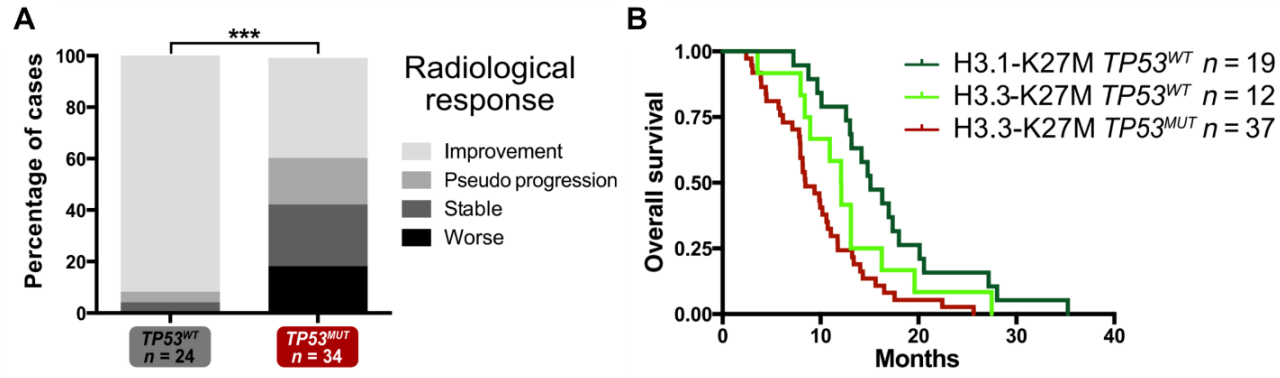

Figure 8: *TP53* mutation in DMG

According to (Werbrouck et al., 2019), *TP53* mutation is associated with:

A- a low response to radiotherapy (RT) in radiological criteria with 4 classes.

B- lower overall survival estimated by using the Kaplan-Meier method.

PDGFRA

Amplification of the gene encoding platelet-derived growth factor receptor α (*PDGFRA*) is found in 30% of DMG tumors, particularly H3.3K27M tumors (Findlay et al., 2022). PDGFRA is involved in numerous downstream signaling pathways, including PI3K/Akt/mTOR, and its over-regulation is sufficient to induce gliomagenesis in both mouse models and human embryonic stem cell models when combined with the H3.3K27M mutation and TP53 loss (Dai et al., 2001; Funato et al., 2016; Larson et al., 2019; Masui et al., 2010; Pathania et al., 2017; Shih and Holland, 2006).

Interestingly, several studies have suggested that PDGFRA could be a lineage-defined factor, as it is overexpressed in oligodendrocyte progenitor cells (OPC). Consequently, in the absence of PRC2 function, PDGFRA might arrest cells at a pre-differentiation stage, maintaining an OPC-like phenotype in the majority of DMG cells (Bruschi et al., 2023; Filbin et al., 2018).

3. A recap of heterogeneity in DMG/DIPG

In the particular case of DMG/DIPG, the predominant presence of the initial alteration H3K27M mutation, coupled with global loss of H3K27me3 and few frequent secondary mutations, renders DMG/DIPG one of the tumor types with a homogeneous background. However, the homogeneity of (epi)genetic of cells infiltrating to other brain structure and cells at original location is yet to be investigated.

1.1. Inter-tumor heterogeneity

Inter-tumor heterogeneity refers to dissimilarities in genotype among tumors, which arise from the distinct genomes of each individual. In the case of DMG, a diverse spectrum of tumoral histology depending on the present mutations underscores the diversity among patients (Auffret et al., 2024; Buczkowicz et al., 2014; Chiang et al., 2020; Warren, 2012). Furthermore, the past decade has witnessed a significant advancement and widespread use of sequencing methods, including whole-genome/exome sequencing, DNA methylation profiling, RNA-sequencing, and more. This progress has provided scientists with valuable insights into the distribution of

common mutations in DMG tumors. In DMG/DIPG, as mentioned above, H3K27M mutation presents up to 90% of cases and even though the other 10% does not harbor this mutation, they share one property which is global loss of H3K27me3. It is possible that the global H3K27me3 loss is the initial alteration to trigger the gliomagenesis but it is the specific type of K27M mutation in combination with other additional mutations that drive the growth of tumor to favor tumor's growth as well as trigger different response to treatment (Aziz-Bose and Monje, 2019).

Analyzing patients' genomes can provide valuable information, promoting precision medicine where patients with the same (epi)genomic mutation or alteration can be grouped to receive distinct therapy strategies to enhance survival rates. It is crucial to consider this complexity when designing new treatment approaches because each subgroup may require a therapy to improve outcomes in children with the same conditions, which is referred as precision therapy. Stereotactic biopsy-driven molecular profiling is a good strategy to obtained these information (Puget et al., 2015).

1.2. Intra-tumor heterogeneity

The evolution of tumors is a well-established concept in oncology, wherein the genomic profiles of original tumors undergo dynamic changes over time, influenced by factors such as temporal progression, spatial location, tumor microenvironment and treatment modalities. Initially, causal mutations could trigger the formation of the primary tumor and as driver mutations accumulate, tumor burden increases, leading to the emergence of diverse subclones (Fig. 9) (Alizadeh et al., 2015). Consequently, tumors at the same anatomical site can comprise multiple subpopulations with distinct molecular signatures and metastatic tumors often exhibit significant differences from their primary counterparts, reflecting adaptations to distinct microenvironments. This is referred as intra-tumor heterogeneity. Scientists have considered intra-tumor heterogeneity as a barrier, challenging the efficacy of conventional therapies that treat tumors as homogeneous entities and potentially fostering resistance mechanisms (Alizadeh et al., 2015; Sun and Yu, 2015; Vinci et al., 2018). Acquiring samples from

different parts or at different time points of the tumor enables the coverage of distinct sets of genetic alterations or the monitoring of tumor evolution (Broniscer et al., 2010; Kambhampati et al., 2015).

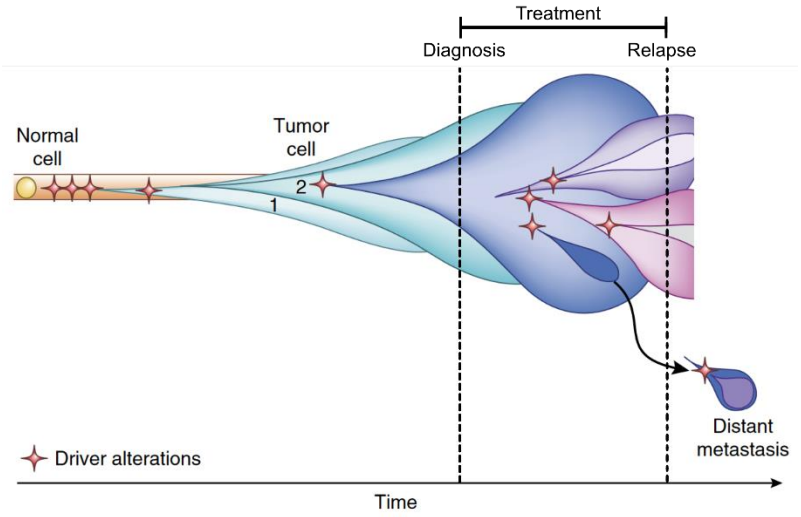

Figure 9: The evolution of tumor clonality
Graph modified from (Alizadeh et al., 2015).

Intra-tumoral heterogeneity arises from a combination of factors, encompassing genetic variances, variations in the microenvironment, pre-existing tolerance or resistance, and possibly new adaptive subpopulations. These factors can be categorized into two groups: cell-autonomous (intrinsic) and non-cell-autonomous (extrinsic) sources (Li, 2022).

Cell-autonomous mechanisms involve various intrinsic factors that exclusively impact mutant cells, such as genetic alterations, epigenetic plasticity, transcription factors (TFs), and the cell-of-origin. Whole-genome/exome sequencing provides insights into the heterogeneous nature of tumors by allowing for the determination of allele frequency of somatic mutations, thus facilitating the identification of the expansion of tumor clones or subclones (Cmero et al., 2020; Dentro et al., 2017). Using the cancer cell fraction or copy number variant analysis in multiple location in DIPG autopsies, H3K27M was detected as the earliest tumorigenic event in DIPG, along with other mutations exhibited predominantly in clones such as ATRX, and NF1, or in combination

with partner gliogenesis-alterations such as *TP53, PPM1D, ACVR1*, and *PIK3R1* (Nikbakht et al., 2016; Vinci et al., 2018) (Fig. 10) (Nikbakht et al., 2016).

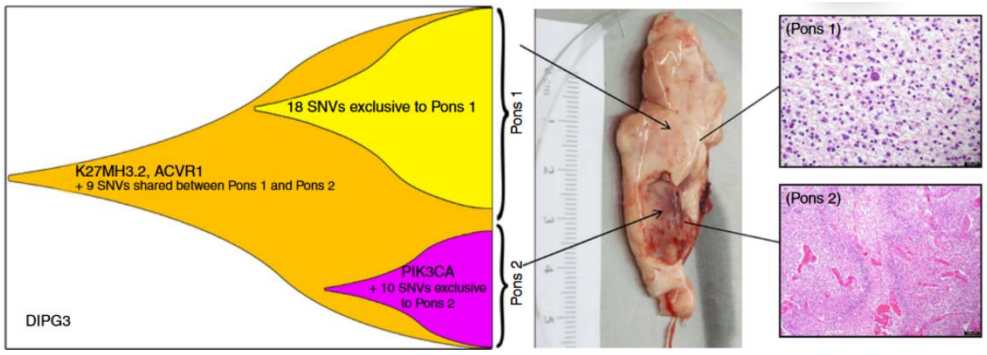

Figure 10: Evolutionary trajectory of a DIPG postmortem sample

Two discrete subclones exhibit distinct histological and genetic profiles despite sharing a common driver mutation, H3.2K27M and *ACVR1*. *PIK3CA* was proposed to emerge early in the evolution of the pons 2 sub-clone (Nikbakht et al., 2016).

Glioma cells not only inherit specific attributes from their cell-of-origin phenotype but also rely on this phenotype to govern their interactions and communication with the tumor microenvironment (TME) through signal transduction pathways to secure an optimal environment for growth (Kluiver et al., 2020; Loveson and Fillmore, 2018; Winkler et al., 2023; Yang et al., 2022). The TME comprises brain cells, immune cells, the extracellular matrix (ECM), and blood vessels. It has been suggested that DIPG subclones exhibiting synergy at the same location may activate each other to become more aggressive, while those forming physical interactions (tumor microtubes) with other cell types in the brain are capable of promoting invasion (Fig. 11A) (Kluiver et al., 2020). An elegant study also revealed that DIPG cells in contact with hyperexcitable neurons, through different mechanisms, might be more proliferative than those without such contact (Fig. 11B) (Venkatesh et al., 2019).

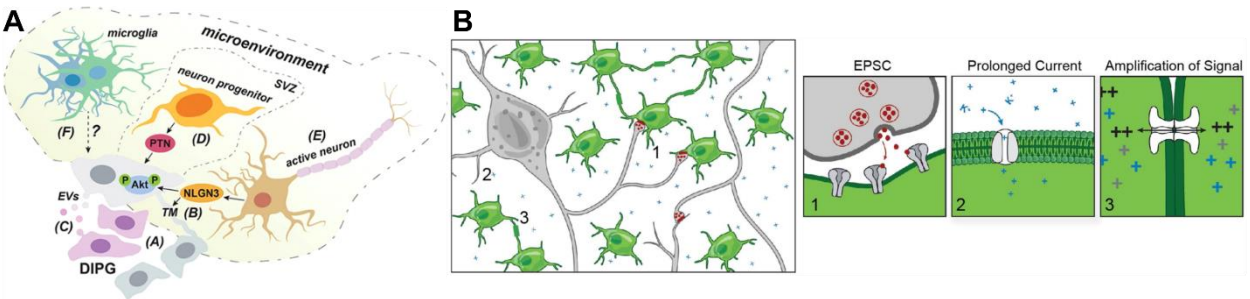

Figure 11: Elements that can promote DMG/DIPG invasion and proliferation

A- Factors in TME that can promote the invasive behaviour of DIPG (Kluiver et al., 2020).

B- Nearby hyperexcitable neurons were suggested to enhance the proliferation of DIPG through different mechanisms: 1- Synaptic connections from neurons to gliomas, with synaptic vesicles (red) and AMPA receptors (grey) (Venkatesh et al., 2019).

4. The disseminating nature of DMG/DIPG

The characteristic infiltrative pattern of DMG refers to a distribution of cancer cells amidst normal tissue rather than the formation of a tumor mass, as observed in many other solid cancers. This diffuse infiltration poses significant challenges for complete surgical resection, primarily due to the intricate task of delineating cancerous from healthy tissue, the heightened risk of disrupting critical brain structures, and the potential for severe neurological consequences. Moreover, there is concern regarding the possibility of "human-induced dissemination" when glioma stem cells are accidentally delivered to a distant location along the trajectory path during biopsy extraction or the addition of an Ommaya catheter. However, empirical evidence suggests that the incidence of such occurrences remains exceedingly low, as documented in prior studies (Lobon-Iglesias et al., 2018a).

The disseminated nature of DMG manifests predominantly during the advanced stages of the disease (Bruschi et al., 2023). Specifically, localized and locoregional dissemination within the pons and adjacent structures, such as the cerebellum and thalamus, has been extensively documented (Caretti et al., 2014) (Fig. 12). Conversely, distant dissemination typically culminates in the formation of metastatic *foci*, which may propagate throughout the CNS, with prevalent sites including supratentorial extensions, leptomeningeal dissemination, and sporadic occurrences within the spinal cord (Buczkowicz et al., 2014; Caretti et al., 2014; Gururangan et al., 2006). Regardless of the specific anatomical location, the diffuse nature of DIPG tumors invariably induces compression and functional perturbations, thereby precipitating a spectrum of neurological sequelae and symptomatic manifestations (Johung and Monje, 2017).

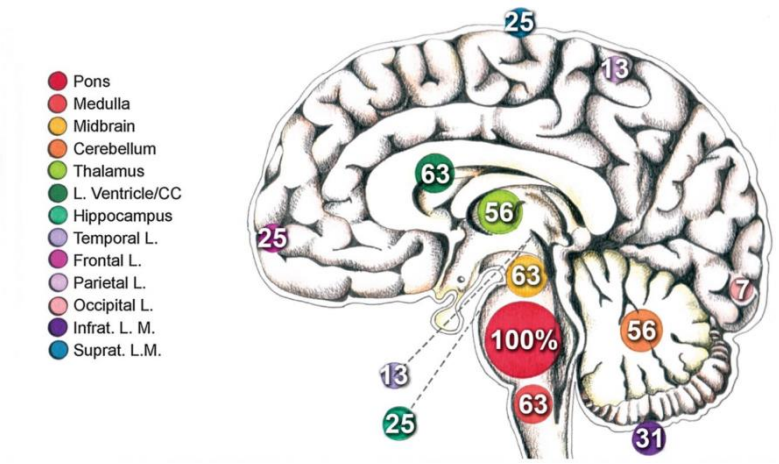

Figure 12: Frequency of tumor spread in subventricular structure of DIPG (Ceretti et al. 2014).

Few exclusive cases were reported throughout the years, in which the presence of extra-neural metastasis with disseminated osseous lesions or diffuse into peritoneum were reported (Bhatt et al., 2020; De Martino et al., 2023; Handis et al., 2021; Lazow et al., 2022; Mohiuddin et al., 2021; Stephens et al., 2019). For example, in De Martino et al. paper, tissue section examining showed a heterogeneous feature with extensive perivascular proliferation and palisading necrosis. Wagner et al. investigated 110 DIPG patients and concluded that the secondary dissemination (happening after diagnosis) did not give any impact on overall survival (OS) of the patients suggesting the short OS resulted from the local tumor progression (Wagner et al., 2006).

So far, the mechanisms underlying the active dissemination of tumor cells from the primary pontine location to other regions of the brain and spine remain enigmatic. In the context of primary brain tumors, there exists a paucity of robust evidence to elucidate whether non-pontine lesions manifest concomitantly with midline structures or represent manifestations of early dissemination, with the latter scenario possibly indicative of delayed diagnoses.

Part II: DMG cell-of-origin and their development in Central Nervous System (CNS)

As previously stated, pHGG do not originate from previously existing pediatric low-

grade gliomas ion contrast to adult glioblastoma (Cohen, 2022; Ryall et al., 2020b). Instead, pHGGs exhibit a distinct biological landscape compared to their adult counterparts (Bax et al., 2010; Paugh et al., 2010). Furthermore, it is noteworthy that DMG or DIPG typically manifests a peak onset during the age range of 6 to 9 years (Liu et al., 2022b; Lobon-Iglesias et al., 2018a; Veldhuijzen van Zanten et al., 2015). This temporal pattern suggests a close association between the initial mutation event and disruptions in normal brain development (Baker et al., 2016). During this developmental phase, the brain undergoes active growth and differentiation characterized by extensive cellular expansion and the maintenance of a reservoir of progenitor cells (Hansen et al., 2013; Zhou et al., 2023). This underscores the significant influence of the cell-of-origin in initiating DMG/DIPG gliomagenesis. They do not only establish the foundational genetic and epigenetic landscape in conjunction with the initiating cancer-causing mutations but may also exert an influence by imparting its inherent migratory capabilities to the cancer cells. In doing so, it potentially contributes to the infiltrative or invasive characteristics exhibited by DMG cells. Therefore, understanding the mechanisms by which the cell-of-origin can drive the infiltrative nature of DMG/DIPG is crucial for finding solutions to restrict the invasive abilities of these gliomas and improve patient survival outcomes.

The available evidence substantiates the hypothesis that the cell-of-origin for DMG likely originates from OPC, or even more primitive lineages such as glial progenitor cells (GPC) and neural stem cells (NSC). This section will delve into the established characteristics of these cell types and their plausible roles in facilitating DMG infiltration and invasiveness. However, the confusion and misunderstandings in the field of stem cells and progenitor cells research have arisen due to the incorrect application of these terms when describing undifferentiated cells in the CNS. Therefore, before going deeper into understanding the development and differentiation of these 3 candidates for cells-of-origin, it is important to have a common definition premise throughout the whole manuscript. For clarity, the following terminologies are used throughout this manuscript (Kriegstein and Alvarez-Buylla, 2009; Martínez-Cerdeño and Noctor, 2018;

Smith, 2006):

- Stem cells: cells with the capacity to continuously renew itself without phenotype alteration and also be able to produce daughter cells with more differentiated characteristics.
- Progenitor cells: dividing cells with more limited proliferation and have a tendency to give rise to more lineage-restricted descendant cell types or undergo terminal differentiation.
- Neural stem cells (NSC): oligopotent and self-renewing primary progenitor cells at different developmental stages with ability to generate lineages forming two distinct populations: neurons and glial cells.
- Glial progenitor cells (GPC): exhibit a reduced capacity for self-renewal, constrained by a finite number of divisions, and their developmental potential is primarily directed toward differentiation into specific glial cell types, encompassing astrocytes and oligodendrocytes.

OPC cells that have the capacity to give rise to oligodendrocytes, which are specialized glial cells charged with the production of myelin.

1. Neural stem cells (NSC)

1.1. NSC during neurogenesis in developing brain

Neurogenesis plays an important role in generating neurons throughout the central nervous system, followed by several other critical processes of brain development, such as neuronal migration, differentiation, axon formation, synaptic development, and establishment of neural circuitry (Taverna et al., 2014). Embryonic NSC undergo a highly coordinated procedure, where multiple steps occur simultaneously to ensure an adequate supply of materials for brain development (Kempermann et al., 2004) yet numerous fundamental questions regarding early NSC development during the fetal and postnatal periods remain unanswered. Hence, the role of NSCs in the context of brain development and gliomagenesis of DMG/DIPG in children remain to be fully

explored.

During the early stages of brain development, from 7 post-conception week (pcw) until 22 pcw (Fig. 13A), in addition to symmetric division, neuroepithelial cells also undergo asymmetric division to generate early neurons and transform into radial glial cells (RGCs) (Hevia et al., 2022; Silbereis et al., 2016). Some of them will also transition into ependymal cells or NSC. These neonatal RGCs/NSCs will subsequently undergo partial divisions to intermediate progenitor cells, giving rise to both neurons and glial cells (astrocytes and oligodendrocytes) (Fig. 13B). NSCs are found in many structures of the embryonic nervous system including both CNS (basal forebrain, cerebral cortex, hippocampus, cerebellum) and peripheral nervous system (neural crest) (Alvarez-Buylla et al., 2001; Carlson, 2019; Gage, 2000; Kriegstein and Alvarez-Buylla, 2009; Laywell et al., 2000; Smith, 2006). In developing CNS, NSCs are confined to the ventricular zone and surrounded by RGC which are accounted for the major neural progenitors. However, the differentiation might involve sub-population of intermediate neural/oligodendrocyte progenitor cells (nIPC or oIPC) with limited number of self-renewal and that their destiny is influenced by both spatial and temporal factors (Haubensak et al., 2004; Kriegstein and Alvarez-Buylla, 2009; Miyata et al., 2004; Noctor et al., 2004).

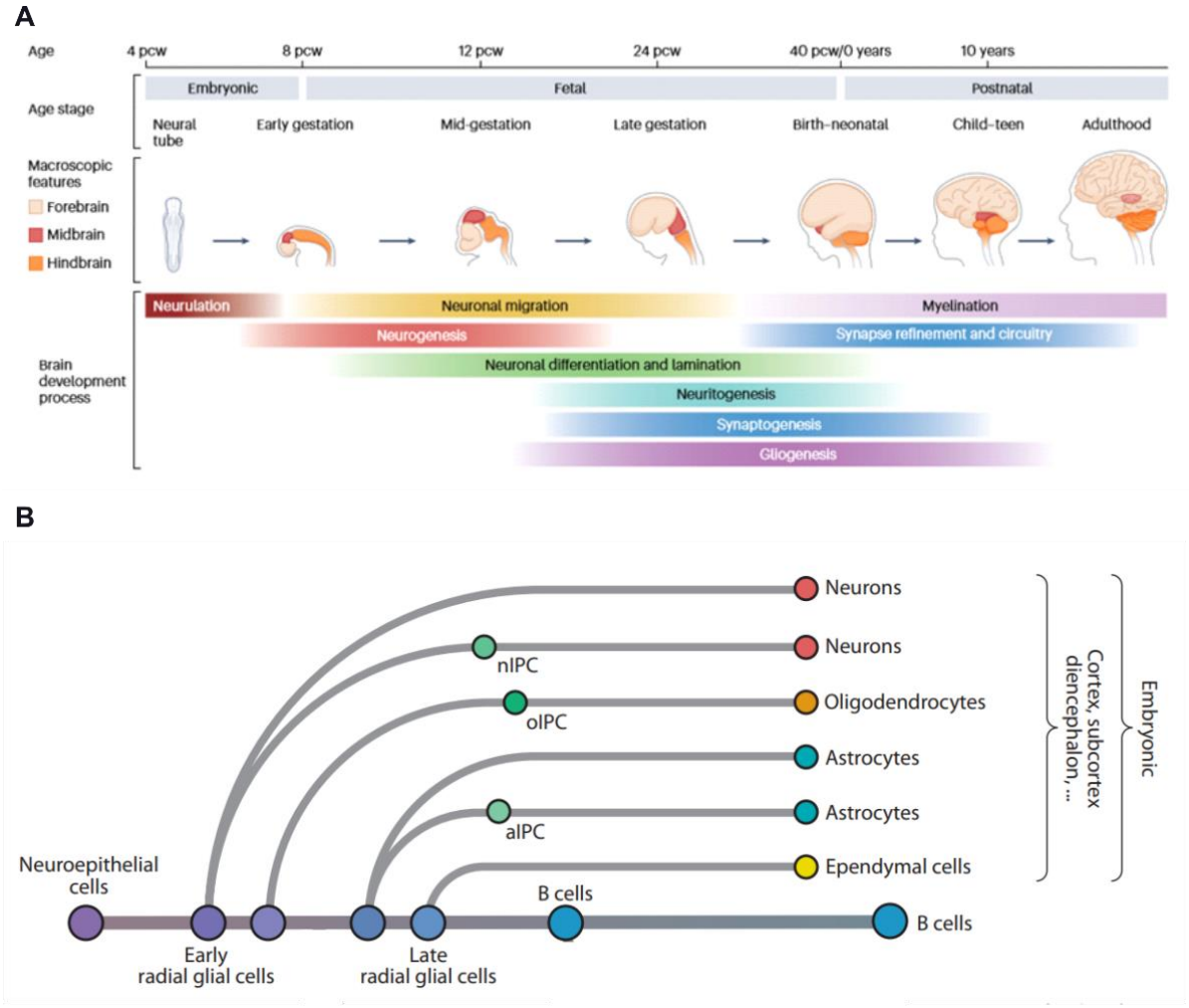

Figure 13: Human brain development timeline and cell lineages

A- Timeline of main events during human brain development (Zhou et al., 2023).

B- Lineage diagram of NSCs (purple and blue dots) during embryonic period. nIPC: intermediate progenitor cells (IPCs) for astryocytes (aIPCs), oligodendrocytes (oIPCs) and neurons (oIPCs). Diagram modified from (Kriegstein and Alvarez-Buylla, 2009).

Notably, NSC appear at early stages of embryo development and subsequently become predominant, with approximately 50% of the viable cells displaying stem-like characteristics at E8 in the embryonic rat model (Kalyani et al., 1997, 1998). However, this percentage rapidly declines, decreasing from 10% at E12 to 1% on postnatal day 1. A similar phenomenon is observed in humans, with hippocampal neurogenesis sharply decreasing to undetectable levels in adults (Sorrells et al., 2018). Nevertheless, a reservoir of NSC persists in either the subventricular zone (SVZ) or the dentate gyrus and serves as a vital source of stem cells for the body. Moreover, hindbrain boundaries,

which act as a barrier separating the midbrain and rhombomere 1 of the hindbrain structure, play a role as a reservoir of NSC via SOX2 and the extracellular matrix proteoglycan chondroitin sulfate (Hutchings et al., 2024; Peretz et al., 2016).

From these original pools, the distribution, amplification, and differentiation of NSC closely follow the developing pattern of the brain, particularly in the hindbrain, which will develop into the pons, the original location of DIPG. Neural differentiation follows the segmental architecture of the hindbrain, resulting in the development of a conserved segmental pattern across neuron, cranial ganglia and neuronal connectivity between hindbrain and others brain structures (Krumlauf and Wilkinson, 2021) (Fig. 14A). Published data have shown that the *Hox* family is deeply involved in the segmentation of the hindbrain (Buckles et al., 2004; Kiecker and Lumsden, 2005; Krumlauf and Wilkinson, 2021; Studer et al., 1996) (Fig. 16A) while a combination of BMPs, Sonic hedgehog, Wnt, and fibroblast growth factors plays a role in regionalizing the brain (Fig. 14B) (Carlson, 2019; Kiecker and Lumsden, 2012). *Hox* genes, together with *Eph* receptors, prevent cell mixing and pattern overlapping between different parts of rhombomeres, as well as guide the migration of neural crest cells and motor neurons (Trainor and Krumlauf, 2000).

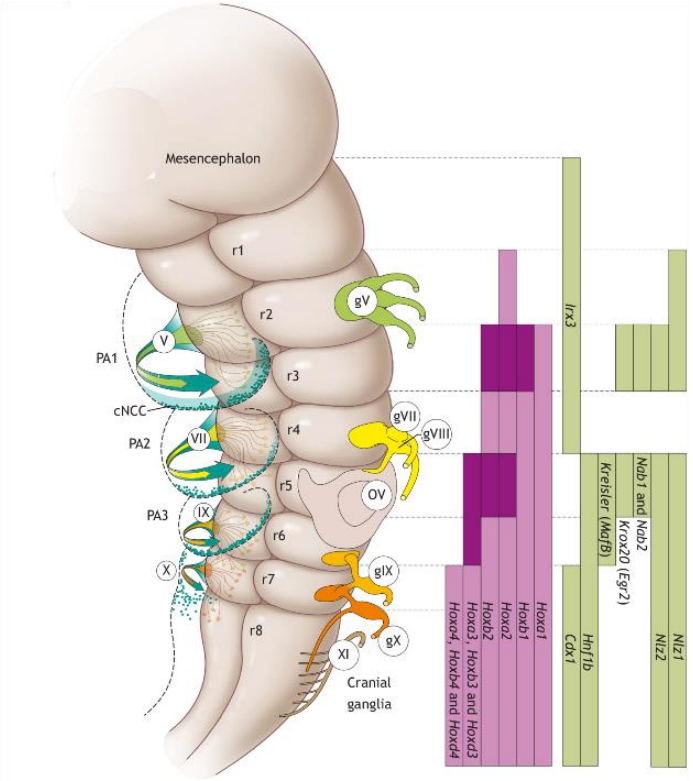

Figure 14: Illustration of individual rhombomeres in ventral view of the developing mouse hindbrain

Rhombomere-specific gene expression domains for key transcription factors governing segmentation and segmental patterning are listed on the right. Figure adapted from (Krumlauf and Wilkinson, 2021).

Additionally, numerous transcription factors have been identified as regulators of both embryonic and adult neurogenesis (Singh et al., 2023). Postmitotic factors such as Ascl1 and Gsh1/2 play pivotal roles in determining the fate choice of NSCs between inhibitory and excitatory phenotypes (Mizuguchi et al., 2006). Members of the basic helix-loop-helix (*bHLH*) family influence the differentiation and lineage commitment of the NSC pool. Homeodomain transcription factors such as PAX6 and SOX2 maintain the delicate balance between stemness and neurogenesis within the NSC pool (Singh et al., 2023).

1.2. NSC as a cell-of-origin of DMG/DIPG

Using DIPG neurosphere culture model, Monje's research team has shown that all tumor cells expressed Nestin, Vimentin, and GFAP, which are three common markers of NSC. Additionally, 37% of the cell culture population was CD133+, with a similar

percentage of CD133+ cells found in immunocytochemistry as well as in the original tumor tissue (Monje et al., 2011).

Moreover, Haag et al. examined injecting several combinations of WT or H3K27M-mutated iOPC and iNSC with or without *TP53* knock-down into the brainstem of 6-week-old NSG mice (Haag et al., 2021). After 12 months, only K27M/shTP53 iNSCs could develop DIPG-like tumors. RCAS/TVA, a powerful human tumor modeling tool, was selected to establish a novel mouse model of DIPG. It demonstrated that introducing PDGFB, TP53 loss and with or without the H3.3K27M mutation to Pax3+/Nestin+/Sox2+ population will create Ki67+, Nestin+, Olig2+, largely GFAP-tumors that could arise within the brainstem structure. It is important to address that these models introduced *PDGFB* to mimic the *PDGFRA* amplification observed in autopsies, even though *PDGFB* has not been detected as overexpressed in biopsies. More importantly, H3.3K27M mutation caused global H3K27me3 reduction as observed in DMG/DIPG tumor (Misuraca et al., 2016). However, H3.3-K27M overexpression and *TP53* knockout give rise to diffuse tumors in the hindbrain and cortex without exogenous PDGFRA activation when targeted to NSC in utero (Larson et al., 2019). Although confirming the tumor-driving potential of H3K27M and providing valuable insight into related epigenetic and transcriptomic changes, these models did not finally clarify the cell of origin question, in part due to limited control over targeting different developmental cell stages.

2. Glial progenitor and oligodendrocyte progenitor cells

Unlike neurogenesis, which initiates during early embryonic development, gliogenesis commences later in this process and persists into postnatal stages. On the other hand, during neurogenesis, bHLH proteins such as Ngn1 combines with Bmp2 expression to form the complex named Smad:p300/CBP:Ngn1 which acts as an astrocyte differentiation inhibitor thus halt the formation of glial cells (Sun et al., 2001). In human, gliogenesis usually starts around week 18 after conception and lasts through by peaking around birth then continues until the next few years later (Silbereis et al., 2016).

Astrocytes and OPC are generated during mid-gestation from RGC (Jakovcevski et al., 2009).

1.1. Gliogenesis in developing brain

Glia account for at least 50% of the cells in the human brain, with two important supportive populations: astrocytes and oligodendrocytes. Once regarded solely as "nervenkitt or nerve glue" responsible for maintaining CNS connections, glial cells have recently gathered increased attention thanks to discoveries revealing their role in early brain development, brain function, neurotransmission, and nutrient transport (Hirbec et al., 2020; Somjen, 1988). These cells play pivotal roles in regulating myelination, involving in saltatory nerve conduction, maintaining homeostatic balance, supporting synaptic function, facilitating nerve signaling, and responding to CNS injuries. This underscores the significance of glial cells in brain function and highlights gliogenesis as one of the most critical processes during CNS development. Gliogenesis comes after the generation of neurons and requires the collaboration of at least three different cues to begin. The first hint is cytokine CT-1 interacts with LIFRβ and gp130 coreceptor trigger JAK signaling then activate the STAT3 TF. This TF then forms a complex with SMADs, downstream components of activated BMP receptors, along with the coactivator p300/CBP. This complex initiates the transcription of *GFAP*, a glial gene, by binding to its promoter region. The Notch pathway is also activated and navigates its downstream effector, RBP-Jκ transcription factor, to activate the *GFAP* promoter. Last but not least, the third cue, NF1 transcription factor, also binds to the *GFAP* promoter. The coordinated interplay of these pathways then regulates the timing of gliogenesis (Fig. 15) (Miller and Gauthier, 2007).

Gliogenesis is typically divided into two parallel processes: astrocytogenesis and oligodendrogenesis. When three specific triggers are met, cells located in the SVZ primarily become gliogenic, and most RGCs begin to detach from the ventricular zone (VZ) and migrate to the SVZ. There, they give rise to astrocytes either directly or through intermediate astrocytic progenitor cells (Miller and Gauthier, 2007) (Fig. 15).

In the hindbrain, it has been reported that oligodendrogenesis could occur at restricted loci on either side of the midline. The progenitor cells in the hindbrain region are resistant to the BMP inhibitor effect, which initiates differentiation with the activation of Olig1/2 (Hardy and Friedrich, 1996; Vallstedt et al., 2005).

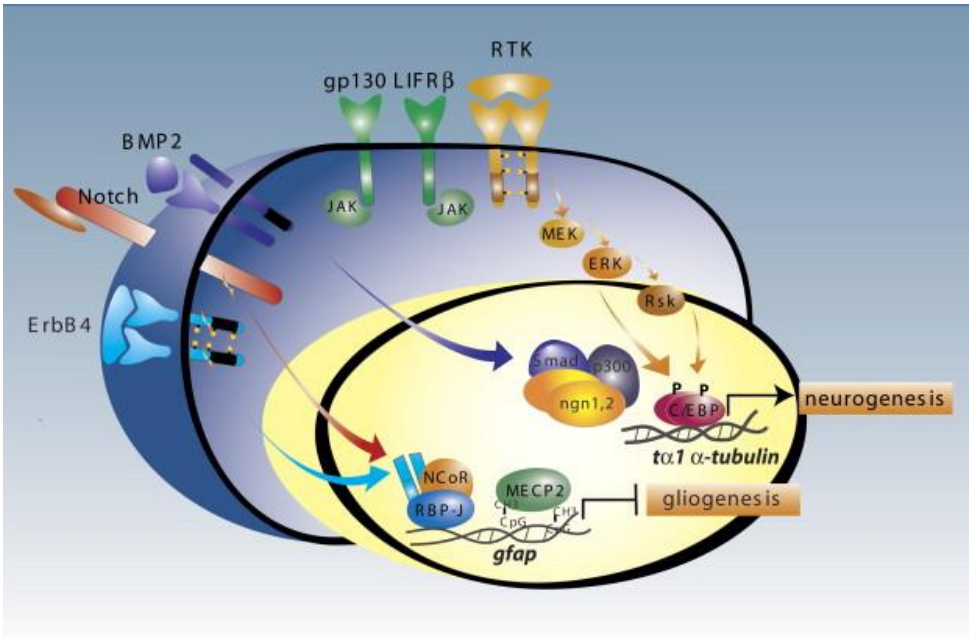

Figure 15: The intrinsic control of neuro-gliogenesis switch
(Miller and Gauthier, 2007)

Astrocytes, an important subset of glial cells, constitute approximately 24-40% of the cellular population within the brain. These cells have gained recognition for their indispensable role in establishing a critical neurovascular connection between neurons and endothelial cells. Their specialized end-feet structures contribute to the maintenance of cerebral homeostasis through the regulation of neurotransmitter, water, and amino acid uptake. Moreover, astrocytes possess the capability to form tripartite synapses, establishing connections between local synaptic circuits and the synapses they envelop. Additionally, these astrocytes express neurotransmitter receptors, enabling them to detect synaptic activity and respond by elevating intracellular calcium levels (Ca^{2+}) and releasing neuroactive substances into the synapses. Astrocytes in white matter are fibrous astrocytes and the ones mainly in gray matter are usually called protoplasmic. The former one creates contact with blood

capillaries and axons while the later one form contact with blood vessels and synapses (Kim et al., 2019) (Fig. 16).

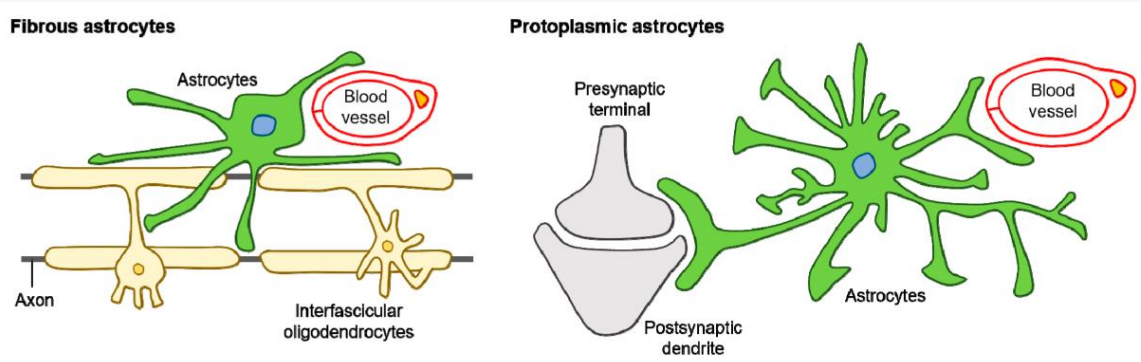

Figure 16: Two types of astrocytes in the CNS.
(Kim et al., 2019).

The development of astrocyte follows a regulated pattern influenced by Scl/tal1, a bHLH TF. This transcription factor collaborates with Olig2 to determine the specific locations where astrocyte progenitor cells (APC) and OPC will originate

1.2. Oligodendrogenesis in developing brain

As mentioned above, the process through which oligodendrocytes are generated from RGC occurs concurrently with astrocytogenesis and is referred to as oligodendrogenesis. This process typically takes place during both embryonic and postnatal CNS development and is crucial for the proper functioning of the human brain, as well as for cognition and learning abilities.

1.2.1. Oligodendrocytes and oligodendrocyte progenitor cells

Oligodendrocytes or OLs for short, are fully developed, non-dividing cells that primarily reside in the white matter of the CNS, which comprises areas in the brain and spinal cord composed exclusively of axons. OLs are responsible for the myelination of the CNS. Myelin refers to a multilayer spiral structure extension, or so-called sheath, of a OL's plasma membrane that wraps around the axon to allow efficient transmission of action potentials and speed up the conduction velocity between neurons within the CNS. One of the distinguishing characteristics between white and grey matter stems

from the presence of myelin, which imparts a translucent, shiny white appearance to the white matter. While mature OLs are frequently illustrated as having compact cell bodies with myelin sheaths extending from the tips of their processes, their morphology, including their myelin structures, varies significantly across different brain regions. In the early stages of oligodendrocyte research, these cells were initially classified into four distinct types based on their cell body shape and the percentage of myelin coverage (Osanai et al., 2022). New research on mice model have shown a connection between neuronal activity, myelination, and the shape of oligodendrocytes. Elevating the activity of neurons in the motor cortex led to an increased population of mature OLs, thicker myelin in the brain, and enhanced motor function in mice (Bonetto et al., 2021; Gibson et al., 2014).

Another significant area of research in gliogenesis is the predecessor of OLs, known as OPC, and their oligodendrogenesis. OLs originate from OPC, which are derived from RGCs in the VZ during the early embryonic period and in the SVZ during the late embryonic period and early postnatal life (Butts et al., 2008). These OPC go through a series of differentiation stages, progressing from immature premyelinating OLs (pre-OLs) to mature OLs that establish contact with neuronal axons and initiate myelin production (Emery, 2010).

OPC are abundant throughout the CNS, comprising approximately 5% of all cells, and they represent a pool of self-renewing cells throughout life (Dawson et al., 2003; Gensert and Goldman, 2001; Richardson et al., 2011). It is noteworthy that not all OPC appearing during the fetal period will maintain their OPC identity into adulthood, as approximately 10-20% of fetal OPC will transition into adult OPC during a later postnatal period, exhibiting distinct morphological and behavioral characteristics. As depicted in figure 17, the bi/tri-polar shape of fetal OPC transforms into a multi-branched form in adult OPC. However, this transformation is not permanent, and adult OPC can switch back to the previous bipolar shape in response to brain injuries and participate in remyelination processes.

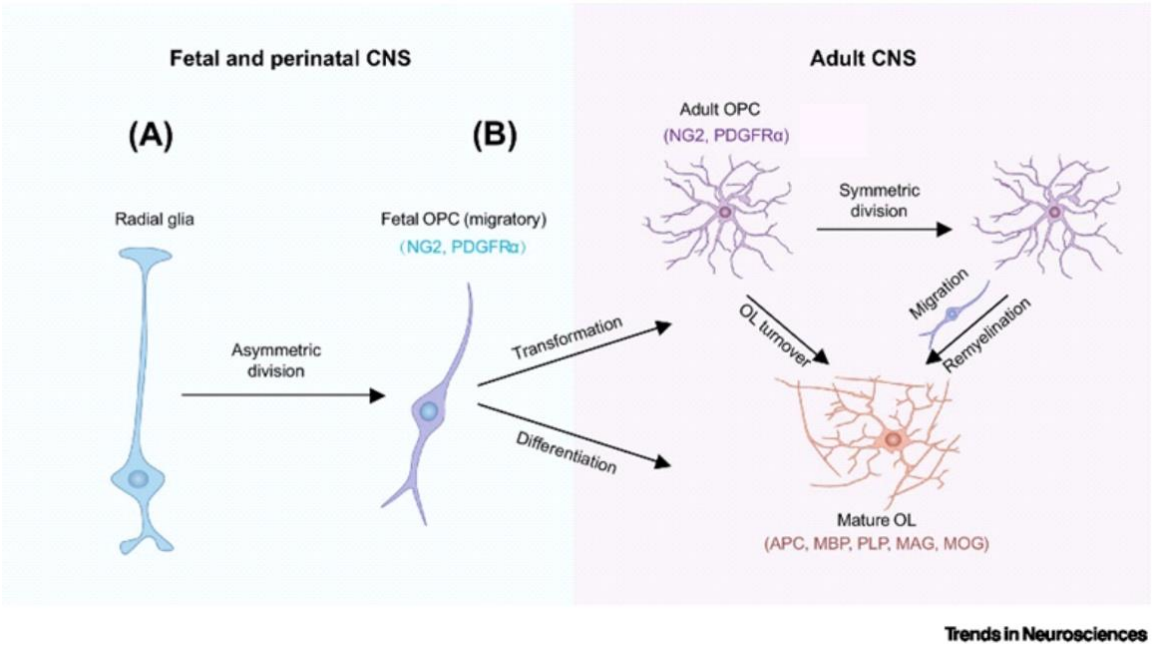

Figure 17: Oligodendrogenesis from RGC to OL

A- RGCs divide asymmetrically to produce fetal OPC.

B- OPC will partly commit to differentiate into OL and the other part will transform to adult OPC as a reservoir for OPC in adult (Yi et al., 2023).

In normal condition, OPC act as a receiver of neural synaptic inputs and they are probably capable to generate action potentials (Káradóttir et al., 2008; Lin and Bergles, 2004). Furthermore, OPC closely interact with the blood-brain barrier and contribute to its maintenance and integrity (Seo et al., 2014). In addition, OPC exhibit immunomodulatory properties, serving as immune cell analogs by surveilling their microenvironment to balance the homeostasis, presenting antigens, and releasing immunomodulatory factors (Falcão et al., 2019; Kirby et al., 2019) (Fig. 18A). On the other hand, OPC establish extensive connections with various brain cell types, including microglia and neurons. Surprisingly, three independent research groups have demonstrated on a mouse model that OPC exhibit gene sets related to the processes of phagocytosis and lysosomal degradation (Fig. 36, right). These cells also appear to play a role in modulating synaptic activity, a function seemingly unrelated to their primary functions in oligodendrogenesis and myelination (Auguste et al., 2022; Buchanan et al., 2022; Xiao et al., 2022). Interestingly, OPC ingest mostly synapses which are likely to be excitatory. However, the specific molecular pathways engaged in these

interactions still remain largely uncharted.

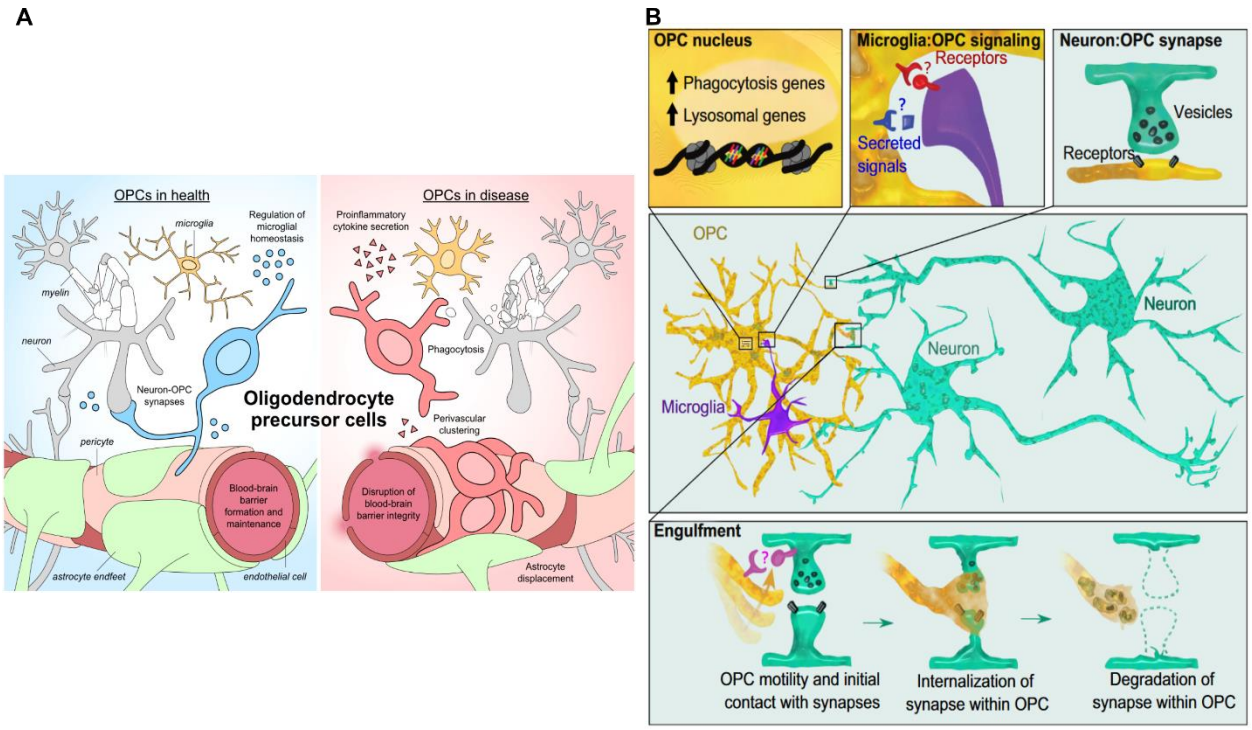

Figure 18: OPC at normal, pathological state and their behavior in brain

A- OPC in healthy and diseased CNS (Akay et al., 2021).

B- OPC interaction in the brain (Buchanan et al., 2023)

1.2.2. Oligodendrogenesis in normal developing CNS

Oligodendrogenesis is one of the most crucial processes in brain development. Consequently, there are several mechanisms involving both transcriptional and epigenetic factors that collaborate together and regulate the normal order of the whole procedure.

At the outset of their journey, RGCs face a crucial choice: to differentiate into either astrocytes or oligodendrocytes. This decision is influenced by the action of histone deacetylases, specifically HDAC3. HDAC3 works in collaboration with p300 to inhibit the expression of genes associated with astroglial differentiation, which includes nuclear factor 1 NF1A, while simultaneously promoting the activation of genes specific to the oligodendroglial lineage (Zhang et al., 2016).

The genesis of oligodendrocytes can be separated into four stages (Table 3) (Butts et al., 2008). In the first stage, RGCs give rise to OPC in the form of motile bipolar cells characterized by a small body and highly proliferative phenotype (Butts et al., 2008). This represents the sole stage during which OPC retain the ability to migrate from their original location to other brain structures before differentiation.

	Undifferentiated		Differentiated	
	Stage 1: OPC	Stage 2: Pro-OL	Stage 3: Immature OL	Stage 4: Mature OL
Morphology	Bipolar	Branching processes	Mature arborization	Myelin sheaths around axons
Motility	YES	NO	NO	NO
Cell division	YES	YES	NO	NO

Table 3: Four main stages of oligodendrogenesis

Table modified from (Butts et al., 2008).

In 2015 Jakovcevski et al. discovered that in human, there are only two waves of OPC during the brain development instead of three waves as reported in rodent. The first wave, known as early OPC, emerges around the 9th gestational week (gw) in the ganglionic eminence and migrates in a form of a gradient towards the cerebral cortex (Jakovcevski and Zecevic, 2005; Jakovcevski et al., 2009). During the first wave, OPC are mitotic and proliferative. The peak number of OPC appears around 15gw in the ganglionic eminence and cortical VZ/SVZ. Following the spreading to dorsal areas and cortical plate, OPC still keep the highest density at the SVZ structure and OPC highly express markers such as *PDGFRA, SOX10, NG2, Olig2, A2B5*. The second wave, referred to as late OPC, becomes apparent around gw15, with small populations appearing in transient subplate layer (Jakovcevski and Zecevic, 2005; Zhou et al., 2021).

Upon reaching their final destination, a homeostatic control mechanism is promptly initiated to maintain the overall population of OPC. OPC actively proliferate while inhibiting the differentiation process, facilitated by the collaboration of several signaling pathways, including BMP4, IGF1, JAK/STAT, Notch, PDGF, and Wnt/β-catenin signaling (Huang et al., 2020; Hughes et al., 2013). Subsequently, as the maturation process begins, guided by the transcription factor NK2 Homeobox 2 (NKX2-2), which

acts as a temporal timing switch (Elbaz and Popko, 2019; Zhu et al., 2014a) in conjunction with other mediators such as *Pdgfra, Olig2, Nk6, Nfat* (Elbaz and Popko, 2019; Sun et al., 2003; Weider et al., 2018; Zhou et al., 2001; Zhu et al., 2014a). Apart from NKX2-2, other transcription factors also play crucial roles in this process, acting as negative regulators of terminal OL differentiation, including *ID2, ID4,* and *HES5*, as well as positive regulators such as *OLIG1, MRF, MASH-1, SIP1,* and *SOX10* (Churchill et al., 2017; Elbaz and Popko, 2019; Kondo and Raff, 2000; Soula et al., 2001; Weng et al., 2012) (Fig. 19). During this phase, OPC transition into pro-oligodendrocytes (pro-OLs), losing their mobility and experiencing reduced mitotic capacity. Pro-OLs begin to express O4, a surface antigen of oligodendrocyte progenitors. Although pro-OL cells continue to divide, this process is hampered by increased expression of p57, an inhibitor of the cell cycle, resulting in slower proliferation.

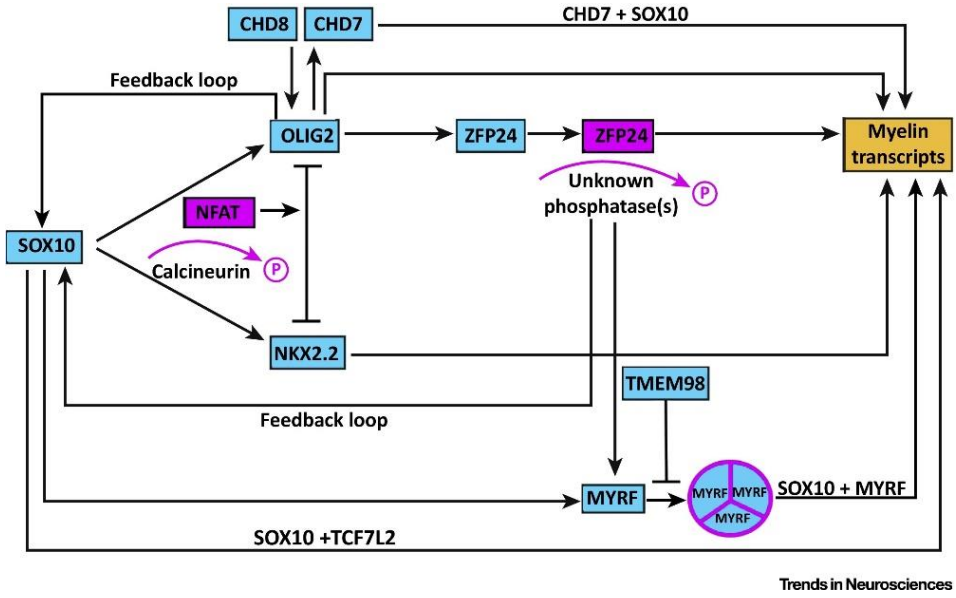

Figure 19: OPC maturation mediated by SOX10 and other interaction proteins (Elbaz and Popko, 2019)

Pro-OLs then are enrolled into 2 stages which are immature and mature OLs. *A2B5*, *PDGFRA* and *NRG2* are inhibited while O4 is still expressed. Immature OLs express galactocerebroside (GalC) and 2',3'-cyclic nucleotide 3'-phosphohydrolase (CNPase) while mature OLs express myelin proteins such as myelin basic protein (MBP), myelin associated glycoprotein (MAG) and myelin oligodendrocyte glycoprotein (MOG). One

of the most important and well-established function of OPC is to form myelin around axon and this process is illustrated briefly in figure 20.

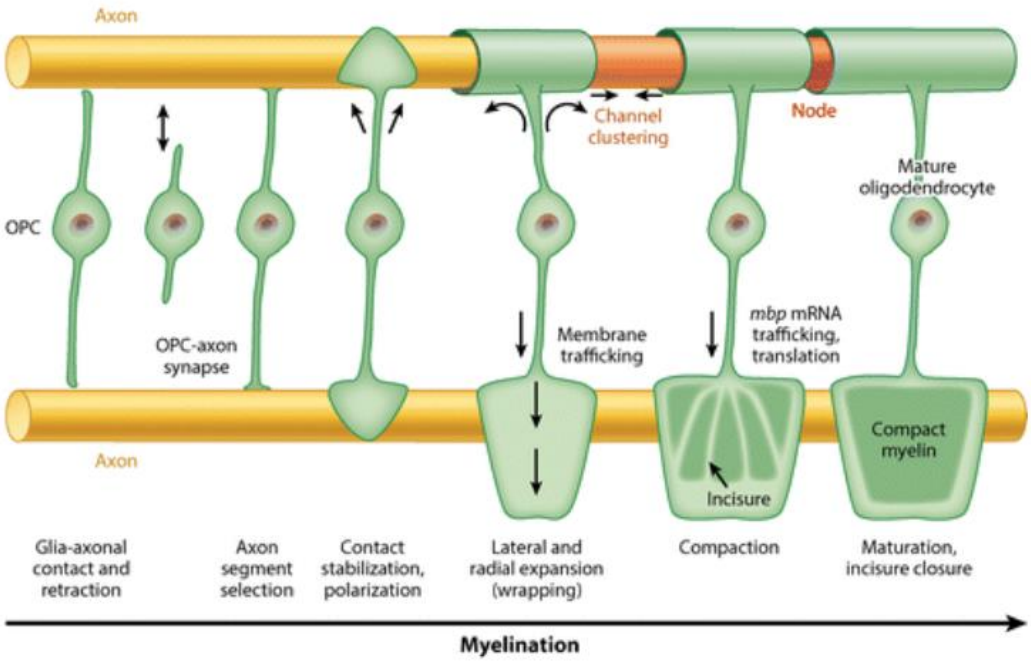

Figure 20: Schematic of myelination process
(Nave and Werner, 2014)

When the pro-OL first makes contact with the axon, its plasma membrane undergoes rapid modification to extend and encircle paranodal loops around the axon. This initial contact triggers a series of molecular rearrangements such as inhibiting Fyn-RhoA-ROCK signaling pathway, enriching the phosphoinositides on the OPC membrane (Baer et al., 2009; Snaidero et al., 2014). Moreover, this process is controlled by Ca^{2+} activity (Kuhn et al., 2019). Myelination increases the diameter of the axon not only by adding myelin sheaths but also by accumulating neurofilaments at the same location (Kuhn et al., 2019). Additionally, Raf-MAPK-ERK1/2 pathway is known for its role in differentiation and myelination as the ablation of both ERK1/2 would lead to hypomyelination (Elbaz and Popko, 2019).

Certainly, existing research indicates that epigenetic processes, including histone modification, DNA methylation, and even microRNAs (miRNAs), have a pivotal role in regulating the progression of the oligodendrocyte lineage. In addition to several TFs

mentioned above that participate in regulating oligodendrogenesis, their expression could be regulated by DNA methylation, histone modification and even miRNAs temporally (Tiane et al., 2019) (Fig. 21). Moreover, signaling pathways and metabolic control also add a hand in oligodendrogenesis. For example, *SREBF1/2*, the two genes relate to fatty acid and cholesterol metabolism, are surprisingly reported to have cell autonomous program in OLs where they participate in synthesizing myelin (Elbaz and Popko, 2019).

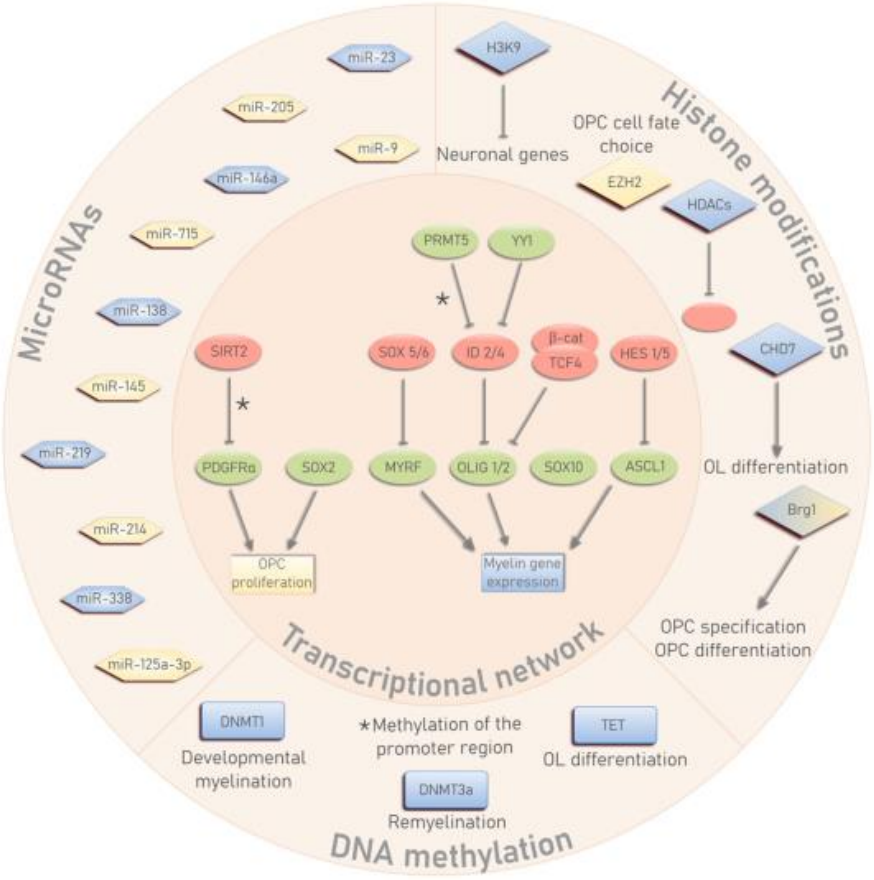

Figure 21: Summary of epigenetic control the oligodendrogenesis (Tiane et al., 2019).

3. Cell-of-origin: when original roots influence future behaviors

It is important to emphasize that the cell-of-origin, which correspond to the normal cells that develop the initial cancer mutation, is not always the same as cancer stem cells (CSC), a cellular sub-population that maintains the stemness of the tumor (Visvader, 2011). A well-accepted model of cell-of-origin is depicted, where the typical

cellular structure involves stem cells that gradually generate general (multipotent) and increasingly specialized progenitor cells, ultimately leading to the formation of all the mature and distinct cell types found in a specific tissue (Fig. 22) (Sutherland and Visvader, 2015). However, it is important to note that pHGG do not develop from pLGG as mentioned in previous part. Therefore, the paradigm indicating that additional genetic and epigenetic alterations accumulate as part of neoplastic progression is not completely suitable in the case of DMG/DIPG.

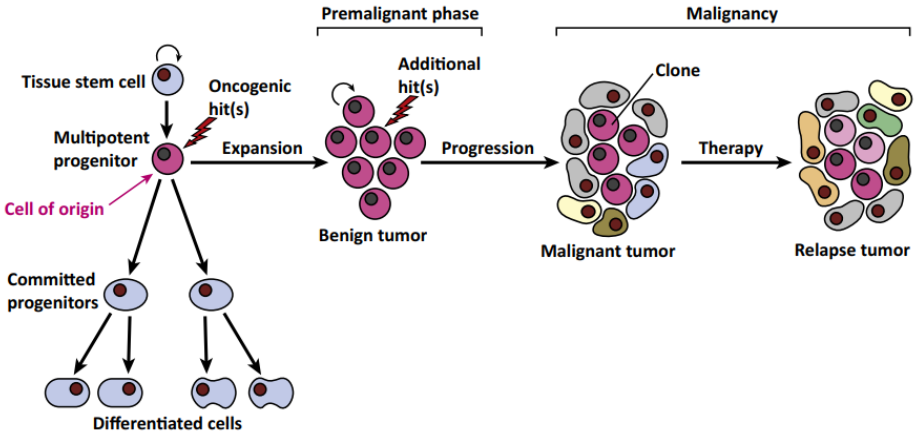

Figure 22: Cell of origin paradigm

The cell of origin paradigm suggests that progenitor cells are the initial ones to undergo genetic alterations and accumulate additional genetic/epigenetic modifications during tumorigenesis (Sutherland and Visvader, 2015).

Furthermore, it has been demonstrated that the nature of this cell significantly influences tumor oncogenesis. For instance, progenitor cells, such as neural progenitors and glial progenitors, exhibit distinct commitments to develop into different final cell types. Consequently, their machinery for differentiation may be programmed to respond differently to the same initiating factors. A study conducted by Haag and colleagues determined that injection of either WT, H3K27M-induced NSC (iNSCs) and induced OPC, either with or without shRNA-mediated *TP53* knockdown, into NSG mice, led to different outcomes. Specifically, only iNSCs carrying K27M/shTP53 were able to develop into tumor lesions after 20-30 weeks (Haag et al., 2021).

Activating the same oncogenic pathway in diverse cell types or contexts can profoundly influence malignant development. Therefore, delineating the cell of origin of DMG/DIPG may provide researchers with deeper insights into the natural biology of these tumors and enhance therapy responsiveness. Studies conducted before 2011 seldom addressed this question (Donaldson et al., 2006; Laigle-Donadey et al., 2008). However, since 2011, numerous studies have endeavored to elucidate the cell-of-origin of DMG/DIPG, yielding substantial insights into this question.

In 2011, Monje et al. reported anatomical and temporal similarities between pontine neural progenitor-like cells in the normal human brain and DIPG, suggesting the former group to be the original cells of DIPG (Monje et al., 2011). Another significant finding in 2015 from Castel et al. classified DIPG into two subgroups, H3.1 and H3.3, as shown in Table 2. RNAseq and gene set enrichment analysis (GSEA) revealed an overexpression of genes related to glioblastoma multiforme (GBM) mesenchymal and astroglial features in the H3.1 subtype, while the H3.3 subtype exhibited an upregulation of GBM proneural and oligodendrocytic genes (Fig. 23A, B). Histological and IHC analyses confirmed a more profound astroglial cell presence in H3.1 and an oligodendrocyte phenotype in H3.3 tumor samples (Fig. 23C) (Castel et al., 2015).

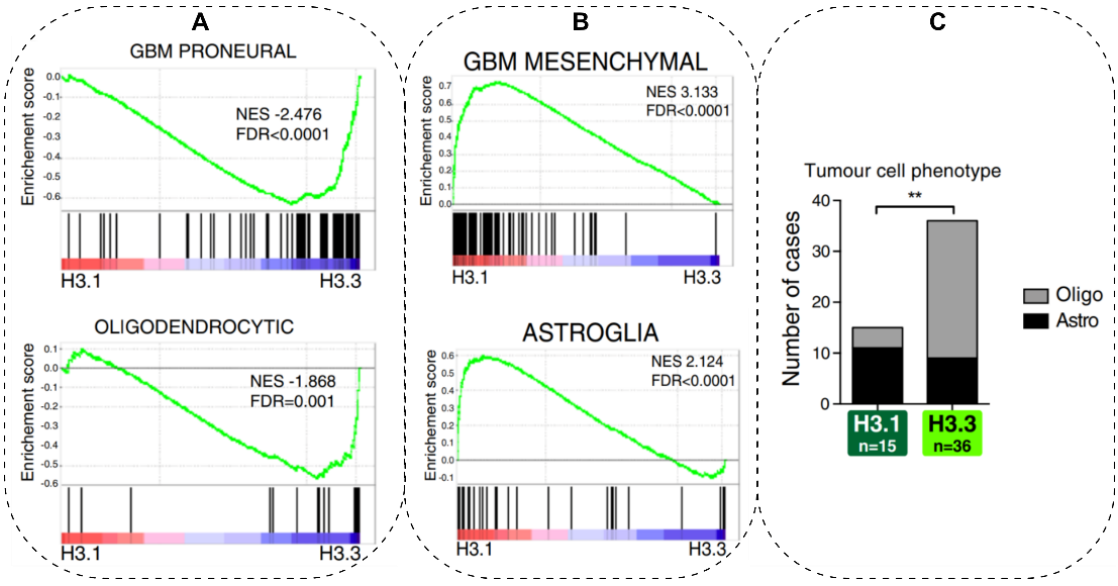

Figure 23: Two different phenotype according to H3 status of DMG/DIPG

A, B: Gene Set Enrichment Analysis presented different cell identity of H3.3K27M and H3.1K27M mutant tumors. C- The IHC histological of tumors (Castel et al., 2015).

However, a few years later, Filbin et al., in a publication in 2018, performed single-cell RNAseq (scRNAseq) profiling of six DIPG tumors, revealing that DIPG tumors are composed of a mixture of cells with OPC-like, oligodendrocytic differentiation (OC-like), and astrocytic differentiation (AC-like), with the most predominant group being OPC-like cells (Filbin et al., 2018). They hypothesized that PRC2 was inhibited during the OPC differentiation into OC, thus resulting in the inactivation of PRC2 and blocking at OPC-like state and maintaining stemness features (Fig. 24).

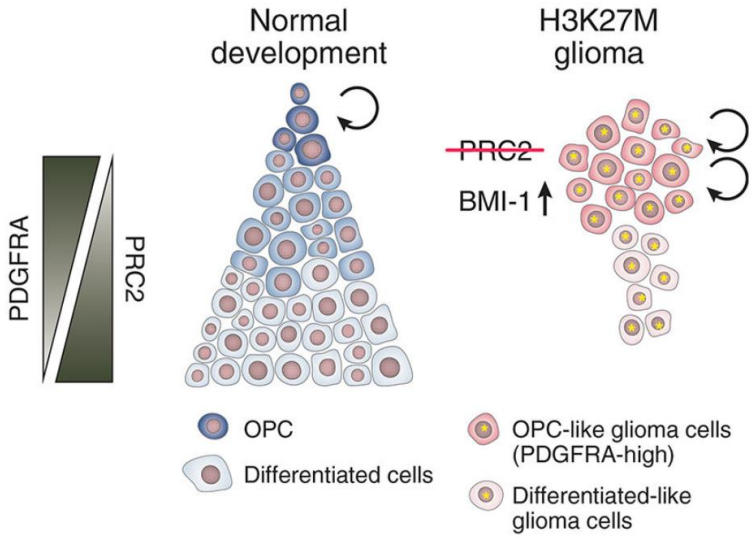

Figure 24: Two scenarios of cell identity

Cellular architecture scenario in (left) normal development; (right) in H3-K27M (Filbin et al., 2018).

Two independent studies from Jessa et al. and Liu et al. in 2022 (Fig. 25) both focused on answering the question of DMG cell-of-origin. The former study demonstrated that the H3K27M mutation arose in discrete lineages with unique identities and maintained the chromatin arrangement of developmental genes associated with OPC. The H3.3-K27M subgroup exhibited a broad spectrum ranging from OPC-like to OC-like and astrocyte-like, as previously reported. They also proposed that H3.1-K27M DMG might develop from more primitive progenitor cells and likely occur in cells derived from the earliest waves of OPC development with NKX6-2+/SHH-. Liu et al. study shared a

similar conclusion among three OPC-like subpopulations of DMG, suggesting that DIPG is more immature compared to DMG from the thalamus.

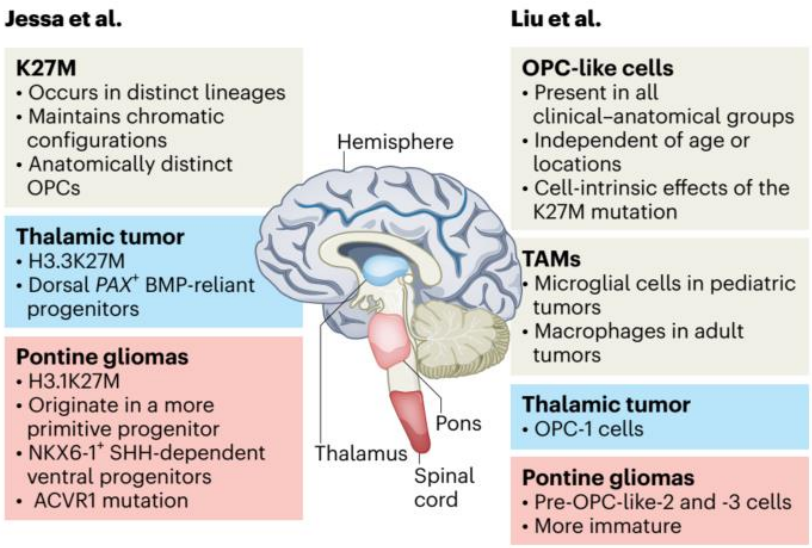

Figure 25: Characteristics of the original cell type in K27M-mutant DMG (Li, 2022).

Part III: The mechanism beyond DMG/DIPG invasiveness and metastasis

Invasiveness and metastasis were first introduced as one of the six main hallmarks of cancer in the seminal review by Hanahan and Weinberg over twenty years ago (Hanahan and Weinberg, 2000). Subsequently, remarkable scientific progress has reinforced this statement, underscoring the importance of understanding the underlying mechanisms. This significance applies not only to cancer in a broader sense but also in gliomas, in particular. Tumor dissemination and metastasis are the main feature closely associated with patient mortality (Chaffer and Weinberg, 2011). Since progenitor cells are believed to be the cells-of-origin of DMG/DIPG and their active migration and mobility might significantly contribute to the diffuse and invasive characteristics of DMG/DIPG, this chapter will initially explore the general migration mechanisms of GPC before delving into the regulation factors specific to the invasion-metastasis cascade in gliomas and DMG/DIPG.

1. Migration mechanism of glial progenitor cells

The fully developed and functional brain results from a meticulously orchestrated expansion of diverse cell populations. During the early stages of brain development, GPCs play a significant role and adhere strictly to a dynamic and precise migration process, which is crucial for the formation and function of the CNS. However, our understanding of GPC migration remains surprisingly limited compared to neuronal migration. Most studies on this topic have been conducted on the adult brain, while the focus of my study is on the developing, postnatal, and pediatric brain. Moreover, it is interesting to note that GPC migration is regionally and temporally specific (Kakita and Goldman, 1999; Levison et al., 1993) and closely collaborates with angiogenesis, dendrite elaboration, and synapse creation (Semple et al., 2013).

In 2022, Tabata and colleagues identified two distinct migration patterns employed by astrocyte progenitor cells to swiftly traverse the developing cortex, referred to as erratic migration and blood-vessel guided migration. The former enables APC to move freely and rapidly within the Intermediate Zone and Cortical Plate. Meanwhile, the latter necessitates the presence of blood vessels, serving as a scaffold to guide APC to their final destination (Tabata et al., 2022). This distinctive migratory characteristic is inherited by the daughter cells of these GFP-positive cells. Given that this unconventional migration markedly differs from the well-established radial migration of neurons, wherein neurons navigate among glial fibers to reach their end-points, it has been termed “erratic migration” (Fig. 26). Although the movements of the cells appear random, characterized by frequent changes in direction, there is an observable tendency for them to orient themselves towards the brain surface.

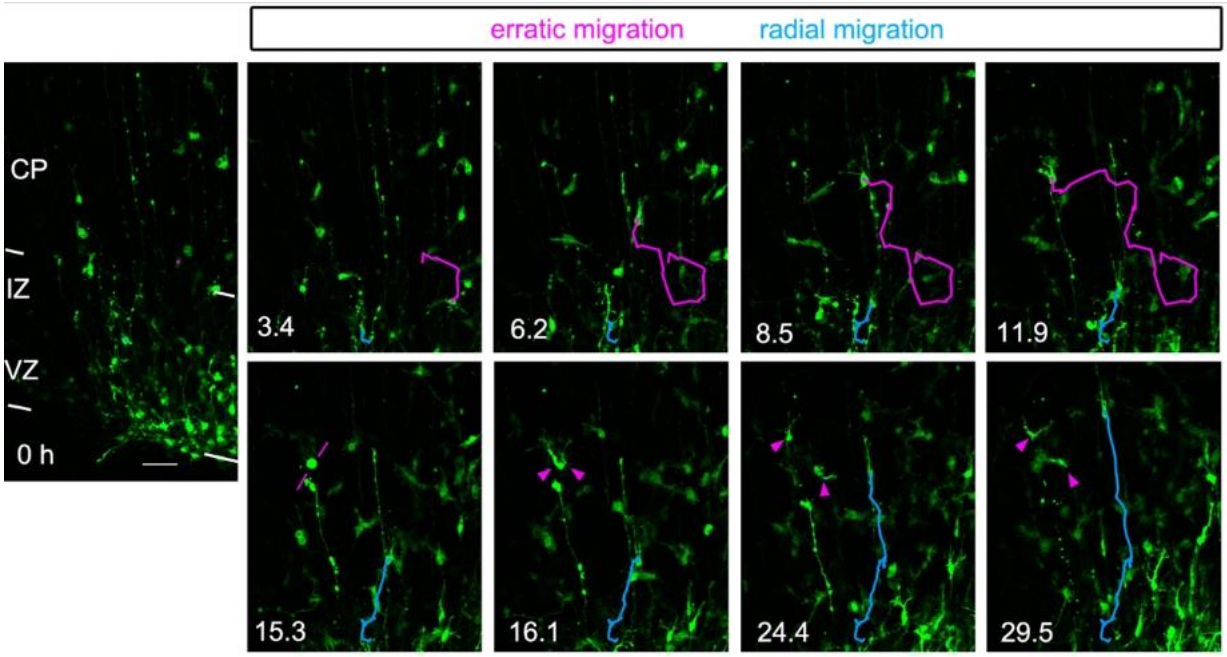

Figure 26: Different migrating modes

Recorded instances of erratic migration (magenta) and radial migration (blue). VZ derived cells were marked through in utero electroporation. The slice at the initiation of the observation is displayed on the left. The cell undergoing erratic migration underwent division at 15.3 hours (h) and persisted in erratic migration (indicated by arrowheads) (Tabata et al., 2022).

These two experimental approaches demonstrated that cells exhibiting erratic migration tendencies differentiate into astrocytes. Moreover, astrocyte-like cells derived from these erratically migrating cells exhibit a wider range of movement directions compared to other cells.

Single-cell RNA-seq analysis of E18 mouse whole-brain revealed that Cxcr4-integrin β1 facilitates the outreach of APC toward blood vessels. Knockdown vectors targeting Integrin β1 *(Itgb1)* significantly extended the distance from blood vessels to APC compared to controls (Miyajima et al., 2023).

One remaining question requiring clarification is how APC switch between these two migratory modes. This transition may be influenced by the differential composition of the ECM in distinct locations. The ECM of the cortical parenchyma comprises proteoglycans, fibronectin, laminin, and various types of collagens (Lau et al., 2013);

whereas the ECM of blood vessels primarily includes collagen, elastin, fibronectin (Fig. 27) and ECM in hindbrain has proteoglycan chondroitin sulphate (Hutchings et al., 2024). The varied proportions of these elements influence the stiffness and characteristics of each ECM. Therefore, the hypothesis posits that once APC cells detect proximity to the ECM of a blood vessel, they trigger blood-vessel guided migration. Additionally, external factors may play a role in this transition, including the secretion of elements in the meninges layer, variations in neuronal layer structures, and the distribution of oxygen and nutrients (Miyajima et al., 2023).

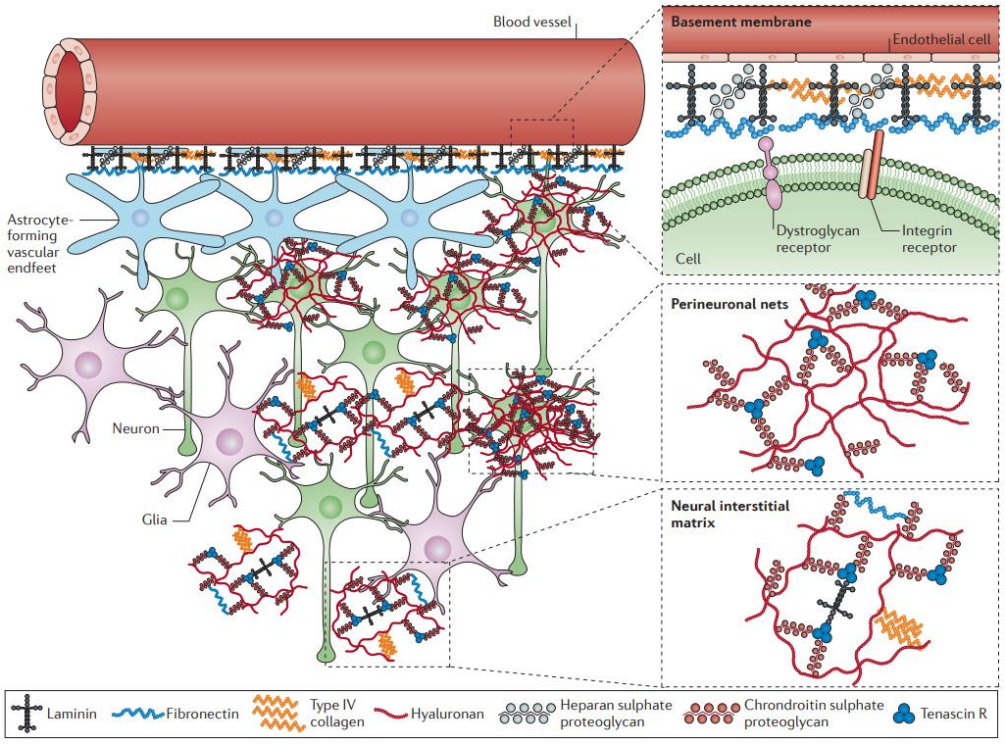

Figure 27: : The basic compartments of the ECM in the CNS
(Lau et al., 2013).

During brain development, OPC are known to be way more migrative than neurons or APC. By using Cre-*lox* system in transgenic mice model, Kessaris et al. uncovered a part of this complex process (Kessaris et al., 2006). The early wave of NKX2-1^{+} OPC begins from the VZ of ventral medial ganglionic eminence (MGE) and anterior entopeduncular (AEP) region approximately at E12.5. They quickly spread to other parts of the

telencephalon and reach cerebral cortex around E16. However, soon after, this population quickly declines and by postnatal day 10 there is only a few lefts in the cortex. Around E15.5, the second wave of OPC which are lateral ganglionic eminence (LGE)-derived or Gsh2^{+} OPC took over the first population and the third wave with Emx1^{+} OPC from dorsal pallium (DP) area usually join this process on the day of birth (Fig. 28) (Chapman et al., 2013; Kessaris et al., 2006; Ono et al., 2001; Tekki-Kessaris et al., 2001). This makes OPC a unique group of proliferative cells in the brain generated from multiple niches (Buchanan et al., 2023).

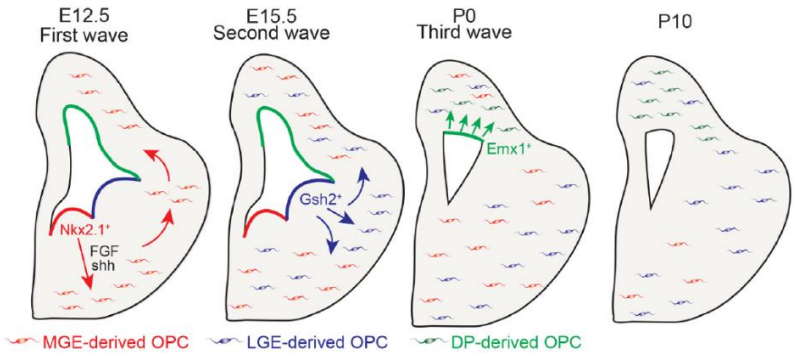

Figure 28: Three waves of OPC during mouse brain development (Tanabe and Yamashita, 2020).

Interestingly, APC and OPC not only belong to the same glial progenitor group but also exhibit a similar migration pattern that involves the participation of blood vessels. Tsai et al. observed the migration of PDGFRα^{+} OPC in the developing mouse brain, noting that 58% elongate their cell bodies along the blood vessel or the abluminal endothelial surface. Among the remaining portion, approximately 67% exhibit at least one part of their process in contact with the vessels (Fig. 29A-C). In human cortex, the first OPC appear in the outer cortex at gw14, aligning with blood vessels, and maintain similar properties until gw18 and gw24 (Fig. 29D-F). Furthermore, the morphology of migrating OPC in mouse and human developing brain is comparable (Tsai et al., 2016).

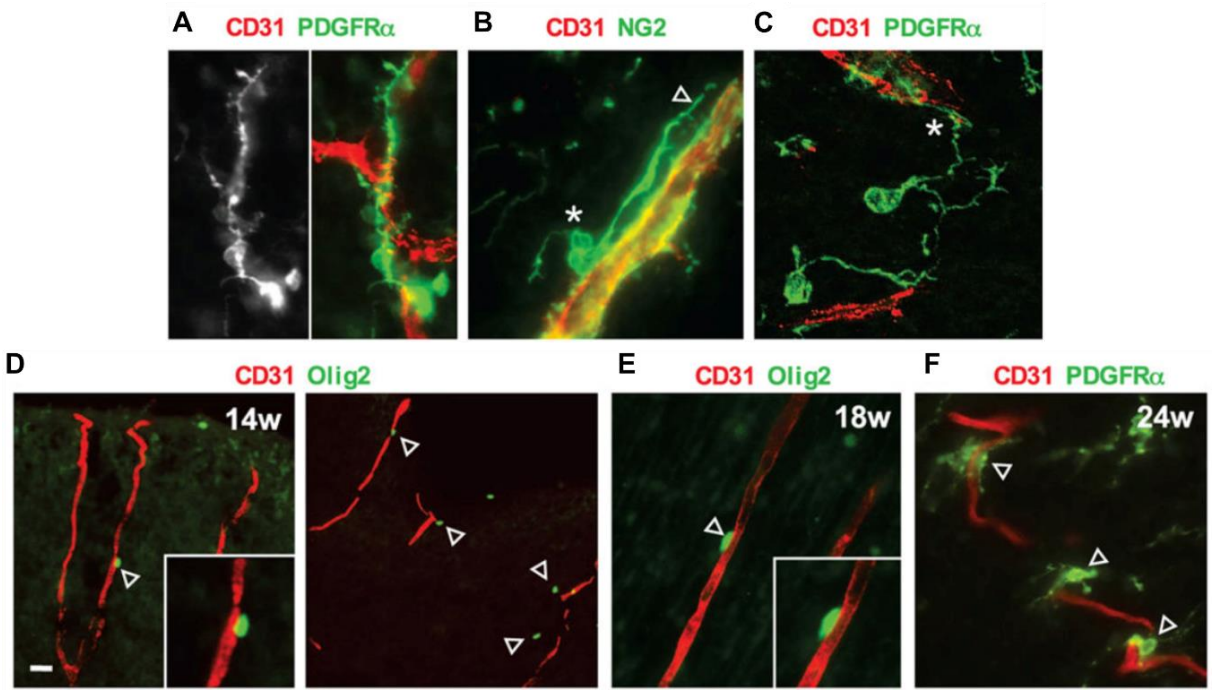

Figure 29: Different modes of OPC migrations using bloos vessels

A- extending alongside vessels.

B- direct contact with the abluminal endothelial surface and featuring a long process among the vessels.

C- exhibit partial interaction with the vessels. (bottom).

D- F: The first OPC appear in the human developing outer cortex in contact with vascular structures at gw14-18-24 (Tsai et al., 2016).

Here, blood vessels serve as a scaffold for OPC, enabling two types of movement: crawling and jumping, with the latter resulting in faster speed. When OPC crawl along a vessel, their cell body maintains contact with one vessel surface, while OPC can jump from one vessel to another by extending one leading process and then translocating the cell body to the target vascular area. Notably, this perivascular migratory behavior of OPC is not restricted to the developing brain but is also present in the spinal cord and postnatal brain (Tsai et al., 2016). Using transgenic mice with disrupted vascular development (lack of orphan G protein–coupled receptor 124 GPR124, essential for vessel germination), Tsai et al. concluded that the endothelial vascular scaffold, but not pericytes, is crucial for OPC perivascular migration. Additionally, OPC express high levels of CXCR4, a direct Wnt target, during embryonic development until the maturation of oligodendrocytes (OL), and the decrease of CXCR4 is associated with a

less migratory phenotype (Chavali et al., 2020; Manukjan et al., 2020; Tsai et al., 2016).

Furthermore, it is well-known that OPC maintain proliferating while migrating and they only exit the cell cycle upon reaching their final destination. Following this, oligodendrocytes undergo terminal differentiation, characterized by a series of transformations including substantial augmentation in lipid biosynthesis and the synthesis of significant quantities of myelin proteins (Wegner, 2008). Surprisingly, the termination of OPC perivascular migration is controlled by the endfoot formation of astrocyte, as indicated by a study conducted on mouse model in 2022 (Su et al., 2023). Figure 30 illustrates the scenario when a migrating OPC reaches the endfeet of the astrocyte wrapping around the blood vessel. Initially, the endfeet of the astrocyte physically block the migration of the OPC. Subsequently, the production of semaphorins Sema3a and 6a interacts with plexin receptors on the OPC surface, promoting the detachment of the OPC from the current perivascular location. Finally, upon detachment, the OPC commits to differentiation and transforms into a myelinating oligodendrocyte (Su et al., 2023).

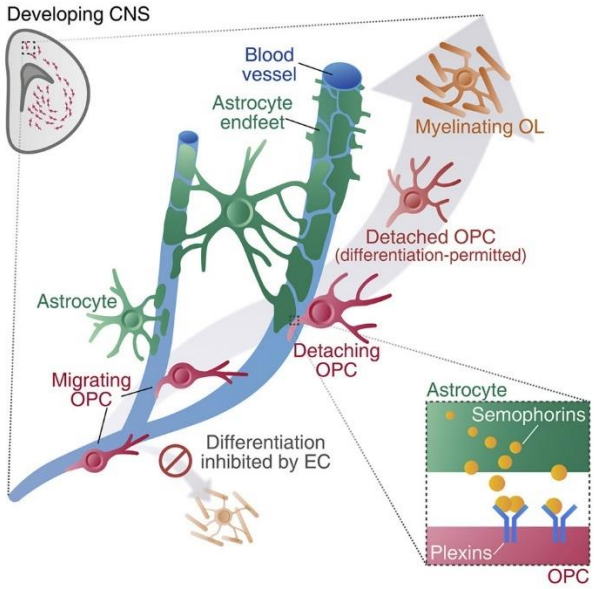

Figure 30: Proposed spatial associations among OPC, astrocytes, and vessels during developmental stages

Red denotes OPC, green represents astrocytes, and blue indicates vessels (Su et al.,

2023).

To date, studies on mice or chicken models have indicated that migration of OPC is controlled by secreted molecules including some growth factors (PDGF, FGF, HGF) (Yan and Rivkees, 2002), chemotropic molecules like netrins and semaphorins (Jarjour et al., 2003; Tsai et al., 2003), and the chemokine CXCL1 (Bradl and Lassmann, 2010; Redwine et al., 1997).

During mouse embryonic stages, it was demonstrated that the existence of Bmp4, Bmp7, and transforming growth factor-beta 1 (Tgfβ1) in meninges and pericytes acts as a repulsive force, directing ventral OPC into the cortex. Conversely, the conditional inhibition of their expression leads to a reduction in OPC migration into the cortex. Furthermore, the absence of Smad4 results in the formation of heterotopia by OPC in ventral areas. These findings suggest a pivotal role for Tgfβ and BMP4/7 in facilitating the migration of ventral OPC (Choe et al., 2014). OPC migration is further facilitated by PDGF-AA through its interaction with the PDGFRα receptor, and there may be a synergistic effect between PDGF and the chemokine CXCL1 (Ellison et al., 1996; Richardson et al., 1988; Robinson et al., 1998). However, in contrast, a study conducted by Tsai et al. in 2002 concluded that CXCL1 inhibits the chemotactic effect of PDGF on OPC in a concentration-dependent manner. Additionally, the combination of this chemokine with its receptor CXCR2 not only hinders migration but also regulates the localization of OPC (Tsai et al., 2002). Another chemokine, CXCL12, has been reported to induce the migration of OPC via CXCR4-activated MEK/ERK and PI3K/AKT pathways. Utilizing the Boyden chamber assay, it was demonstrated that CXCL12 functions as a chemoattractant to OPC, leading to a significant upregulation of p-ERK and p-AKT, two key proteins in the MEK/ERK and PI3K/AKT pathways (Tian et al., 2018).

In addition to the secretion of molecules, various contact-mediated mechanisms rely on the ECM (Frost et al., 2010; Hood and Cheresh, 2002; Kiernan et al., 1996), neuronal axons, vascular and cell surface molecules to regulate OPC migration (Niehaus et al., 1999; Schnädelbach et al., 2000). Integrin αvβ1, fibronectin, and merosin on the ECM

have been identified as promoters of OPC migration (Frost et al., 2010; Milner et al., 1996), while the glycoprotein tenascin-C has been reported to be antiadhesive for OPC, inhibiting their migration (Frost et al., 2010; Kiernan et al., 1996). A fascinating characteristic of OPC is their ability to balance attracting and repulsing regulations, ensuring an even distribution throughout the CNS. This homeostasis control is not limited to brain development but persists throughout life, allowing OPC to adapt rapidly in response to myelinated cell loss due to injury or disease (Hughes et al., 2013). Despite numerous proposed mechanisms explaining how OPC in the adult brain can rapidly target locations of cell loss for myelination, the process by which OPC achieve even migration throughout the CNS remains undisclosed.

Given the substantial evidence supporting the OPC-like phenotype in the majority of DMG cells, it is hypothesized that these DMG cells may also possess an advantage in terms of migration within the CNS, akin to OPC. Consequently, unraveling the unanswered question concerning the mechanism of OPC migration could provide insights into limiting the invasive and infiltrative characteristics of DMG.

2. Invasion and metastasis in high grade gliomas

This section delves into three fundamental terminologies:

- Infiltration: In contrast to certain tumors that manifest distinct and well-defined borders, DMG do not exhibit solid tumor formations and lack clearly delineated borders. Instead, they display a diffuse, invasive pattern.
- Invasion: Refers to the capacity of cancer cells to breach tissue barriers, indicating their ability to penetrate surrounding tissues.
- Metastasis: Signifies the process through which cancer cells disperse from the primary site of the original tumor to distant locations within the brain or the body, giving rise to secondary tumors.

HGG are known for their rapid and aggressive growth compared with LGG. They infiltrate surrounding brain tissue quickly and making complete resection challenging.

Similar to other type of cancer, metastasis in HGG constitutes the leading cause of mortality of cancer patients (Chaffer and Weinberg, 2011; Lah et al., 2020).

In general, there are five key steps of metastasis that are well-studied for epithelial cancers which are invasion, intravasation, circulation, extravasation and colonization (Fig. 31). Initially, cancer cells become aggressive, initiating local invasion. Then, these invasive cancer cells enter blood vessels, a process referred to as intravasation, or lymphatic vessels, enabling them to depart from the primary site. Following this, they must survive the circulation step, navigating through the bloodstream and lymphatic system to reach distant organs and tissues. Upon reaching the new location, extravasation occurs, facilitating their exit from circulation and invasion into the new tissue. Ultimately, the uncontrolled growth of these cancer cells rapidly gives rise to secondary tumors, contributing to the spread of the tumor throughout the body (Chaffer and Weinberg, 2011; Fares et al., 2020; Hanahan and Weinberg, 2011).

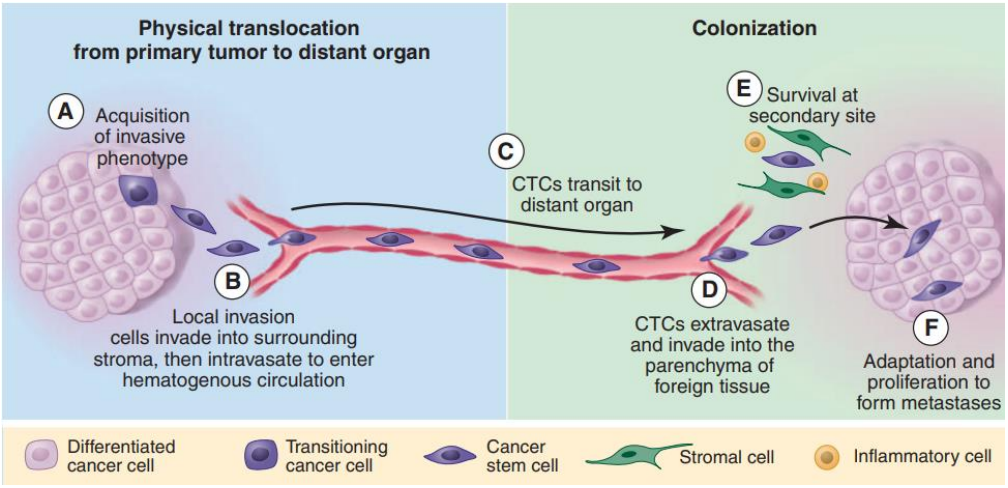

Figure 31: Five basic stages of the cancer metastatic process in general

The metastatic cascade comprises five crucial stages, namely invasion (A), intravasation (B), circulation (C), extravasation (D-E), and colonization (F) (Chaffer and Weinberg, 2011).

However, it is crucial to highlight that HGG rarely form extracranial metastases but primarily exhibit extensive invasion within the CNS (Lun et al., 2011). Reported cases of distant metastasis most commonly manifest as foci in the spinal cord, with sporadic instances of bone metastasis documented (Fabi et al.; Sun et al., 2017; Yung et al., 1983).

Hence, the stages of intravasation and extravasation in glioma metastasis are substituted by the invasion along the white matter tracts or blood vessels of glioma cells, deviating from the penetration mechanism observed in other types of cancers (Cha and Kim, 2017).

Several factors contribute to the initiation of metastasis, recognized as the fourth and final stage in cancer progression. Notably, cancer cells in the early stages of the disease typically lack the propensity to metastasize. The progression to the metastatic stage necessitates the fulfillment of a set of hallmarks and criteria. Over time, accumulating genetic, epigenetic, and molecular alterations equip cancer cells with properties conducive to metastasis, including cellular plasticity and mobility. External physical factors, such as treatment or surgery, can also serve as triggers (Lobon-Iglesias et al., 2018b). Furthermore, the metastatic process requires modifications and triggers in the surrounding elements to create a supportive environment for cancer cells to invade. Examples include epithelial-to-mesenchymal transition (EMT), remodeling of the ECM/the tumor microenvironment (TME), and the identification of new favorable sites (Massagué and Obenauf, 2016; Welch and Hurst, 2019; Gui and Bivona, 2022; Fares et al., 2020; Hapach et al., 2019). EMT is a process wherein less-mobile epithelial cells undergo a transition to acquire a more mobile phenotype, namely the mesenchymal phenotype. This intricate process involves a complex interplay of various factors, including focal adhesion and cytoskeleton dynamics, signaling pathways, as well as cell-cell and cell-ECM interactions (IWADATE, 2016; Pu et al., 2020; Xu et al., 2023).

Prior observations have indicated that GBM cells employ diverse pathways for invasion. Specifically, these routes include the white matter tracts, the brain parenchyma, the perivascular space, and the leptomeningeal space, each characterized by distinct structural and compositional features (Cha and Kim, 2017). GB uses white matter tracts or perivascular space as migratory routes as neurons and neuroblasts (Cuddapah et al., 2014; de Gooijer et al., 2018) and they infiltrate the tissue either as individual cells or collective invasion (Seano and Jain, 2020). Moreover, GBM are able to actively modify

the ECM composition by upregulating tenascin-C, hyaluronan, vitronectin, collagens, and downregulating thrombospondin and versican (Bellail et al., 2004; de Gooijer et al., 2018; Xia et al., 2015) (Fig. 32).

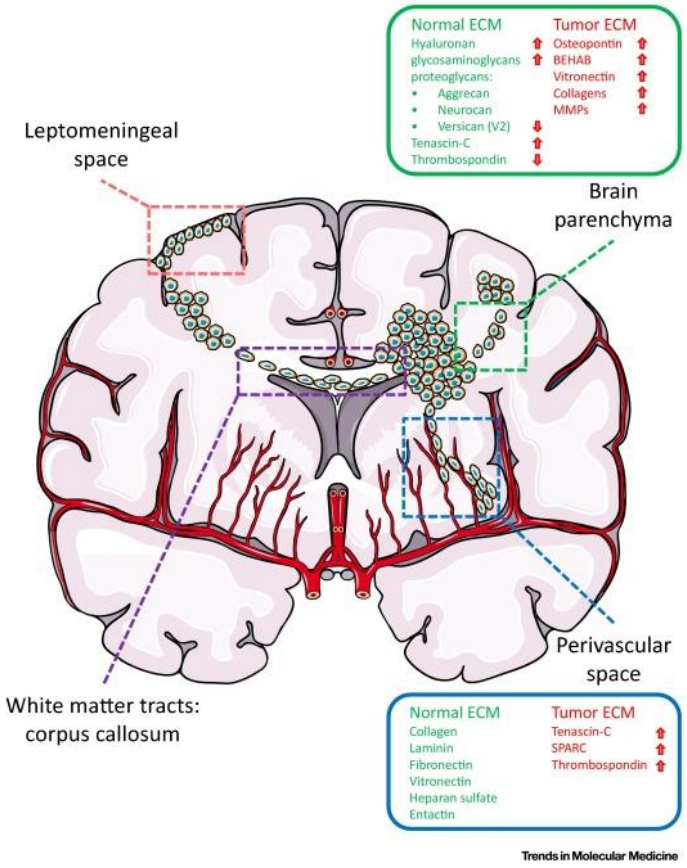

Figure 32: Four invasion routes of GBM and their distinct components compared with normal ECM

(de Gooijer et al., 2018).

However, the composition of TME could vary from one HGG to the others. For example, the blood tumor barrier (BTB) is mostly preserved in DMG and Sonic Hedgehog SHH-driven medulloblastoma (Fig. 33A) while it is disrupted with non-uniform pericyte vessel coverage is shown for HGG and WNT-driven medulloblastoma(Fig. 33B) (Pasqualini et al., 2020).

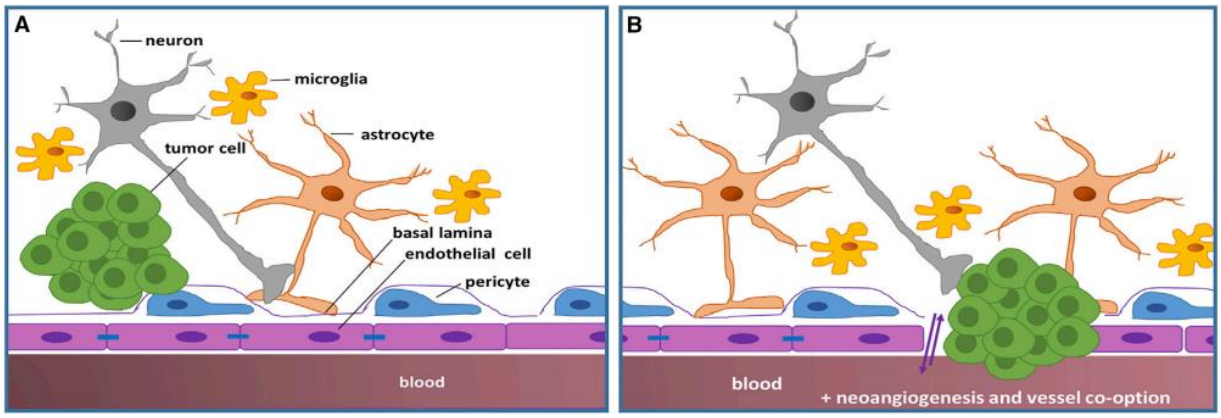

Figure 33: TME distinct components

The attributes of distinct components within the TME exhibit notable variations based on tumor histology and its molecular characteristics (Pasqualini et al., 2020).

More intriguingly, GBM has been documented to exploit neuronal mechanisms to enhance its invasive potential (Venkataramani et al., 2022). In addition to the phenotype changes observed with or without contact with astrocytes, as mentioned in Chapter I (Fig. 14), GBM cells also exhibit formation of tumor microtubes (TM), facilitating the emulation of three movement patterns observed in neuronal cells: protrusion, retraction, and TM generation via branching. This gives rise to three primary invasion modes in GBMs: translocation (where the soma moves by shortening the TM length), locomotion (where the soma follows the protruding TM), and branching migration (involving extensive branching combined with TM protrusion and retraction) (Venkataramani et al., 2022) (Fig. 33). Notably, these mechanisms closely resemble those observed in the migration of other neural progenitor cells, as discussed in the previous section (Nadarajah and Parnavelas, 2002; Nadarajah et al., 2001; Tabata et al., 2022; Tsai et al., 2016). Furthermore, GBM cells not associated with astrocytes may receive input from neurons via the α-amino-3-hydroxy-5-methyl-4-isoxazolepropionic acid receptor (AMPAR), thereby stimulating TM formation and cell invasion.

Additionally, these glioblastoma cells also establish connections with normal astrocytes through gap junctions (Varn et al., 2022) (Fig. 34A). More interestingly, studies on glioblastoma models have demonstrated that neural cells in the microenvironment establish specific intercellular connections with gliomas in different ways depending on

the tumor cell state (Fig. 34B) (Taylor and Monje, 2022). In contrast, stationary glioblastoma cells with astrocyte-like and mesenchymal-like phenotypes create an inter-glioma-connecting network through gap junctions, exhibiting NPC-like, OPC-like, and neuron-like phenotypes or form synapses with neurons but do not establish connections with other glioma cells. (Fig. 34A). Moreover, they also tend to become the invasive drivers and display an enrichment of neuronal and OPC/NPC gene expression signatures (Varn et al., 2022).

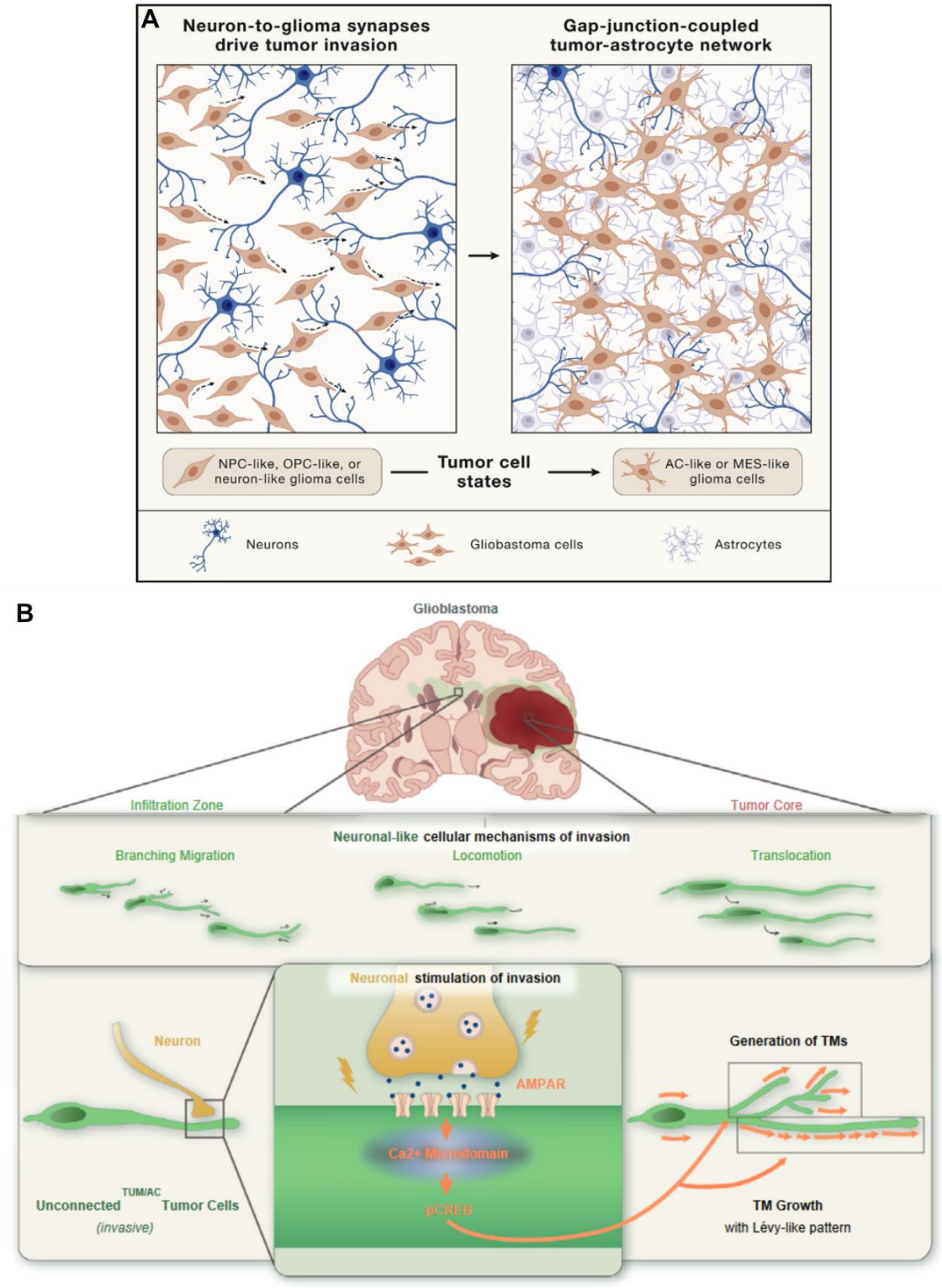

Figure 34: GBM interconnection and interaction with neural cells type

A- Two different interconnection types of invasive and stationary glioblastoma networks (Taylor and Monje, 2022).

B- Neuronal-like characteristics of GBM and its interaction with astrocytes and neurons to promote invasion (Venkataramani et al., 2022).

Some evidence substantiates the extensive involvement of other neural progenitor cells within the glioma microenvironment in glioma invasion. Notably, neuroligin-3 (NLGN3) produced by neurons serves to stimulate glioma expansion, and gliomagens recruited by microglia play a crucial role in promoting glioma proliferation. Additionally, neural progenitors in the lateral ventricle SVZ recruit a multimeric protein complex comprising pleiotrophin (PTN), secreted protein acidic and rich in cysteine (SPARC), SPARC-like protein 1 (SPARCL1), and heat shock protein 90B (HSP90B). This complex generates a gradient of chemoattractants, facilitating the migration of glioma cells through the Rho/ROCK signaling pathway (Qin et al., 2017) (Fig. 35).

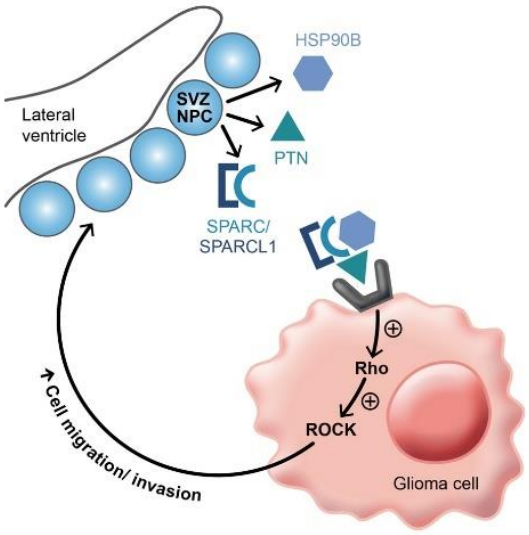

Figure 35: Glioma invasion into SVZ following chemoattractant

The schematic depicts glioma invasion into the SVZ relying on a chemoattractant complex (PTN, HSP90B, and SPARC/SPARCL1) secreted by NPCs. This complex activates the RhoA/ROCK signaling pathway, facilitating invasion (Qin et al., 2017).

Finally, the invasiveness of gliomas may align with the characteristics of their cell of origin from which they originate. This inherent nature encompasses interactions with various neural and neural progenitor cell types, engagement with the microenvironment, and the utilization of a well-established migratory machinery.

3. Invasion and metastasis in DMG/DIPG

DMG/DIPG represents a rare HGG occurring in children, indicating that the brain and

CNS are still in a developmental stage unlike that of adults. In fact, notable distinctions exist in the composition and functionality of CNS cells between these two age groups, thereby endowing DMG/DIPG with a distinct narrative compared to high-grade gliomas in adults (Schroeder et al., 2014). Therefore, even though DMG/DIPG shares certain commonalities with other HGG in terms of invasion and metastasis, it presents a distinct phenotype, posing considerable challenges for scientists seeking effective strategies to impede its invasiveness.

Many studies have extensively investigated established factors such as H3K27M, TP53, ACVR1, and PDGFRA, with numerous trials conducted (Kluiver et al., 2020). Despite these efforts, none of these factors has yet resulted in a significant breakthrough. In contrast, recent discoveries have illuminated the critical role of interactions with neurons in glioma pathogenesis. This is particularly intriguing in the case of DIPG, as these cancer cells lack a clear tumor border and infiltrate into other neural cell populations. Additionally, attention is being directed toward cell-autonomous mechanisms driving invasion and metastasis, as well as other contributing factors. To gain a better understanding of DMG/DIPG invasion and metastasis, Bruschi et al. from my host laboratory recently has conducted a study involving 72 DMG patients. Their findings categorized DMG tumors into three groups based on metastatic states. The first group (34% of cases) was characterized as metastasis-free, displaying local tumor evolution strictly confined to the pons. The second group comprised metastasis-free, further subdivided into loco-regionally extending tumors with cancer cells detected in contiguous extrapontine structures. The third group contained tumor with distant evolution encompassing cases with intracranial and spinal metastases (28%). Further analysis revealed a negative correlation between parenchymal invasion rate and survival outcomes, leading to the conclusion that the invasiveness of DMG tumors is inversely related to patient survival rates (Bruschi et al., 2023) (Fig. 36).

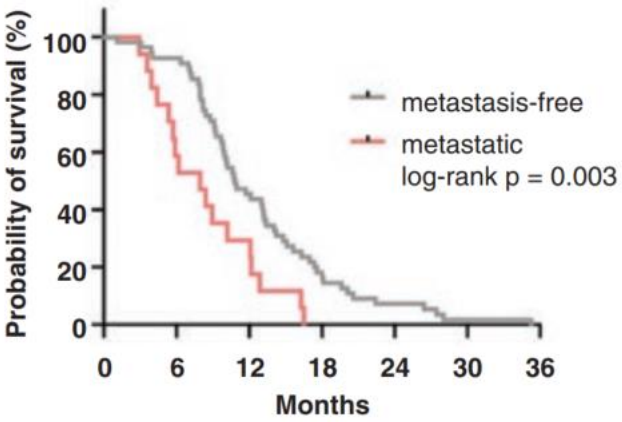

Figure 36: Survival rate between patients with and without metastasis

The Kaplan-Meier curves depict the overall survival (months) of patients with metastatic (n=17) and metastatic-free (n=17) upon assessment at the first place. local-to-locoregional progression (n = 53) compared to those with metastatic progression (n = 17) upon assessment at the first relapse.

While a mesenchymal phenotype in other HGG often correlates with increased invasiveness, this relationship appears to be inverted in DMG/DIPG (Carro et al., 2010; Meel et al., 2018; Mikheeva et al., 2010; Tso et al., 2006). Bulk RNA-sequencing conducted on both 2D and 3D culture reported a different discovery when the phenotype of 3D DMG tumoroids and their parental biopsies were not categorized according to the histone H3 mutation status but their invasive behavior. The transcriptional profiles from DIPG 3D culture and biopsy showed that highly invasive models expressed OPC identity while low invasive ones had upregulated of genes related to EMT (Fig. 37) (Bruschi et al., 2023) in models derived from DMG patients as well as parental biopsy supported this observation. Specifically, the group demonstrating moderate invasiveness exhibited characteristics of the mesenchymal phenotype, while the subset with higher invasiveness displayed features reminiscent of OPC-like properties (Bruschi et al., 2023; Castel et al., 2015).

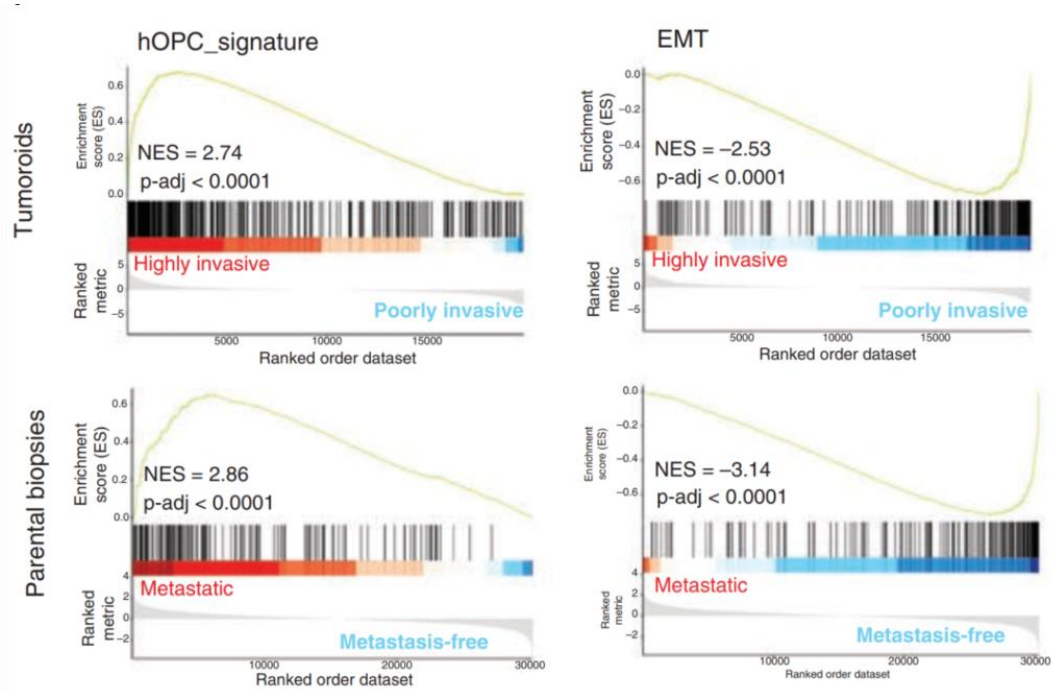

Figure 37: Phenotype of highly and low-invasive models

GSEA analysis showed an enrichment of OPC signatures in highly invasive DIPG models whilst low-invasive models showed elevated expression of genes linked to EMT transition regulators and reduced levels of the epithelial marker E-cadherin (Bruschi et al., 2023).

To delve deeper into the involving genes, the analysis included Differential Expression Genes (DEG) and GSEA, revealing downregulation of several genes associated with ECM remodeling and focal adhesion in the metastasis-free DMG. In contrast, a heightened expression of genesets linked to angiogenesis was observed in less invasive DMG. Supported by evidence from pathohistological assessments of biopsies and MRI images, these findings suggest that, unlike other HGG, less-invasive DMG tend to remodel the microenvironment, promoting neo-vessel formation and establishing a favorable microenvironment. Conversely, highly invasive DMG exhibit a predominant capacity for tissue penetration and invasion into other brain structures.

Additionally, in another study, approximately 10% of the DIPG cell population was found to establish electrophysiologically functional synapses with neurons. These neurons can activate the depolarization of glioma cells, leading to the triggering of signaling pathways that promote the proliferation and growth of cancer cells.

(Venkatesh et al., 2019).

Taken together, these studies underscore that DMG/DIPG cells exhibiting an OPC-like phenotype possess the ability to form *bona fide* synapses with neurons, maintain a single-cell state, and demonstrate high invasiveness. In contrast, DMG/DIPG cells with a mesenchymal-like phenotype can interconnect both with each other and with astrocytes through gap junctions. They recruit angiogenesis and remodel the extracellular matrix (ECM), creating a supportive and autonomous microenvironment on-site. Consequently, this group exhibits low invasive behavior.

Bruschi et al. conducted different functional analysis to elucidate the factors contributing to the differences between low and high invasive groups (Fig. 38A). A hypothesis was postulated, suggesting that the overexpressed of the BMP7 in high invasive group triggers cell-autonomous machinery via ALK receptor, subsequently hijacking the normal OPC migration during brain development and obtained ameboid-like motility (Fig. 38B). This aberrant mechanism is proposed to drive high-invasive DMG to invade distant areas (Bruschi et al., 2023). This observation is noteworthy, as another BMP ligand, BMP4, has been documented to attenuate the stemness characteristics of DIPG and function as a suppressor of DIPG tumor growth (Sun et al., 2022) whilst complex BMP4/BMP7 was mentioned as an element to promote ventral OPC invasion.

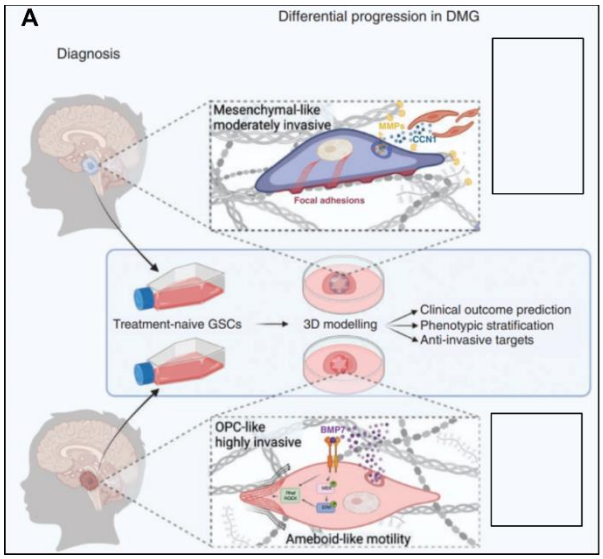

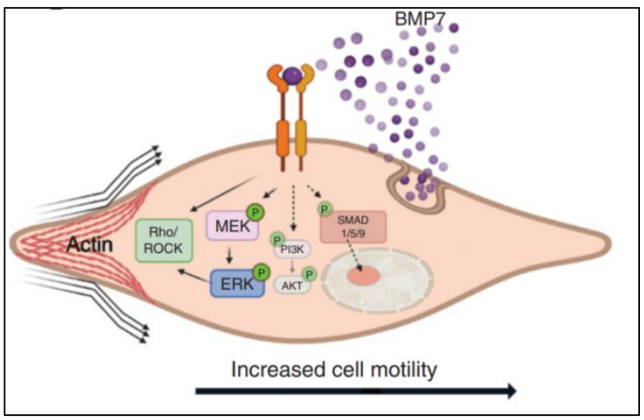

Figure 38: Distinct DMG entities and BMP7 signaling pathway in DMG

A- Two main entities of DMG with distinct gene expression and metastasis profile.

B- B- The signaling pathway triggered by secreted BMP7. Scheme modified from (Bruschi et al., 2023).

Additionally, DMG/DIPG is characterized as a "cold tumor" due to its markedly low presence of T cells within the microenvironment and its inherently low inflammatory signature profile (Lieberman et al., 2019; Lin et al., 2018; Pachocki and Hol, 2022). Notably, the percentage of T lymphocytes in DMG pre-treatment and autopsy samples is a 2%, contrasting sharply with the range of 7-50% observed in GBM (Lin et al., 2018). This deficiency extends to the lack of macrophages, pivotal in promoting metastasis and angiogenesis in glioma, as well as cytokines and chemokines known for their roles in inducing invasion and metastasis in glioma (Lin et al., 2023) (Fig. 39). While this characteristic diminishes the number of candidate key factors influencing the infiltration and metastasis of DMG/DIPG, it concurrently intensifies the challenge of identifying novel treatments for the metastatic features and achieving consistent data across different studies.

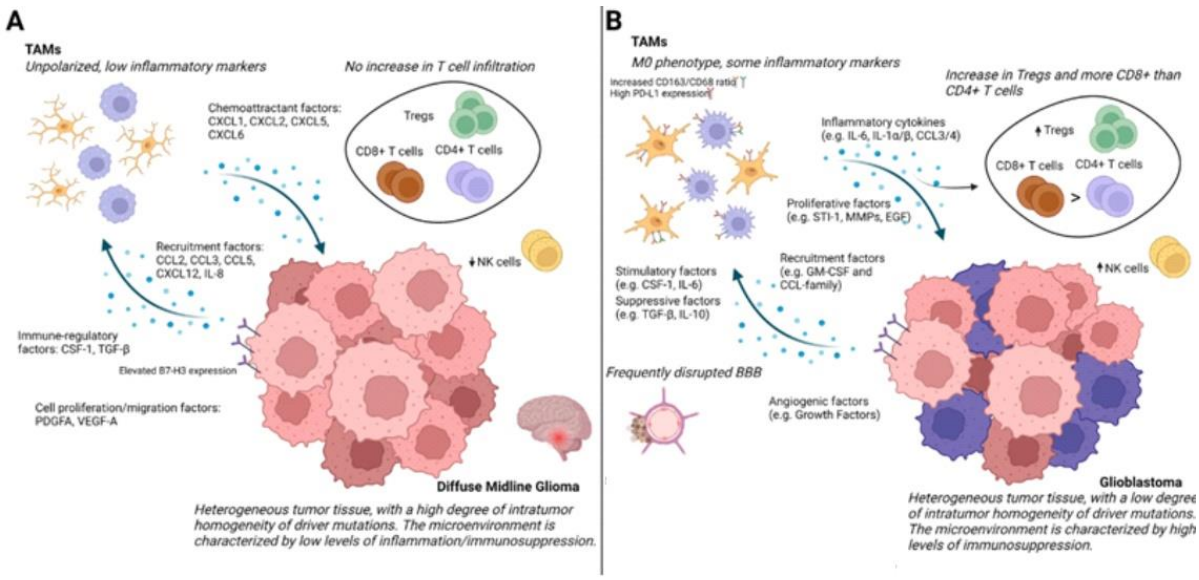

Figure 39: Distinct immune microenvironment between DMG and GBM

A- DMG consist unpolarized tumor-associated macrophages (TAM) population and have less cytokines/chemokines than

B- Immuno microenvironment in GBM.

Schematic modified from (Pachocki and Hol, 2022).

Concerning the extra-neural metastasis of DMG/DIPG, a case report authored by De Martino et al. identified 14 cases in the existing literature (De Martino et al., 2023), This paucity of occurrences suggests a rare phenomenon, resulting in limited sample availability and posing challenges for further research endeavors.

With the provided evidence, it can be inferred that the invasion of DMG/DIPG exhibits similarities with OPC migration, previously identified as their cell of origin. Furthermore, the metastasis of DMG/DIPG exhibits commonalities in cues with OPC migration. Consequently, the modification of OPC features in the context of DMG/DIPG may emerge as a novel approach to mitigate metastasis in affected patients, presenting a promising avenue for therapeutic intervention. In the majority of cases, these tumor lesions tend to manifest in regions that are readily accessible to cerebrospinal tracts, raising the possibility of dissemination via cerebrospinal fluid flow, leading to the seeding of tumor cells at new sites (Sethi et al., 2011; Vanan and Eisenstat, 2015). However, the precise triggers that would prompt DMG cells to initiate metastasis and the mechanisms that dictate their selection of secondary locations remain elusive questions in need of exploration.

Additionally, there is precedent in previous glioma metastases research demonstrating the migration of tumor cells through white matter pathways. Furthermore, it is imperative to underscore that numerous metastatic behaviors have been observed post-treatment, providing compelling evidence of the influence of radiation and chemotherapy on the tumor's characteristics and its ability to alter the microenvironment, thereby facilitating the metastatic potential of favorable DMG tumor cells.

Thus, mitigating the invasiveness of DMG tumors could be a promising therapeutic strategy to improve the overall survival rate of patients with DMG. This is particularly pertinent in my research project, where I focus on understanding the invasive characteristics of DMG/DIPG tumors with the aim of identifying novel targetable

elements to mitigate invasion and metastasis, ultimately improving survival outcomes.

OBJECTIVES OF PHD PROJECT

Exploring the relationship between cell identity and migration ability constitutes a substantial body of biological research as it may lead to reprogramming means to impede the extension of gliomas cells. Interestingly, despite many hypotheses and evidence about the cell-of-origin of DMG/DIPG, as well as more updated information about the interaction between DMG/DIPG cells and the tumor microenvironment, there are not many studies that specifically focus on tackling the role of cell fate in regulating the invasive and metastatic behavior of DMG/DIPG.

Over the last decade our laboratory has developed, in collaboration with Necker Hospital (Hôpital Necker-Enfants malades), a unique cohort of patient-derived DMG/DIPG cellular models cultivated both in 2D and 3D. These cell lines not only harbor the H3K27M mutation but also faithfully mirror the inter-patient heterogeneity. Notably, as presented in the introduction, an in vitro 3D-invasion assay could predict the metastatic evolution and disease progression observed in patients. Therefore, these models are highly relevant for studying the invasiveness of DMG/DIPG. The available bulk RNAseq information obtained from these cells cultivated in 3D model was a starting point for initiating my PhD project.

My PhD project delves into the intricate relationship between cell identity and the invasive potential of DMG/DIPG. My primary objectives were as follows:

(1) Identification and validation of candidate gene: Utilizing primary data obtained from bulk RNA-seq performed on 3D model, the project looks to identify candidate genes with significant implications for cell fate which expression correlates with the invasive capabilities of DMG/DIPG cells. Following the identification process, the project aimed at elucidating the role of the candidate gene(s) in modulating cell invasion through functional analyses of DMG/DIPG cell lines after its knock-down.

(2) Study the genetic and epigenetic role of the candidate gene: In order to decipher the role of the gene of interest in regulating cell identity and the invasion process, as well as identifying its downstream, we performed both transcriptome profiling with bulk RNA-seq and chromatin location of the gene of interest and the histone mark H3K27ac using CUT&Tag.

RESULTS

I. Identification and validation of a candidate gene regulating invasion in DMG/DIPG: *NKX2-2*

1. Identification of potential regulators of the invasion process in DIPG by combining gene expression and phenotypical profiling

The study by Bruschi and colleagues not only stands as one of the key discoveries of my host team in recent years, but it also marks the starting point of my Ph.D. project (Bruschi et al., 2023). It identified how the heterogeneity in the invasion process in Diffuse Intrinsic Pontine Glioma (DIPG), classified in local, locoregional or metastatic, impacted survival in patients. Additionally, utilizing patient-specific 3D avatar models that accurately depict interindividual invasiveness, his study generated transcriptomic data for both organoids and primary tumors.

Briefly, RNA-seq profiling was conducted on 17 DMG organoids after 21 of culture after embedding in Matrigel. Unsupervised clustering identified 13 organoids associating with high invasion rate and 4 with low invasion rate in the 3D-invasion assay. Unsupervised hierarchical clustering of samples based on their expression profiles revealed two primary clusters: C1 comprising 4 organoids with low invasion rate and C2 comprising 13 organoids associated with high invasion rate in the 3D invasion assay. Indeed, this clustering pattern strongly correlated with the invasion capabilities of the respective glioma stem-like cells (GSC) and the metastatic development in the corresponding patients. These differentially expressed genes offered insights into the

molecular mechanisms underlying the observed variations in invasiveness. This suggests that the variation in invasiveness exhibited in both primary tumors and patient-derived organoids mostly rely on transcriptional processes.

A pre-ranked list, derived from differential gene expression analysis of DIPG cells from each cluster with low or high invasion rate was used as input data for Gene Set Enrichment Analysis (GSEA) and compared to predefined set of genes, which represents a molecular function, biological process or cellular component. The analysis from Bruschi et al. revealed that upon dividing DMG into moderate and highly invasive subgroups, the genesets relating to OPC were upregulated in highly invasive tumors (C2) while mesenchymal signatures were found overexpressed in the low invasive tumors (C1).

Looking in more details within the expression profile of the highly invasive cluster C2, the OPC identity is supported by the overexpression of transcription factors related to OPC differentiation. Notably, *NKX2-2* is the most overexpressed gene (Fig. 40A; adj-*p*-value=0.0018) in C2 organoids cluster and its expression positively correlates with the invasion score of GSC in 3D (Fig. 40B; Pearson r^2=0.04711, *p*-value=0.0023). We next analyzed the expression level of *NKX2-2* in DMG tumors categorized depending on the development of metastasis during the course of the disease in the corresponding patients. Despite a relatively low number of tumor analyzed (n=17), we observed an overall higher *NKX2-2* expression in tumors of patients developing metastasis, albeit not reaching statistical significance (Fig. 40C).

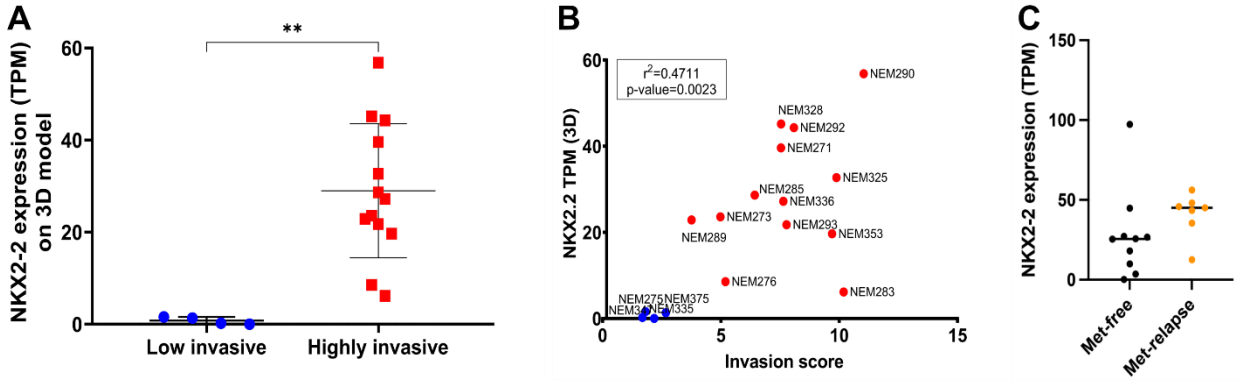

Figure 40: NKX2-2 expression in GSC 3D models and patient tumors

A- Differential expression of *NKX2-2* in organoids 3D models categorized based on their low (C1) versus high invasive (C2) clusters (p-value = 0.0018).

B- Correlation between *NKX2-2* expression level in organoids and corresponding GSC invasion score, determined through 3D invasion assay (linear regression, p-value = 0.0023).

C- *NKX2-2* expression in DIPG patient tumors collected at diagnosis further categorized by upon the metastatic evolution during the course of the disease (p-value = 0.27).

Among the top 10 differentially expressed genes, I identified *NKX2-2* and *OLIG2* that related to OPC differentiation and identification as two candidate genes linking cell fate and invasion in DMG/DIPG. NKX2-2 is NK2 Homeobox 2, a transcription factor (TF) that belongs to the NK2 family of homeobox TFs. Its roles include regulating pancreatic beta cell differentiation, participating in the development of the CNS through the SHH signaling pathway to initiate ventral patterning, and specifically contributing to the initiation of oligodendrocyte differentiation. While OLIG2 has been the subject of some publications (Anderson et al., 2017; Liao et al., 2021), the role of NKX2-2 in DMG/DIPG remains unexplored, making it an interesting potential candidate gene. Consequently, NKX2-2 was selected for investigation, with the aim of understanding its role in regulating DMG/DIPG invasiveness and the mechanism underlying invasion via cell identity.

2. Validation of *NKX2-2* knock-down (KD) in DIPG cells

In order to investigate the possible roles of *NKX2-2* in regulating invasion of DIPG cells, we performed a loss-of-function approach. Findings from my Master 2 internship project in the lab revealed that transfection of short-interfering RNAs (siRNAs) in our patient-derived DIPG cells (henceforth, GSC) was not an option due to the strong induction of cytotoxicity. Consequently, I opted for transduction of lentiviral vectors coding short hairpin RNA (shRNA) in order to achieve stable knockdown of *NKX2-2*.

Five different predesigned shRNAs targeting *NKX2-2* in the pLKO.1-TRC lentiviral vector backbone were used and one shRNA did not pass the sequencing verification

step. Among the four other NKX2-2 shRNAs, we eliminated the one which could not reduce up to 50% of the NKX2-2 expression or higher cell toxicity. Finally, two NKX2-2-targeting shRNAs with more than 50% of reduction of NKX2-2 were selected for further investigation, referred to as shNKX2-2.1 and shNKX2-2.5. Additionally, two shRNA sequences – non-targeting control shRNA (shADDGENE) and non-mammalian control shRNA (shCOO2) were used as controls.

The selected cell lines used in the study, along with their main genetic alteration, are presented in Table 4. These cell lines were chosen based on their average to high *NKX2-2* expression and their moderate to high invasion scores. In other words, their selection was guided by their proximity to the linear regression. In addition to the key causal histone mutation H3K27M H3.3, these four cell lines encompass other known secondary alterations, such as *TP53*, *PPM1D*, and PI3K/AKT/mTOR pathway mutations, as well as *PDGFRA* amplification. Given the time limitation, my research focused predominantly on the effect of NKX2-2 depletion in DIPG cells that possess the H3.3-K27M mutation. Initial experiments using GSC harboring H3.1-K27M mutation demonstrated a marked increased sensitivity to *NKX2-2* depletion thus hindered subsequent analyses, such as cell's ability to form spheres when embedded in Matrigel (Fig. 41).

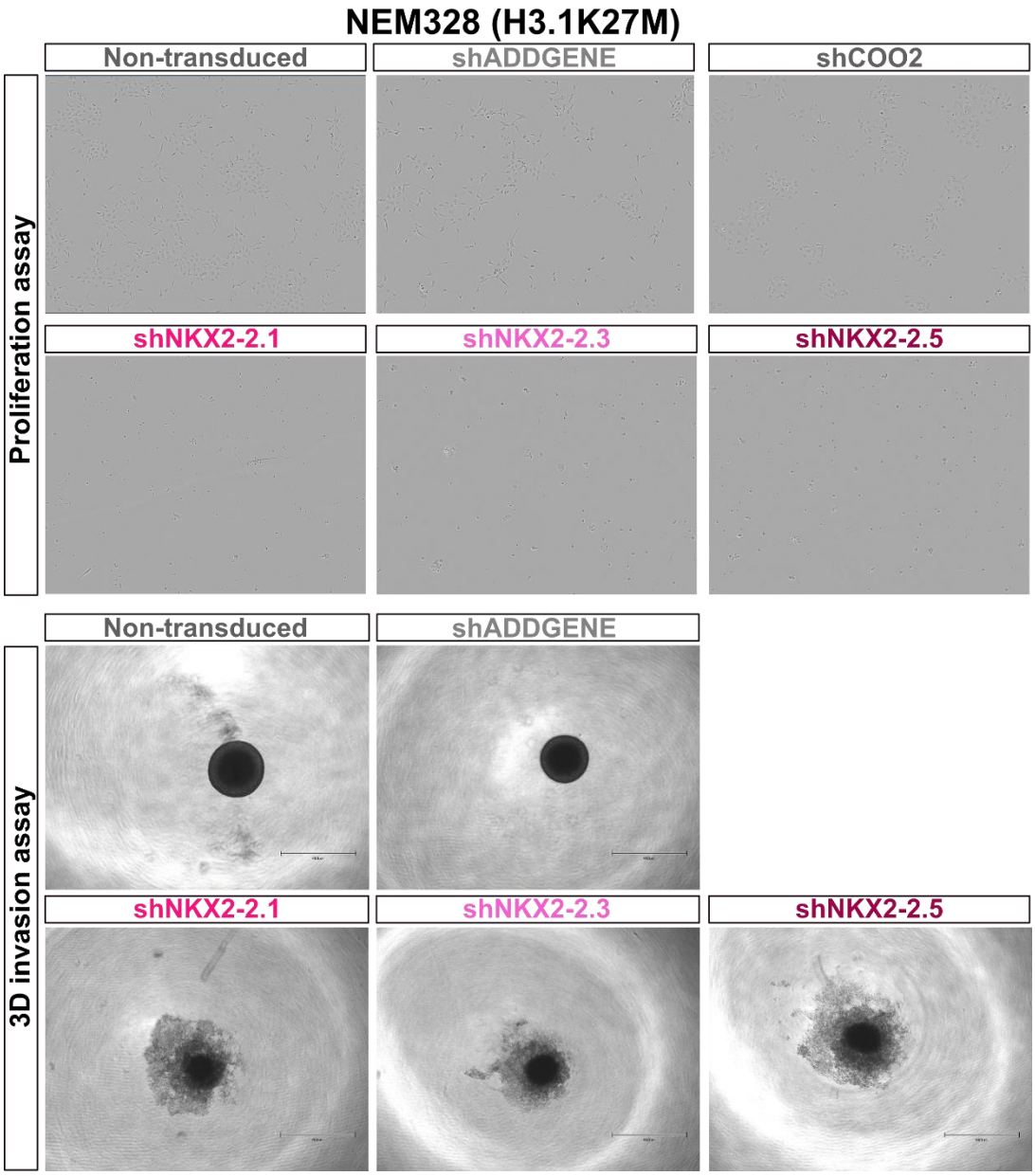

Figure 41: Cytotoxicity of NKX2-2 depletion on GSC DIPG H3.1 NEM328

A- caused massive cell death compared with control conditions

B- could not form spheres in 3D culture model.

Following viral production and titration, DIPG GSC were transduced at multiplicity of infection (MOI) of 0.5 or 1. After transduced-cell selection with puromycin over two days, RNA was extracted and *NKX2-2* knock-down was confirmed by RT-qPCR. The two control shRNAs showed equivalent *NKX2-2* expression, indicating that shCOO2, the non-mammalian target shRNA, did not interfere with the NKX2-2 levels compared to the ADDGENE shRNA. With these two shRNAs shNKX2-2.1 and shNKX2-5, we obtained

a reproducible knockdown, achieving more than 50% reduction in *NKX2-2* expression with low MOIs (Fig. 42). The two NKX2-2-shRNAs caused moderately similar knockdown efficiency in terms of decreasing NKX2-2 levels.

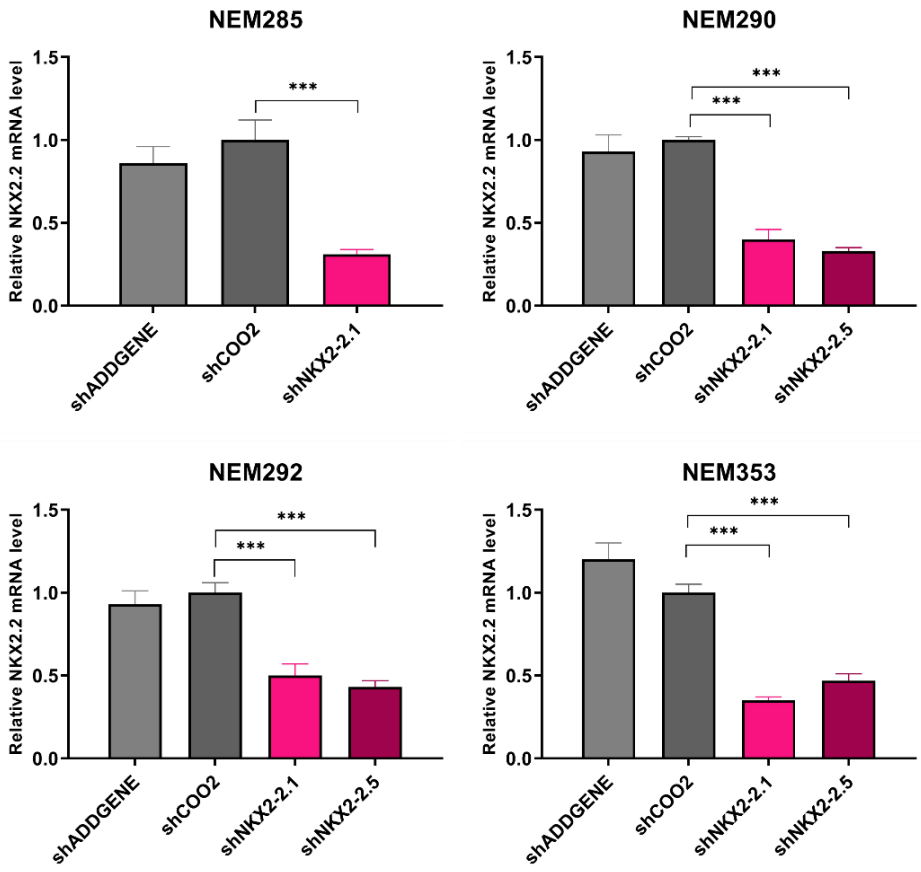

Figure 42: Assessment of knockdown efficiency of NKX2-2 in GSC following shRNA transduction

The mRNA expression of *NKX2-2* in shRNA-transduced GSC was examined by RT-qPCR 48 hours after treatment with puromycin. NKX2-2 expression was normalized to *TBP* expression, and compared to non-treated GSC using the comparative $2^{-\Delta\Delta CT}$ method. Statistical analysis was performed using Student's t-test (***: $p < 0.001$).

3. Study the impact of *NKX2-2* KD on DIPG cells invasion

To evaluate the invasiveness of DIPG following the attenuation of this transcription factor, four days following transduction the same cells that were used to profile *NKX2-2* KD were aggregated as tumorspheres during 2 days and further embedded in Matrigel. Cell invasion was monitored using a live video-microscope (Incucyte) for 40 hours. Despite equivalent tumorspheres size at 0h, at 40h GSC with *NKX2-2* KD

exhibited a smaller occupied area compared to the control conditions, linked to a decrease in invasion (Fig. 43).

The inverted brightfield images showed that, initially, the glioma spheres across all four conditions within the same cell model exhibited similar sizes. However, by the 40h post-embedding into Matrigel, the gliospheres derived from GSC harboring *NKX2-2*-targeting shRNAs were smaller compared with the two control conditions with the most visualizable ones were NEM285, NEM292 and NEM290. Exhibited reduced size compared to those in the two control conditions, with the most pronounced reductions observed in conditions NEM285, NEM292, and NEM290. Furthermore, within the subset of GSC transfected with NKX2-2 shRNAs, shNKX2-2.5 induced a significantly smaller gliosphere size compared to shNKX2-2.1.

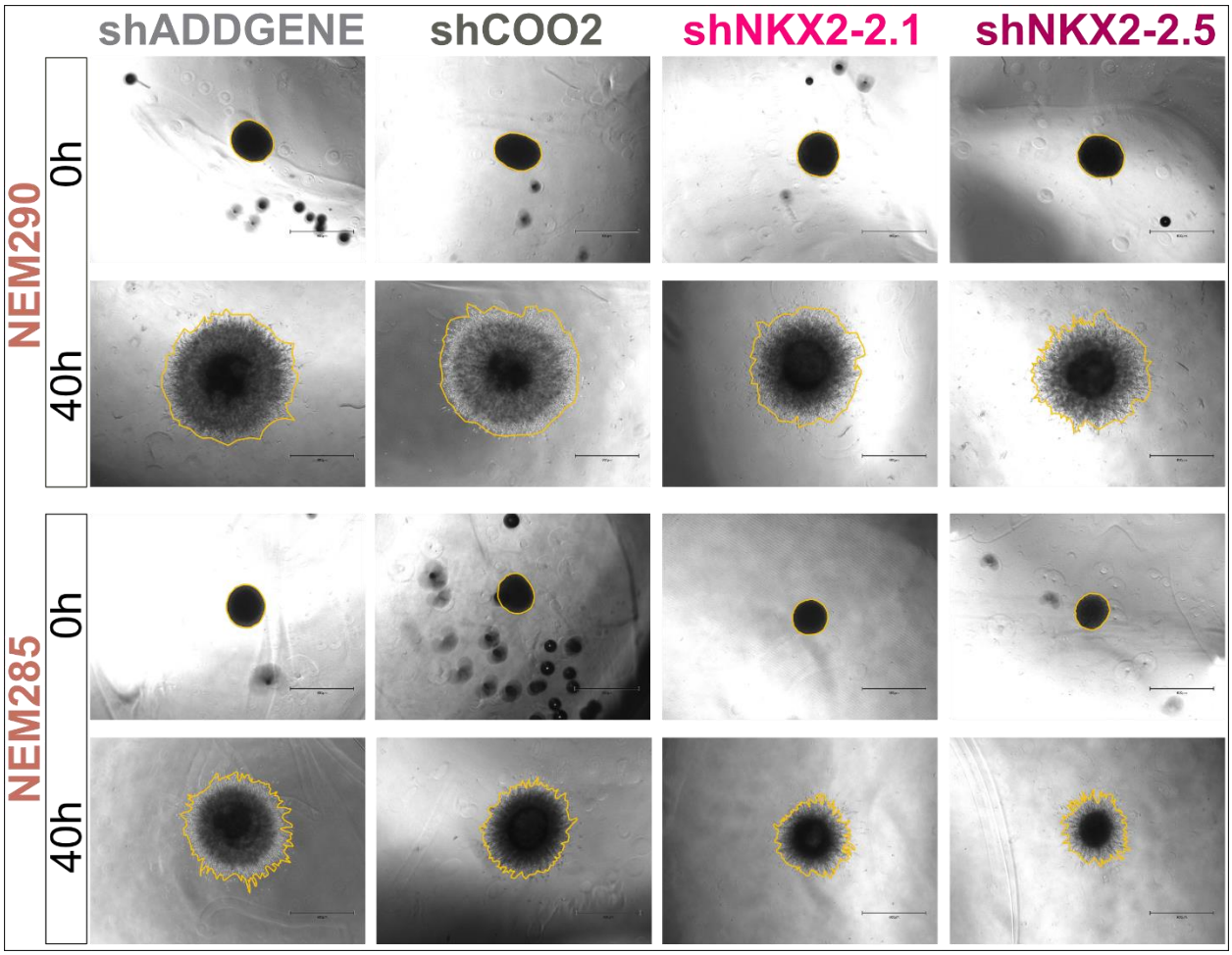

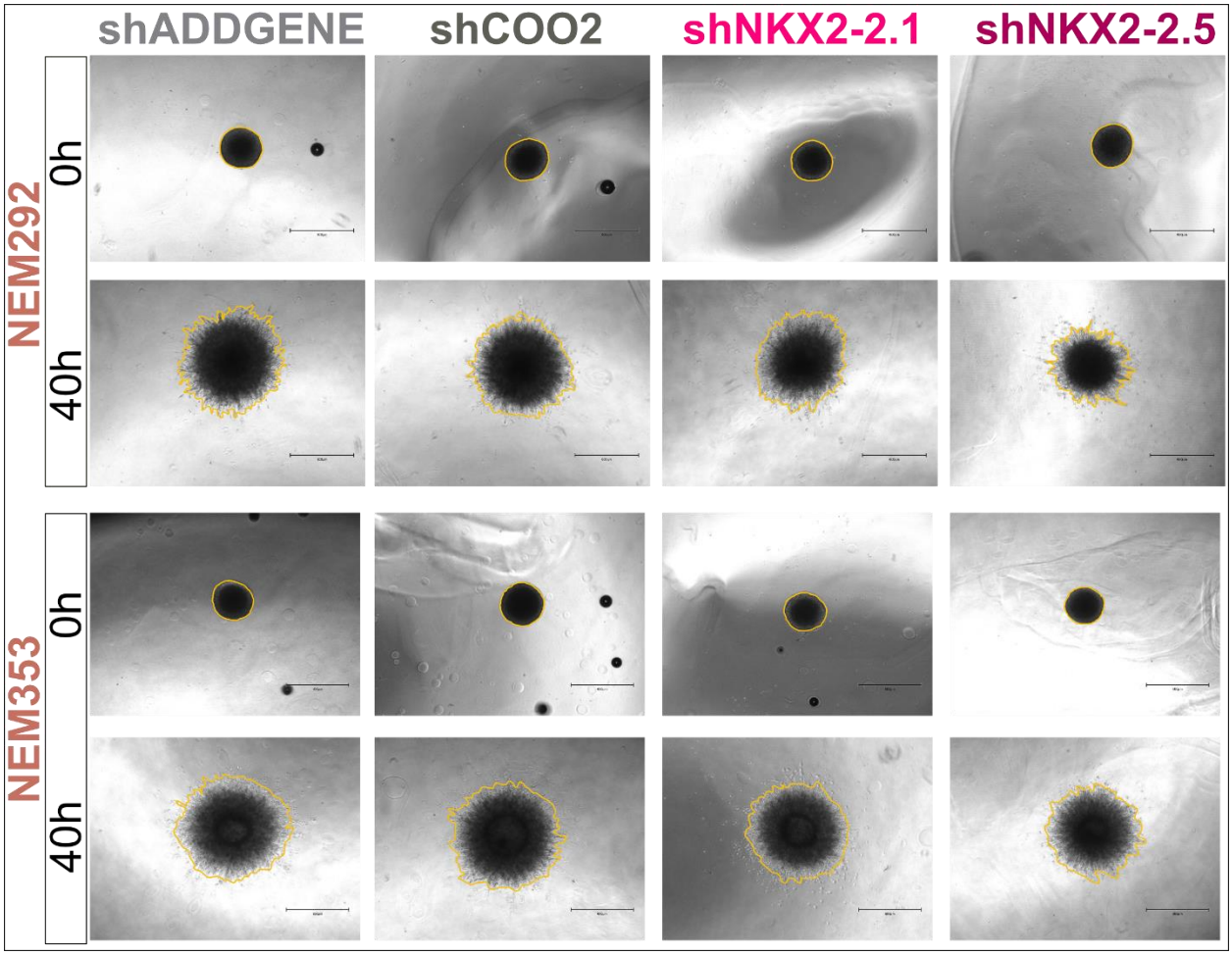

Figure 43: Images of the 3D invasion assay of gliomasphere on four selected GSC NEM290, NEM285, NEM292 and NEM353 transduced with control and NKX2-2-targeting shRNAs

Yellow lines outlining the surface area occupied by the initial gliomasphere at 0h and by invading GSC were manually drawn using ImageJ. Scale bar= 600 µm.

Relative quantification of invasion scores was achieved by normalizing surface area data at each time point to the 0h time point of each condition on 9 replicate spheres. The experiment was repeated at least twice for each cell model (n≥2). The invasion scores of control conditions varied among GSC models while maintaining the order of invasiveness of non-transduced models (Table 4). NEM290 gliomaspheres exhibited the highest invasion on Matrigel, with a score of 10.07 for COO2 control shRNA, followed by NEM353-shCOO2 with a moderate score of 6.09 at 40h. Two models, NEM292 and NEM285, achieved the lowest scores of 5.34 and 4.94, respectively (Fig. 44).

When comparing the invasion areas of GSC at 40h in the different conditions, the results corroborated the observations mentioned earlier with statistical differences between GSC with control shRNAs vs. sh*NKX2-2* (Fig. 44). Notably, shNKX2-2.5 had a more significant effect, showing an average decrease in invasiveness of 33.35% across all four models, compared to a 15.23% decrease with shNKX2-2.3. However, the effect varied among the different GSC. For example, the invasion score of NEM353 decreased by 6.4% to 16.3%, which was less than the other cell lines. All other cases showed a reduction of at least 19%, with the exception of NEM292 transduced with shNKX2-2.1.

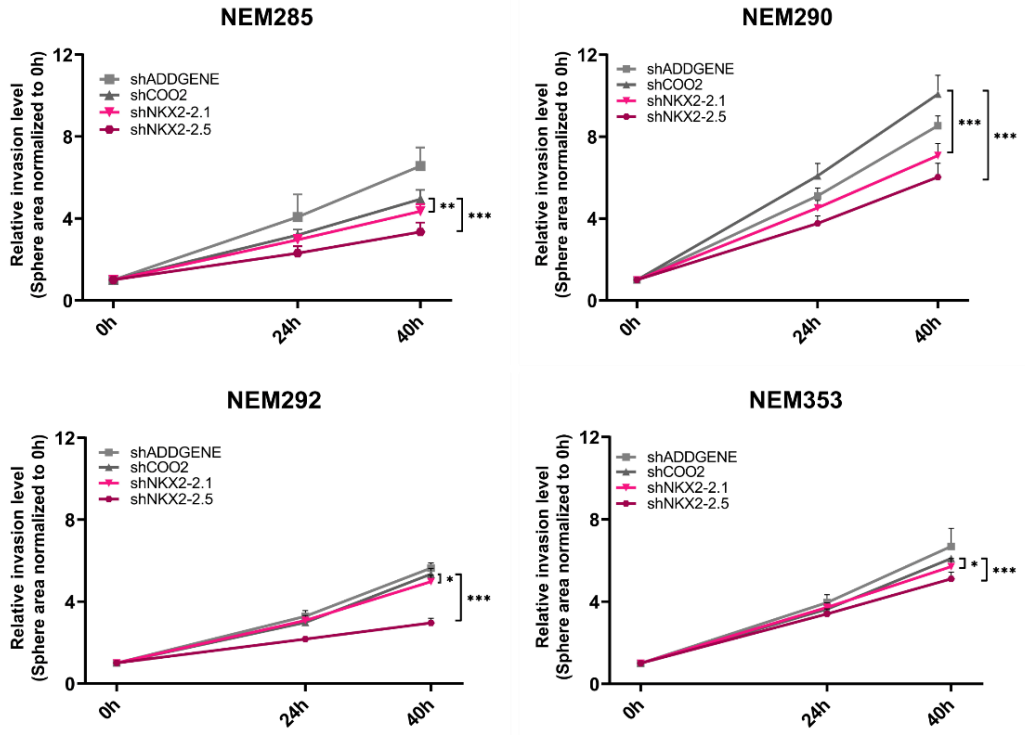

Figure 44: Impact of *NKX2-2* KD on the 3D invasion score of 4 DIPG GSC models

The area occupied by cells at 24h and 40h was compared to the initial timepoint for each replicate tumorspheres (n=9 for each condition). Statistical analysis was performed using Student's t-test on the score at 40h (*: $p < 0.05$; **: $p < 0.01$; ***: $p < 0.001$).

Taking the average decrease in invasion score resulting from the application of two NKX2-2-shRNAs, the analysis unveiled a subtle correlation between the initial expression level of *NKX2-2* and the magnitude of decrease in invasion score subsequent to *NKX2-2* KD, with a p-value of 0.0381 (Fig. 45).

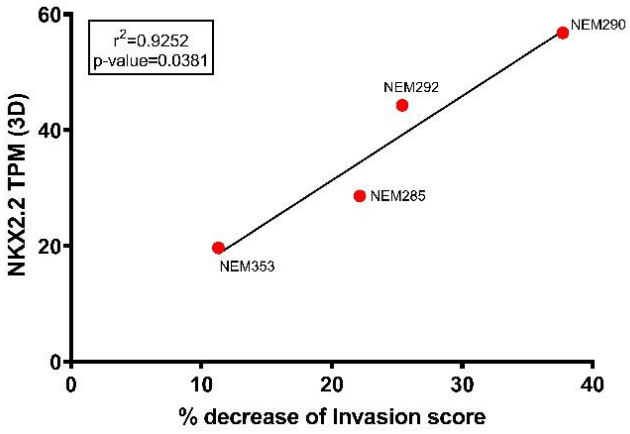

Figure 45: Correlation between initial NKX2-2 expression level in tumoroids and corresponding average percentage decrease in GSC invasion score

Data was analyzed using linear regression, p-value = 0.0381.

In conclusion, by using shRNAs I was successful in achieving a knockdown of NKX2-2 on four DIPG cell lines and that it led to a reduction in the invasion score of gliomaspheres compared to the conditions with control shRNAs at 40hrs post Matrigel embedding. Thus, reducing *NKX2-2* by 2- or 3-fold impacted negatively the invasion capacities of DIPG cells.

4. Analysis the impact of *NKX2-2* KD on DIPG cells proliferation in 2D culture

In order to assess if the observed changes in the invasion score in the 3D model could be attributed solely to an altered invasive behavior, or might it be biased by changes in the growth rate of GSC when subjected to NKX2-2-shRNAs, we then conducted proliferation experiments.

For this, we plated GSC 4 days post transduction in 24-wells plates and their proliferation was followed for seven days using video-microscopy (Incucyte). We focused in particular on two specific timepoints: at 40 hours post-plating for comparison with the 40h time point on the 3D invasion assay, and the other at day 7 to assess the long-term impact of *NKX2-2* knockdown on the growth of GSC.

The DIPG models exhibited varying rates of proliferation. Notably, the comparison of GSC transduced with shCOO2 revealed that NEM290 and NEM292 demonstrated the

highest proliferative capacities, with a confluency increase of 17.5 and 12.7 times, respectively, while NEM285 displayed the least proliferation, with only 4.4 times increase in confluency after 7 days (Fig. 46). Despite the differing proliferation speeds among the DIPG models, no significant differences were observed at 40 hours post-seeding between the control- and NKX2-2-shRNA conditions in all four models. However, cells transduced with NKX2-2-shRNAs exhibited slower growth compared to those with control-shRNAs over longer culture. Overall, the reduction in *NKX2-2* level had a more pronounced impact on NEM290, NEM292, and NEM285, resulting in an average decrease of proliferation 2.2, 1.7, and 1.6 times, respectively, while the effect on NEM353 was only 1.2.

A discrepancy emerged between the two NKX2-2-shRNAs, with shNKX2-2.5 demonstrating a stronger effect than shNKX2-2.1 in three out of four GSC models specifically, NEM290, NEM292, and NEM353. Transduction on NEM285 did not show any significant difference between cells transduced with shNKX2-2.1 and shNKX2-2.5.

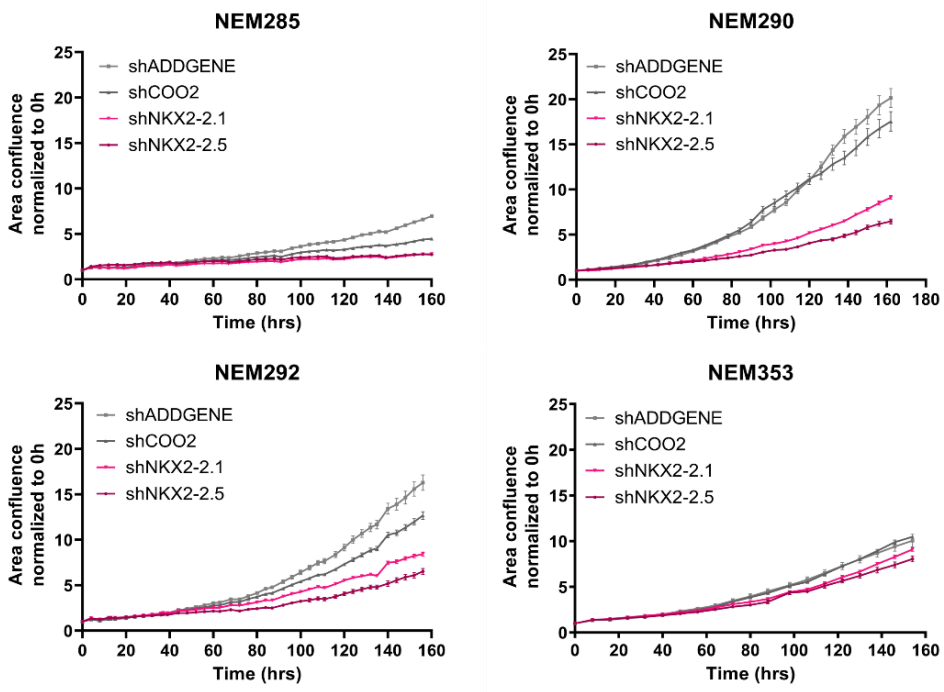

Figure 46: Proliferation curves of GSC tranduced with control shRNAs and NKX2-2-shRNAs

Cell images were recorded using video-microscopy (Incucyte S3, Sartorius), with

images captured at four-hour intervals. The cell mask tool was used to detect cell surface area, followed by area confluence analysis, which involved dividing the cell surface area at each time point by that at the initial time point. The experiment was designed with triplicate wells per condition.

To understand the cause of this decrease in proliferation, I examined image series captured through video-microscopy at each time point. It revealed that the transduction of shNKX2-2 into selected GSC did not induce cellular toxicity, as evidenced by the absence of recorded massive cell death. The presence of cell death was checked by video microscopy images during the proliferation assay, and dead cells were detected using trypan blue at the endpoint of the assay. The results showed that there was less than 10% cell death in each condition.

The observed slowdown in cell proliferation could potentially be due to senescence, a cell cycle arrest that might be triggered secondary to *NKX2-2* knock-down. To test this hypothesis, I chose to use a β-galactosidase (β-gal) assay.

β-gal assay was conducted on two models, NEM290 and NEM353, chosen for their notably divergent alterations in proliferation rates post *NKX2-2* knock-down. Specifically, in NEM290, the introduction of shNKX2-2.1 resulted in a 1.9-fold decrease in proliferation rate, concomitant with a marked increase in the percentage of senescent cells, rising from 7.5% to 14.2% when compared to the shCOO2 condition (Fig. 47). Conversely, in NEM353, no significant disparity was observed between these two conditions, with an average of 26.76% senescent cells.

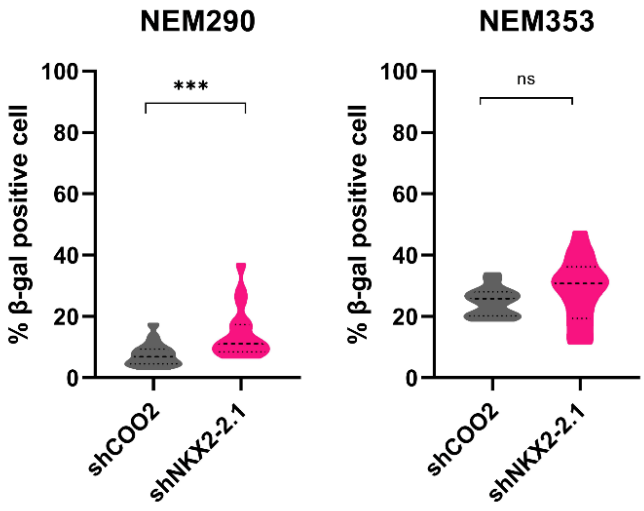

Figure 47: SA-β-gal assay detected the senescence on NEM290 and NEM353

Statistical analysis was performed using Student's t-test (*: $p < 0.05$; **: $p < 0.01$; ***: $p < 0.001$).

According to these data, it was concluded that reducing *NKX2-2* expression leads to a less proliferative phenotype in the four selected DIPG models at varying levels. β-gal assay should be replicated to have a statistical result and conclusion of the contribution of senescence to the divergent effects observed across the models.

5. *NKX2-2* depletion and its consequence on DIPG cells morphology

Images derived from video-microscopy during the proliferation assay, unveiled a discernible alteration in cell morphology between GSC harboring control shRNAs and those incorporating shNKX2-2. However, it is imperative to note that these observations exhibit notable variability among distinct GSC models. Notably, in the case of NEM290, the cells transduced with control shCOO2 demonstrated a typical bipolar or tripolar shape with a small cell body, characteristic of OPC morphology (Fig. 48A, yellow arrows). Conversely, NEM290-shNKX2-2.1 exhibited a rounder and flatter morphology (Fig. 48A, pink arrows).

Consequently, the cell projections of NEM290-shRNAs appeared shorter than those in the control conditions. To validate this observation, cells were fixed and stained for the nucleus and actin filaments. Subsequently, images were analyzed using ImageJ with

the NeuroJ plugin. Specifically, cell projections were manually selected and measured using the Neuro tracing function. The results confirmed that NEM290 transduced with NKX2-2-shRNAs exhibited shorter projections compared to the control ones (Fig. 48B, Fig. 50).

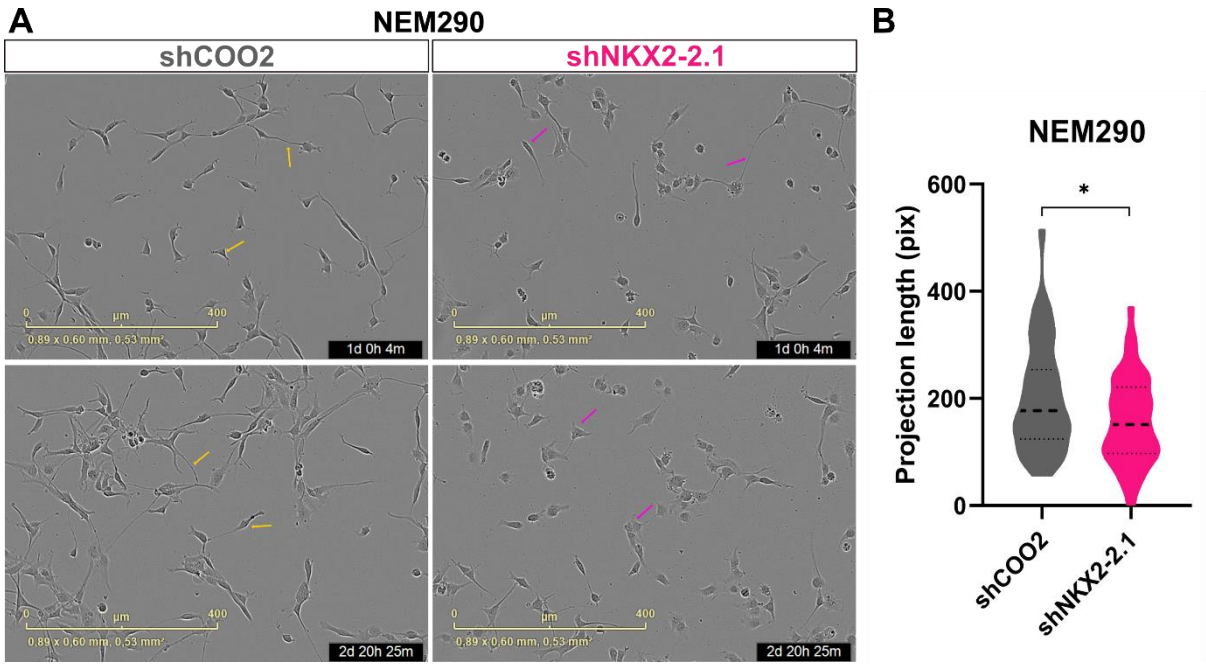

Figure 48: Cell morphology of NEM290 at phase-contrast and quantification of projection length

A- Images of NEM290 expressing control- or NKX2-2-shRNAs were captured using a phase-contrast microscope at a magnification of 10X.

B- Quantification of cellular projection lengths performed on more than 40 cells (n=1). Scale bar 400um. Statistical analysis was performed using Student's t-test (*: $p < 0.05$).

Interestingly, consistent findings were observed in the GSC NEM353 cell line, wherein cells subjected to *NKX2-2* knockdown exhibited significantly shorter projections when compared to the control shCOO2 (Fig. 49A, Fig. 50). In contrast, NEM292 did not show any difference as in the trend observed in NEM290 and NEM353, as the measurements of cell process length were not significantly different from the control (Fig. 49B, Fig. 50).

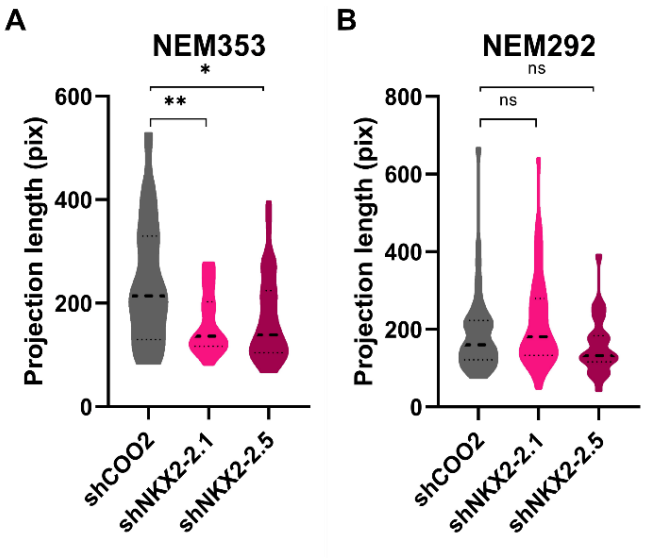

Figure 49: Quantification of cellular projection lengths on two GSC models

A- NEM353

B- NEM292

n=1. Statistical analysis was performed using Student's t-test (ns, non-significant; *: $p < 0.05$; **: $p < 0.01$; ***).

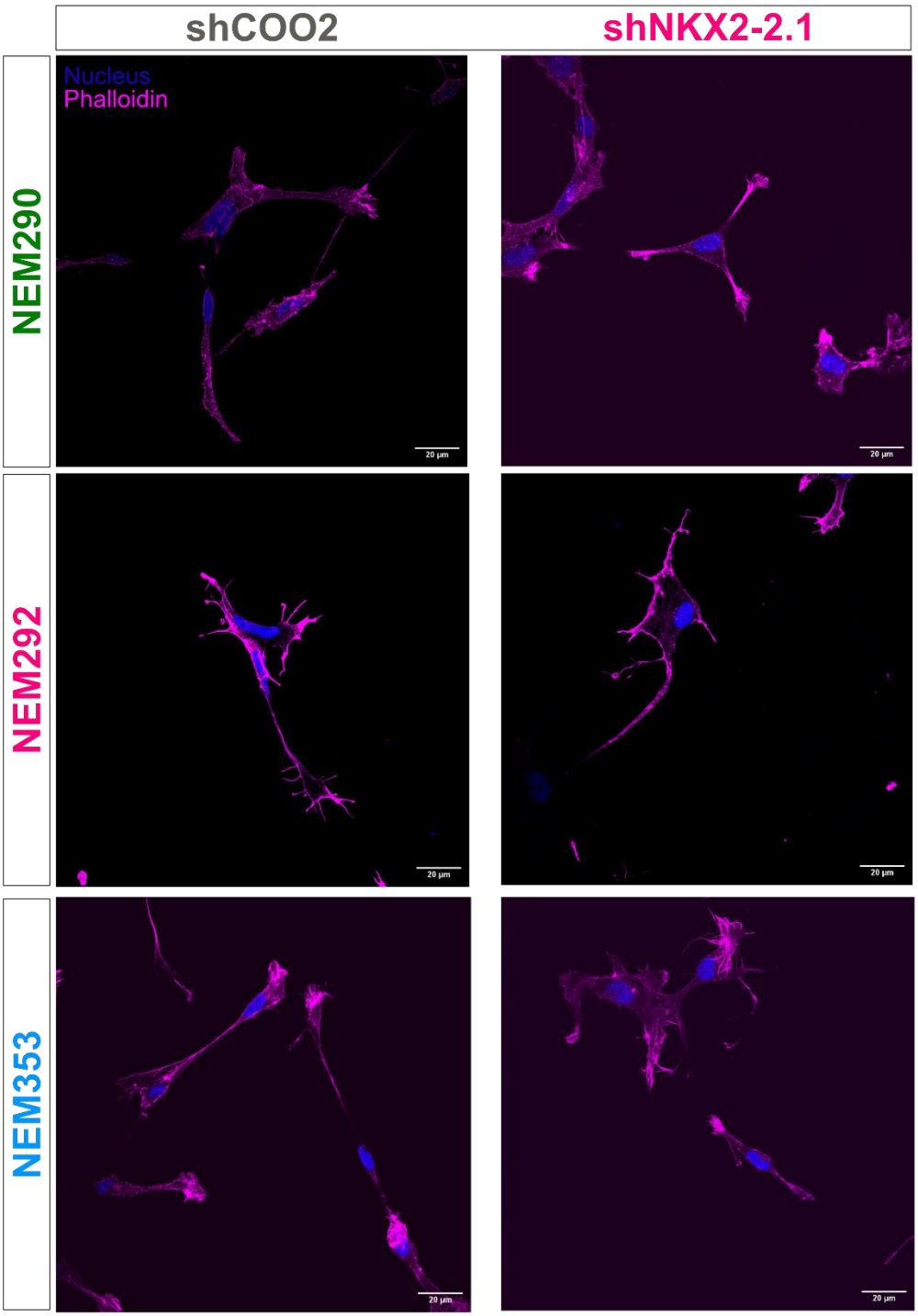

Figure 50: Cell morphology of GSC pre- and post- *NKX2-2* KD

IF images compared cell morphology of all three GSC transduced with target control shRNA (COO2) and NKX2-2-target shRNA (NKX2-2.1). nucleus (blue) F-actin (phalloidin, magenta). The images were captured using microscopy Leica SP8 at a magnification of 40X. Scale bar: 20µm.

In contrast, it is noteworthy to observe that NEM285 cells subjected to NKX2-2-

targeting shRNAs exhibited a discernible trend toward the development of longer and thinner cellular processes when compared to those treated with the control shRNA (Fig. 51). No quantification data based on IF images were recorded due to a technical issue encountered during the experiment, resulting in the absence of the COO2-control shRNA condition. This intriguing morphological distinction underscores the potential influence of *NKX2-2* expression modulation on the intricacies of cellular projections, warranting further investigation and detailed characterization for a comprehensive understanding of its impact on cellular morphology.

Figure 51: Phase-contrast video microscope images of NEM285 with COO2-control shRNA and NKX2-2-targeting shRNAs

The images were captured using video microscopy at a magnification of 10X. Scale bar: 300 µm.

Furthermore, irrespective of the GSC models utilized, following transduction with NKX2-2-shRNAs, a diverse array of cell morphologies manifested within the population. These morphologies included round and flat cells, as well as bipolar/tripolar cells with simple projections and those exhibiting more intricate and complex structures in their projections.

Together, these findings imply that the knockdown of *NKX2-2* induces alterations in cell morphology, giving rise to rounder and flatter cell shapes with shorter projections in NEM290 and NEM353. Nevertheless, this phenomenon was not observed in NEM292 and NEM285.

II. Functional study of *NKX2-2*

1. Identification of Differentially Expressed Genes (DEG) in transcriptome of DIPG GSC with *NKX2-2* KD

The first part of my PhD project allowed the identification of the transcription factor NKX2-2 and its influence on the invasion process in GSC. Subsequently, we aimed to delve deeper into the functional ramifications of NKX2-2 depletion and its role in driving the invasion of GSC gliomaspheres, investigating whether it entails a shift in cell identity. Consequently, bulk RNAseq was executed on 3D tumoroid samples derived from four selected cell lines under four conditions: employing two control shRNAs and two NKX2-2 targeting shRNAs.

DIPG tumoroids were generated by embedding 100,000 cells in Matrigel and cultured in GSC completed medium. Six days post-embedding, seven tumoroids were collectively pooled, and total RNA was extracted. Subsequent to RNA qualification and quantification, the samples were sent for bulk RNAseq (Integragen), generating on average 70 million paired-end reads. The analysis was conducted utilizing the in-house modification of DEBrowser (Kucukural et al., 2019).

We first applied a cell model normalization of was applied following model normalization on RNA-sequencing data of gliomaspheres from four cell models under four experimental conditions (two controls shRNAs and two with shRNAs targeting NKX2-2). We then conducted a Principal Component Analysis (PCA) using the 3000 genes with most-variable expression in the dataset. Each point on the plot represents a sample, with the distance between points reflecting the similarity of their gene expression profiles. This PCA unveiled that the first axis accounted for 38% of the variance, while the second axis explained 16%. Collectively, these axes showcased a separation between the control and NKX2-2-shRNA groups (Fig. 52A). Remarkably, while GSC samples from the two control conditions (shADD and shCOO2) clustered closely together, a notable disparity was observed among GSC expressing NKX2-2-

specific shRNA, manifesting a more dispersed distribution along the axis, even within the same cell model. Interestingly, sample regrouped according to NKX2-2 targeting shRNA (i.e. shNKX2-2.1 or .5) and not according to GSC models. Along both PC1 and PC2, NEM285 and NEM353 samples clustered closest to each other, suggesting that overall, these two GSC models might share more similarities than compared to NEM290 and NEM292 models. On the other hand, the two shNKX2-2-expressing NEM292 samples exhibited a long distance between each other, despite both undergoing gene knockdown of the same target gene, NKX2-2 (Fig. 52A). Their positions on the PCA plot suggest divergent transcriptional responses.

We next performed a differential gene expression analysis between the samples with controls and NKX2-2-targeting shRNAs. It is illustrated in the volcano plot where each point represents a gene with the x-axis indicating the fold change in gene expression and the y-axis representing the statistical significance of the change (Fig. 52B). Precisely, we identified 1007 differentially expressed genes (DEG) between two groups with an adjusted p-value of less than 0.01 and a log2 fold-change (log2FC) expression threshold set at 1.5. Among these, 695 exhibited up-regulation (depicted as red dots), while 312 demonstrated down-regulation (depicted as blue dots) in cells with NKX2-2 depletion. Interestingly, 386 genes were upregulated with a log2FC greater than 1, whereas only 37 genes demonstrated downregulation greater than 1 log2FC. Additionally, 21 genes within the down-regulated group exhibited a log adjusted p-value greater than 10, whereas this number in the up-regulated genes was only 2.

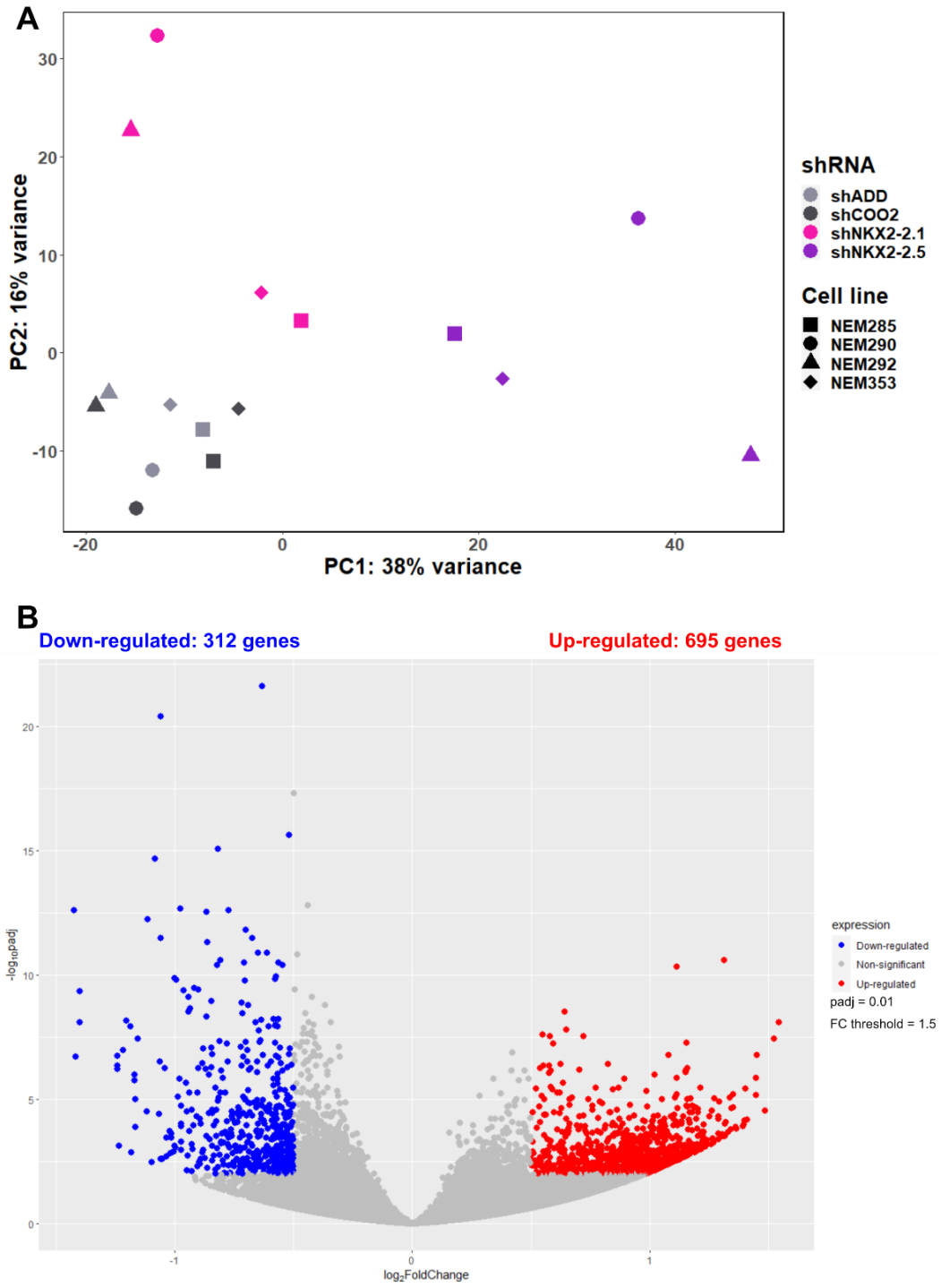

Figure 52: PCA and volcano plot of RNAseq data of GSC with and without NKX2-2 KD

A- PCA was performed on the expression data of the 3,000 most variable genes in GSC transduced with control shRNAs (depicted in light and dark grey) and GSC transduced with NKX2-2 shRNAs (shown in pink and violet). PC1 accounted for 38% of the variance, while PC2 explained 16% of the variance.

B- The volcano plot illustrates the DEG in cells expressing NKX2-2-shRNAs compared to control shRNAs, with a log2FC cutoff at 1.5. Significance is determined by an adjusted p-value of less than 0.01. Significantly up-regulated

genes are represented in red, while significantly down-regulated genes are in blue. Non-significantly deregulated genes are shown by grey dots.

2. Gene Ontology (GO) and Gene Set Enrichment Analysis (GSEA) of DEG after NKX2-2 depletion

Subsequently, we examined the lists of DEG using Gene Ontology (GO) analysis provided by the ToppFun platform to comprehend the biological processes associated with these two gene sets. Gene ontologies with 10 hit counts or fewer were filtered out, and the terms were ranked based on q-value FDR (False Discovery Rate) using Benjamini-Hochberg procedure. It was observed that terms related to the *cell surface*, *transmembrane signaling activity*, *external side of plasma membrane, external side of plasma membrane*, *extracellular matrix (ECM), collagen-containing ECM, G protein-coupled receptor (GPCR) activity, monoatomic ion channel complex, nervous system process* and *side of membrane* were the ten most enriched in genes increased in expression in GSC with *NKX2-2*-KD, with more than 21 hit count genes on the list (Fig. 53). Among these top ten, if considering the terms that shared more than 80% of the gene list as one, then the overexpressed genes after *NKX2-2* knock-down were involved in these five main enriched ontologies, which are: *cell surface, transmembrane signaling activity, ECM, nervous system* and *side of membrane*.

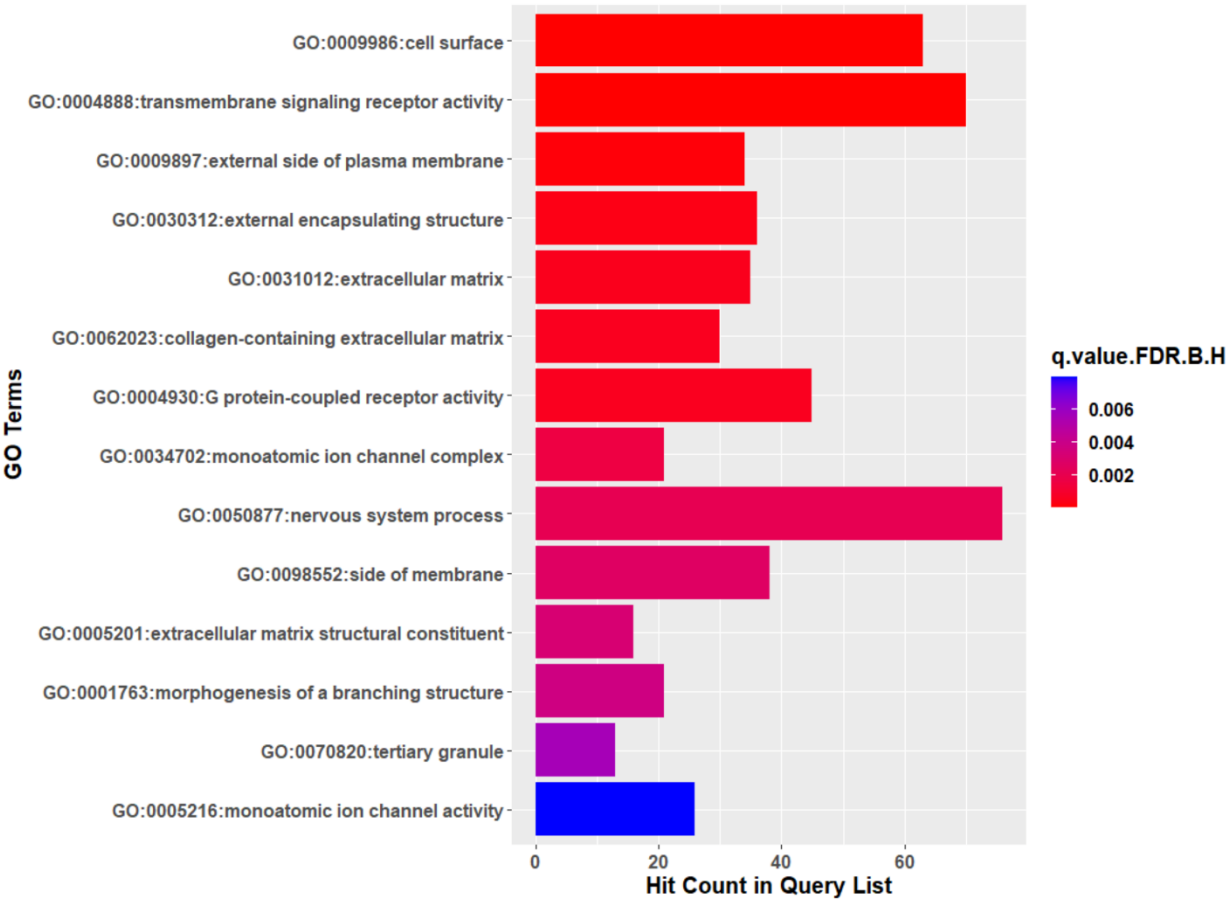

Figure 53: Gene Ontology (GO) analysis of overexpressed genes after *NKX2-2* KD p-value cut-off FDR of Benjamini and Hochberg <=0.01.

The analysis of the four-most enriched gene ontologies reveal only a single redundant gene, namely C5AR1 (Complement C5a Receptor 1). While literature on C5AR1 in gliomas remains limited, a single-cell study published in 2020 identified the C5AR1-RPS19 interaction as one of the most prevalent signaling cross-talk mechanisms between tumor and microenvironment in their GBM patient cohort (Caruso et al., 2020).

Among the top-10 most enriched gene ontologies, there is no redundant gene. However, 9 genes were found as common out of 208 genes in at least 5 out of 10 gene ontologies, which are: *LILRB2, FCN1, FGA, MUSK, CXCR5, LILRA1, CTSS, CHRFAM7A* and *EFNA5* (Table 4).

Genes	Brief function
LILRB2	Encodes a protein belonging to the leukocyte immunoglobulin-like receptor (LIR) family, involved in immune response regulation
FCN1	Encodes a protein called ficolin-1, involved in innate immune defense by recognizing and binding to pathogens
FGA	Encodes the alpha chain of fibrinogen, which is involved in blood clotting and wound healing
MUSK	Encodes a receptor tyrosine kinase that plays a key role in the formation and maintenance of neuromuscular junctions
CXCR5	Encodes a chemokine receptor that is primarily expressed on B cells and is involved in the migration of B cells to lymphoid tissues
LILRA1	Encodes a protein belonging to the leukocyte immunoglobulin-like receptor (LIR) family, involved in immune response regulation
CTSS	Encodes cathepsin S, a lysosomal protease involved in antigen processing and presentation in the immune system
CHRFAM7A	Encodes a cholinergic receptor, which may play a role in neurological functions and diseases
EFNA5	Encodes a member of the ephrin family, which are cell surface molecules that interact with Eph receptors to regulate cell adhesion and repulsion, influencing cell migration and axon guidance

Table 4: Functions of frequent common genes among top 10-most enriched GO of up-regulated genes

These results suggested that knocking-down the expression of NKX2-2 in GSC models appears to alter various signaling pathways related to cell surface modifications associated with cell adhesion and junctions.

Interestingly, there were fewer down-regulated DEGs compared to the up-regulated gene list. However, there were more GO terms associated enriched in this list, with 52 terms, while this number was only 22 for the up-regulated list. With the same filter and ranking applied to the up-regulated gene list, it revealed that shRNA-mediated *NKX2-2* knock-down significantly reduced the expression of genes related to *postsynaptic specialization membrane, cell surface, cell body, sulfur compound binding, glycosaminoglycan binding, cell adhesion, somatodendritic comportment* and *circulatory system development* (Fig. 54).

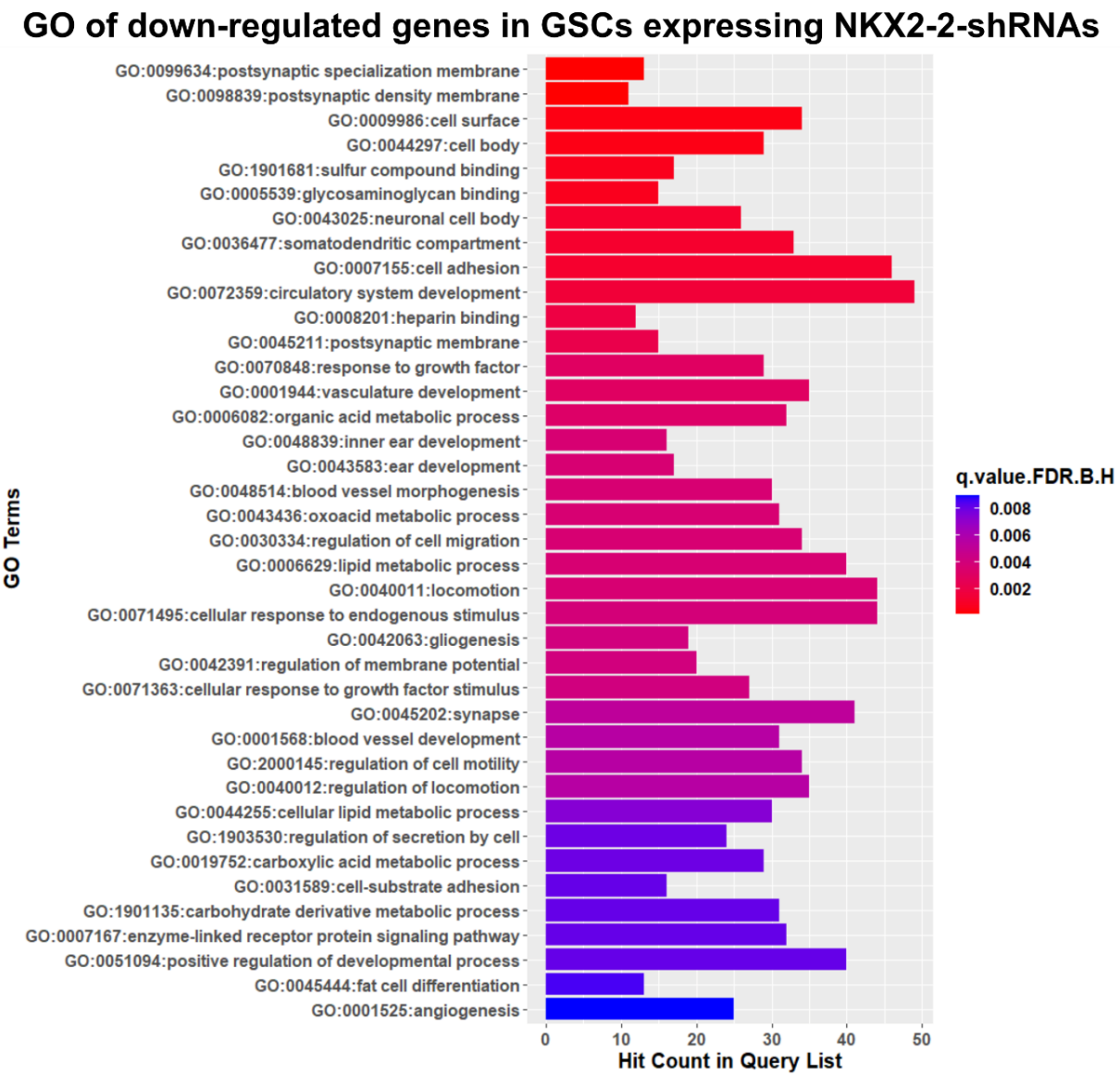

Figure 54: GO terms of down-regulated genes in *NKX2-2* KD cells

GO terms showing significant enrichment were identified within ontologies related to DEGs in GSC expression NKX2-2-shRNAs with a cut-off q-value FDR of Benjamini and Hochberg <=0.01.

The top four enriched gene ontologies did not exhibit any shared genes. However, 10 genes (out of 152 genes) were found to be common among at least five gene ontologies within the top ten most enriched categories: *ACTN2, NLGN3, PTPRF, PTPRZ1, RGS7BP, GRIK4, KCNK2, NTRK2, TGFB1* and *CCN3* (table 5). Notably, PTPRF and CCN3 were prevalent, appearing in eight and seven gene ontologies, respectively.

Genes	Full name	Brief function
ACTN2	Actinin Alpha 2	Actin-binding protein involved in cytoskeletal organization and muscle contraction
NLGN3	Neuroligin 3	Synaptic cell adhesion molecule involved in synapse formation and function
PTPRF	Protein Tyrosine Phosphatase Receptor Type F	Phosphatase involved in the regulation of cell signaling pathways
PTPRZ1	Protein Tyrosine Phosphatase Receptor Type Z1	Involved in neuronal development and plasticity
RGS7BP	Regulator of G-Protein Signaling 7 Binding Protein	Modulates signaling by G protein-coupled receptors
GRIK4	Glutamate Ionotropic Receptor Kainate Type Subunit 4	Glutamate receptor involved in synaptic transmission
KCNK2	Potassium Two Pore Domain Channel Subfamily K Member 2	Potassium channel involved in the regulation of membrane potential
NTRK2	Neurotrophic Tyrosine Kinase Receptor Type 2	Receptor for neurotrophins involved in neuronal survival and differentiation
TGFB1	Transforming Growth Factor Beta 1	Growth factor involved in various cellular processes including proliferation, differentiation, and apoptosis
CCN3	Cellular Communication Network Factor 3	Regulates cell proliferation, adhesion, migration, and survival

Table 5: Functions of frequent common genes among top 10-most enriched GO of down-regulated genes

Based on these results, *NKX2-2* is likely involved in multiple signaling pathways governing neuronal functions, such as neurotransmitter regulation and synapse transmission; or formation of neuron-tumor synapses. Furthermore, the reduction in *NKX2-2* expression levels resulted in the downregulation of genes involved in cytoskeletal organization, cell proliferation, and adhesion.

Remarkably, both overexpressed and down-regulated genes are implicated in cell surface modification, with 63 genes showing upregulation and 34 genes displaying downregulation. Conducting another GO analysis on each gene list revealed that the upregulated cell surface genes are associated with *transmembrane signaling receptors, binding processes, cell adhesion, immune cell activation, and antigenic binding*. Conversely, the downregulated genes are more involved in *positive regulation of phosphate metabolic processes, kinase activity, cell adhesion*, and *the MAPK cascade*.

To complement GO analyses, we performed a Gene Set Enrichment Analysis (GSEA) for examination of specific pre-ranked gene sets associated with pathways and functions. Interestingly, we observed that the DMG tumoroids post-*NKX2-2* depletion overexpressed genes associated with a neuroblasts signature (HNBM) than the control group (NES = 1.88, FDR < 0.001)(La Manno et al., 2016) (Fig. 55A). In contrast, gliospheres transduced with control shRNAs showed enriched expression of human Oligodendrocyte Progenitor Cell (HOPC) and human Radial Glia-Like 2B (HRGL2B) markers (NES = -2.92 and -2.55, respectively, FDR < 0.001) (Fig. 55B).

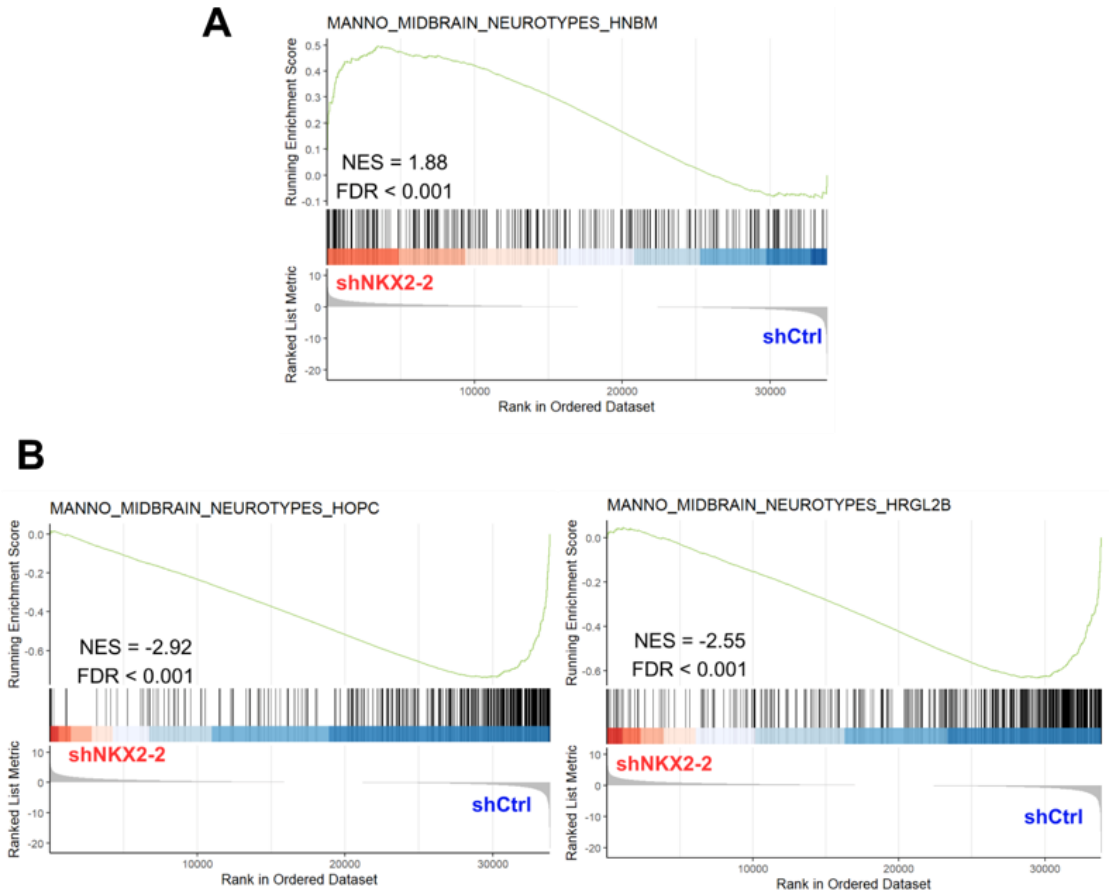

Figure 55: GSEA identified significantly enriched gene sets GSEA identified gene sets exhibiting significant overlaps with

A- genes that are overexpressed in GSC expressing shNKX2-2 compared to the control group and

B- genes that are downregulated in GSC expressing shNKX2-2 compared to the control group. The x-axis reflects the rank order of genes, while the barcode visually represents each individual gene of the gene set. The running enrichment score, depicted by a green line, illustrates the extent of enrichment, and each

plot provides information on the NES and FDR.

In addition, the markers associated with epithelial to mesenchymal transition (EMT) were identified as enriched among cells in the control condition (NES = -1.8, FDR < 0.001). Two other gene sets were notably identified as significantly activated (FDR < 0.01): angiogenesis (NES = -1.99) and apical junction (NES = -1.49) (Fig. 56).

The ten most downregulated genes associated with the EMT are *ITGAV, THBS2, IGFBP4, ADAM12, SGCD, NID2, MATN2, PRRX1, EFEMP2* and *COL11A1*. These genes are been reported to contribute to mediating cell-cell and cell-matrix interactions, as well as regulating the migratory machinery of cells.

The four selected GSC models were categorized into highly invasive cells, and the GSEA confirmed their OPC-like phenotype, with an additional radial-glial phenotype. Surprisingly, upon reduction of *NKX2-2* expression, GSC lost their OPC-like highly invasive phenotype albeit not showing an EMT gene signature characteristic of low invasive cells, as reported previously (Bruschi et al., 2023). Instead, they transitioned to a neuroblast identity, exhibiting down-regulation of EMT, angiogenesis and apical junction signatures compared to control conditions (Fig. 56).

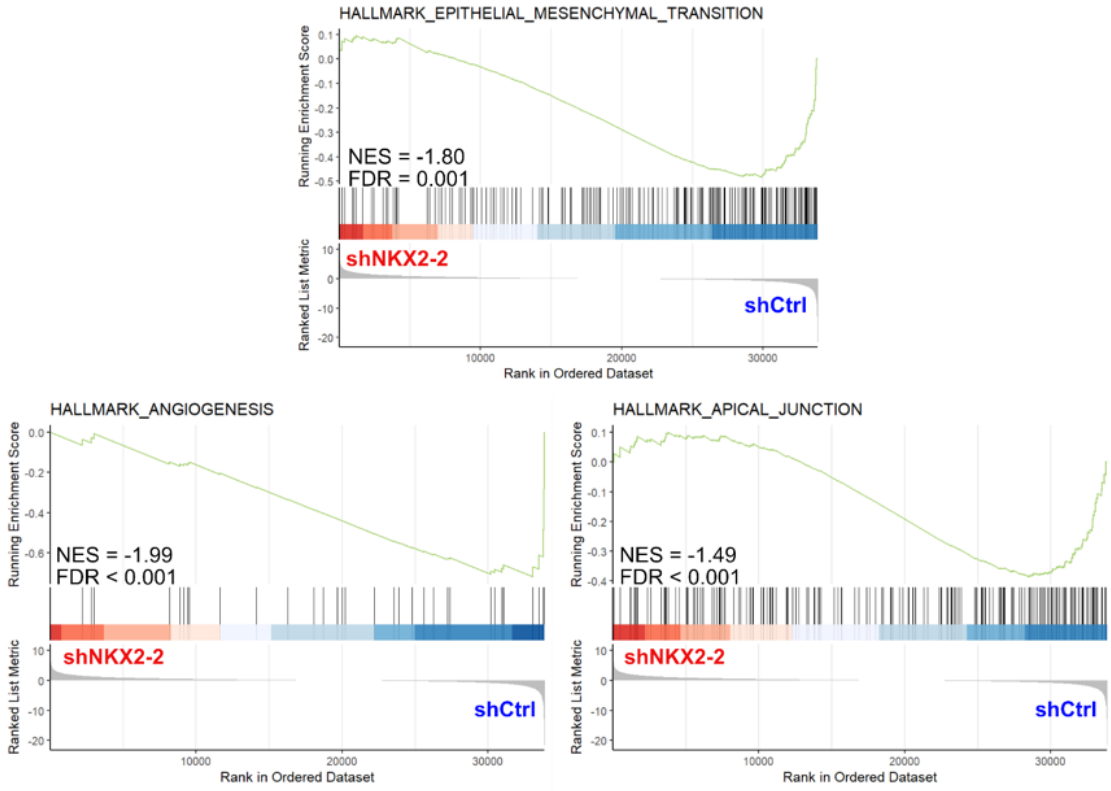

Figure 56: Enriched GSEA in GSC expressing control shRNAs over NKX2-2 shRNAs group

Geneset associated with EMT, angiogenesis and apical junction signatures were enriched in control condition compared with GSC *NKX2-2* KD condition.

3. Identification of common regulated genes associated with *NKX2-2* expression and High/Low invasion phenotype of DIPG GSC

Since transduction of NKX2-2-specific shRNAs on GSC resulted in a less invasive behavior, we aimed to investigate whether they exhibit similar enrichment patterns to tumoroids transcriptomic data from Bruschi *et al.* study, where highly invasive and moderately invasive 3D-GSC were compared (Bruschi et al., 2023). For this, we derived a specific GSEA geneset containing significantly differentially expressed genes from the study (n=339 upregulated genes and n=547 downregulated genes). GSEA was performed using the same pre-ranked gene list as in the GSEA analysis above. The results revealed that, as expected, GSC expressing control shRNAs exhibited an enrichment of genes up-regulated in highly invasive GSC 3D models (MB_UP). Interestingly, *NKX2-2* KD led to the enrichment of genes up-regulated in the

moderately invasive group (MB_DOWN) (Fig. 57) which correlated with the less invasive phenotype of this condition.

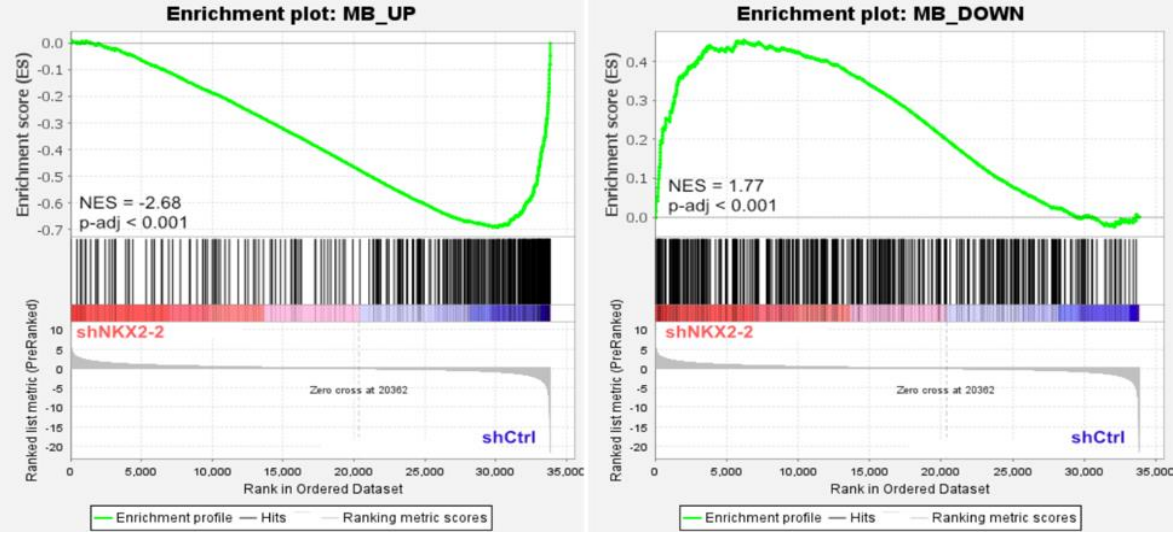

Figure 57: Comparison between differentially expressed genes of RNAseq data of this project and Bruschi et al. study

GSEA was carried out on genesets based on differentially expressed genes between highly and poorly invasive GSC in the study by Bruschi *et al.,* (Bruschi et al., 2023) using the pre-ranked gene list comparing shNKX2-2 vs. shCTRL GSC resemble highly invasive GSC whereas shNKX2-2 GSC resemble moderately invasive GSC.

Examining these data more closely, we identified 28 common genes between the up-regulated genes in highly invasive Glioma Stem Cells (GSC) and the up-regulated genes in GSC expressing control shRNAs. In other words, these genes were downregulated following *NKX2-2* knockdown and were typically overexpressed in highly invasive GSC. The majority of them are associated with cell adhesion and migration, as well as neuronal development and signaling pathways.

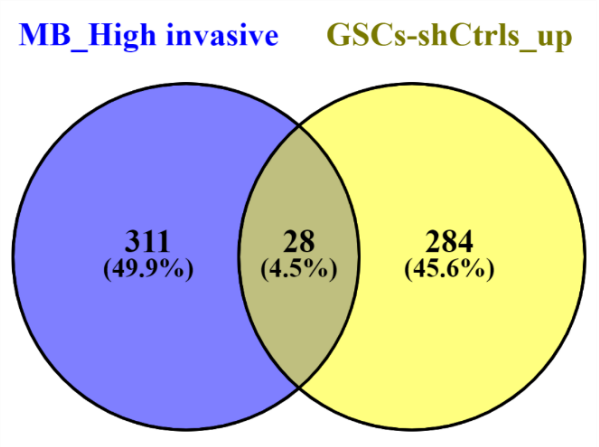

Common genes	Annotation	Function
NKX2-2	NK2 homeobox 2	Transcription factor involved in oligodendrocyte differentiation
ADGRA1	Adhesion G protein-coupled receptor A1	Part of the G protein-coupled receptor family, role in cell adhesion
ACSL6	Acyl-CoA synthetase long-chain family member 6	Involved in fatty acid metabolism
C2orf72	Chromosome 2 open reading frame 72	Associated with neurological disorders
SORCS3	Sortilin-related VPS10 domain-containing receptor 3	Regulates protein trafficking, involved in insulin signaling
AJAP1	Adherens junctions-associated protein 1	Associated with cell adhesion and migration
IGLON5	IgLON family member 5	Implicated in autoimmune neurodegenerative diseases
SOX8	SRY-box transcription factor 8	Transcription factor involved in embryonic development
TBX21	T-box transcription factor TBX21	Transcription factor expressed in specific region of telencephalon and involve in brain development, immune system regulation.
LHFPL3	Lipoma HMGIC fusion partner-like 3	May play a role in hearing
BRINP1	BMP/retinoic acid-inducible neural-specific protein 1	Involved in neuronal development and plasticity
TMEM132E	Transmembrane protein 132E	Involved in neural development, possibly linked to psychiatric disorders
RAPGEF4	Rap guanine nucleotide exchange factor 4	Involved in cell signaling and neuronal development
TAFA5	FAM19A5/Tafa5	Associated with brain development and function
RAP1GAP	Rap1 GTPase-activating protein	Regulates cell adhesion and migration
FGFBP3	Fibroblast growth factor-binding protein 3	Binds to fibroblast growth factors, potential role in cell growth
ACTN2	Actinin alpha 2	Structural protein in muscle cells
CSGALNACT1	Chondroitin sulfate N-acetylgalactosaminyltransferase 1	Involved in glycosaminoglycan biosynthesis
SUSD4	Sushi domain-containing protein 4	Cell adhesion molecule, potential role in cancer
FBXL16	F-box/LRR-repeat protein 16	Part of the ubiquitin-proteasome system, involved in protein degradation
CDHR1	Cadherin-related family member 1	Cadherin-related family member 1, cell adhesion molecule
TSPAN7	Tetraspanin-7	Involved in cell signaling and adhesion
PCDHAC2	Protocadherin alpha subfamily C2	Protocadherin alpha subfamily C2, cell adhesion molecule
HES4	Hes family bHLH transcription factor 4	Transcription factor, involved in cell fate determination
TSPAN11	Tetraspanin-11	Involved in cell signaling and adhesion
PDGFA	Platelet-derived growth factor subunit A	Growth factor, important in cell proliferation and development
TSPAN12	Tetraspanin-12	Involved in cell signaling and adhesion
GNG7	Guanine nucleotide-binding protein G(I)/G(S)/G(O) subunit gamma-7	Part of a G protein complex, involved in signaling pathways

Figure 58: Number and function of common genes between genes overexpressed in high invasive GSC models and overexpressed in GSC shCTLs

Venn diagram illustrating the number of common genes between the upregulated genes in High Invasion (Bruschi et al., 2023) and the upregulated genes in GSC expressing control shRNAs, along with the comprehensive list of these identified genes.

The same analysis was repeated for up-regulated genes in GSC expressing NKX2-2-shRNAs and in Low invasive models. There were 25 commons genes associating mainly to extracellular matrix, connective tissue, and epithelial cells (Fig. 59).

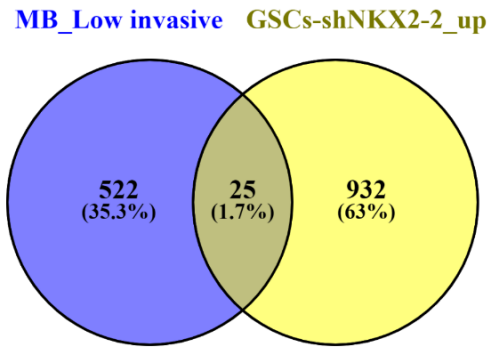

Common genes	Annotation	Function
SLC12A8	Solute Carrier Family 12 Member 8	Involved in ion transport, potential role in electrolyte balance.
BOC	Biregional CDO Homolog	Part of Hedgehog signaling pathway, implicated in development.
NEDD4L	Neural Precursor Cell Expressed, Developmentally Down-Regulated 4-Like	Regulator of protein degradation, involved in ubiquitination.
LRIG3	Leucine-Rich Repeats and Immunoglobulin-Like Domains 3	May play a role in cell adhesion and signaling.
PGM2L1	Phosphoglucomutase 2-Like 1	Function not well-defined, potential role in glucose metabolism.
FAM227A	Family with Sequence Similarity 227 Member A	Role not well-defined, requires further investigation.
TLL2	Tolloid-Like 2	Metalloproteinase involved in extracellular matrix remodeling.
NEK10	NIMA (Never In Mitosis Gene A)-Related Kinase 10	Regulator of cell cycle progression and mitosis.
IL1A	Interleukin 1 Alpha	Proinflammatory cytokine involved in immune response.
GBP2	Guanylate Binding Protein 2	Involved in host defense against pathogens.
TP63	Tumor Protein P63	Transcription factor crucial for epithelial development.
MIR3142HG	MIR3142 Host Gene	Host gene for a microRNA, specific function may vary.
FAM78B	Family with Sequence Similarity 78 Member B	Role not well-defined, requires further investigation.
SAMD3	Sterile Alpha Motif Domain Containing 3	May play a role in immune response and signal transduction.
SH3RF2	SH3 Domain-Containing Ring Finger 2	Involved in protein ubiquitination and degradation.
COL21A1	Collagen Type XXI Alpha 1 Chain	Structural component of collagen, role in connective tissue.
IL31RA	Interleukin 31 Receptor A	Receptor for interleukin-31, involved in immune response.
CRYBG1	Crystallin Beta-Gamma Domain Containing 1	Role not well-defined, potential involvement in eye development.
COL24A1	Collagen Type XXIV Alpha 1 Chain	Structural component of collagen, role in connective tissue.
KRT18	Keratin 18	Structural protein in epithelial cells.
GALNT6	N-Acetylgalactosaminyltransferase 6	Involved in glycosylation processes.
ADAMTSL1	ADAMTS-Like 1	Metalloproteinase with various roles in extracellular matrix.
COL1A2	Collagen Type I Alpha 2 Chain	Structural component of collagen, role in connective tissue.
SLIT3	Slit Guidance Ligand 3	Axon guidance and cell migration during development.
ABCA13	ATP Binding Cassette Subfamily A Member 13	Involved in cellular transport processes.

Figure 59: Number and function of common genes between genes overexpressed in

low invasive GSC models and overexpressed in GSC shNKX2-2s

Venn diagram displaying the shared genes between the overexpressed gene sets in GSC with Low Invasion and the upregulated genes in GSC expressing NKX2-2 shRNAs, along with a detailed list of these identified genes.

In summary, the downregulation of *NKX2-2* expression through shRNA transduction in four H3.3 DIPG GSC cell lines resulted in a reduction in invasion scores in 3D invasion assays. Although the decrease in invasiveness was not directly proportional to the reduction in *NKX2-2* levels, a modest correlation was observed with the initial expression levels of *NKX2-2* in DIPG cells. Furthermore, *NKX2-2* KD also slowed down the proliferation of GSC models and potentially induced alterations in cell morphology, characterized by shorter cell projections and changes in cell senescence. RNAseq analysis revealed that H3.3 DIPG GSC exhibited a transition from their original OPC-like identity to a neuroblast identity following *NKX2-2* KD, without acquiring the expected EMT phenotype associated with moderately invasive DIPG models. Additionally, GO and GSEA analyses suggested that NKX2-2 is involved in several signaling pathways regulating neurotransmitter regulation, synapse transmission, cytoskeletal reorganization, as well as cell proliferation and adhesion.

4. Epigenetic study of *NKX2-2* and histone mark H3K27ac in DIPG GSC

The transcriptomic data obtained from RNAseq provided us the changes in gene expression levels upon *NKX2-2* knock-down. Thereafter, a deeper investigation of *NKX2-2* epigenetic activity was conducted with the aim of identifying the genomic location of this transcription factor and therefore confirm the direct downstream genes regulated by *NKX2-2* as well as its influence on histone modifications in DIPG GSC.

In the recent years, a new method named Cleavage Under Targets and Tagmentation (or CUT&Tag for short) has been developed to analyze protein interaction with DNA which is based on the similar principles with ChIP-seq but with several advantages (Kaya-Okur et al., 2019). This strategy utilizes the Tn5 transposase to cleave chromatin and integrate the NGS adapters for the library preparation step. It exhibits increased sensitivity compared to ChIP-seq, attributed to its direct targeting of DNA bound by

the protein of interest. Consequently, it affords superior resolution while minimizing background noise. Moreover, this protocol requires less input material than ChIP-seq, is amenable to fresh samples, does not require sonication to avoid losing material, and boasts a shorter manipulation time than its ChIP-seq counterpart.

For this experiment, 500 000 cells of 3 GSC were transduced with control shC002 and shNKX2-2.1. Cells were harvested and processed freshly according to the recommended protocol. After cells were bound by Concanavalin A, 1 µg of *NKX2-2*-specific antibody or H3K27ac-target antibody was added, and samples were incubated overnight at 4°C. The secondary antibody compatible with the first antibody was incubated the next day, followed by the binding of pA-Tn5 transposase and then tagmentation. Subsequently, DNA was extracted by phenol/chloroform and collected by ethanol precipitation. The DNA was amplified by PCR with 14 cycles to insert the unique indexed primers and then purified twice. Library quality and quantity were confirmed by Bioanalyzer using the High Sensitivity DNA kit and by Qubit using 1X dsDNA High Sensitivity, respectively, before being sent for sequencing with 10M sequence reads. However, NEM290-shC002 targeted *NKX2-2* was performed with 1.3M sequence reads due to the low concentration of the library.

A bioinformatician in the lab processed the data and performed the analysis according to the nf-core/cutandrun pipeline (Ewels et al., 2020). Since it was the first time that the CUT&Tag technique was performed in my host laboratory and there has been no report about using the *NKX2-2* specific antibody for CUT&Tag, it was important to verify the Quality Control (QC) of the sequenced samples. The mean Quality Scores showed that after adapter trimming, all the sequences fell into Phred score 30 or above (except for a few beginning base pairs of *NKX2-2* CUT&Tag sample of NEM292 expression COO2 shRNA (Fig. 60A, green line). Besides that, all samples showed an overall high alignment rate with more than 99% and the pair ends (PE) mapped uniquely was more than 47% for all samples (Fig. 60B).

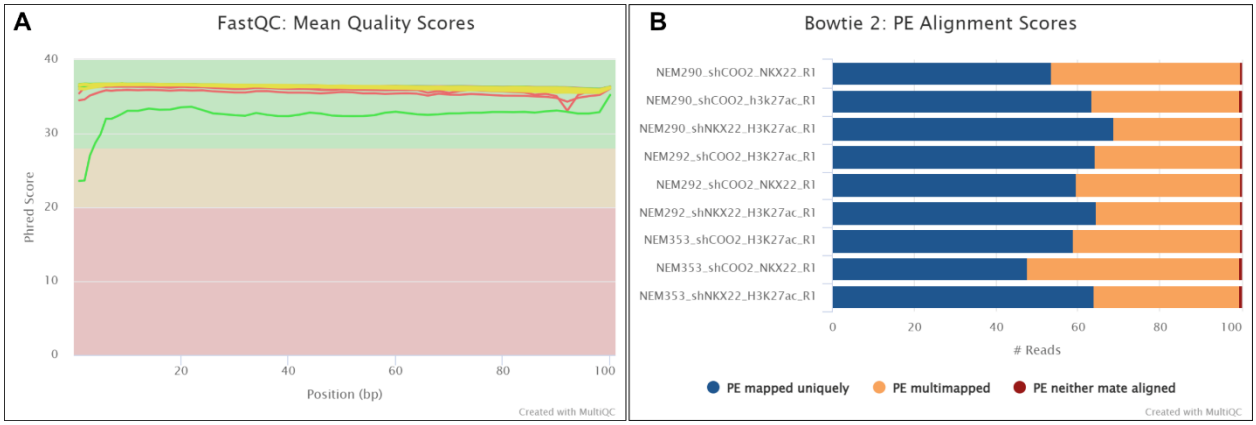

Figure 60: Quality control report of CUT&Tag data

A- After adapter trimming, Mean quality scores across each base position for the sequencing reads; a green box signifies successful QC, while orange and read boxes indicate warning and failure, respectively. Yellow lines: NEM290; Red line: NEM353; Green line: NEM292.

B- Percentage of reads aligning using Bowtie2 to the reference.

Overall, all six sequencing results passed the quality control check and were deemed suitable for further analysis.

1.1. Genome-wide profile of *NKX2-2* in DIPG cells

A heatmap was generated to visualize the enrichment peaks of *NKX2-2* across the three control-shRNA samples. The *NKX2-2* CUT&Tag peaks in NEM292, exhibited the highest global intensity among the three cell lines, exceeding 15. Following this, NEM353 showed an intensity of 2, with NEM290 displaying the least intensive peak signal (Fig. 61A).

The *NKX2-2* binding peaks were enriched at upstream regions (±3kb) from the TSS, and signals were detected around the Transcription End Site (TES) in all three selected GSC. It is noteworthy that, despite NEM292 exhibiting fewer peaks than the other two cell lines, it unexpectedly showed stronger intensity compared to NEM290 and NEM353, with the peak intensity being over 1.25, while the data for NEM290 and NEM353 were above 0.8 and 1, respectively (Fig. 61B).

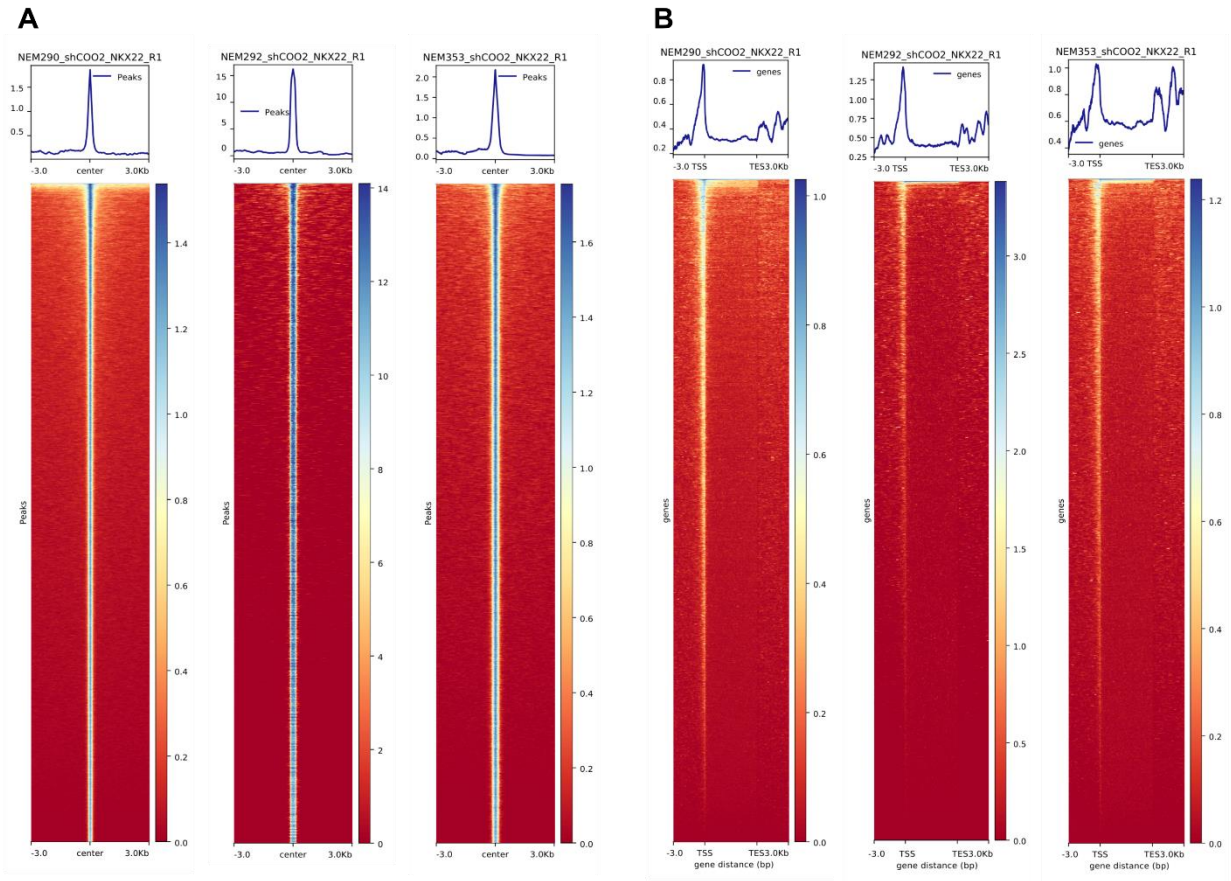

Figure 61: Heatmap visualization NKX2-2 peaks in GSC expression control shRNA:

A- Heatmap illustrating *NKX2-2* enrichment in peaks.

B- Heatmap displaying *NKX2-2* enrichment around genes in three DIPG GSC cell lines under the control-shRNA condition.

In the control-shRNA groups of NEM290, NEM292, and NEM353, a total of 4 838, 3 480 and 27 700 peaks of *NKX2-2* were detected, respectively. This indicates a significantly higher number of significant *NKX2-2* peaks detected in NEM353 compared to the others, about 5.7 times and 7.9 times higher than NEM290 and NEM292, respectively. Meanwhile, the difference between NEM290 and NEM292 was 1 358 peaks, accounting for 28%-39% of the total peaks of each of these models (Fig. 62A). However, despite the substantial disparity in peak quantity, the average peak width under control conditions for these three GSC models did not correspond with peak numbers. Overall, NEM290 had the largest *NKX2-2* peaks while NEM292 had the narrowest ones, measuring 431.5 and 361.4 bp, respectively (Fig. 62B).

Interestingly, the peak annotation revealed that despite variations in the number of recorded peaks, all GSC showed most enrichment in promoters (<1kb), introns and distal intergenic regions. Both NEM292 and NEM353 shared a similar pattern with the majority of *NKX2-2* peaks equally enriched in introns, promoters (<1kb), and distal intergenic regions (Fig. 62C, D). In contrast, NEM290 exhibited a different pattern, with the majority of peaks detected in the promoter (<1kb) region and fewer peaks in introns or distal intergenic regions (Fig. 62D). Accordingly, the distance for the majority of peaks relative to the Transcription Start Site (TSS) was at <1kb from the TSS or at 10-100kb (Fig. 62E). This suggests direct binding of *NKX2-2* to gene expression regulation sites and that *NKX2-2* binds both to proximal enhancers and distal enhancers to regulate gene expression potentially contributing to tissue-specific or developmental gene regulation.

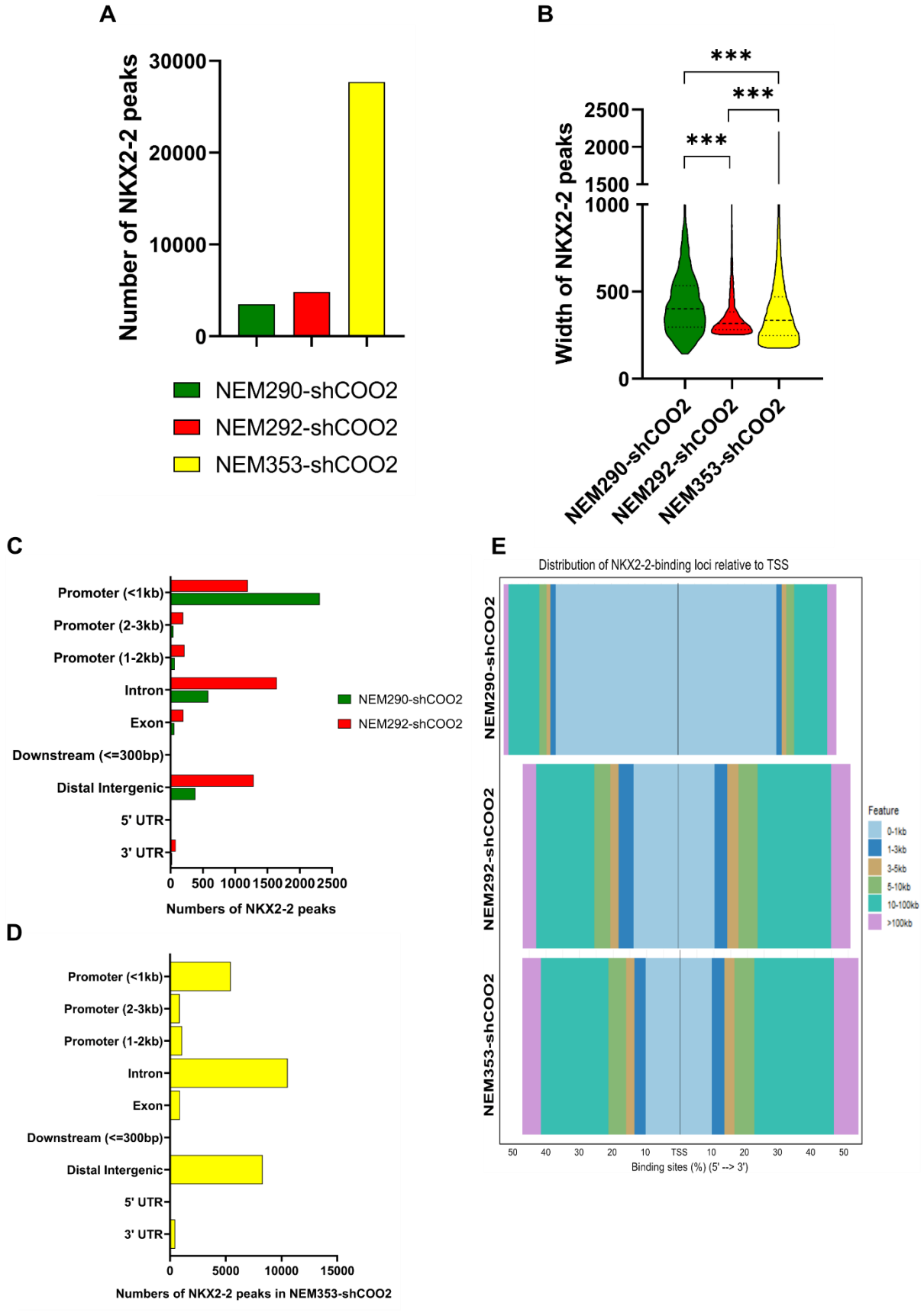

Figure 62: Overall about NKX2-2 peaks in GSC control shRNA

A- Total number of *NKX2-2* binding peaks under the control-shRNA condition in GSC NEM290 (green), NEM292 (red), and NEM353 (yellow)

B- Width distribution of *NKX2-2* binding peaks.

C- Annotation of *NKX2-2* binding peaks on GSC NEM290 and NEM292 carrying control shCOO2.

D- Annotation of *NKX2-2* binding peaks on GSC NEM353-shCOO2.

E- Distribution of *NKX2-2* binding peaks relative to the TSS.

Biological process gene ontology analysis was next conducted using the Toppfun portal to examine the enriched processes associated with genes nearest to *NKX2-2* peaks, with the top 20 most-enriched processes in each model selected for display (Fig. 63A). Overall, all GSC models shared three commonalities (815 genes) related to neuron development, CNS development, and neuron projection development. Consistent with previous findings, NEM292 and NEM353 exhibited eight additional shared biological processes related to cytoskeleton organization, cell projection morphogenesis, and synapse organization, underscoring the importance of cytoskeletal dynamics, neuronal connectivity, and synaptic function. In addition to these similarities, each model displayed distinct features reflecting various aspects of neuronal differentiation, connectivity, and tissue organization (Fig. 63B, C). NEM290 demonstrated enrichment in a different set of processes (638 genes) related to intracellular transport, organelle organization, and the mitotic cell cycle. This suggests a focus on processes essential for cellular division and organelle maintenance, which may indirectly contribute to neuronal development. Conversely, nearest genes to *NKX2-2* peaks exclusively found in NEM292 (976 genes) were enriched in cell adhesion, synapse organization, and synaptic signaling, indicating a particular emphasis on neuronal connectivity and communication. Meanwhile, results from NEM353 showed enrichment in processes related to GTPase-mediated signal transduction, circulatory system development, and actin organization, suggesting potential interactions between neural and vascular development pathways (9635 genes) (Fig. 63B, C).

Interestingly, the results showed that all three GSC shCTL shared peaks near cadherin genes such as *CDH1, CDH2, CDH11*, and *CDH13*, suggesting the involvement of *NKX2-*

2 KD in the modulation of cell-cell adhesion.

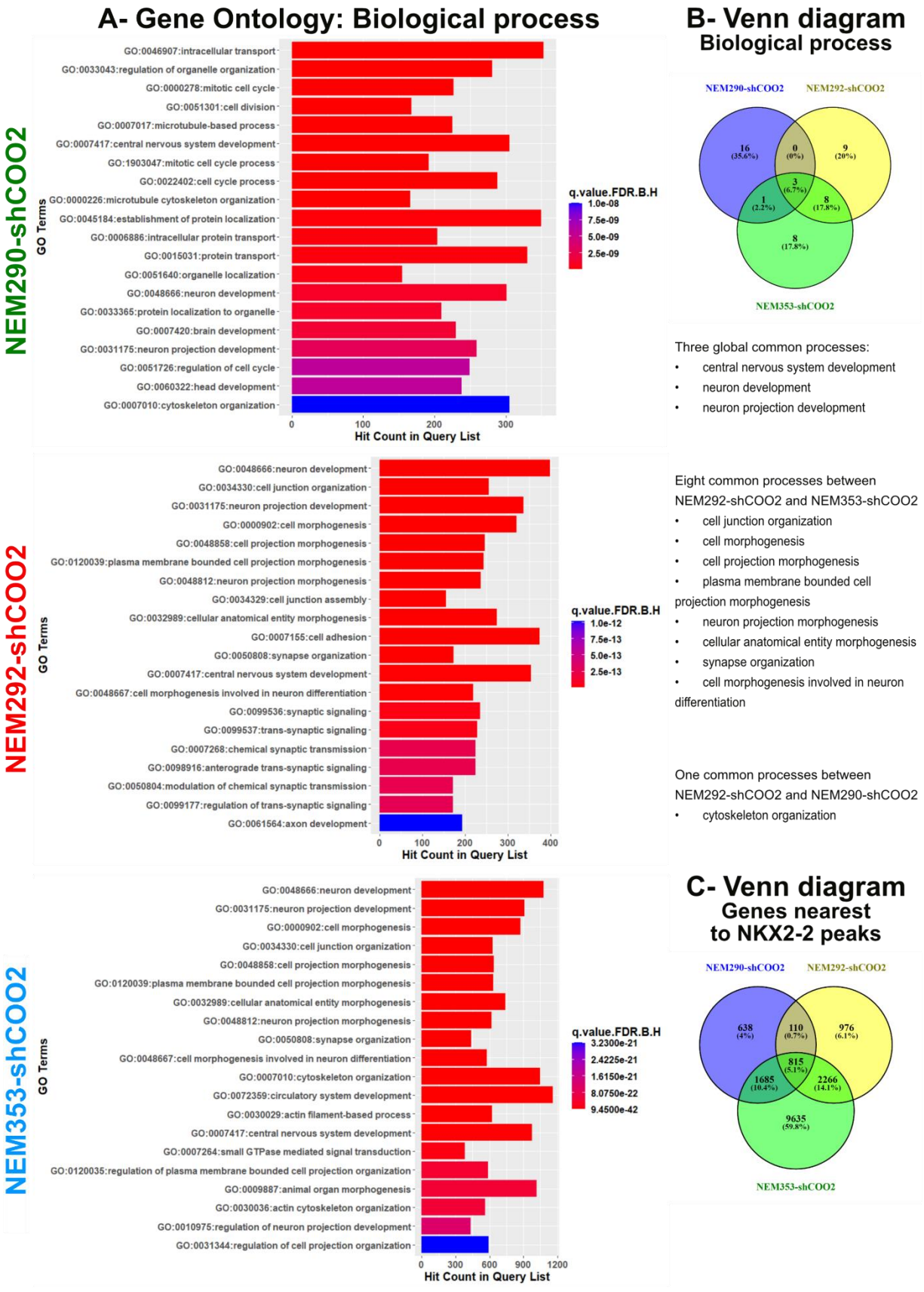

Three global common processes:

- central nervous system development
- neuron development
- neuron projection development

Eight common processes between NEM292-shCOO2 and NEM353-shCOO2

- cell junction organization
- cell morphogenesis
- cell projection morphogenesis
- plasma membrane bounded cell projection morphogenesis
- neuron projection morphogenesis
- cellular anatomical entity morphogenesis
- synapse organization
- cell morphogenesis involved in neuron differentiation

One common processes between NEM292-shCOO2 and NEM290-shCOO2

- cytoskeleton organization

Figure 63: Biological process analysis of genes proximal to NKX2-2 binding peaks

A- Biological process analysis of genes proximal to NKX2-2 binding peaks

B- Venn diagram comparing biological process enriched between three GSC models carrying COO2-control shRNAs

C- Venn diagram comparing genes-nearest-to-peaks in COO2-control shRNAs GSC models.

Peak intensity at locus of genes related to neuron development showed that NEM290 (green) had the cleanest profile, while peaks in NEM353 (rose) were weaker compared to the others (Fig. 64).

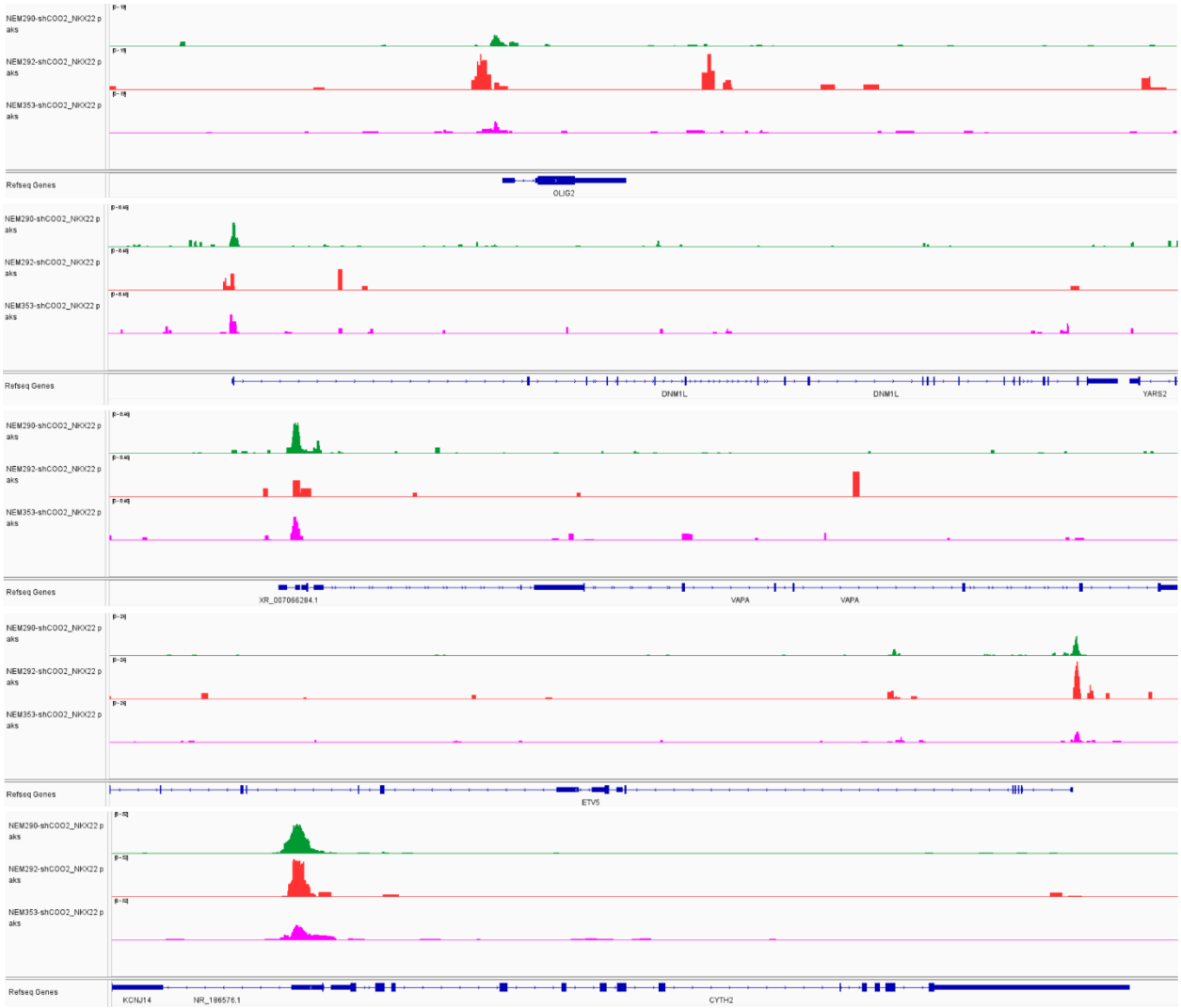

Figure 64: IGV visualization of NKX2-2 peaks at different locus of genes related to neuron development

Order from top to bottom: OLIG2, DNM1L, VAPA, ETV5, CYTH2.

I then focused on the Reactome pathway analysis of genes associated with *NKX2-2*

binding peaks to further investigate the potential functions of these genes and understand the role of *NKX2-2* in regulating its target genes. The results revealed that among the three GSC models with control shRNAs, the most closely related pathway, and the only redundant one, was the RHO GTPase cycle. This pathway is crucial for modulating glioma cell invasion by rearranging the actin cytoskeleton (Fortin Ensign et al., 2013; Kwiatkowska et al., 2012) (Fig. 65). Notably, the *NKX2-2* peaks were found to be involved in pathways related to cell cycle progression and microtubule and cytoskeleton dynamics, all of which are crucial for cell division progression. Additionally, NEM292 and NEM353 shared a few other common pathways, such as the neuronal system and the RAC1 GTPase cycle, indicating a more extensive involvement in neuronal development and synaptic transmission. However, transcription factor *NKX2-2* in NEM292 seemed to play a role on cell-cell interactions and synaptic plasticity, while in NEM353, it appeared to be more involved in angiogenesis (Fig. 65).

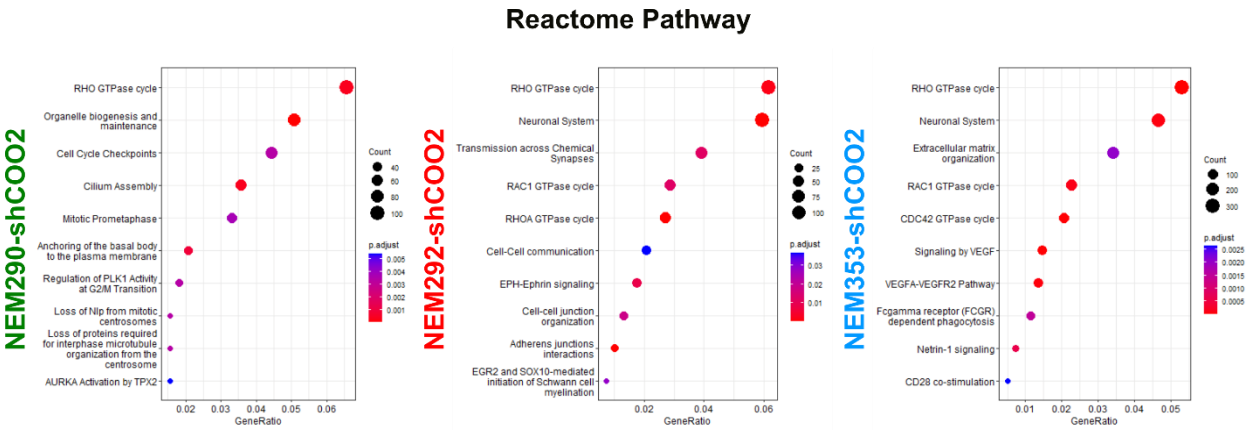

Figure 65: Reactome pathway analysis of genes proximal to *NKX2-2* binding peaks

NKX2-2 has been identified as a dual transcription factor, capable of acting as either an activator or a suppressor (Fadul et al., 2015; Muhr et al., 2001; Watada et al., 2000). By intersecting the differentially expressed genes identified from RNAseq data with the genes nearest to NKX2-2 peaks obtained from CUT&Tag data, a deeper understanding of NKX2-2's role in specific biological processes or target genes can be achieved.

However, comparing the number of similar genes between genes related to NKX2-2 peaks with either overexpressed genes or underexpressed genes did not yield a

dominant result for either condition. Therefore, I could not make any assumptions about the role of NKX2-2 in NEM290 and the other two models (Fig. 66).

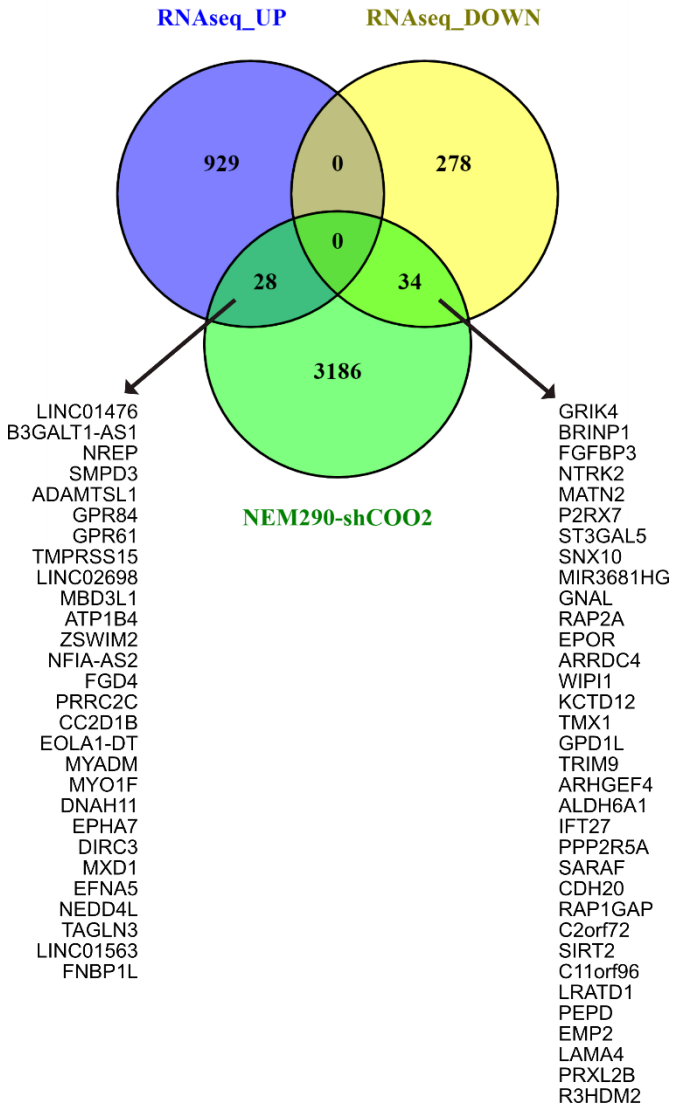

Figure 66: Intersecting DEG from RNAseq data and gene-nearest to NKX2-2 peaks

RNA_UP: Overexpressed genes in RNAseq; RNA_DOWN: Downregulated genes in RNAseq.

The overexpressed or downregulated genes identified from RNAseq data were compared with NKX2-2 peaks detected in at least 2 out of 3 shCOO2 GSC samples. Eight upregulated genes were found to have NKX2-2 binding sites nearby in all three GSC expressing shCOO2. These genes include LINC02698, NEDD4L, MYO1F, MXD1, ZSWIM2, DIRC3, EFNA5, and NREP (Fig. 67). Analysis of peaks shared in at least 2 GSC shCOO2 samples revealed that NKX2-2 acted as an inhibitor of 90 genes,

predominantly involved in various cellular processes such as cell-cell communication (EPHA7, GPR149, IL15, and AGTR2), cytoskeleton dynamics and migration (MYO1F, FGD4, and MYH11), cell fate determination and tissue patterning (PAX7, TFAP2B, and ERG), ECM and cell-cell adhesion (DSP, COL6A5, and BOC), as well as neuronal development and synaptic function (EFNA5, NREP, and SVOP).

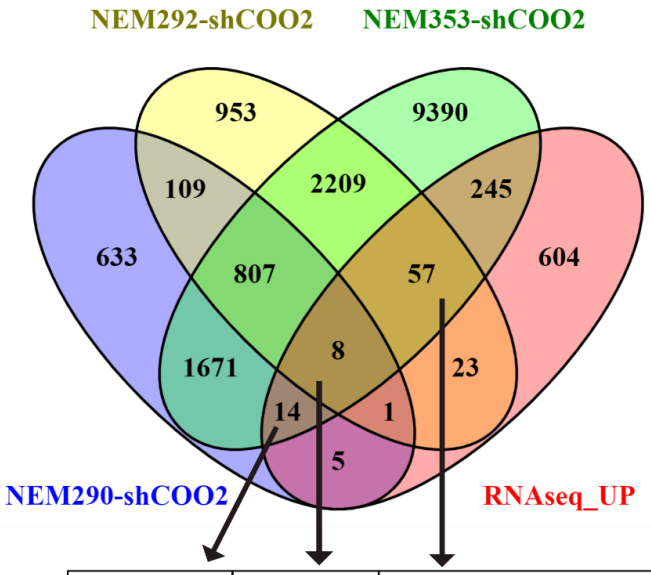

CC2D1B	LINC02698	PAX7	MGAT4C	LINC00494	HCP5
FNBP1L	NEDD4L	LDC1P	SVOP	LINC01271	ADGRF1
PRRC2C	MYO1F	CSF3R	CATSPERB	MIR99AHG	TFAP2B
FGD4	MXD1	RSPO1	PLA2G4F	KCNJ15	LINC02532
SMPD3	ZSWIM2	LINC01725	EWSAT1	ERG	LINC02534
LINC01563	DIRC3	SMG7-AS1	FAM169B	UMODL1	TRDN
LINC01476	EFNA5	CACNA1S	MYH11	ZNRF3-AS1	TRPV6
MYADM	NREP	RYR2	MYOCD	RIBC2	UNC5D
B3GALT1-AS1		LINC01516	CELF4	BOC	CLVS1
EPHA7		CRTAC1	MUC16	COL6A5	SULF1
DNAH11		MUC5B	PLB1	GPR149	LINC01231
ADAMTSL1		IQSEC3	LINC01122	IL15	SHOC1
ATP1B4		LMO3	SLC4A5	SLIT3	GLRA2
EOLA1-DT		LRIG3	SH2D6	DSP	XACT
					AGTR2

Figure 67: Common genes between overexpressed gene in RNAseq data and NKX2-2 peaks to the nearest-gene annotation.

Genes	Full name	Brief function
LINC02698	Long non-coding RNA (lncRNA)	Further experimental studies would needed to be done
NEDD4L	Neural precursor cell expressed developmentally down-regulated 4-like	Regulating of ion channels, membrane transporters, and signaling pathways
MYO1F	Myosin 1F	Interacting with actin filaments and generating mechanical force to drive cellular movement and membrane dynamics
MXD1	MAX dimerization	By repressing the transcription of target genes, MXD1 regulates various cellular processes, including cell cycle progression, differentiation, and apoptosis
ZSWIM2	Zinc Finger SWIM-Type Containing 2	Further experimental studies would needed to be done
DIRC3	Disrupted In Renal Carcinoma 3	May play a role in tumor development and progression
EFNA5	Ephrin-A5	Mediating cell-cell communication and regulating cell adhesion, migration, axon guidance, and synaptogenesis. EFNA5 specifically has been implicated in neuronal development, synaptic plasticity, and angiogenesis
NREP	Neuronal Regeneration-Related Protein	Regulating neurite outgrowth, axon guidance, and synaptic function thus may play a role in neuronal development, repair, and maintenance processes in the central nervous system

Table 6: Function of over-regulated genes which are near to NKX2-2 peaks

There were 11 downregulated genes common among all three GSC control samples that also exhibited nearby NKX2-2 peaks. In total, considering a peak as common if it was detected in 2 out of 3 samples, there were 66 genes overlapped with the NKX2-2 peaks list. Consequently, NKX2-2 may act as an activator of genes involved in cell signaling regulation (PPP2R5A, ARRDC4, EPOR, ARHGEF4, TRIM9, PTPRU, PTPRF, and RAPGEF4), ion channel activity (GRIK4, P2RX7, KCNK2, and KCNIP1), cell adhesion and interaction (CDH20, AJAP1, LAMA4, and TSPAN11), as well as neuronal functions including axon guidance and synaptic function (NTRK2, SEMA5A, ITGB8, LHFPL3, and DAAM) (Fig. 68).

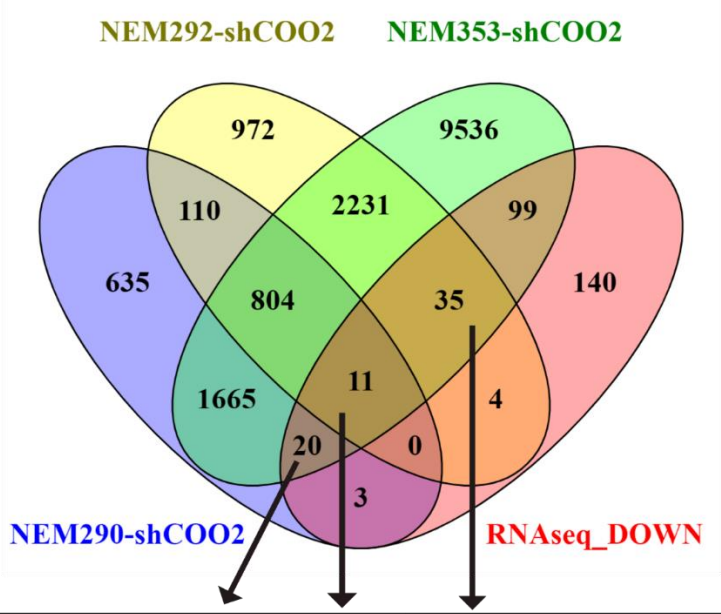

FGFBP3	C2orf72	PPP2R5A	AJAP1	NT5M	ITGB8
C11orf96	LAMA4	GRIK4	PTPRU	RAB31	ADCYAP1R1
R3HDM2	SNX10	ARRDC4	PTPRF	RAPGEF4	PDE1C
P2RX7	NTRK2	WIPI1	KCNK2	TAFA5	VWC2
KCTD12	BRINP1	CDH20	SUSD4	MGLL	LHFPL3
RAP2A		EPOR	PLPP4	KIT	
TRIM9		ARHGEF4	CHST15	SEMA5A	
TMX1		IFT27	ADAM12	GHR	
ALDH6A1		GPD1L	SCART1	RGS7BP	
GNAL		SARAF	B4GALNT4	MCTP1	
PEPD		MATN2	TSPAN11	SGCD	
SIRT2			CPM	KCNIP1	
MIR3681HG			SAMD4A	DAAM2	
LRATD1			BEGAIN	AKAP7	
ST3GAL5			NTN1	FAM20C	

Figure 68: Common genes between down-expressed gene in RNAseq data and NKX2-2 peaks to the nearest-gene annotation.

1.2. Genome-wide changes of H3K27ac profiles in DIPG cells with and without *NKX2-2*-shRNA

Given the impossibility of directly studying the interaction between the *NKX2-2* transcription factor and DNA in GSC samples with *NKX2-2* targeting shRNA, my next objective was to investigate the impact of *NKX2-2* knockdown through an indirect approach. H3K27ac is a histone modification associated with active enhancers and promoters. The binding of *NKX2-2* to its specific gene sequences might lead to the deposition of H3K27ac and the activation of nearby genes. Furthermore, H3K27ac also marks accessible chromatin regions, which can facilitate the binding of transcription

factors such as *NKX2-2*. Here, I would like to correlate the H3K27ac transcription activity with the NKX2-2 expression. Therefore, examining the binding peaks of H3K27ac with and without the presence of *NKX2-2* shRNA could provide valuable insights not only into the interplay between *NKX2-2* and H3K27ac.

Interestingly, while all three GSC exhibited signal enrichment within a ±3kb around the TSS and weak signal around the TES, NEM290 displayed distinct H3K27ac binding peak data compared to NEM292 and NEM353. In NEM290, H3K27ac CUT&Tag peaks with control-shRNA showed the highest intensity (almost 3) along upstream regions (±3kb) from the TSS, but this intensity dramatically dropped to 0.8 with the introduction of *NKX2-2*-shRNA. Conversely, NEM292 and NEM353 exhibited a similar signal density of about 0.6 under control conditions, with a slight increase to 0.8 following the decrease in *NKX2-2* expression (Fig. 69A).

This trend was similarly observed when examining histone modifications around the peak center, where there was an approximate 3-fold decrease in intensity with *NKX2-2* knockdown in NEM290, while peak enrichment at the center increased in NEM292 and NEM353 following *NKX2-2* knockdown (Fig. 69B).

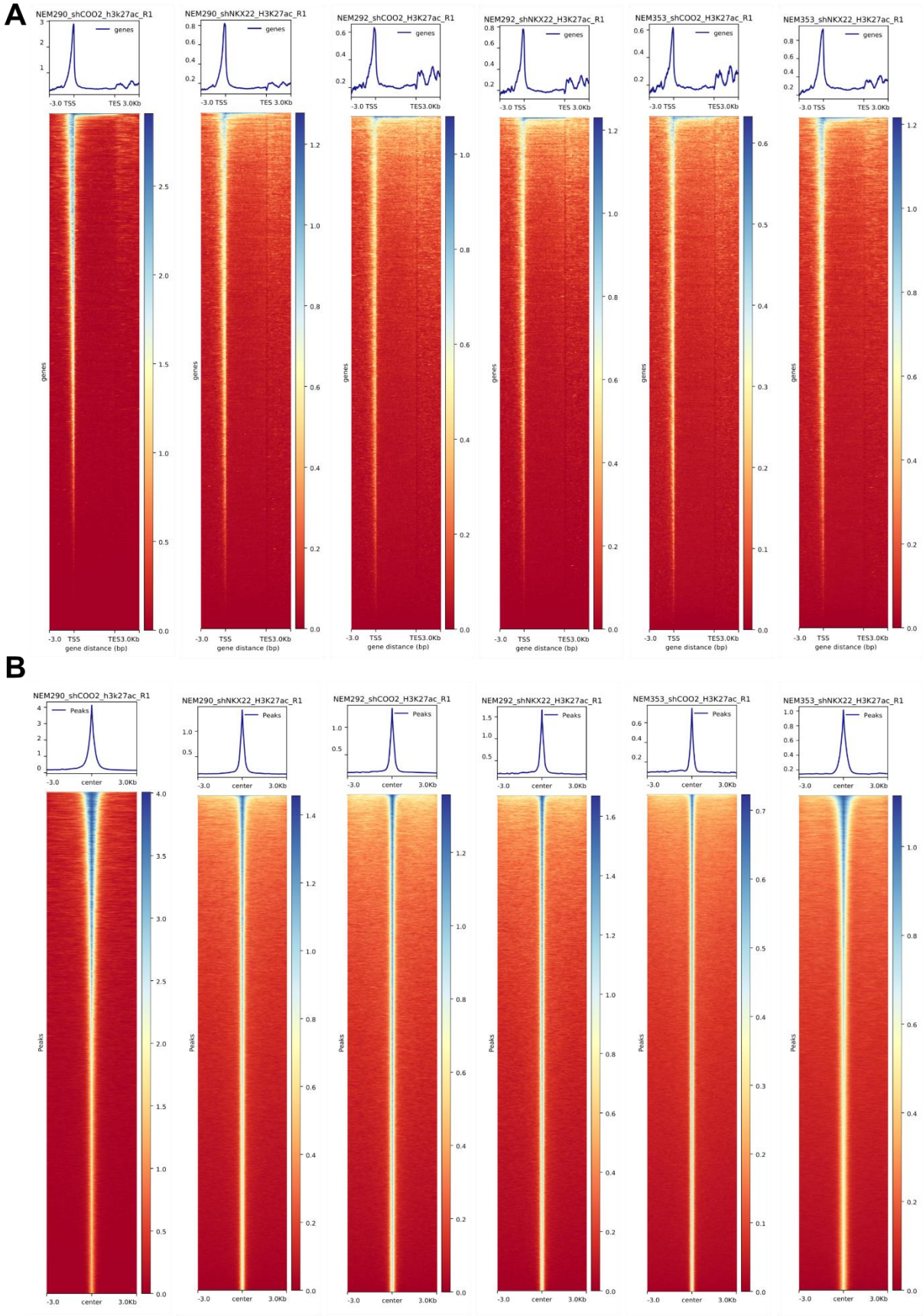

Figure 69: Heatmap visualization NKX2-2 peaks in GSC expression control shRNA

A- Heatmap depicting H3K27 peaks around genes in three DIPG GSC cell lines under the control-shRNA and *NKX2-2*-shRNA condition

B- Heatmap representing the enrichment of H3K27ac in peaks.

The results obtained from the analysis of H3K27ac peaks revealed notable variations among the three GSC models upon the knock-down of *NKX2-2*. Both NEM290 and NEM353 demonstrated a reduction in peaks following the knock-down of *NKX2-2*. Specifically, in NEM290, the number of peaks decreased from 12 752 under the shCOO2 control condition to 6 492 under shNKX2-2, while in NEM353, it decreased from 6 937 to 4 739 under the respective conditions. Conversely, NEM292 displayed a contrasting trend, with a substantial increase in total peaks observed after the introduction of shRNA targeting *NKX2-2*. Under the shCOO2 control condition, NEM292 exhibited 4 434 peaks, whereas this number significantly rose to 13 638 after the knockdown of *NKX2-2*. Among three GSC models, NEM290 displayed the most significant enriched H3K27ac peaks under the control condition compared to the others (Fig. 70A). Analysis of peaks width revealed that both NEM290 and NEM292 exhibited narrower peaks after *NKX2-2* knock-down, whereas NEM353 displayed broader peaks following the knock-down (Fig. 70B). These observations underscore the necessity of increasing the replication of this experiment to confirm the results.

The variations in peak numbers observed within each cell model are reflected in their global enrichment properties. Peak annotation analysis revealed that the majority of H3K27ac peaks were primarily enriched in promoters (<1kb), intronic regions, and distal intergenic regions, maintaining a consistent ranking of peak abundance across the models (Fig. 70C). Concerning the distance of peaks relative to the TSS, all models exhibited peaks within distances of 0-1kb and 10-100kb from the TSS (Fig. 70D). Interestingly, NEM292 and NEM353 displayed a slight increase in peaks within the <1kb region from the TSS, whereas a slight reduction in peaks located less than 1kb from the TSS was observed in NEM290 (Fig. 70D).

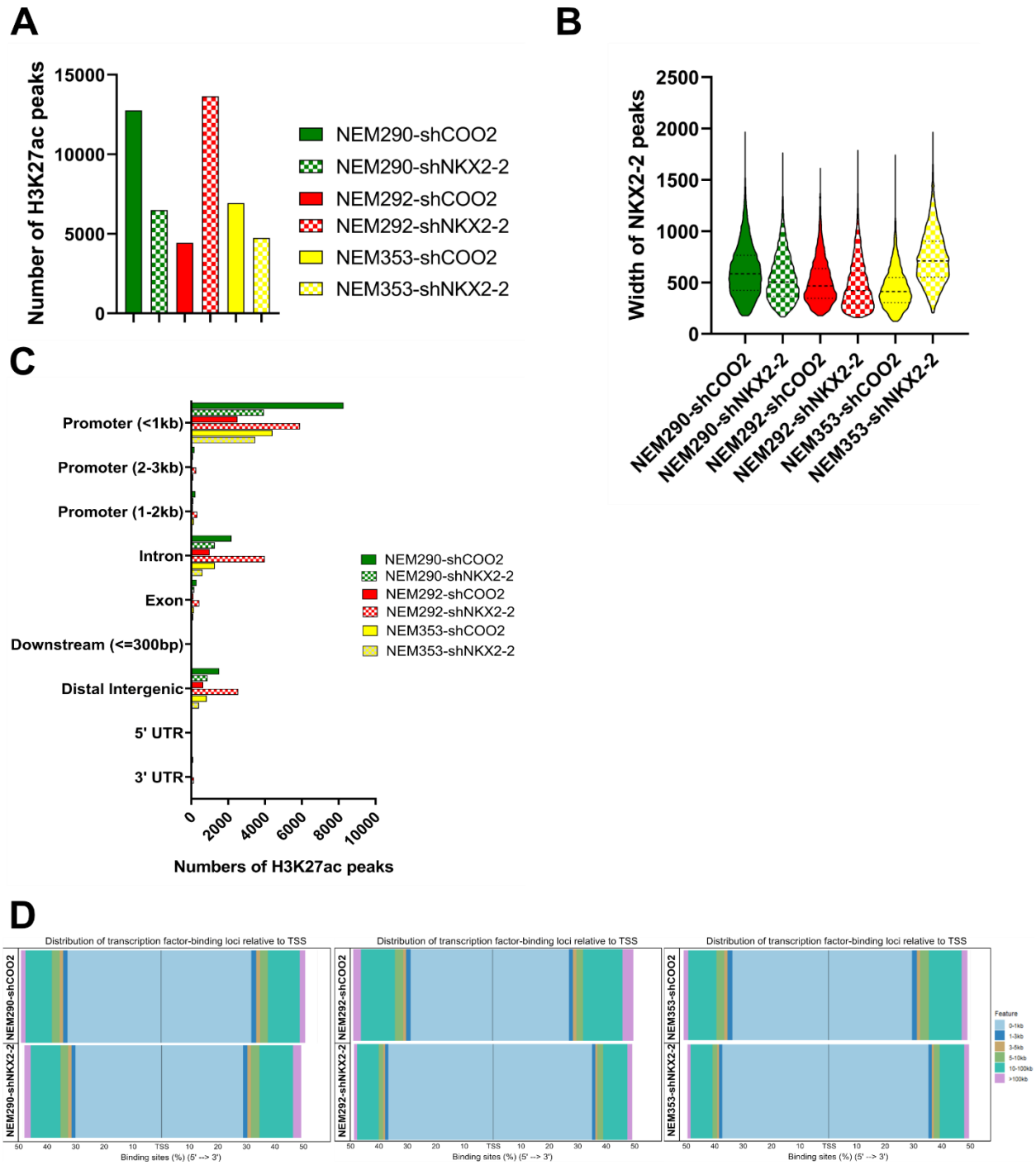

Figure 70: Overall about H3K27ac peaks in GSC control shRNA and GSC *NKX2-2* KD

A- Total number of H3K27ac binding peaks under the control-shRNA and *NKX2-2*-shRNA conditions in GSC NEM290 (green), NEM292 (red), and NEM353 (yellow).

B- Width distribution of H3K27ac binding peaks.

C- Annotation of H3K27ac binding peaks.

D- Distribution of H3K27ac binding peaks relative to the TSS.

The gene ontology analysis of control condition on NEM290, NEM292, and NEM353

revealed both shared and unique biological processes enriched in each cell model (Fig. 71A, B, C). NEM290-shCOO2 exhibited a diverse range of processes, including those involved in intracellular transport, mitotic cell cycle regulation, and establishment of protein localization. Additionally, processes related to DNA metabolism, cell division, and microtubule dynamics were prominent. Unique to NEM290-shCOO2 was the involvement of processes such as modification-dependent macromolecule catabolism and cell morphogenesis, highlighting its distinct functional landscape. In contrast, NEM292-shCOO2 demonstrated enrichment in mRNA metabolism, protein catabolic processes, and membrane organization, suggesting its role in gene expression regulation and cellular homeostasis. Notably, DNA repair processes, RNA splicing and histone modification were exclusive to NEM292-shCOO2 (792 genes), emphasizing its importance in maintaining genomic integrity. On the other hand, NEM353-shCOO2 shared several processes with NEM290-shCOO2 (2 915 genes), including those related to intracellular transport, mitotic cell cycle regulation, and DNA metabolism. Additionally, NEM353-shCOO2 exhibited unique processes such as regulation of cellular stress response and small GTPase-mediated signaling, indicating its involvement in cellular stress adaptation and signaling pathways. These findings underscore the complex and multifaceted nature of biological processes in DIPG GSC models.

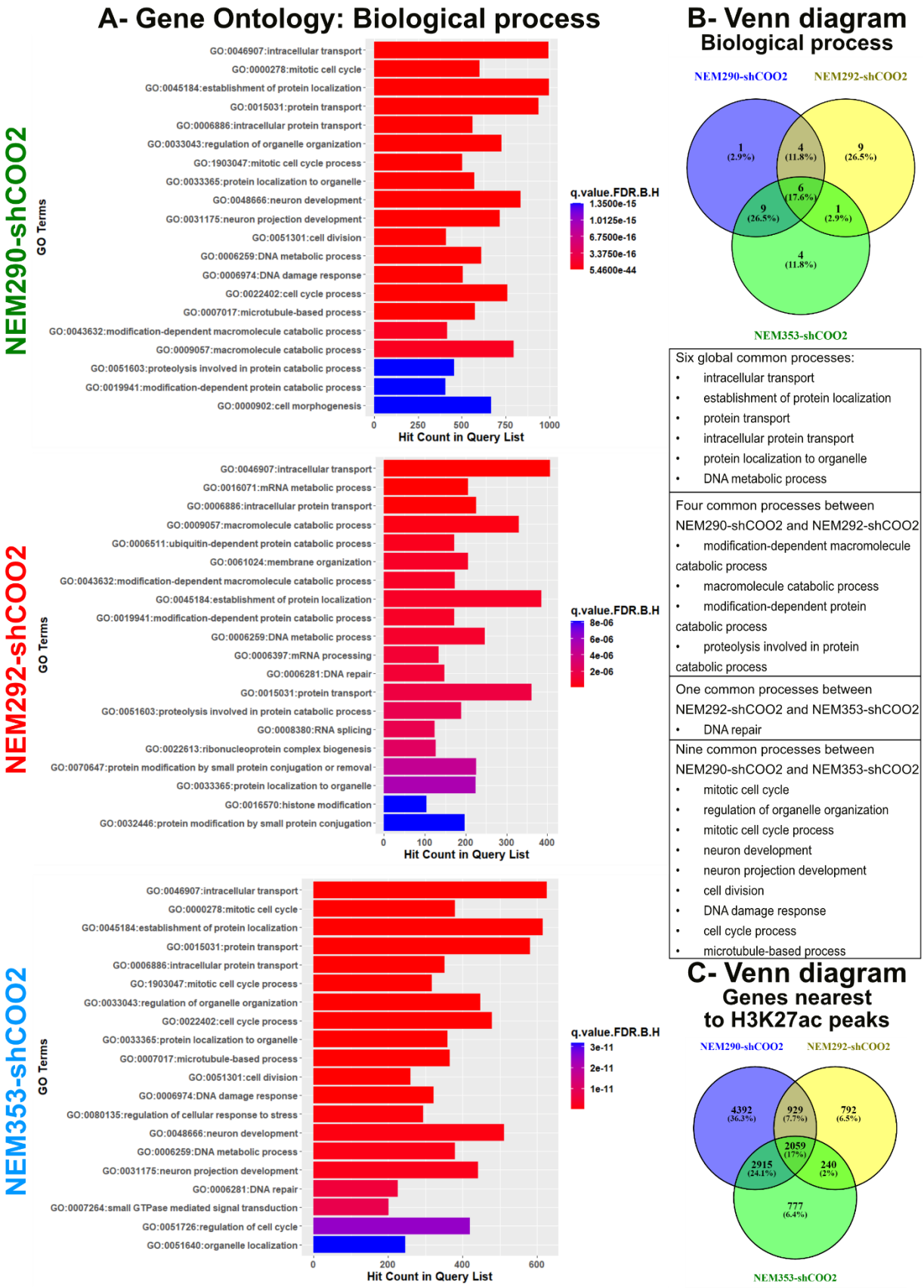

Figure 71: Biological process analysis of genes proximal to H3K27ac binding peaks

A- Biological process analysis of genes proximal to H3K27ac binding peaks.

B- Venn diagram comparing biological process enriched between three GSC models carrying COO2-control shRNAs.

C- Venn diagram comparing genes-nearest-to-H3K27ac peaks in COO2-control shRNAs GSC models.

Comparing the genes nearest to H3K27ac peaks under both control and *NKX2-2* knock-down conditions underscored the expected involvement of H3K27ac as it marked all active genes, across all cell lines and conditions. Notably, NEM292 exhibited the most pronounced changes following decreased *NKX2-2* expression levels, with 13 distinct biological processes affected, representing over 35% of the total processes identified. The exclusive processes associated with H3K27ac peaks after *NKX2-2* knockdown, such as regulation of organelle organization, neuron development, and mitotic cell cycle, shed light on the specific roles of *NKX2-2* in coordinating cellular differentiation, organization, and proliferation. Furthermore, the presence of processes like neuron projection development and cytoskeleton organization in NEM292 suggests a specialized function of *NKX2-2* in neuronal development and cellular morphology, potentially influencing crucial aspects such as cell migration, neurite outgrowth, and synaptic connectivity (Fig. 72A, B).

In contrast, NEM290 and NEM353 exhibited fewer exclusive biological processes, with 8 and 7 identified, respectively. These processes, including mRNA metabolic process, microtubule-based transport, and mRNA processing in NEM290, and mRNA splicing, microtubule cytoskeleton organization, and chromosome organization in NEM353, underscore the heterogeneity among DIPG GSC models and highlight the distinct roles of *NKX2-2* in each cell line. Notably, there was no overlap in the specifically altered processes between NEM290 and NEM292, further emphasizing the unique impact of *NKX2-2* on each cell line and suggesting divergent regulatory mechanisms underlying their cellular processes (Fig. 72B).

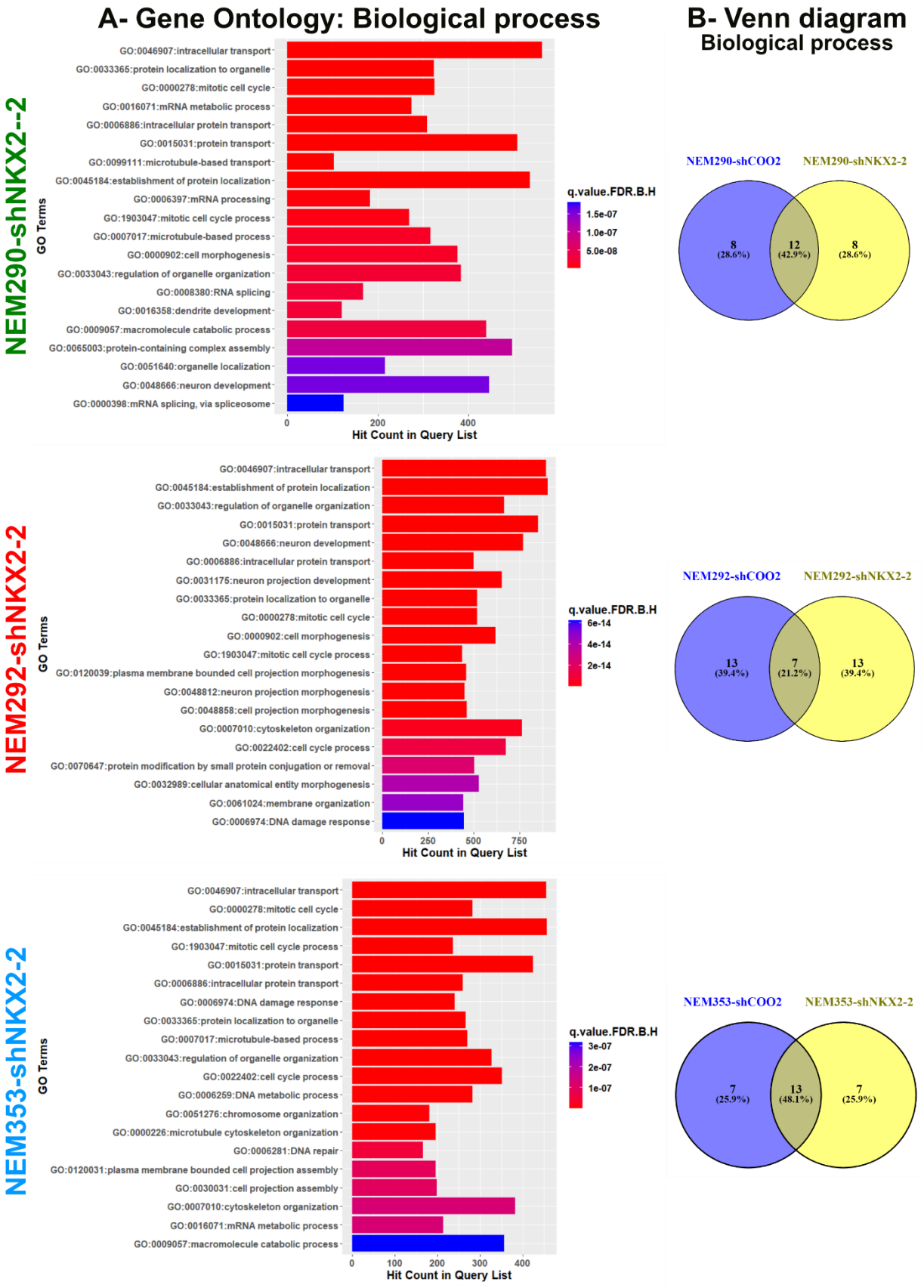
A- Gene Ontology: Biological process
B- Venn diagram
Biological process
NEM290-shNKX2--2
GO:0046907:intracellular transport
GO:0033365:protein localization to organelle
GO:0000278:mitotic cell cycle
GO:0016071:mRNA metabolic process
GO:0006886:intracellular protein transport
GO:0015031:protein transport
GO:0099111:microtubule-based transport
GO:0045184:establishment of protein localization
GO:0006397:mRNA processing
GO:1903047:mitotic cell cycle process
GO:0007017:microtubule-based process
GO:0000902:cell morphogenesis
GO:0033043:regulation of organelle organization
GO:0008380:RNA splicing
GO:0016358:dendrite development
GO:0009057:macromolecule catabolic process
GO:0065003:protein-containing complex assembly
GO:0051640:organelle localization
GO:0048666:neuron development
GO:0000398:mRNA splicing, via spliceosome
GO Terms
0
200
400
Hit Count in Query List
q.value.FDR.B.H
1.5e-07
1.0e-07
5.0e-08
NEM290-shCOO2
NEM290-shNKX2-2
8
(28.6%)
12
(42.9%)
8
(28.6%)
NEM292-shNKX2-2
GO:0046907:intracellular transport
GO:0045184:establishment of protein localization
GO:0033043:regulation of organelle organization
GO:0015031:protein transport
GO:0048666:neuron development
GO:0006886:intracellular protein transport
GO:0031175:neuron projection development
GO:0033365:protein localization to organelle
GO:0000278:mitotic cell cycle
GO:0000902:cell morphogenesis
GO:1903047:mitotic cell cycle process
GO:0120039:plasma membrane bounded cell projection morphogenesis
GO:0048812:neuron projection morphogenesis
GO:0048858:cell projection morphogenesis
GO:0007010:cytoskeleton organization
GO:0022402:cell cycle process
GO:0070647:protein modification by small protein conjugation or removal
GO:0032989:cellular anatomical entity morphogenesis
GO:0061024:membrane organization
GO:0006974:DNA damage response
GO Terms
0
250
500
750
Hit Count in Query List
q.value.FDR.B.H
6e-14
4e-14
2e-14
NEM292-shCOO2
NEM292-shNKX2-2
13
(39.4%)
7
(21.2%)
13
(39.4%)
NEM353-shNKX2-2
GO:0046907:intracellular transport
GO:0000278:mitotic cell cycle
GO:0045184:establishment of protein localization
GO:1903047:mitotic cell cycle process
GO:0015031:protein transport
GO:0006886:intracellular protein transport
GO:0006974:DNA damage response
GO:0033365:protein localization to organelle
GO:0007017:microtubule-based process
GO:0033043:regulation of organelle organization
GO:0022402:cell cycle process
GO:0006259:DNA metabolic process
GO:0051276:chromosome organization
GO:0000226:microtubule cytoskeleton organization
GO:0006281:DNA repair
GO:0120031:plasma membrane bounded cell projection assembly
GO:0030031:cell projection assembly
GO:0007010:cytoskeleton organization
GO:0016071:mRNA metabolic process
GO:0009057:macromolecule catabolic process
GO Terms
0
100
200
300
400
Hit Count in Query List
q.value.FDR.B.H
3e-07
2e-07
1e-07
NEM353-shCOO2
NEM353-shNKX2-2
7
(25.9%)
13
(48.1%)
7
(25.9%)

Figure 72:

A- Biological process analysis of genes proximal to H3K27ac binding peaks in *NKX2-2* knocked down models

B- Venn diagram comparing biological process enriched between GSC models carrying COO2-control shRNAs and *NKX2-2*-targeting shRNAs.

By examining the peaks of both H3K27ac and NKX2-2 at the genes mentioned above, we observed co-localization of these two peaks in all samples. Importantly, the intensity of H3K27ac peaks decreased when the cells expressed NKX2-2 targeting shRNA (Fig. 73).

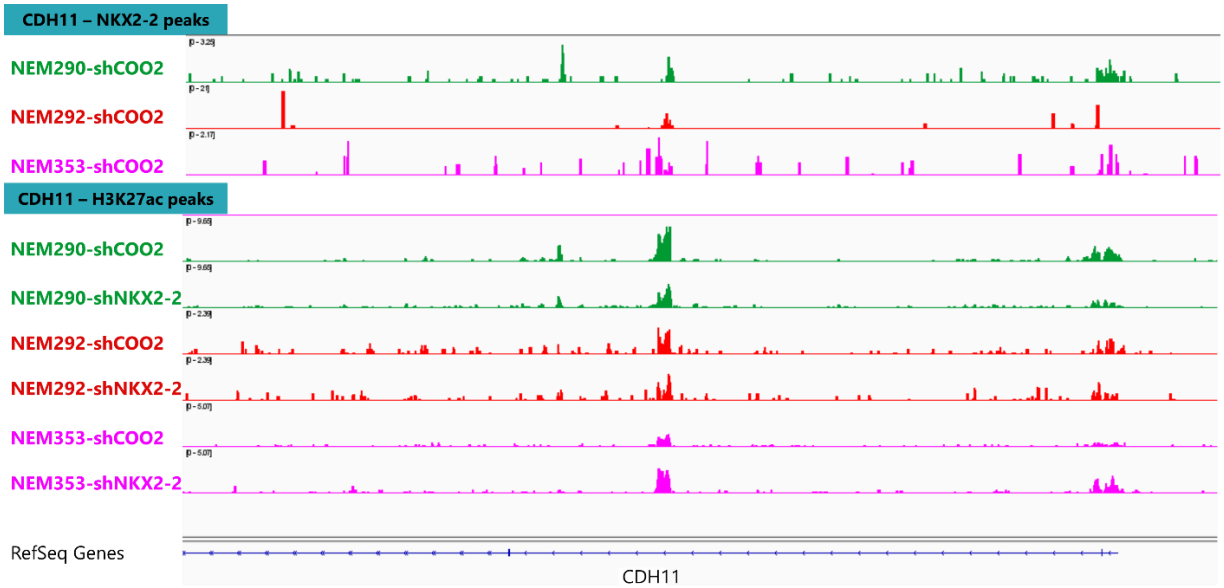

Figure 73: IGV illustrate H3K27ac and NKX2-2 peaks at *CDH11* loci

H3K27ac has been reported to be abnormally activated at high levels at super-enhancers (SEs), which are large clusters of enhancers associated with oncogenes or cell fate genes (Lavarone et al., 2019). To investigate whether the reduction of *NKX2-2* expression would have any influence on this phenomenon, the landscape of SEs was characterized in both control and *NKX2-2*-shRNA GSC cultures based on H3K27ac marks. SEs were annotated with their nearest genes to the TSS. Both NEM292 and NEM353 witnessed an increase in detectable SEs after *NKX2-2* knockdown (3.8 times and 1.7 times, respectively), while NEM290 showed a decrease in SE numbers (2.4 times) (Fig. 74).

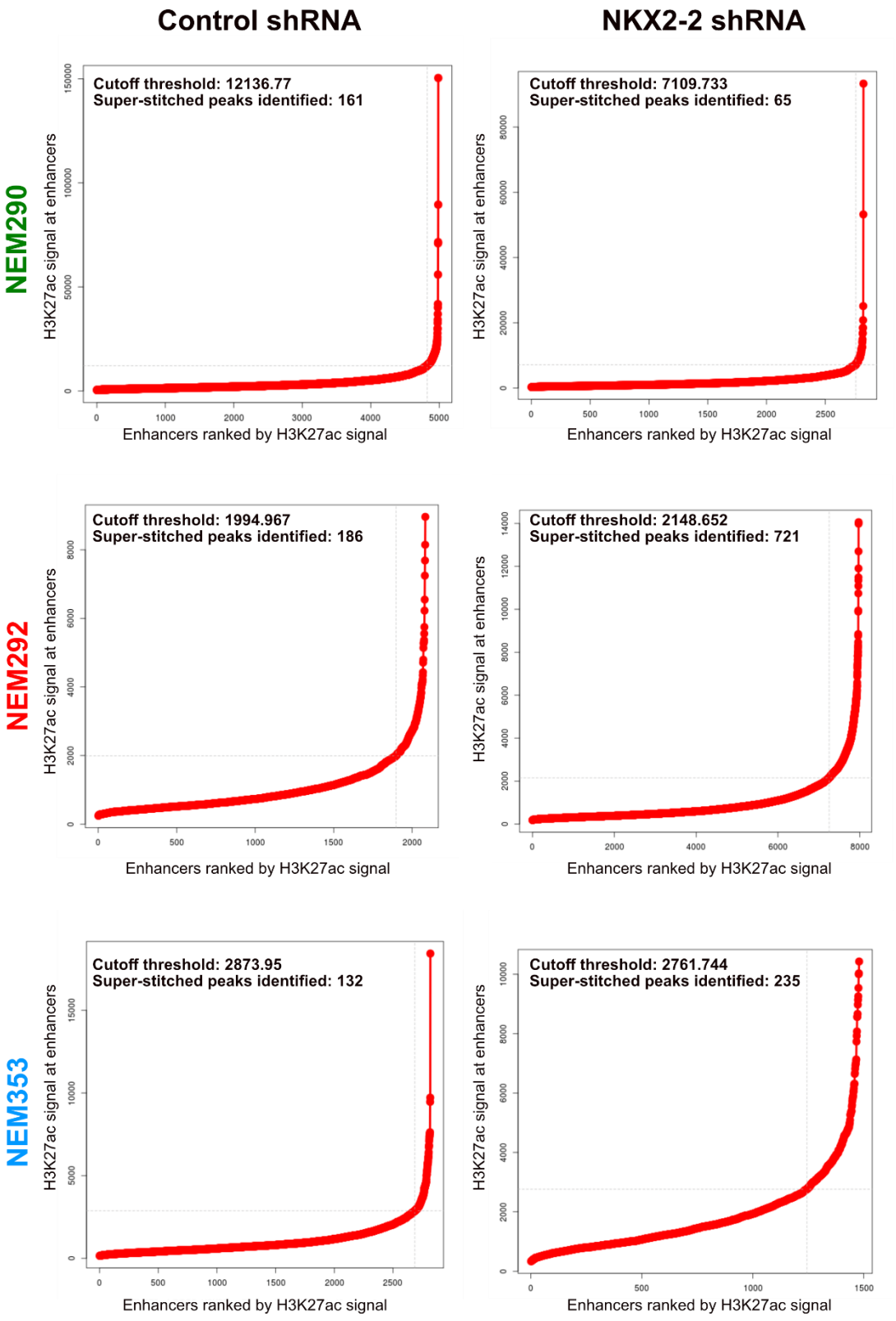

Figure 74: Super-Enhancers (SE) of H3K27ac detected in both control shRNA and NKX2-2 KD samples

Enhancers ranked by H3K27ac signal. Super enhancers (SEs) are identified with signal higher than cutoff threshold.

Gene Ontology analysis of SE-associated genes in each condition of three GSC models (with a p-value cutoff of 0.05) revealed interesting insights. Specifically, there were no significantly enriched ontologies in NEM290, regardless of the expression level of *NKX2-2*, and in NEM292-shCOO2 (Fig. 75). In NEM292, genes associated with SEs and expressing COO2 control shRNA were found to be linked with the basement membrane. Conversely, in NEM353, there was an enrichment observed in the extracellular matrix (ECM) cell component, irrespective of *NKX2-2* status. Notably, despite sharing SEs related to ECM, SEs on the BMP7 locus were exclusively detected in NEM353 expressing *NKX2-2* shRNA. Furthermore, upon the knockdown of *NKX2-2*, an enrichment of the ossification ontology was observed in NEM353-shNKX2-2. Genes such as *BMP7*, *GLI2*, *DDR2*, *LRP3*, among others, contributed to this enrichment, suggesting a potential regulatory role of *NKX2-2* in ossification-related processes.

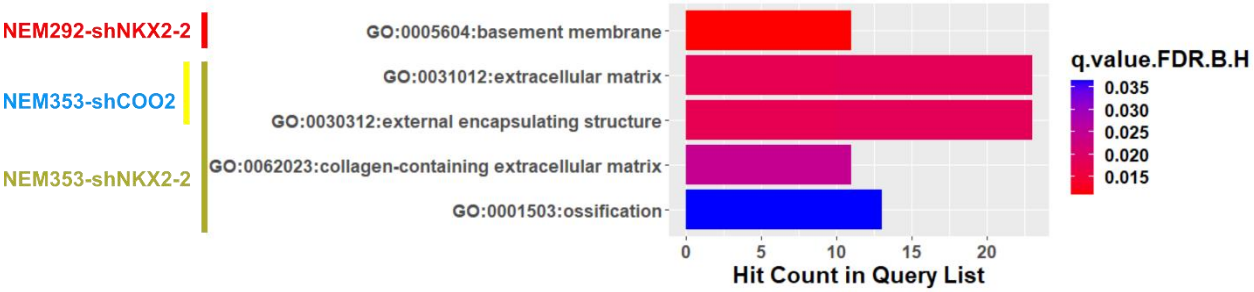

Figure 75: Gene ontology analysis of SE-associated genes in studied GSC models

There were 72 common SEs which appeared in either 2 or or all three shCOO2 control samples (Fig. 76A). In the comparison of cells expressing *NKX2-2* shRNA, it was demonstrated that NEM292 shared a greater similarity in SEs with NEM353 than with NEM290. This observation aligns with the finding that *NKX2-2* exhibits a higher degree of binding to similar genomic locus in NEM292 compared to NEM290 (Fig. 76B). Overlapping this list with the SEs list of GSC expressing *NKX2-2* shRNA using Venn diagram showed that there were 15 common SEs that were lost after *NKX2-2* knockdown. Among these 15 SEs, one was located near *FZD3*, a gene encoding a protein called Frizzled-3, which is a receptor for Wnt signaling proteins. WNT signaling pathway has been reported to play an important role in the regulation of self-renewal

and differentiation of CNS as well as the development of gliomas and DIPG (Lee et al., 2016; Zuccarini et al., 2018), in which a therapeutic treatment combining inhibitors of Wnt/β-catenin and PI3K/mTOR was proposed to treat DIPG (Sharma et al., 2023). Visualization of the FZD3 locus revealed a decrease in H3K27ac SE peak intensity upon *NKX2-2* knockdown compared to the control condition in NEM290. However, the opposite observation was made in NEM292 and NEM353, where loss of SE peaks was consistent but there is gain of a single higher and broader H3K27ac peak in the *NKX2-2* knockdown condition (Fig. 76D).

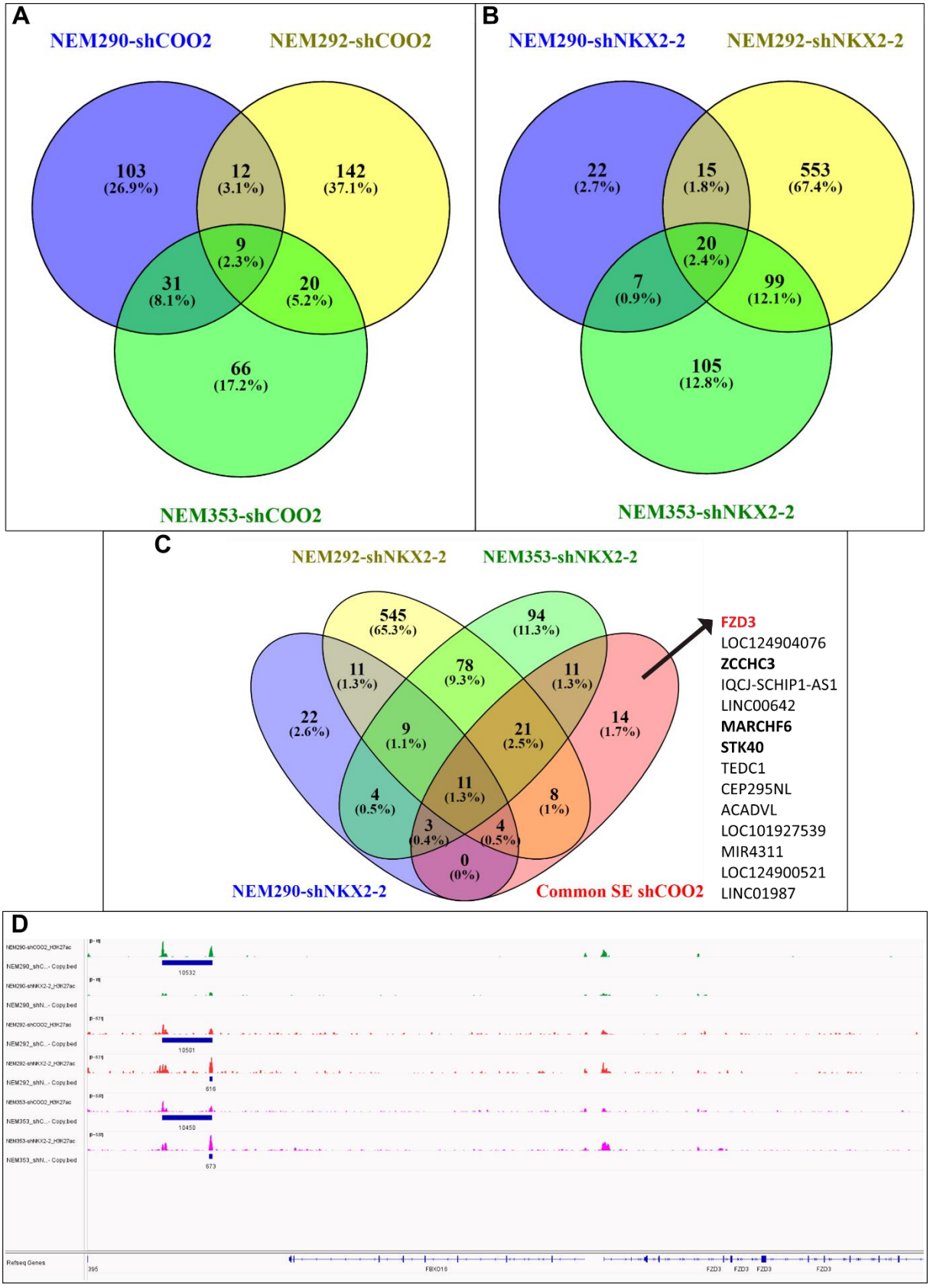

Figure 76

A- Venn diagram illustrating the super-enhancers (SEs) identified by H3K27ac

marks in: A- NEM290, NEM292 and NEM353 expressing control shCOO2

B- NEM290, NEM292 and NEM353 expressing *NKX2-2* targeting shRNAs

C- Overlapping Venn diagram in B and the SEs detected in 2/3 or 3/3 GSC shCOO2 samples. Gene list indicated the genes related to SE which expressed exclusively in shCOO2 control condition.

D- Visualization by IGV of H3K27ac CUT&Tag signal across *FZD3* locus in both GSC carrying control and NKX2-2 specific shRNA; with the presence of .BED file to identify enriched peaks.

In the analysis of differentially expressed genes derived from RNA-seq data and overlapping transcripts associated with SEs, a total of 14 upregulated genes and 17 downregulated genes were identified (Fig 77). Notably, none of these genes pertain to the cell identity of either OPCs or medial neuroblasts. Conversely, no shared upregulated genes exclusively associated with SEs were observed either in control conditions or following *NKX2-2* KD. Among the downregulated genes, two common genes were identified, which were downregulated by *NKX2-2* KD and associated with SEs: *RNU1-2* (RNA, U1 small nuclear 2) and *LMTK3* (Lemur Tyrosine Kinase 3). Notably, only the SE linked with *RNU1-2* was lost following *NKX2-2* knockdown. Additionally, GNG7 is the only downregulated gene that appeared to be similarly associated with SEs in two out of three GSC with *NKX2-2* targeting shRNA (Fig. 77B).

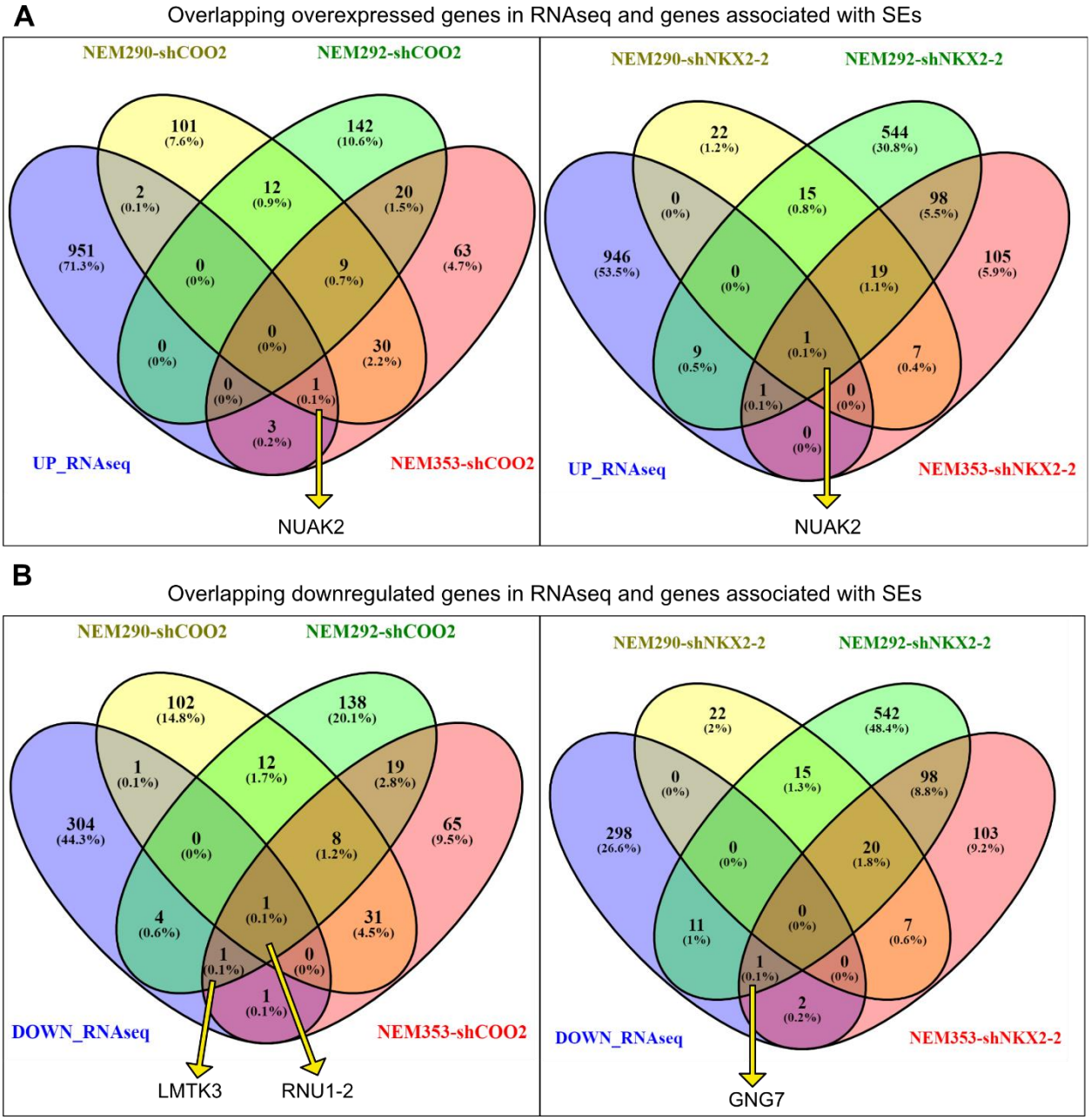

Figure 77: Overlapping DEG data from RNAseq and genes related to SE from CUT&Tag

A Venn diagram illustrating the overlap of the following sets:

A- Upregulated genes from RNAseq analysis and SE-associated genes from CUT&Tag experiment

B- Downregulated genes from bulk RNAseq and SE-associated genes.

DISCUSSION & PERSPECTIVES

Discussion

In my PhD project, my aim was to identify regulators of invasion in Diffuse Midline Gliomas/Diffuse Intrinsic Pontine Gliomas (DMG/DIPG) cells in order to find ways to target their invasive behavior. It has been reported that DIPG cells originate from Oligodendrocyte Progenitor Cells (OPC) or Neural Stem Cells (NSC) and that the nature of gliomas cell-of-origin may influence the oncogenesis and some behaviors of DIPG cells (Castel et al., 2015; Haag et al., 2021; Monje et al., 2011). Moreover, not only until recently that there is a study report the direct link between DIPG metastasis and survival rate of patients (Bruschi et al., 2023), which suggests that the highly motile feature of OPC (Binamé et al., 2013) and NSC (Fukushima et al., 2002) could contribute to the infiltrative phenotype and thus indicate that alteration of cell identity might be a potential approach to inhibit the invasion of DIPG. Additionally, I sought to elucidate the underlying mechanism by which this gene exerts its influence on these two critical aspects of DIPG. Notably, this area of DIPG research has received limited attention in previous studies. This Discussion part will summarize and emphasize the insights gained from my PhD project into these aspects, while also analyze the study's limitation and propose perspectives for future research.

1. Modulating NKX2-2 expression in DIPG patient-derived cells leads to different invasion and proliferation profile

The preliminary findings from the study by Bruschi et al. combining 3D invasion assays and bulk RNA sequencing (RNAseq) of 3D organoid models have highlighted *NKX2-2* as a potential candidate gene involved in regulating DMG invasion. It was observed that the expression level of *NKX2-2* positively correlates with invasion scores, with significantly higher expression levels noted in highly invasive DIPG cell models compared to those with low to moderate invasion potential. While no significant correlation was observed between *NKX2-2* expression in patient tumors and the

metastasis status of the patients, a trend was noted, with the majority of metastasis-free patients expressing lower levels of *NKX2-2* compared to patients with metastasis or relapse. Notably, two models expressed markedly high *NKX2-2* levels in the metastasis-free group, while one tumor exhibited lower *NKX2-2* expression in the metastasis group. To validate these findings, future studies could include a larger cohort of patient tumors with clinical follow-up to increase the sample size and enhance the precision of the results notably in the delay of appearance of metastases.

NKX2-2 is a master transcription factor belonging to the NKX family of homeodomain-containing proteins. It plays crucial roles in various developmental processes, with numerous studies published on its role in regulating cell fate choice during pancreatic β-cell development (Anderson et al., 2009; Desai et al., 2008, 2008; Flanagan et al., 2014; Gutiérrez et al., 2017; Sussel et al., 1998; Watada et al., 2003). In the central nervous system, NKX2-2 is involved in ventral neuronal patterning by specifying neuronal identity through the Sonic hedgehog and WNT signaling pathways (Briscoe et al., 1999; Dias et al., 2020; Jarrar et al., 2015; Lei et al., 2006). Additionally, NKX2-2 has been reported to play a critical role as a temporal determinant in OPC differentiation (Dugas et al., 2006; Fu et al., 2002; Qi et al., 2001; Soula et al., 2001; Zhu et al., 2014b). In the context of cancer, NKX2-2 has been implicated in inhibiting the self-renewal of glioma-initiating cells, and its suppression function is essential in the oncogenesis of Ewing's sarcoma (Muraguchi et al., 2011; Owen et al., 2008). Former studies have addressed OPCs as the cell-of-origin of DMG/DIPG (Filbin et al., 2018; Jessa et al., 2022b; Liu et al., 2022a) and research by Nagaraja et al. indicated that NKX2-2 is associated with the oligodendroglial lineage and Super-Enhancers (SE) in DIPG (Nagaraja et al., 2017). However, to date, no study has directly linked *NKX2-2* expression to the invasiveness of DMG/DIPG.

Through a loss-of-function approach utilizing shRNA to specifically target and knock-down (KD) *NKX2-2* expression, all four Gliomas Stem-like Cells (GSC) models exhibited a decrease in invasion at 40 hours post-embedding spheroids into artificial extracellular

matrix (ECM) to form 3D organoid structures. Interestingly, the reduction in invasion scores appeared to be independent of the degree of decrease in *NKX2-2* expression level, although a subtle correlation with the initial expression level of *NKX2-2* was noted.

Therefore, my PhD study represents the first attempt to investigate the relationship between *NKX2-2* and cell behavior in DIPG patient-derived cell lines, providing compelling evidence that *NKX2-2* is positively correlated with invasiveness.

In my initial investigations, it became apparent that GSC harboring the H3.1-K27M mutation exhibited heightened sensitivity to NKX2-2 depletion. This sensitivity posed challenges for further experimentation, particularly in the formation of spheres in Matrigel. Consequently, my PhD project shifted focus towards studying the role of *NKX2-2* in four selected H3.3-K27M DIPG patient-derived cell models: NEM285, NEM290, NEM292, and NEM353. The unexpected cytotoxicity observed in H3.1-K27M DIPG NEM328 cells presents a perplexing challenge. This cell line was selected for study due to its high invasion score of 7.37, placing it within the high invasive group. Despite this selection, investigation into the genetic alterations of this cell line compared to others did not yield any direct clues regarding potential synergistic or synthetic lethality effects between *NKX2-2* KD and available alterations in this H3.1-K27M cell line. Adding to the complexity is the divergence in phenotype observed between H3.1-K27M and H3.3-K27M DIPG models. While H3.3-K27M DIPG models typically exhibit an OPC-like phenotype, H3.1-K27M DIPG has been reported to display a less aggressive astroglial and mesenchymal phenotype (Castel et al., 2015). However, the recent study by Bruschi et al. has suggested that the OPC-like phenotype may be more strongly correlated with invasion behaviors, irrespective of the H3K27M status (Bruschi et al., 2023). Further experiments on other H3.1-K27M DIPG models with high or moderate invasiveness should be conducted to determine whether the observed cytotoxicity is specific to the NEM328 cell line or represents a broader phenomenon across H3.1-K27M DIPG models. Gathering additional data before drawing conclusions

will provide a more comprehensive understanding of the implications of *NKX2-2* KD in this context.

Subsequent results indicated that *NKX2-2* KD also led to a deceleration in cell proliferation in 2D culture models but with less than 10% of cell death. This suggests that the decreased proliferation rate might be attributed to other pathway triggers rather than cell cytotoxicity caused by the depletion of NKX2-2. Additionally, the Senescence-Associated β-galactosidase assay suggested that senescence could play a role in the decrease of cell proliferation in the NEM290 model but no significant effect of this process was observed in NEM353. Further replicated experiments across all four cell lines are necessary to obtain reliable results and give a conclusion on association between *NKX2-2* KD and senescence in highly invasive DIPG models, enhancing the overall information obtained from the study.

2. Modulating NKX2-2 expression in DIPG GSC altered cell identity

The Gene Set Enrichment Analysis (GSEA) comparing GSC transduced with control shRNAs and *NKX2-2* shRNAs with GSC from Bruschi et al. data showed the same trend of enriched gene sets between control samples from my data and highly invasive cells and between *NKX2-2* knock-down cells and poor invasive cells. One information to keep in mind is that the durations of tumoroid culture between the two experiments were different. In my experiment, tumoroids were cultured for 6 days in Matrigel to capture early cellular modifications in response to *NKX2-2* KD and to minimize the impact of different cell proliferation rate between models. In contrast, Bruschi et al. study cultured tumoroids for 21 days (Bruschi et al., 2023) resulting in increased cell proliferation and reduced Matrigel concentration in the tumoroid structure compared to my setup. This might explain the low number of common genes between control shRNA samples and highly invasive cells 28 genes, 4.5%. However, the overall similarity in enriched gene sets once again confirmed the highly invasive nature of GSC expressing control shRNAs. This indicated that the transduction process did not interfere the invasion behavior of the cells, and that further underscores that deletion

of NKX2-2 leaded to a less invasive profile in DIPG.

Interestingly, *NKX2-2* KD cells only share a few genes with low invasive GSC models indicating that while GSC after NKX2-2 reduction may exhibit some similarities with low invasive GSC, they did not fully acquire the phenotype of mildly invasive GSC reported in Bruschi et al. study. Therefore, *NKX2-2* KD did not reprogram the high invasive GSC to a low invasive epithelial-to-mesenchymal transition (EMT) state. This raises a question whether high invasive and low invasive DIPG originate from the same cell type, which require further lineage-tracing experiments to provide further insights. Alternatively, this outcome could be explained by the inadequacy of *NKX2-2* KD alone to completely reprogram highly invasive GSC into low invasive GSC. Instead, the GSEA of my bulk RNAseq results suggested that *NKX2-2* KD is sufficient to induce a direct transition from an OPC-like phenotype in control shRNA conditions to a medial neuroblast phenotype upon *NKX2-2* KD. Additionally, *NKX2-2* knock-down cells even exhibited reduced expression of signatures associated with EMT, a hallmark of poorly invasive or less aggressive DIPG phenotypes (Bruschi et al., 2023; Castel et al., 2015), as well as angiogenesis and apical junctional markers. This is consistent with the results of the 3D invasion assay, where GSC transduced with *NKX2-2* shRNAs did not achieve an invasion score as low as the poorly invasive GSC models (above 3 and less than 2, respectively). Neuroblasts are immature neurons that migrate from NSC pools to their final locations in various regions of the brain during early postnatal development (Aoyagi et al., 2018). The migration cascade of these cells is mediated by insulin-like growth factor I (IGF) and fibroblast growth factor 2 (FGF2), with tight involvement of blood vessels and astrocytes around the rostral migratory stream (Motamed et al., 2019; Porter et al., 2022). Therefore, decreased motility in neuroblasts would correlate with lower expression of genes related to these elements. According to my 3D tumoroid RNAseq data, there was a significant downregulation of genes related to biological processes such as angiogenesis, blood vessel morphogenesis, postsynapse formation, and cell-substrate adhesion. It is also noteworthy that our DIPG GSC models consistently indicate that EMT signatures are associated with less invasive and

infiltrative behavior, contrary to the conventional understanding that EMT promotes cancer invasiveness and metastasis (Hanahan and Weinberg, 2000, 2011; Kluiver et al., 2020; Kumar et al., 2017; Lamouille et al., 2014; Meel et al., 2018; Sanders et al., 2020). Recent study conducted in the lab has unveiled a migration mode associated with EMT, wherein mesenchymal signals augment the presence of focal adhesions across a broader area and induce actin stress fibers, thereby reducing cell mobility and migration (Bruschi et al., 2023).

Taken together, all the data suggest that the reduction in invasion behavior of GSC in 3D models following NKX2-2 depletion could occur through a mechanism different from that demonstrated in the study by Bruschi et al. This disparity may be influenced by the reprogramming in a new neuroblast phenotype. Thus, it is suggested that *NKX2-2* KD induces a cellular identity shift towards a neuroblast phenotype, leading to reduced invasion due to an environment less conducive to neuroblast migration. This environment is characterized by decreased formation of blood vessels, reduced interaction with growth factors, diminished cell-substrate adhesion, and decreased postsynaptic transmission.

Interestingly, alterations in cell morphology were observed, characterized by shorter cell projections and a flatter cell shape in the NEM290 and NEM353 models, but not in the NEM292 model. The results were obtained once by analyzing several images. To confirm this conclusion, it is necessary to perform another replication under the same cell conditions. Considering that my experiment set up did not co-culture GSC with other cell types of the brain, this could be a outcome of an autonomous mechanism or an autocrine signaling which cause an alteration in focal adhesion and reorganization of the cytoskeleton (Bodor et al., 2020). Interestingly, this finding bears resemblance to the behavior of NKX2-2 in Ewing's sarcoma cells, where NKX2-2 represses mesenchymal features such as actin stabilization and adhesion (Fadul et al., 2015). The result from my chromatin location analysis (CUT&Tag) revealed enriched binding of NKX2-2 peaks near genes encoding cadherins (*CDH1, CDH2, CDH11 and CDH13)* in all

cell lines. However, among these genes, while all cadherin genes showed a downregulation trend, there was only *CDH11* downregulation got a p-adjust value less than 0.005. Furthermore, co-localization of H3K27ac and NKX2-2 peaks near *CDH11* was detected in NEM290 and NEM292. Accompanied by a reduction in H3K27ac peak intensity after NKX2-2 depletion, this finding suggests that NKX2-2 influences binding of H3K27ac at *CDH11* locus and may act as an activator of *CDH11*. A recent study has reported underexpression of CDH11 in H3-K27M gliomas (Sanders et al., 2020). CDH11 has been reported as regulator of stem cell fate (Alimperti and Andreadis, 2015) and as a marker of mesenchymal phenotype, enhancing cell survival in glioblastoma (Kaur et al., 2012). Additionally, Li et al. concluded that CDH11 inhibit the formation of actin stress fibers, EMT, and the WNT signaling pathway, thereby inhibit carcinoma tumor cells invasion (Li et al., 2012). Moreover, it is noteworthy that H3K27ac peaks intensity increased in NEM353 *NKX2-2* KD cells, emphasizing the heterogeneity among GSC models. Overall, these data suggest that NKX2-2 acts as an activator of CDH11, and the reduction of NKX2-2 levels triggers a cascade involving CDH11, leading to cytoskeleton remodeling and increased cell adhesion. This, in turn, results in alterations in cell morphology and a less invasive phenotype. Further functional experiments (such as Western blotting, immunofluorescence, treatment with CDH11 inhibitor) should be conducted in combination with phenotypic assays (3D invasion, proliferation) to gain deeper insight into this process.

Even though *NKX2-2* KD generally resulted in decreased invasion ability and proliferation rate of DIPG GSC, its role among the selected DIPG GSC models in my study varies. Principal Component Analysis (PCA) of RNAseq data revealed divergent transcriptional responses of DIPG cells to *NKX2-2* KD. This observation was corroborated by the results from NKX2-2 peak binding analysis, which indicated only a few common genes nearest to NKX2-2 peaks in all selected GSC, with significant dissimilarities between each pair of the GSC models. Similarly, when comparing H3K27ac peaks in GSC expressing control shRNA versus those expressing NKX2-2 targeting shRNAs, notable differences were observed. Interestingly, the comparison of

genes nearest to NKX2-2 enriched peaks and H3K27ac peaks revealed that cell lines with more similarities in terms of NKX2-2 binding sites did not necessarily have more H3K27ac peaks in common. This phenomenon could be attributed to the inter-tumor heterogeneity in DIPG, which has been extensively documented from various perspectives ranging from tumor histology to molecular landscape and response to treatment (Bruschi et al., 2023; Buczkowicz et al., 2014; Chiang et al., 2020; Mackay et al., 2017).

Interestingly, contrary to my obtained results where *NKX2-2* KD led to decrease of invasion score and cell proliferation, NKX2-2 has been shown to be a tumor suppressor in Osteosarcoma and its overexpression inhibited the osteosarcoma cells invading into Matrigel (Chen et al., 2018). The structure of NKX2-2 comprises three highly conserved domains with distinct functions: the tinman (TN) domain, the DNA binding homeodomain (HD), and the NKX2-specific domain (SD). Moreover, the transcriptional activation domain (TAD) located in the C-terminus region has been reported as an activation domain and play a critical role to determine the suppressor or activator role of the cells (Chen et al., 2018; Owen et al., 2008; Zhang et al., 2020). The differing roles of NKX2-2 in DIPG compared to osteosarcoma or Ewing's sarcoma may be attributed to the activation or inactivation of the TAD. To elucidate which domain is responsible for the activation role of NKX2-2 in DIPG, testing a series of truncated FLAG-tagged *NKX2-2* constructs in rescue experiments would be a feasible approach. This would provide insights into the specific domains of *NKX2-2* implicated in its function in DIPG.

Given the reported dual role of *NKX2-2*, functioning both as an activator and an inhibitor, there is considerable interest in elucidating its intricate role in DIPG GSC. However, the comparison of overlap of differentially expressed gene in RNAseq with genes-nearest to NKX2-2 binding sites from the CUT&Tag experiment did not provide a clear conclusion regarding whether NKX2-2 acts as an activator or a suppressor in the DIPG GSC. Indeed, an equivalent number of common genes were detected between the CUT&Tag data and either the upregulated or downregulated genes from RNAseq

data.

The majority of NKX2-2 peaks were identified in promoter regions (<1kb), introns, and distal intergenic regions, which aligns with expectations for a transcription factor (Spitz and Furlong, 2012). Typically, transcription factors NKX2-2 bind to proximal enhancers for adjacent transcriptional activation, intronic regions for alternative splicing or enhancer activity, and distal intergenic regions for distal enhancer. The results showed that NKX2-2 binds to enhancers of genes related to central nervous system (CNS) development, neuron development, and neuron projection development across all GSC models, reaffirming its fundamental role during brain development. This finding aligns with previous studies implicating NKX2-2 in the determination of neuronal identity, wherein it blocks motor neurons via the Sonic Hedgehog signaling (Shh) pathway or intrinsically programs the timing of Gli gene activity, indirectly influencing the timing of developmental steps (Briscoe et al., 1999; Dias et al., 2020).

Additionally, in all three DIPG GSC models, NKX2-2 peaks were found in in all COO2 control samples, proximity to genes related to the noncanonical WNT planar cell polarity (WNT/PCP) and RHO GTPase signaling pathway, including WNT7A, ARHGEF4/28, and ARHGAP24, genes are involved in cell motility and cytoskeleton remodeling (Akilesh et al., 2011; Chen et al., 2021; Fukumoto et al., 2015; Taniuchi et al., 2018; Yu et al., 2011). One point to consider when analyzing NKX2-2 peaks among the three conditions is the scattered peaks observed in NEM292-shCOO2 and the substantial number of peaks detected in NEM353-shCOO2, which may introduce bias into the analysis. Moreover, SE analysis of H3K27ac peaks revealed a common SE at FZD3, which is related to the noncanonical WNT signaling pathway. Among all GSC models, there was enrichment of the RHO GTPase pathway in NEM292 and NEM353 despite the presence of NKX2-2 shRNA, indicating that NKX2-2 is just one of the factors contributing to the enrichment of the RHO GTPase pathway. Furthermore, Reactome Pathway and Biological Process analysis of NKX2-2 peaks indicated a common enrichment of the RHO GTPase cycle and cytoskeleton organization. This finding is

consistent with a previous study showing that H3.3-K27M DIPG tumors preferentially express WNT/PCP pathway signals, with a correlation observed with Rho family member A (RhoA), a member of the RHO GTPase family, and with cytoskeleton modulation (Nagaraja et al., 2019). To my knowledge, NKX2-2 has been reported to implicate in the canonical WNT signaling pathway (Lei et al., 2006) but not the noncanonical WNT pathway, making this observation particularly noteworthy. However, it is still not clear to what extent NKX2-2 contributes to the function of the WNT/PCP pathway and how much it is involved in the RHO GTPase cycle.

The RNAseq data reveals that both NEM292 and NEM353 DIPG models exhibit downregulation of genes associated with synapse and postsynaptic membrane functions, including Neuroligin-3 (NLGN3) and Glutamate Ionotropic Receptor Kainate Type Subunit 4 (GRIK4). Studies have demonstrated that NLGN3, when secreted by postsynaptic cells or directly from OPC, can bind to its receptor on glioma membranes. This binding event activates the PI3K-mTOR pathway, leading to the upregulation of glioma growth (Venkatesh et al., 2015, 2017). Additionally, functional synapses formed between neurons and glioma cells, mediated by AMPA (α-amino-3-hydroxy-5-methyl-4-isoxazole propionic acid) receptors contribute to tumor growth (Venkataramani et al., 2022). Specifically, glioma cell membrane depolarization induced by these synapses stimulates tumor proliferation. Furthermore, *NKX2-2* also exhibited enriched peaks at Ephrin-A5 (*EFNA5*), an important gene to early phases of synaptogenesis and was down-regulated after NKX2-2 depletion. These data suggest that NKX2-2 might play a role in modulating neuron-glioma synaptic interactions or cell-cell interconnection and that depletion of NKX2-2 might impede DIPG cells migration and proliferation in more complex environment involving cell-cell interactions.

However, it's important to note that the CUT&Tag data lacks replication due to time constraints. Additionally, this is the first instance of using the specific antibody targeting NKX2-2 for a CUT&Tag experiment in our lab, and this experimental setup has not been conducted previously. Data seem to indicate that for NEM292 NKX2-2

CUT&Tag did not work so well, and signal-to-noise ratio is rather low in NEM353 Consequently, there are no comparable CUT&Tag results for NKX2-2 to assess. Therefore, it is necessary to increase the number of replicates in the data and it light be needed to optimize the concentration of the primary antibody targeting NKX2-2 to enhance the peak signal and improve specificity.

In recent years, targeting transcription factors has emerged as a potential strategy for cancer treatment. Various approaches can be employed, including inhibiting the interaction between a transcription factor and its cofactors, blocking the transcription factor's binding site, or regulating the expression level of the transcription factor by modulating ubiquitylation and subsequent proteasome degradation (Bushweller, 2019; Spitz and Furlong, 2012). In the case of the master transcription factor NKX2-2, mutated NKX2-2 have resulted in neonatal lethality, underscoring the critical role of NKX2-2 not only in brain development but also in maintaining the normal functioning of cells, tissues, or organs (Auerbach et al., 2020; Flanagan et al., 2014). Moreover, research on NKX2-2 in OPCs has revealed the involvement of a repressor complex comprising HDAC1, GRG3, and DNMT3A that interacts with NKX2-2 at the CT and TN domains (Zhu et al., 2014b). A ChIP-seq and super enhancer analysis on DIPG cell lines revealed that NKX2-2 is associated with a super enhancer in 1 out of 4 DIPG cell lines (Nagaraja et al., 2017).

Perspectives

The first perspective involves supplementing the replication of certain experiments to ensure reliable and robust results. This includes comparing cell projection and morphology before and after *NKX2-2* KD on DIPG H3.3-K27M models, evaluating the impact of NKX2-2 *KD* on DIPG H3.1-K27M cell lines, optimizing the CUT&Tag experiment, and conducting at least one additional replicate.

Albeit existing work identified the role of NKX2-2 in cell fate, my study is the first study of NKX2-2 on DMG/DIPG patient-derived cell models. Since my PhD project did not

involve gene domain analysis, drawing a definitive conclusion regarding whether NKX2-2 acts primarily as a repressor or activator in H3.3 DIPG highly invasive GSC cells, is challenging. Therefore, it would be intriguing to assess the specific contribution of each structural domain of NKX2-2 to DIPG GSC models. This could be achieved by designing various deletion mutants targeting each domain and investigating the effects on GSC behavior upon introduction of these derivatives. Additionally, this approach will shed light on whether any co-activators or co-repressors are recruited to *NKX2-2* binding locations to coordinate the regulation of downstream genes.

Due to time constraints, some analyses based on the CUT&Tag data were not completed. It is imperative to prioritize completing these aspects to extract more insights from the experiment. Firstly, conducting a differential analysis of enriched H3K27ac peaks between control and *NKX2-2* knockdown conditions is essential. This will provide a more precise comparison of changes in enriched peaks regarding H3K27ac binding with and without NKX2-2 depletion. Secondly, performing motif binding discovery to identify *de novo* NKX2-2 motif bindings, in addition to testing published NKX2-2 motif bindings on public databases such as JASPAR and TFBSshape will be crucial. This is expected to offer insights into any potential co-activators or co-repressors of NKX2-2.

Furthermore, since my data point toward a role of NKX2-2 in regulation of the noncanonical WNT/PCP signaling pathway was proposed, it will be important to validate this by conducting some functional experiments such as western blot or immunofluorescence to evaluate the modulation of the pathway.

Although the 3D tumoroid model provides a relevant platform that recapitulates tumor behavior in patients, it is important to acknowledge its limitations. In this project, only Matrigel was utilized as the ECM, and a single DIPG cell line was employed. While this model is adequate for studying the cell-autonomous behavior of DIPG patient-derived models, it lacks the complexity of interactions between different cell types and various brain-specific ECM components. Since the inception of my PhD, I have endeavored to

establish an interface organotypic brain slice culture as an alternative model to validate the function of NKX2-2 in DIPG within a more complex system, retaining the complexity in terms of ECM and cell types. Additionally, injecting DIPG cells with or without *NKX2-2* knockdown into these brain slices could provide further insights.

To conclude, my PhD project is the first study to identify NKX2-2 as a dual regulator of invasion and cell identity in DMG/DIPG H3.3-K27M. Through this research, I have made the following discoveries:

1. Knocking-down the expression of *NKX2-2* led to a reduction in the invasion ability and cell proliferation of DIPG H3.3-K27M cells, and this effect was independent of the degree of decrease in *NKX2-2* levels.
2. NKX2-2 depletion did not reprogram highly-invasive DIPG cells with an OPC-like phenotype to a low-invasive mesenchymal cell fate. Instead, reducing *NKX2-2* expression induced a cell identity conversion from OPC-like to neuroblast with less invasive behavior.
3. NKX2-2 is suggested to be an activator of *CDH11*, involved in cell morphology alteration and cell invasion modulation.
4. *NKX2-2* is reported to be implicated in the RHO GTPase and noncanonical WNT/PCP pathway regarding cytoskeleton remodeling and regulating invasiveness. Potential downstream genes include *WNT7A*, *ARHGEF4/28, ARHGAP24, and FZD3*.
5. *NKX2-2* is proposed to play a role in modulating neuron-glioma synaptic interaction and gliomas interconnection, and the depletion of NKX2-2 might impede DIPG cell migration and proliferation in a more complex environment involving cell-cell interactions.

Cellular models and cell-culture

Glioma stem-like cell (GSC) models were derived from diagnostic biopsies of primary DIPG tumors. GSC were cultured in flasks coated with laminin (10 µg/mL; Gibco, cat# 23017-015) at 37°C and 5% CO2 in NeuroCult™ NS-A Basal medium (StemCell Technologies, cat# 05750) supplemented with NeuroCult™ NS-A Proliferation supplement (StemCell Technologies, cat# 05753), heparin (2 µg/mL; StemCell Technologies, cat# 07980), epithelial growth factor/fibroblast growth factor (EGF/FGF, 20 ng/mL; Miltenyi, cat# 130-097-751 and 130-093-843), platelet-derived growth factor (PDGF, 10 ng/mL; Miltenyi, cat# 130-108-160). Selected DIPG GSC models are listed in Table 4.

Cell line	H3 subtype	Tumor progression (MRI)	NKX2-2 expression (TPM, RNAseq) (Bruschi et al., 2023)	3D Invasion score (Bruschi et al., 2023)	TP53 mutation (Y/N)	PPM1D mutation (Y/N)	PI3K/AKT /mTOR mutation (Y/N)	PDGFRA amplification (Y/N)
NEM285	H3.3	Local-regional	28.63	6.26	Y	N	Y	N
NEM290	H3.3	Metastatic	56.79	10.86	Y	N	N	N
NEM292	H3.3	Metastatic	44.28	7.92	Y	N	N	N
NEM353	H3.3	Metastatic	19.66	9.52	N	Y	Y	Y

Table 7: Annotation of selected DIPG GSC

Main molecular, clinical characteristics, NKX2-2 expression and invasion score of the DIPG tumors from which GSC were derived.

For viral productions; human embryonic kidney HEK293T cell line was cultured at 37°C and 5% CO2 in Dulbecco's Modified Eagle Medium (DMEM) GlutaMAX™ (Gibco, cat# 10566016) supplemented with 10% fetal bovine serum (FBS) and 1% Penicillin/Streptomycin (P/S; Life Technologies, cat# 15140148).

For all cell types, the medium was refreshed every 2-3 days. Once the confluence reached approximately 85% of the surface, cells were passed after being dissociated

by StemPro™ Accutase™ (Gibco, cat# A11105) for GSC and TrypLE™ (ThermoFisher Scientific, cat# 12604013) for HEK293T cells.

3D patient-derived tumor-organoid culture

A total of 100 000 dissociated GSC cells were counted and resuspended in an appropriate volume of complete medium to yield 5 µl of medium per tumor-organoid. Fifteen replicates were prepared per condition to ensure the successful formation of tumor-organoid for further experiments.

To sterilize two PCR plates and parafilm, 70% ethanol was used. Parafilm was placed on the first PCR plate, and wells were created on the it by gently pressing down and using a hand to smooth the surface. The upper plate was then removed, and the mold was snap-frozen onto the lower PCR plate on dry ice for 1 minute before being gently transferred to a petri dish. A volume of 20 µl of Matrigel (Corning, cat# 356234, 8.9mg/ml) was added to each tumor cells using a large-bore pipette tip. After thoroughly mixing the cell-Matrigel mixture, 25 µl of this mix was pipetted onto the mold using cold tips, forming a dome-shaped structure after pipetting. The mold was then placed on a flat surface in the incubator for at least 30 minutes to allow polymerization to occur. Subsequently, the mold was held over a petri dish while using a 10 ml pipette to wash the tumor-organoids with complete GSC medium supplemented with 1% P/S. The tumor-organoids were allowed to stabilize in the normal incubator overnight before being transferred to an agitator in the incubator.
The cultures were maintained under constant shaking for 6 days following a previously described protocol (Hubert et al., 2016). The complete GSC medium was refreshed every 2 days. Finally, seven tumoroids were pooled together and centrifugated at 200g for 4 minutes to remove exceed medium. The organoids were dissociated by adding cold PBS and gentle pipetting to break the Matrigel structure. Trypan Blue was added to a little sample to check cell viability. Cell suspension was centrifuged at 300g in 5 minutes and the PBS removed before being snap freezing on dry ice to preserve them until RNA extraction was performed.

Lentiviral shRNA cloning

shRNAs targeting *NKX2-2* were pre-designed by Sigma Aldrich and ordered in the pLKO-U6-hPGK (pLKO.1-TRC) lentiviral vector backbone. Two negative control shRNAs, non-hairpin insert control shADDGENE (Addgene, cat# 10879) and non-mammalian targeting control shC002 (Sigma-Aldrich), were cloned into the same pLKO.1-TRC backbone.

shRNA	Target sequence	Selection in bacterial cells	Selection in mammalian cells
shADDGENE	No shRNA inserts	Ampicillin	Puromycin
shC002	TTGGTGCTCTTCATCTTGTTG	Ampicillin	Puromycin
shNKX2-2.1	CGCCGTGTTTACAGAATGTTT	Ampicillin	Puromycin
shNKX2-2.5	CCTGCCGGACACCAACGATGA	Ampicillin	Puromycin

Table 8: Target sequences of the control and NKX2-2-targeting shRNA

The sequences of all plasmids were confirmed by Sanger sequencing using the pLKO.1_5 primer (5'-3': GACTATCATATGCTTACCGT) before being amplified using the NucleoBond® Xtra Midi kit (Macherey-Nagel, cat# 740410.50), and the plasmidic DNA of their corresponding MIDI preparations was quantified by spectrophotometry with NanoDrop™ 2000 (ThermoFisher Scientific, ND-2000).

Lentiviral production and transduction

Lentiviral particles were produced in HEK293T cells with at passage lower than 25. One day before transfection, HEK293T cells were plated in a T175 flask at a density of 200 000 cells/cm^2 in DMEM GlutaMAX supplemented with 10% FBS and 1% PS. The culture media were refreshed 1 hour before transfection. Transfection was performed using the psPax2 and pMD2.g second-generation packaging plasmids (Addgene cat# 12260 and cat# 12259) with the jetPRIME transfection kit (Polyplus, cat# 101000001) following the manufacturer's recommendations. The molar ratio between

psPax2:pMD2.g:transgene was 1:1:1.3. Cell culture medium was replaced 24 hours post-transfection in a biosafety level 3 laboratory with 17 ml of DMEM GlutaMAX medium containing only 1% P/S.

48 hours post-transfection, the supernatant was harvested and centrifuged for 5 minutes at 5000 rpm to pellet the detached cells. The supernatant was then gently transferred to ultracentrifuge tubes and centrifuged for 1 hour and 10 minutes at 22,000 rpm at 4°C to concentrate the viral particles. Subsequently, the supernatant was removed and 110 µl of cold PBS was added to the virus pellet, and the ultracentrifuge tubes were covered with parafilm and kept at 4°C. After 1 hour, the virus pellet was resuspended, and the suspension was centrifuged at 2500 rpm for 1 minute to pellet the debris before aliquoting the virus suspension at 10 µl per tube.

To determine the number of infecting particle, concentrated virus suspensions were titrated on the DIPG H3.3 GSC. Cells were plated at 100,000 cells/well in duplicates in a laminin-coated 12-well plate a day before the titration. Medium was replaced with 500 µl of fresh medium 1 hour before the titration. A five-fold dilution series was prepared from highly concentrated virus suspensions with a total of 6 dilutions, and 10 µl of each dilution was added drop by drop to each well. Medium was changed 4 hours post-transduction, and three days after transduction, half of the cell population was passaged to a new plate in complete medium supplemented with puromycin at a concentration of 2 µg/ml, while the other half was transferred to a plate with complete medium without puromycin. Two days post-puromycin selection, the percentage of transduced cells was calculated by manual cell counting.

The virus titer was calculated using the following formulas:

$$\%\ \text{transduced cells} = \frac{\text{Number of cells treated with puromycin}}{\text{Number of cells without puromycin}}$$

$$\text{Titer (TU/ul)} = \frac{\%\ \text{transduced cells} \times \text{initial cell number}}{100 \times V_{(\text{virus added to each well})} \times \text{dilution factor}}$$

Once the titer was determined, selected DIPG patient-derived GSC were transduced with a multiplicity of infection (MOI) of 0.5 to 1. Positive cells were selected by treating with puromycin at a concentration of 2 µg/mL for two days.

RT-qPCR

Cell pellets were collected by centrifugation for 5 minutes at 1,300rpm. Subsequently, total RNA was extracted using the RNeasy Mini kit (QIAGEN, cat#74104). To determine total RNA quantity and purity, UV absorbance was measured using a measure Nanodrop (Thermo). Reverse transcription (RT) was performed using 0.5-1ug total RNA combined in a master mix of 20 µl made on ice, containing 50ng/µL ReadyMade™ Random Hexamer Primers (2 µl; Integrated DNA Technologies, cat# 51-01-18-01), 50ng/µL anchored Oligo-dT primers (1 µl; Integrated DNA Technologies, cat# 51-01-15-08), 1X Reaction buffer (4 µl; ThermoFisher Scientific, cat# EP0442), 3.3mM dNTP (2 µl; Sigma Aldrich, cat# 04 738420001), RevertAid Reverse Transcriptase (1 µl), and nuclease-free water. One cycle of RT included 10 minutes at 25°C followed by 60 minutes at 42°C and finished with 10 minutes at 70°C.

Subsequently, the template DNA was diluted 10 times before launching qPCR with specified primers targeting *NKX2-2* (Table 6) using GoTaq® qPCR Master Mix (2X; Promega, cat# A6002). Real-time quantification was performed with triplication. The thermocycler program was run on the ViiA 7 System (ThermoFisher Scientific) with a program of a 10-minute denaturation stage at 95°C, followed by 40 cycles of denaturation at 95°C for 15 seconds, primer annealing at 60°C for 1 minute, and primer extension at 95°C for 15 seconds. Following that, a final extension was performed at 60°C for 1 minute, followed by 15 seconds of incubation at 95°C. The expression of the house-keeping gene *TBP* (TATA Binding Protein) was utilized as an internal calibrator, hence the threshold cycle (C_T) values of *NKX2-2* were normalized using the expression of the TBP housekeeping gene. Then the C_T of the all conditions were normalized with the shCOO2 control shRNA and the relative fold change of gene expression was calculated using the comparative 2-ΔΔCT method (Schmittgen and Livak, 2008).

Statistical analysis was performed using Student's t-test (***: $p < 0.001$).

Genes	Forward primer (5'→3')	Reverse primer (5'→3')
TBP	CACGAACCACGGCACTGATT	TTTTCTTGCTGCCAGTCTGGAC
NKX2-2	GCC TTC AGT ACT CCC TGC AC	GTC ATT GTC CGG TGA CTC GT

Table 9: List of primers used for RT-PCR

3D-invasion assay

GSC transduced with shRNA constructs and selected with puromycin were dissociated using StemPro™ Accutase™. Subsequently, 100 µl of complete GSC media was used to plate 15,000 cells per well on 96-well round-bottomed plates with ultra-low adherence (PrimeSurface, cat# 9096UZ). The cells were allowed to settle on a stable surface and kept for 48 hours at 37°C, 5% CO2, and 95% relative. Gliomaspheres were collected in 5 µl of complete media using wide bore pipette tip and embedded in 25 µL of Matrigel basement membrane matrix (Corning, cat# 356234, 8.9 mg/ml) using chilled pipette tips. Polymerization occurred over the next 30 minutes at 37°C, after which gliomaspheres were transferred to 24-well plates with 1 ml of complete GSC media supplemented with 1% P/S for individual tracking. Images of GSC invasion in Matrigel were captured at 0, 24, and 40 hours after embedding. The gliomasphere surface area was manually defined using Fiji software with $n \geq 9$ replicates. The invasion score was calculated by normalizing the relative surface area of each gliomasphere to its initial size at 0-hour.

Cellular proliferation assay

GSC stably carrying control and *NKX2-2* targeting shRNAs were seeded at a density of 10 000 cells/cm^2 in fully supplemented cell culture medium in a 24-well plate. Cell proliferation was monitored for 6 days using a video-microscope (Incucyte S3, Sartorius), with images captured at 4-hour intervals. Cell area was detected by modifying the cell mask parameters, followed by area confluence analysis using the

provided Incucyte software to determine the proliferation rate under the specified experimental conditions.

Senescence-Associated β-Galactosidase assay

Senescence was assessed utilizing the β-Galactosidase Cell Staining kit (Cell Signaling, cat#8960). Initially, GSC were plated at a density of 9 000 cells/cm^2 in a 24-well plate. At 48 hours post-seeding, the medium was aspirated and the cells were rinsed with PBS to remove any excess medium. Subsequently, the cells were fixed with 200 µL of Fixation solution for 15 minutes at room temperature, followed by two washes with PBS. The cells were then incubated with 200 µL of β-galactosidase staining solution in each well overnight at 37°C in a dry incubator, with parafilm seal. Images were captured using an inverted microscope, and β-galactosidase-positive cells were manually quantified using QuPath software.

Immunofluorescence

GSC stably expressing shRNAs were plated at a density of 100,000 cells per laminin-coated coverslip in 1.5 mL of complete medium. Two days post-seeding, the cells were fixed in 500 µl of 4% paraformaldehyde (PFA) for 5 minutes at room temperature (RT). After three washes with 1X PBS, the cell membrane was permeabilized by adding 500 µl of 0.5% Triton X-100 for 5 minutes at RT, followed by another three washes with PBS. Fixed and permeabilized cells were then incubated for 1 hour at RT in darkness with Hoechst (Thermo Fisher, cat# 33342) at a concentration of 1µg/ml to stain the nucleus, and Alexa Fluor® 647 Phalloidin (Cell Signaling, cat# 8940) at concentration of 3.3µM to stain F-actin. Images were captured using a Leica SP8 Confocal Microscope. Cell processes were manually tracked and quantified using the NeuroJ plugin in ImageJ.

RNA extraction of 3D-organoids

RNA extraction was conducted using TRIzol™ LS Reagent (Life Technologies, cat# 10296010) following the manufacturer's protocol. Initially, 1 ml of cold Trizol LS was

added to each pellet and thoroughly mixed using a 19G or 21G needle combined with vortexing. Next, 320 µl of chloroform was added, followed by vortexing for 10 seconds. After incubating at room temperature for 10 minutes, centrifugation was performed at 12,000g at 4°C for 15 minutes. The transparent upper layer containing RNA was carefully transferred to a new 2 ml Eppendorf tube without touching the DNA ring. The volume of this solution was checked before adding an equal volume of isopropanol and 1 µl of GlycoBlue (Thermo Fisher Scientific, cat# AM9515). The solution was homogenized by flipping the tubes a few times, followed by incubation at room temperature for 10 minutes and centrifugation at 4°C at 12,000g for 10 minutes. The supernatant was discarded, and the RNA pellet was washed three times with 1 ml of 75% ethanol, followed by centrifugation at 4°C at 12,000g for 5 minutes. After the final wash, the RNA pellet was air-dried for a few minutes and then eluted in 20 µl of RNase-free water during the final step. RNA quantity was assessed using the Qubit™ RNA High Sensitivity (HS) Assay Kit (Thermo Fisher, cat# Q32852) on a Qubit Fluorometer (Thermo Fisher). Quality analysis was performed using the 2100 Bioanalyzer (Agilent) with the RNA 6000 Nano kit (Agilent, cat# 5067-1511). Samples qualified for sequencing only if they exhibited a satisfactory profile and RIN>7.

Bulk RNA-sequencing and analysis

Total RNA was sent to Integragen SA sequencing service facility. Illumina sequencing libraries were prepared following the depletion of ribosomal RNA. Subsequently, 70 million paired-end 100 nucleotides long reads (PE100) were generated on a NovaSeq. Precisely, raw sequencing data were processed using the nf-core RNAseq pipeline (version 20.11.0-edge). Sequence quality was assessed with FastQC (version 0.11.9) before alignment to the human reference genome hg38 (GRCh38) using the STAR aligner (version 2.6.1d). Aligned sequences were then quantified at the gene level with Salmon (version 1.4.0) using gene positions from the Gencode v36 annotation file. The count matrix was filtered to remove genes with less than 10 reads across all samples. TPM normalization was performed to compare gene expression levels between and

within individuals. VST normalization was additionally performed to correct non-biological variation and visualize sample distribution based on their transcriptomic profiles. A batch effect correction was applied using the ComBat function from the R package SVA (version 3.38.0) by adjusting data based on the cell line model. Principal component analysis (PCA) was performed using the plotPCA function from the R package DESeq2 (version 1.30.0). Differential expression analysis was conducted with DESeq2 (version 1.30.0) using pre-filtered raw count data. A linear regression normalization was performed, followed by a Wald test to determine if gene expression was significantly different between predefined group of samples. The p-value associated with the statistical test was adjusted using the Benjamini-Hochberg method to control for false discovery rate.

Gene Ontology (GO) analysis was conducted using the ToppFun tool, with an adjusted p-value threshold below 0.01 to validate significantly enriched GO terms. Gene Set Enrichment Analysis (GSEA) was performed using GSEA software (v4.3.2) with a pre-ranked list of DEGs, using default settings. Venn diagram was used to select common elements between conditions (Oliveros, 2007).

Cleavage Under Targets and Tagmentation (CUT&Tag) and analysis

GSC transduced with shCTRL and ShNKX2-2.1 were harvested and prepared for CUT&Tag using the CUT&Tag-IT™ Assay kit (Anti-Mouse; Active Motif, cat# 53165) according to the manufacturer's instructions. Cells were detached using Accutase, and cold PBS was used to resuspend the cells. After cell counting, 500 000 cells per sample were transferred to a new 1.5 ml Eppendorf tube. The cell suspension was centrifuged at 600g for 3 minutes at RT. Next, 1 ml of 1X Wash buffer at RT was added to the pellet, followed by another centrifugation. The pellet was then resuspended in 1.5 ml of 1X Wash buffer in a 2 ml tube and kept on ice.

Concanavalin A beads were prepared by adding 20 µl of beads to 1.6 ml of 1X binding buffer and mixed well before placing the tube on a magnetic stand for 2 minutes to remove all the liquid. The tube was then taken off the magnetic stand, and 1.5 ml of

Binding buffer was added and cell mixed before another clearance step on the magnetic stand for 2 minutes to remove all liquid. The Concanavalin A beads were resuspended in 20 µl of 1X Binding buffer at RT and slowly added to the prepared cell sample. The cell-Concanavalin A bead mix was inverted a few times to mix and placed on an end-to-end rotator for 10 minutes at RT. Beads were washed away using the magnetic stand, and the bead-bound cells were resuspended in 50 µl Antibody buffer. Then, 1 µg of primary antibody was added to the sample and gently mixed by pipetting. Two primary antibodies were used: Histone H3K27ac antibody (1 µg; Active Motif, cat# 39133, rabbit) and NKX2-2 antibody (1 µg; Developmental Studies Hybridoma Bank DSHB, cat# 74.5A5, mouse). The sample was incubated at 4°C. After overnight incubation, the liquid was removed using the magnetic stand, and 1 µl of guinea pig anti-rabbit secondary antibody or 1ul of rabbit anti-mouse secondary antibody diluted in 100 µl Dig-wash buffer was added to the sample. The sample was mixed at RT for 60 minutes using a nutator, combined with gentle pipetting every 15 minutes. At the end of the incubation time, the liquid was removed using the magnetic stand, and 1 ml of Dig-wash buffer was added to the sample before discarding on the magnetic stand. The wash step was repeated two more times, followed by a pA-Tn5 transposomes binding step with 125 µl of supplemented Tagmentation buffer. The sample was incubated at 37°C for 1 hour using a thermomixer at 350 rpm. The tagmentation process was stopped, and DNA was solubilized by adding subsequently EDTA, SDS, and Proteinase K to the sample according to the manufacturer's protocol, followed by full-speed vortexing for 2 seconds and incubation at 55°C for 1 hour. DNA was then column purified and eluted in 35 µl of DNA purification elution buffer and further stored at -20°C. Next, library was prepared by PCR amplification with i7 and i5 indexing primers, using Q5 polymerase following the recommendation of supplier. Libraries were purified by a 2-step cleanup protocol. First, 30 µl of Mag-Bind® TotalPure NGS beads were added to each sample and vortexed briefly, followed by 5 minutes of incubation at RT. Then, 80 µl of supernatant was collected using a magnetic stand, and 25 µl of beads were added to the supernatant with 5 minutes of incubation

at RT. After that, the sample tube was placed on the magnetic stand, and once the solution was cleared, the supernatant was aspirated. After two washing with 80% ethanol, samples were eluted in 20 µl DNA elution buffer for 5 minutes at RT. Library concentration was quantified using Qubit, and the library profile was verified by Bioanalyzer using the DNA High Sensitivity Kit. Finally, CUT&Tag libraries were sent to Integragen SA for 100 bp paired-end sequencing on the NovaSeq™6000 S2 system.

After obtaining raw data, low-quality reads and adapters were trimmed and removed from the raw sequencing data using Trimgalore (v0.6.6), and FastQC (v0.11.9) was used to check read quality pre- and post-trimming. Processed reads were then aligned to the human reference genome hg38 using Bowtie2 (v2.2.2). Duplicates were removed using Picard (v2.27.4), followed by peak calling using the MACS2 (v2.2.7.1) peak caller. Duplicates were removed using Picard (v2.27.4), followed by peak calling using the MACS2 (v2.2.7.1) peak caller, with a threshold of 10 applied to select enriched peaks. Heatmaps by gene and peak were generated using deepTools (v3.5.1). All of these analyses were performed by a bioinformatician in the lab following protocol nf-core/cut&run (v3.1). The annotation of peak enrichment of NKX2-2 and H3K27ac was conducted using ChIPseeker (v1.30.3). The genomic distribution of peaks was visualized using IGV (v2.16.1) with BigWig files. Super-enhancers were detected using ROSE tool (v0.1) (Lovén et al., 2013; Whyte et al., 2013). Briefly, enriched regions of H3K27ac CUT&Tag were considered as constituent enhancers and were stitched together if they were located within 12.5 kb and ± 2 kb away from TSS. These stitched regions were ranked based on their signal intensity to define SE.

Statistical analysis

All statistical analysis was conducted on GraphPad Prism 8 software. Unless otherwise noted, data are presented as means ± standard deviation (SD). Statistical comparisons were carried out using the unpaired Student t-test for two-tailed P values (* $P < 0.05$, ** $P < 0.01$, *** $P < 0.001$, **** $P < 0.0001$).

PUBLICATIONS

Modeling the Interaction between the Microenvironment and Tumor Cells in Brain Tumors

Claudia Pasqualini, Tatsuya Kozaki, Marco Bruschi, Thi Hai Hoa Nguyen, Véronique Minard-Colin, David Castel, Jacques Grill, Florent Ginhoux.

Neuron, 2020

BIBLIOGRAPHY

Akamandisa, M.P., Nie, K., Nahta, R., Hambardzumyan, D., and Castellino, R.C. (2019). Inhibition of mutant PPM1D enhances DNA damage response and growth suppressive effects of ionizing radiation in diffuse intrinsic pontine glioma. Neuro-Oncol. *21*, 786–799. https://doi.org/10.1093/neuonc/noz053.

Akay, L.A., Effenberger, A.H., and Tsai, L.-H. (2021). Cell of all trades: oligodendrocyte precursor cells in synaptic, vascular, and immune function. Genes Dev. *35*, 180–198. https://doi.org/10.1101/gad.344218.120.

Akilesh, S., Suleiman, H., Yu, H., Stander, M.C., Lavin, P., Gbadegesin, R., Antignac, C., Pollak, M., Kopp, J.B., Winn, M.P., et al. (2011). Arhgap24 inactivates Rac1 in mouse podocytes, and a mutant form is associated with familial focal segmental glomerulosclerosis. J. Clin. Invest. *121*, 4127–4137. https://doi.org/10.1172/JCI46458.

Alimperti, S., and Andreadis, S.T. (2015). CDH2 and CDH11 act as regulators of stem cell fate decisions. Stem Cell Res. *14*, 270–282. https://doi.org/10.1016/j.scr.2015.02.002.

Alizadeh, A.A., Aranda, V., Bardelli, A., Blanpain, C., Bock, C., Borowski, C., Caldas, C., Califano, A., Doherty, M., Elsner, M., et al. (2015). Toward understanding and exploiting tumor heterogeneity. Nat. Med. *21*, 846–853. https://doi.org/10.1038/nm.3915.

Alvarez-Buylla, A., García-Verdugo, J.M., and Tramontin, A.D. (2001). A unified hypothesis on the lineage of neural stem cells. Nat. Rev. Neurosci. *2*, 287–293. https://doi.org/10.1038/35067582.

Anderson, J.L., Muraleedharan, R., Oatman, N., Klotter, A., Sengupta, S., Waclaw, R.R., Wu, J., Drissi, R., Miles, L., Raabe, E.H., et al. (2017). The transcription factor Olig2 is important for the biology of diffuse intrinsic pontine gliomas. Neuro-Oncol. *19*, 1068–1078. https://doi.org/10.1093/neuonc/now299.

Anderson, K.R., Torres, C.A., Solomon, K., Becker, T.C., Newgard, C.B., Wright, C.V., Hagman, J., and Sussel, L. (2009). Cooperative Transcriptional Regulation of the Essential Pancreatic Islet Gene *NeuroD1* (*Beta2*) by Nkx2.2 and Neurogenin 3*. J. Biol. Chem. *284*, 31236–31248. https://doi.org/10.1074/jbc.M109.048694.

Aoyagi, Y., Hibi, T., Kimori, Y., Sawada, M., Kawakami, R., Sawamoto, K., and Nemoto, T. (2018). Heterogeneous distribution of doublecortin-expressing cells surrounding the rostral migratory stream in the juvenile mouse. J. Comp. Neurol. *526*, 2631–2646. https://doi.org/10.1002/cne.24521.

Auerbach, A., Cohen, A., Ofek Shlomai, N., Weinberg-Shukron, A., Gulsuner, S., King, M.-C., Hemi, R., Levy-Lahad, E., Abulibdeh, A., and Zangen, D. (2020). NKX2-2 Mutation Causes Congenital Diabetes and Infantile Obesity With Paradoxical Glucose-Induced Ghrelin Secretion. J. Clin. Endocrinol. Metab. *105*, dgaa563.

https://doi.org/10.1210/clinem/dgaa563.

Auffret, L., Ajlil, Y., Tauziède-Espariat, A., Kergrohen, T., Puiseux, C., Riffaud, L., Blouin, P., Bertozzi, A.-I., Leblond, P., Blomgren, K., et al. (2024). A new subtype of diffuse midline glioma, H3 K27 and BRAF/FGFR1 co-altered: a clinico-radiological and histomolecular characterisation. Acta Neuropathol. (Berl.) *147*, 2. https://doi.org/10.1007/s00401-023-02651-4.

Auguste, Y.S.S., Ferro, A., Kahng, J.A., Xavier, A.M., Dixon, J.R., Vrudhula, U., Nichitiu, A.-S., Rosado, D., Wee, T.-L., Pedmale, U.V., et al. (2022). Oligodendrocyte precursor cells engulf synapses during circuit remodeling in mice. Nat. Neurosci. *25*, 1273–1278. https://doi.org/10.1038/s41593-022-01170-x.

Aziz-Bose, R., and Monje, M. (2019). Diffuse intrinsic pontine glioma: molecular landscape and emerging therapeutic targets. Curr. Opin. Oncol. *31*, 522–530. https://doi.org/10.1097/CCO.0000000000000577.

Baer, A.S., Syed, Y.A., Kang, S.U., Mitteregger, D., Vig, R., ffrench-Constant, C., Franklin, R.J.M., Altmann, F., Lubec, G., and Kotter, M.R. (2009). Myelin-mediated inhibition of oligodendrocyte precursor differentiation can be overcome by pharmacological modulation of Fyn-RhoA and protein kinase C signalling. Brain *132*, 465–481. https://doi.org/10.1093/brain/awn334.

Baker, S.J., Ellison, D.W., and Gutmann, D.H. (2016). Pediatric Gliomas as Neurodevelopmental Disorders. Glia *64*, 879–895. https://doi.org/10.1002/glia.22945.

Bax, D.A., Mackay, A., Little, S.E., Carvalho, D., Viana-Pereira, M., Tamber, N., Grigoriadis, A.E., Ashworth, A., Reis, R.M., Ellison, D.W., et al. (2010). A Distinct Spectrum of Copy Number Aberrations in Pediatric High-Grade Gliomas. Clin. Cancer Res. *16*, 3368–3377. https://doi.org/10.1158/1078-0432.CCR-10-0438.

Bellail, A.C., Hunter, S.B., Brat, D.J., Tan, C., and Van Meir, E.G. (2004). Microregional extracellular matrix heterogeneity in brain modulates glioma cell invasion. Int. J. Biochem. Cell Biol. *36*, 1046–1069. https://doi.org/10.1016/j.biocel.2004.01.013.

Bender, S., Tang, Y., Lindroth, A.M., Hovestadt, V., Jones, D.T.W., Kool, M., Zapatka, M., Northcott, P.A., Sturm, D., Wang, W., et al. (2013). Reduced H3K27me3 and DNA Hypomethylation Are Major Drivers of Gene Expression in K27M Mutant Pediatric High-Grade Gliomas. Cancer Cell *24*, 660–672. https://doi.org/10.1016/j.ccr.2013.10.006.

Bhatt, N.S., Houser, K., Belongia, M., Ellison, D.W., Foy, A., Jarzembowski, J., Kelly, T., Maheshwari, M., Suchi, M., and Knipstein, J. (2020). Diffuse Midline Glioma With Osseous Metastases at Diagnosis: A Case Report. J. Pediatr. Hematol. Oncol. *42*, e673. https://doi.org/10.1097/MPH.0000000000001598.

Binamé, F., Sakry, D., Dimou, L., Jolivel, V., and Trotter, J. (2013). NG2 Regulates Directional Migration of Oligodendrocyte Precursor Cells via Rho GTPases and Polarity Complex Proteins. J. Neurosci. *33*, 10858–10874. https://doi.org/10.1523/JNEUROSCI.5010-12.2013.

Bodor, D.L., Pönisch, W., Endres, R.G., and Paluch, E.K. (2020). Of Cell Shapes and Motion: The Physical Basis of Animal Cell Migration. Dev. Cell *52*, 550–562. https://doi.org/10.1016/j.devcel.2020.02.013.

Bonetto, G., Belin, D., and Káradóttir, R.T. (2021). Myelin: A gatekeeper of activity-dependent circuit plasticity? Science *374*, eaba6905. https://doi.org/10.1126/science.aba6905.

Boros, J., Arnoult, N., Stroobant, V., Collet, J.-F., and Decottignies, A. (2014). Polycomb Repressive Complex 2 and H3K27me3 Cooperate with H3K9 Methylation To Maintain Heterochromatin Protein 1α at Chromatin. Mol. Cell. Biol. *34*, 3662–3674. https://doi.org/10.1128/MCB.00205-14.

Bradl, M., and Lassmann, H. (2010). Oligodendrocytes: biology and pathology. Acta Neuropathol. (Berl.) *119*, 37–53. https://doi.org/10.1007/s00401-009-0601-5.

Briscoe, J., Sussel, L., Serup, P., Hartigan-O'Connor, D., Jessell, T.M., Rubenstein, J.L.R., and Ericson, J. (1999). Homeobox gene Nkx2.2 and speci®cation of neuronal identity by graded Sonic hedgehog signalling. *398*. .

Broniscer, A., Baker, J.N., Baker, S.J., Chi, S.N., Geyer, J.R., Morris, E.B., and Gajjar, A. (2010). Prospective collection of tissue samples at autopsy in children with diffuse intrinsic pontine glioma. Cancer *116*, 4632–4637. https://doi.org/10.1002/cncr.25405.

Bruschi, M., Midjek, L., Ajlil, Y., Vairy, S., Lancien, M., Ghermaoui, S., Kergrohen, T., Verreault, M., Idbaih, A., De Biagi, C.A.O., et al. (2023). Diffuse midline glioma invasion and metastasis rely on cell-autonomous signaling. Neuro-Oncol. noad161. https://doi.org/10.1093/neuonc/noad161.

Buchanan, J., Elabbady, L., Collman, F., Jorstad, N.L., Bakken, T.E., Ott, C., Glatzer, J., Bleckert, A.A., Bodor, A.L., Brittain, D., et al. (2022). Oligodendrocyte precursor cells ingest axons in the mouse neocortex. Proc. Natl. Acad. Sci. *119*, e2202580119. https://doi.org/10.1073/pnas.2202580119.

Buchanan, J., Costa, N.M. da, and Cheadle, L. (2023). Emerging roles of oligodendrocyte precursor cells in neural circuit development and remodeling. Trends Neurosci. *46*, 628–639. https://doi.org/10.1016/j.tins.2023.05.007.

Buckles, G.R., Thorpe, C.J., Ramel, M.-C., and Lekven, A.C. (2004). Combinatorial Wnt control of zebrafish midbrain–hindbrain boundary formation. Mech. Dev. *121*, 437–447. https://doi.org/10.1016/j.mod.2004.03.026.

Buczkowicz, P., Bartels, U., Bouffet, E., Becher, O., and Hawkins, C. (2014). Histopathological spectrum of paediatric diffuse intrinsic pontine glioma: diagnostic and therapeutic implications. Acta Neuropathol. (Berl.) *128*, 573–581. https://doi.org/10.1007/s00401-014-1319-6.

Bushweller, J.H. (2019). Targeting transcription factors in cancer — from undruggable to reality. Nat. Rev. Cancer *19*, 611–624. https://doi.org/10.1038/s41568-019-0196-7.

Butts, B.D., Houde, C., and Mehmet, H. (2008). Maturation-dependent sensitivity of oligodendrocyte lineage cells to apoptosis: implications for normal development and disease. Cell Death Differ. *15*, 1178–1186. https://doi.org/10.1038/cdd.2008.70.

Caretti, V., Bugiani, M., Freret, M., Schellen, P., Jansen, M., Van Vuurden, D., Kaspers, G., Fisher, P.G., Hulleman, E., Wesseling, P., et al. (2014). Subventricular spread of diffuse intrinsic pontine glioma. Acta Neuropathol. (Berl.) *128*, 605–607. https://doi.org/10.1007/s00401-014-1307-x.

Carlson, B.M. (2019). Human embryology and developmental biology (St. Louis, Missouri: Elsevier).

Carro, M.S., Lim, W.K., Alvarez, M.J., Bollo, R.J., Zhao, X., Snyder, E.Y., Sulman, E.P., Anne, S.L., Doetsch, F., Colman, H., et al. (2010). The transcriptional network for mesenchymal transformation of brain tumors. Nature *463*, 318–325. https://doi.org/10.1038/nature08712.

Caruso, F.P., Garofano, L., D'Angelo, F., Yu, K., Tang, F., Yuan, J., Zhang, J., Cerulo, L., Pagnotta, S.M., Bedognetti, D., et al. (2020). A map of tumor–host interactions in glioma at single-cell resolution. GigaScience *9*, giaa109. https://doi.org/10.1093/gigascience/giaa109.

Castel, D., Philippe, C., Calmon, R., Le Dret, L., Truffaux, N., Boddaert, N., Pagès, M., Taylor, K.R., Saulnier, P., Lacroix, L., et al. (2015). Histone H3F3A and HIST1H3B K27M mutations define two subgroups of diffuse intrinsic pontine gliomas with different prognosis and phenotypes. Acta Neuropathol. (Berl.) *130*, 815–827. https://doi.org/10.1007/s00401-015-1478-0.

Castel, D., Kergrohen, T., Tauziède-Espariat, A., Mackay, A., Ghermaoui, S., Lechapt, E., Pfister, S.M., Kramm, C.M., Boddaert, N., Blauwblomme, T., et al. (2020). Histone H3 wild-type DIPG/DMG overexpressing EZHIP extend the spectrum diffuse midline gliomas with PRC2 inhibition beyond H3-K27M mutation. Acta Neuropathol. (Berl.) *139*, 1109–1113. https://doi.org/10.1007/s00401-020-02142-w.

Cha, J., and Kim, P. (2017). Biomimetic Strategies for the Glioblastoma Microenvironment. Front. Mater. *4*. .

Chaffer, C.L., and Weinberg, R.A. (2011). A Perspective on Cancer Cell Metastasis. Science *331*, 1559–1564. https://doi.org/10.1126/science.1203543.

Chan, K.-M., Fang, D., Gan, H., Hashizume, R., Yu, C., Schroeder, M., Gupta, N., Mueller, S., James, C.D., Jenkins, R., et al. (2013). The histone H3.3K27M mutation in pediatric glioma reprograms H3K27 methylation and gene expression. Genes Dev. *27*, 985–990. https://doi.org/10.1101/gad.217778.113.

Chapman, H., Waclaw, R.R., Pei, Z., Nakafuku, M., and Campbell, K. (2013). The homeobox gene Gsx2 controls the timing of oligodendroglial fate specification in mouse lateral ganglionic eminence progenitors. Dev. Camb. Engl. *140*, 2289–2298. https://doi.org/10.1242/dev.091090.

Chavali, M., Ulloa-Navas, M.J., Pérez-Borredá, P., Garcia-Verdugo, J.M., McQuillen, P.S., Huang, E.J., and Rowitch, D.H. (2020). Wnt-Dependent Oligodendroglial-Endothelial Interactions Regulate White Matter Vascularization and Attenuate Injury. Neuron *108*, 1130-1145.e5. https://doi.org/10.1016/j.neuron.2020.09.033.

Chen, H., Liu, W., Zhong, L., Liao, D., Zhang, R., Kang, T., and Wu, Y. (2018). NKX2-2 Suppresses Osteosarcoma Metastasis and Proliferation by Downregulating Multiple Target Genes. J. Cancer *9*, 3067–3077. https://doi.org/10.7150/jca.26382.

Chen, Y., Chen, Z., Tang, Y., and Xiao, Q. (2021). The involvement of noncanonical Wnt signaling in cancers. Biomed. Pharmacother. *133*, 110946. https://doi.org/10.1016/j.biopha.2020.110946.

Chiang, J., Diaz, A.K., Makepeace, L., Li, X., Han, Y., Li, Y., Klimo, P., Boop, F.A., Baker, S.J., Gajjar, A., et al. (2020). Clinical, imaging, and molecular analysis of pediatric pontine tumors lacking characteristic imaging features of DIPG. Acta Neuropathol. Commun. *8*, 57. https://doi.org/10.1186/s40478-020-00930-9.

Choe, Y., Huynh, T., and Pleasure, S.J. (2014). Migration of Oligodendrocyte Progenitor Cells Is Controlled by Transforming Growth Factor β Family Proteins during Corticogenesis. J. Neurosci. *34*, 14973–14983. https://doi.org/10.1523/JNEUROSCI.1156-14.2014.

Churchill, A.J., Gutiérrez, G.D., Singer, R.A., Lorberbaum, D.S., Fischer, K.A., and Sussel, L. (2017). Genetic evidence that Nkx2.2 acts primarily downstream of Neurog3 in pancreatic endocrine lineage development. eLife *6*, e20010. https://doi.org/10.7554/eLife.20010.

Cmero, M., Yuan, K., Ong, C.S., Schröder, J., Corcoran, N.M., Papenfuss, T., Hovens, C.M., Markowetz, F., and Macintyre, G. (2020). Inferring structural variant cancer cell fraction. Nat. Commun. *11*, 730. https://doi.org/10.1038/s41467-020-14351-8.

Cohen, A.R. (2022). Brain Tumors in Children. N. Engl. J. Med. *386*, 1922–1931. https://doi.org/10.1056/NEJMra2116344.

Cuddapah, V.A., Robel, S., Watkins, S., and Sontheimer, H. (2014). A neurocentric perspective on glioma invasion. Nat. Rev. Neurosci. *15*, 455–465. https://doi.org/10.1038/nrn3765.

Dai, C., Celestino, J.C., Okada, Y., Louis, D.N., Fuller, G.N., and Holland, E.C. (2001). PDGF autocrine stimulation dedifferentiates cultured astrocytes and induces oligodendrogliomas and oligoastrocytomas from neural progenitors and astrocytes in vivo. Genes Dev. *15*, 1913–1925. https://doi.org/10.1101/gad.903001.

Da-Veiga, M.-A., Rogister, B., Lombard, A., Neirinckx, V., and Piette, C. (2022). Glioma Stem Cells in Pediatric High-Grade Gliomas: From Current Knowledge to Future Perspectives. Cancers *14*, 2296. https://doi.org/10.3390/cancers14092296.

Dawson, M.R.L., Polito, A., Levine, J.M., and Reynolds, R. (2003). NG2-expressing glial progenitor cells: an abundant and widespread population of cycling cells in the adult rat CNS. Mol. Cell. Neurosci. *24*, 476–488. https://doi.org/10.1016/S1044-7431(03)00210-0.

De Martino, L., Picariello, S., Russo, C., Errico, M.E., Spennato, P., Papa, M.R., Normanno, N., Scimone, G., Colafati, G.S., Cacchione, A., et al. (2023). Extra-neural metastases in pediatric diffuse midline gliomas, H3 K27-altered: presentation of two cases and literature review. Front. Mol. Neurosci. *16*, 1152430. https://doi.org/10.3389/fnmol.2023.1152430.

Dentro, S.C., Wedge, D.C., and Van Loo, P. (2017). Principles of Reconstructing the Subclonal Architecture of Cancers. Cold Spring Harb. Perspect. Med. *7*, a026625. https://doi.org/10.1101/cshperspect.a026625.

Desai, S., Loomis, Z., Pugh-Bernard, A., Schrunk, J., Doyle, M.J., Minic, A., McCoy, E., and Sussel, L. (2008). Nkx2.2 regulates cell fate choice in the enteroendocrine cell lineages of the intestine. Dev. Biol. *313*, 58–66. https://doi.org/10.1016/j.ydbio.2007.09.047.

Dias, J.M., Alekseenko, Z., Jeggari, A., Boareto, M., Vollmer, J., Kozhevnikova, M., Wang, H., Matise, M.P., Alexeyenko, A., Iber, D., et al. (2020). A Shh/Gli-driven three-node timer motif controls temporal identity and fate of neural stem cells. Sci. Adv. *6*, eaba8196. https://doi.org/10.1126/sciadv.aba8196.

Donaldson, S.S., Laningham, F., and Fisher, P.G. (2006). Advances Toward an Understanding of Brainstem Gliomas. J. Clin. Oncol. *24*, 1266–1272. https://doi.org/10.1200/JCO.2005.04.6599.

Duchatel, R.J., Jackson, E.R., Alvaro, F., Nixon, B., Hondermarck, H., and Dun, M.D. (2019). Signal Transduction in Diffuse Intrinsic Pontine Glioma. PROTEOMICS *19*, 1800479. https://doi.org/10.1002/pmic.201800479.

Dugas, J.C., Tai, Y.C., Speed, T.P., Ngai, J., and Barres, B.A. (2006). Functional Genomic Analysis of Oligodendrocyte Differentiation. J. Neurosci. *26*, 10967–10983. https://doi.org/10.1523/JNEUROSCI.2572-06.2006.

Elbaz, B., and Popko, B. (2019). Molecular Control of Oligodendrocyte Development. Trends Neurosci. *42*, 263–277. https://doi.org/10.1016/j.tins.2019.01.002.

Ellison, J. a., Scully, S. a., and de Vellis, J. (1996). Evidence for neuronal regulation of oligodendrocyte development: Cellular localization of platelet-derived growth factor α receptor and A-chain mRNA during cerebral cortex development in the rat. J. Neurosci. Res. *45*, 28–39. https://doi.org/10.1002/(SICI)1097-4547(19960701)45:1<28::AID-JNR3>3.0.CO;2-J.

Emery, B. (2010). Regulation of Oligodendrocyte Differentiation and Myelination. Science *330*, 779–782. https://doi.org/10.1126/science.1190927.

Fabi, A., Vidiri, A., Carapella, C., Pace, A., Occhipinti, E., Caroli, F., Mirri, A., Carlini, P., and Cognetti, F. Bone Metastasis from Glioblastoma Multiforme Without Central Nervous System Relapse: A Case Report.

Fadul, J., Bell, R., Hoffman, L.M., Beckerle, M.C., Engel, M.E., and Lessnick, S.L. (2015). EWS/FLI utilizes NKX2-2 to repress mesenchymal features of Ewing sarcoma. Genes Cancer *6*, 129–143. .

Falcão, A.M., van Bruggen, D., Marques, S., Meijer, M., Jäkel, S., Agirre, E., Samudyata, Floriddia, E.M., Vanichkina, D.P., ffrench-Constant, C., et al. (2019). Disease-specific oligodendrocyte lineage cells arise in multiple sclerosis. Nat. Med. *24*, 1837–1844. https://doi.org/10.1038/s41591-018-0236-y.

Fang, D., Gan, H., Cheng, L., Lee, J.-H., Zhou, H., Sarkaria, J.N., Daniels, D.J., and Zhang, Z. (2018). H3.3K27M mutant proteins reprogram epigenome by sequestering the PRC2 complex to poised enhancers. eLife *7*, e36696. https://doi.org/10.7554/eLife.36696.

Fares, J., Fares, M.Y., Khachfe, H.H., Salhab, H.A., and Fares, Y. (2020). Molecular principles of metastasis: a hallmark of cancer revisited. Signal Transduct. Target. Ther. *5*, 1–17. https://doi.org/10.1038/s41392-020-0134-x.

Filbin, M.G., Tirosh, I., Hovestadt, V., Shaw, M.L., Escalante, L.E., Mathewson, N.D., Neftel, C., Frank, N., Pelton, K., Hebert, C.M., et al. (2018). Developmental and oncogenic programs in H3K27M gliomas dissected by single-cell RNA-seq. Science *360*, 331–335. https://doi.org/10.1126/science.aao4750.

Findlay, I.J., De Iuliis, G.N., Duchatel, R.J., Jackson, E.R., Vitanza, N.A., Cain, J.E., Waszak, S.M., and Dun, M.D. (2022). Pharmaco-proteogenomic profiling of pediatric diffuse midline glioma to inform future treatment strategies. Oncogene *41*, 461–475. https://doi.org/10.1038/s41388-021-02102-y.

Flanagan, S.E., De Franco, E., Lango Allen, H., Zerah, M., Abdul-Rasoul, M.M., Edge, J.A., Stewart, H., Alamiri, E., Hussain, K., Wallis, S., et al. (2014). Analysis of Transcription Factors Key for Mouse Pancreatic Development

Establishes NKX2-2 and MNX1 Mutations as Causes of Neonatal Diabetes in Man. Cell Metab. *19*, 146–154. https://doi.org/10.1016/j.cmet.2013.11.021.

Fontebasso, A.M., Schwartzentruber, J., Khuong-Quang, D.-A., Liu, X.-Y., Sturm, D., Korshunov, A., Jones, D.T.W., Witt, H., Kool, M., Albrecht, S., et al. (2013). puge. Acta Neuropathol. (Berl.) *125*, 659–669. https://doi.org/10.1007/s00401-013-1095-8.

Force, L.M., Abdollahpour, I., Advani, S.M., Agius, D., Ahmadian, E., Alahdab, F., Alam, T., Alebel, A., Alipour, V., Allen, C.A., et al. (2019). The global burden of childhood and adolescent cancer in 2017: an analysis of the Global Burden of Disease Study 2017. Lancet Oncol. *20*, 1211–1225. https://doi.org/10.1016/S1470-2045(19)30339-0.

Fortin, J., Tian, R., Zarrabi, I., Hill, G., Williams, E., Sanchez-Duffhues, G., Thorikay, M., Ramachandran, P., Siddaway, R., Wong, J.F., et al. (2020). Mutant ACVR1 Arrests Glial Cell Differentiation to Drive Tumorigenesis in Pediatric Gliomas. Cancer Cell https://doi.org/10.1016/j.ccell.2020.02.002.

Frost, E., Kiernan, B.W., Faissner, A., and ffrench-Constant, C. (2010). Regulation of Oligodendrocyte Precursor Migration by Extracellular Matrix: Evidence for Substrate-Specific Inhibition of Migration by Tenascin-C. Dev. Neurosci. *18*, 266–273. https://doi.org/10.1159/000111416.

Fu, H., Qi, Y., Tan, M., Cai, J., Takebayashi, H., Nakafuku, M., Richardson, W., and Qiu, M. (2002). Dual origin of spinal oligodendrocyte progenitors and evidence for the cooperative role of Olig2 and Nkx2.2 in the control of oligodendrocyte differentiation. Development *129*, 681–693. https://doi.org/10.1242/dev.129.3.681.

Fukumoto, M., Kurisu, S., Yamada, T., and Takenawa, T. (2015). α-Actinin-4 Enhances Colorectal Cancer Cell Invasion by Suppressing Focal Adhesion Maturation. PLOS ONE *10*, e0120616. https://doi.org/10.1371/journal.pone.0120616.

Fukushima, N., Yokouchi, K., Kawagishi, K., and Moriizumi, T. (2002). Differential neurogenesis and gliogenesis by local and migrating neural stem cells in the olfactory bulb. Neurosci. Res. *44*, 467–473. https://doi.org/10.1016/S0168-0102(02)00173-6.

Funato, K., Major, T., Lewis, P.W., Allis, C.D., and Tabar, V. (2016). Use of human embryonic stem cells to model pediatric gliomas with H3.3K27M histone mutation.

Gage, F.H. (2000). Mammalian Neural Stem Cells. Science *287*, 1433–1438. https://doi.org/10.1126/science.287.5457.1433.

Gatta, G., Peris-Bonet, R., Visser, O., Stiller, C., Marcos-Gragera, R., Sánchez, M.-J., Lacour, B., Kaatsch, P., Berrino, F., Rutkowski, S., et al. (2017). Geographical variability in survival of European children with central nervous system tumours. Eur. J. Cancer *82*, 137–148. https://doi.org/10.1016/j.ejca.2017.05.028.

Gensert, J.M., and Goldman, J.E. (2001). Heterogeneity of cycling glial progenitors in the adult mammalian cortex and white matter. J. Neurobiol. *48*, 75–86. .

Gibson, E.M., Purger, D., Mount, C.W., Goldstein, A.K., Lin, G.L., Wood, L.S., Inema, I., Miller, S.E., Bieri, G., Zuchero, J.B., et al. (2014). Neuronal Activity Promotes Oligodendrogenesis and Adaptive Myelination in the Mammalian Brain. Science *344*, 1252304. https://doi.org/10.1126/science.1252304.

de Gooijer, M.C., Guillén Navarro, M., Bernards, R., Wurdinger, T., and van Tellingen, O. (2018). An Experimenter's Guide to Glioblastoma Invasion Pathways. Trends Mol. Med. *24*, 763–780. https://doi.org/10.1016/j.molmed.2018.07.003.

Grill, J., and Bhangoo, R. (2007). Recent development in chemotherapy of paediatric brain tumours. Curr. Opin. Oncol. *19*, 612–615. https://doi.org/10.1097/CCO.0b013e3282f03152.

Gui, P., and Bivona, T.G. (2022). Evolution of metastasis: new tools and insights. Trends Cancer *8*, 98–109. https://doi.org/10.1016/j.trecan.2021.11.002.

Gururangan, S., McLaughlin, C.A., Brashears, J., Watral, M.A., Provenzale, J., Coleman, R.E., Halperin, E.C., Quinn, J.,

Reardon, D., Vredenburgh, J., et al. (2006). Incidence and patterns of neuraxis metastases in children with diffuse pontine glioma★. J. Neurooncol. *77*, 207–212. https://doi.org/10.1007/s11060-005-9029-5.

Gutiérrez, G.D., Bender, A.S., Cirulli, V., Mastracci, T.L., Kelly, S.M., Tsirigos, A., Kaestner, K.H., and Sussel, L. (2017). Pancreatic **β** cell identity requires continual repression of non–**β** cell programs. J. Clin. Invest. *127*, 244–259. https://doi.org/10.1172/JCI88017.

Haag, D., Mack, N., Benites Goncalves Da Silva, P., Statz, B., Clark, J., Tanabe, K., Sharma, T., Jäger, N., Jones, D.T.W., Kawauchi, D., et al. (2021). H3.3-K27M drives neural stem cell-specific gliomagenesis in a human iPSC-derived model. Cancer Cell *39*, 407-422.e13. https://doi.org/10.1016/j.ccell.2021.01.005.

Hamisch, C., Kickingereder, P., Fischer, M., Simon, T., and Ruge, M.I. (2017). Update on the diagnostic value and safety of stereotactic biopsy for pediatric brainstem tumors: a systematic review and meta-analysis of 735 cases. J. Neurosurg. Pediatr. *20*, 261–268. https://doi.org/10.3171/2017.2.PEDS1665.

Hanahan, D., and Weinberg, R.A. (2000). The Hallmarks of Cancer. Cell *100*, 57–70. https://doi.org/10.1016/S0092-8674(00)81683-9.

Hanahan, D., and Weinberg, R.A. (2011). Hallmarks of Cancer: The Next Generation. Cell *144*, 646–674. https://doi.org/10.1016/j.cell.2011.02.013.

Handis, C., Tanrıkulu, B., Danyeli, A.E., and Özek, M.M. (2021). Spinal intramedullary H3K27M mutant glioma with vertebral metastasis: a case report. Childs Nerv. Syst. *37*, 3933–3937. https://doi.org/10.1007/s00381-021-05119-6.

Hansen, D.V., Lui, J.H., Flandin, P., Yoshikawa, K., Rubenstein, J.L., Alvarez-Buylla, A., and Kriegstein, A.R. (2013). Non-epithelial stem cells and cortical interneuron production in the human ganglionic eminences. Nat. Neurosci. *16*, 1576–1587. https://doi.org/10.1038/nn.3541.

Hapach, L.A., Mosier, J.A., Wang, W., and Reinhart-King, C.A. (2019). Engineered models to parse apart the metastatic cascade. Npj Precis. Oncol. *3*, 1–8. https://doi.org/10.1038/s41698-019-0092-3.

Hardy, R.J., and Friedrich, V.L., Jr (1996). Oligodendrocyte progenitors are generated throughout the embryonic mouse brain, but differentiate in restricted foci. Development *122*, 2059–2069. https://doi.org/10.1242/dev.122.7.2059.

Harutyunyan, A.S., Krug, B., Chen, H., Papillon-Cavanagh, S., Zeinieh, M., De Jay, N., Deshmukh, S., Chen, C.C.L., Belle, J., Mikael, L.G., et al. (2019). H3K27M induces defective chromatin spread of PRC2-mediated repressive H3K27me2/me3 and is essential for glioma tumorigenesis. Nat. Commun. *10*, 1262. https://doi.org/10.1038/s41467-019-09140-x.

Haubensak, W., Attardo, A., Denk, W., and Huttner, W.B. (2004). Neurons arise in the basal neuroepithelium of the early mammalian telencephalon: A major site of neurogenesis. Proc. Natl. Acad. Sci. U. S. A. *101*, 3196–3201. https://doi.org/10.1073/pnas.0308600100.

Hevia, C.F., Engel-Pizcueta, C., Udina, F., and Pujades, C. (2022). The neurogenic fate of the hindbrain boundaries relies on Notch3-dependent asymmetric cell divisions. Cell Rep. *39*, 110915. https://doi.org/10.1016/j.celrep.2022.110915.

Hirbec, H., Déglon, N., Foo, L.C., Goshen, I., Grutzendler, J., Hangen, E., Kreisel, T., Linck, N., Muffat, J., Regio, S., et al. (2020). Emerging technologies to study glial cells. Glia *68*, 1692–1728. https://doi.org/10.1002/glia.23780.

Hochart, A., Escande, F., Rocourt, N., Grill, J., Koubi-Pick, V., Beaujot, J., Meignan, S., Vinchon, M., Maurage, C.A., and Leblond, P. (2015). Long survival in a child with a mutated K27M-H3.3 pilocytic astrocytoma. Ann. Clin. Transl. Neurol. *2*, 439–443. https://doi.org/10.1002/acn3.184.

Hoeman, C.M., Cordero, F.J., Hu, G., Misuraca, K., Romero, M.M., Cardona, H.J., Nazarian, J., Hashizume, R., McLendon, R., Yu, P., et al. (2019). ACVR1 R206H cooperates with H3.1K27M in promoting diffuse intrinsic pontine glioma pathogenesis. Nat. Commun. *10*, 1023. https://doi.org/10.1038/s41467-019-08823-9.

Hoffman, L.M., DeWire, M., Ryall, S., Buczkowicz, P., Leach, J., Miles, L., Ramani, A., Brudno, M., Kumar, S.S., Drissi, R., et al. (2016). Spatial genomic heterogeneity in diffuse intrinsic pontine and midline high-grade glioma: implications for diagnostic biopsy and targeted therapeutics. Acta Neuropathol. Commun. *4*, 1. https://doi.org/10.1186/s40478-015-0269-0.

Hoffman, L.M., Veldhuijzen van Zanten, S.E.M., Colditz, N., Baugh, J., Chaney, B., Hoffmann, M., Lane, A., Fuller, C., Miles, L., Hawkins, C., et al. (2018). Clinical, Radiologic, Pathologic, and Molecular Characteristics of Long-Term Survivors of Diffuse Intrinsic Pontine Glioma (DIPG): A Collaborative Report From the International and European Society for Pediatric Oncology DIPG Registries. J. Clin. Oncol. *36*, 1963–1972. https://doi.org/10.1200/JCO.2017.75.9308.

Hood, J.D., and Cheresh, D.A. (2002). Role of integrins in cell invasion and migration. Nat. Rev. Cancer *2*, 91–100. https://doi.org/10.1038/nrc727.

Huang, W., Bhaduri, A., Velmeshev, D., Wang, S., Wang, L., Rottkamp, C.A., Alvarez-Buylla, A., Rowitch, D.H., and Kriegstein, A.R. (2020). Origins and Proliferative States of Human Oligodendrocyte Precursor Cells. Cell *182*, 594-608.e11. https://doi.org/10.1016/j.cell.2020.06.027.

Hughes, E.G., Kang, S.H., Fukaya, M., and Bergles, D.E. (2013). Oligodendrocyte progenitors balance growth with self-repulsion to achieve homeostasis in the adult brain. Nat. Neurosci. *16*, 668–676. https://doi.org/10.1038/nn.3390.

Hutchings, C., Nuriel, Y., Lazar, D., Kohl, A., Muir, E., Genin, O., Cinnamon, Y., Benyamini, H., Nevo, Y., and Sela-Donenfeld, D. (2024). Hindbrain boundaries as niches of neural progenitor and stem cells regulated by the extracellular matrix proteoglycan chondroitin sulphate. Dev. Camb. Engl. *151*, dev201934. https://doi.org/10.1242/dev.201934.

IWADATE, Y. (2016). Epithelial-mesenchymal transition in glioblastoma progression. Oncol. Lett. *11*, 1615–1620. https://doi.org/10.3892/ol.2016.4113.

Jain, S.U., Rashoff, A.Q., Krabbenhoft, S.D., Hoelper, D., Do, T.J., Gibson, T.J., Lundgren, S.M., Bondra, E.R., Deshmukh, S., Harutyunyan, A.S., et al. (2020). H3 K27M and EZHIP Impede H3K27-Methylation Spreading by Inhibiting Allosterically Stimulated PRC2. Mol. Cell *80*, 726-735.e7. https://doi.org/10.1016/j.molcel.2020.09.028.

Jakovcevski, I., and Zecevic, N. (2005). Sequence of oligodendrocyte development in the human fetal telencephalon. Glia *49*, 480–491. https://doi.org/10.1002/glia.20134.

Jakovcevski, I., Filipovic, R., Mo, Z., Rakic, S., and Zecevic, N. (2009). Oligodendrocyte Development and the Onset of Myelination in the Human Fetal Brain. Front. Neuroanat. *3*, 5. https://doi.org/10.3389/neuro.05.005.2009.

Jansen, M.H., Veldhuijzen van Zanten, S.E., Sanchez Aliaga, E., Heymans, M.W., Warmuth-Metz, M., Hargrave, D., van der Hoeven, E.J., Gidding, C.E., de Bont, E.S., Eshghi, O.S., et al. (2015). Survival prediction model of children with diffuse intrinsic pontine glioma based on clinical and radiological criteria. Neuro-Oncol. *17*, 160–166. https://doi.org/10.1093/neuonc/nou104.

Jarjour, A.A., Manitt, C., Moore, S.W., Thompson, K.M., Yuh, S.-J., and Kennedy, T.E. (2003). Netrin-1 Is a Chemorepellent for Oligodendrocyte Precursor Cells in the Embryonic Spinal Cord. J. Neurosci. *23*, 3735–3744. https://doi.org/10.1523/JNEUROSCI.23-09-03735.2003.

Jarrar, W., Vauti, F., Arnold, H.-H., and Holz, A. (2015). Generation of a Nkx2.2Cre knock-in mouse line: Analysis of cell lineages in the central nervous system. Differentiation *89*, 70–76. https://doi.org/10.1016/j.diff.2015.03.001.

Jessa, S., Mohammadnia, A., Harutyunyan, A.S., Hulswit, M., Varadharajan, S., Lakkis, H., Kabir, N., Bashardanesh, Z., Hébert, S., Faury, D., et al. (2022a). K27M in canonical and noncanonical H3 variants occurs in distinct oligodendroglial cell lineages in brain midline gliomas. Nat. Genet. *54*, 1865–1880. https://doi.org/10.1038/s41588-022-01205-w.

Jessa, S., Mohammadnia, A., Harutyunyan, A.S., Hulswit, M., Varadharajan, S., Lakkis, H., Kabir, N., Bashardanesh, Z., Hébert, S., Faury, D., et al. (2022b). K27M in canonical and noncanonical H3 variants occurs in distinct

oligodendroglial cell lineages in brain midline gliomas. Nat. Genet. *54*, 1865–1880. https://doi.org/10.1038/s41588-022-01205-w.

Johung, T.B., and Monje, M. (2017). Diffuse Intrinsic Pontine Glioma: New Pathophysiological Insights and Emerging Therapeutic Targets. Curr. Neuropharmacol. *15*, 88–97. https://doi.org/10.2174/1570159X14666160509123229.

Jones, C., Perryman, L., and Hargrave, D. (2012). Paediatric and adult malignant glioma: close relatives or distant cousins? Nat. Rev. Clin. Oncol. *9*, 400–413. https://doi.org/10.1038/nrclinonc.2012.87.

Jovanovich, N., Habib, A., Head, J., Hameed, F., Agnihotri, S., and Zinn, P.O. (2023). Pediatric diffuse midline glioma: Understanding the mechanisms and assessing the next generation of personalized therapeutics. Neuro-Oncol. Adv. *5*, vdad040. https://doi.org/10.1093/noajnl/vdad040.

Justin, N., Zhang, Y., Tarricone, C., Martin, S.R., Chen, S., Underwood, E., De Marco, V., Haire, L.F., Walker, P.A., Reinberg, D., et al. (2016). Structural basis of oncogenic histone H3K27M inhibition of human polycomb repressive complex 2. Nat. Commun. *7*, 11316. https://doi.org/10.1038/ncomms11316.

Kakita, A., and Goldman, J.E. (1999). Patterns and Dynamics of SVZ Cell Migration in the Postnatal Forebrain: Monitoring Living Progenitors in Slice Preparations. Neuron *23*, 461–472. https://doi.org/10.1016/S0896-6273(00)80800-4.

Kalyani, A., Hobson, K., and Rao, M.S. (1997). Neuroepithelial Stem Cells from the Embryonic Spinal Cord: Isolation, Characterization, and Clonal Analysis. Dev. Biol. *186*, 202–223. https://doi.org/10.1006/dbio.1997.8592.

Kalyani, A.J., Piper, D., Mujtaba, T., Lucero, M.T., and Rao, M.S. (1998). Spinal Cord Neuronal Precursors Generate Multiple Neuronal Phenotypes in Culture. J. Neurosci. *18*, 7856–7868. https://doi.org/10.1523/JNEUROSCI.18-19-07856.1998.

Kambhampati, M., Perez, J.P., Yadavilli, S., Saratsis, A.M., Hill, A.D., Ho, C.-Y., Panditharatna, E., Markel, M., Packer, R.J., and Nazarian, J. (2015). A standardized autopsy procurement allows for the comprehensive study of DIPG biology. Oncotarget *6*, 12740–12747. .

Káradóttir, R., Hamilton, N.B., Bakiri, Y., and Attwell, D. (2008). Spiking and non-spiking classes of oligodendrocyte precursor glia in CNS white matter. Nat. Neurosci. *11*, 450–456. https://doi.org/10.1038/nn2060.

Karremann, M., Gielen, G.H., Hoffmann, M., Wiese, M., Colditz, N., Warmuth-Metz, M., Bison, B., Claviez, A., van Vuurden, D.G., von Bueren, A.O., et al. (2018). Diffuse high-grade gliomas with H3 K27M mutations carry a dismal prognosis independent of tumor location. Neuro-Oncol. *20*, 123–131. https://doi.org/10.1093/neuonc/nox149.

Kaur, H., Phillips-Mason, P.J., Burden-Gulley, S.M., Kerstetter-Fogle, A.E., Basilion, J.P., Sloan, A.E., and Brady-Kalnay, S.M. (2012). Cadherin-11, a Marker of the Mesenchymal Phenotype, Regulates Glioblastoma Cell Migration and Survival In Vivo. Mol. Cancer Res. *10*, 293–304. https://doi.org/10.1158/1541-7786.MCR-11-0457.

Kempermann, G., Jessberger, S., Steiner, B., and Kronenberg, G. (2004). Milestones of neuronal development in the adult hippocampus. Trends Neurosci. *27*, 447–452. https://doi.org/10.1016/j.tins.2004.05.013.

Kessaris, N., Fogarty, M., Iannarelli, P., Grist, M., Wegner, M., and Richardson, W.D. (2006). Competing waves of oligodendrocytes in the forebrain and postnatal elimination of an embryonic lineage. Nat. Neurosci. *9*, 173–179. https://doi.org/10.1038/nn1620.

Khuong-Quang, D.-A., Buczkowicz, P., Rakopoulos, P., Liu, X.-Y., Fontebasso, A.M., Bouffet, E., Bartels, U., Albrecht, S., Schwartzentruber, J., Letourneau, L., et al. (2012). K27M mutation in histone H3.3 defines clinically and biologically distinct subgroups of pediatric diffuse intrinsic pontine gliomas. Acta Neuropathol. (Berl.) *124*, 439–447. https://doi.org/10.1007/s00401-012-0998-0.

Kiecker, C., and Lumsden, A. (2005). Compartments and their boundaries in vertebrate brain development. Nat. Rev. Neurosci. *6*, 553–564. https://doi.org/10.1038/nrn1702.

Kiecker, C., and Lumsden, A. (2012). The Role of Organizers in Patterning the Nervous System. Annu. Rev. Neurosci. *35*, 347–367. https://doi.org/10.1146/annurev-neuro-062111-150543.

Kiernan, B.W., Götz, B., Faissner, A., and ffrench-Constant, C. (1996). Tenascin-C inhibits oligodendrocyte precursor cell migration by both adhesion-dependent and adhesion-independent mechanisms. Mol. Cell. Neurosci. *7*, 322–335. https://doi.org/10.1006/mcne.1996.0024.

Kim, Y., Park, J., and Choi, Y.K. (2019). The Role of Astrocytes in the Central Nervous System Focused on BK Channel and Heme Oxygenase Metabolites: A Review. Antioxidants *8*, 121. https://doi.org/10.3390/antiox8050121.

Kirby, L., Jin, J., Cardona, J.G., Smith, M.D., Martin, K.A., Wang, J., Strasburger, H., Herbst, L., Alexis, M., Karnell, J., et al. (2019). Oligodendrocyte precursor cells present antigen and are cytotoxic targets in inflammatory demyelination. Nat. Commun. *10*, 3887. https://doi.org/10.1038/s41467-019-11638-3.

Kleiblova, P., Shaltiel, I.A., Benada, J., Ševčík, J., Pecháčková, S., Pohlreich, P., Voest, E.E., Dundr, P., Bartek, J., Kleibl, Z., et al. (2013). Gain-of-function mutations of PPM1D/Wip1 impair the p53-dependent G1 checkpoint. J. Cell Biol. *201*, 511–521. https://doi.org/10.1083/jcb.201210031.

Kluiver, T.A., Alieva, M., van Vuurden, D.G., Wehrens, E.J., and Rios, A.C. (2020). Invaders Exposed: Understanding and Targeting Tumor Cell Invasion in Diffuse Intrinsic Pontine Glioma. Front. Oncol. *10*, 92. https://doi.org/10.3389/fonc.2020.00092.

Kondo, T., and Raff, M. (2000). The Id4 HLH protein and the timing of oligodendrocyte differentiation. EMBO J. *19*, 1998–2007. https://doi.org/10.1093/emboj/19.9.1998.

Kriegstein, A., and Alvarez-Buylla, A. (2009). The Glial Nature of Embryonic and Adult Neural Stem Cells. Annu. Rev. Neurosci. *32*, 149–184. https://doi.org/10.1146/annurev.neuro.051508.135600.

Krug, B., Harutyunyan, A.S., Deshmukh, S., and Jabado, N. (2021). PRC2 in the driver's seat of childhood and young adult brain tumours. Trends Cell Biol. *31*, 814–828. https://doi.org/10.1016/j.tcb.2021.05.006.

Krumlauf, R., and Wilkinson, D.G. (2021). Segmentation and patterning of the vertebrate hindbrain. Dev. Camb. Engl. *148*, dev186460. https://doi.org/10.1242/dev.186460.

Kucukural, A., Yukselen, O., Ozata, D.M., Moore, M.J., and Garber, M. (2019). DEBrowser: interactive differential expression analysis and visualization tool for count data. BMC Genomics *20*, 6. https://doi.org/10.1186/s12864-018-5362-x.

Kuhn, S., Gritti, L., Crooks, D., and Dombrowski, Y. (2019). Oligodendrocytes in Development, Myelin Generation and Beyond. Cells *8*, 1424. https://doi.org/10.3390/cells8111424.

Lah, T.T., Novak, M., and Breznik, B. (2020). Brain malignancies: Glioblastoma and brain metastases. Semin. Cancer Biol. *60*, 262–273. https://doi.org/10.1016/j.semcancer.2019.10.010.

Laigle-Donadey, F., Doz, F., and Delattre, J.-Y. (2008). Brainstem gliomas in children and adults. Curr. Opin. Oncol. *20*, 662–667. https://doi.org/10.1097/CCO.0b013e32831186e0.

La Manno, G., Gyllborg, D., Codeluppi, S., Nishimura, K., Salto, C., Zeisel, A., Borm, L.E., Stott, S.R.W., Toledo, E.M., Villaescusa, J.C., et al. (2016). Molecular Diversity of Midbrain Development in Mouse, Human, and Stem Cells. Cell *167*, 566. https://doi.org/10.1016/j.cell.2016.09.027.

Larson, J.D., Kasper, L.H., Paugh, B.S., Jin, H., Wu, G., Kwon, C.-H., Fan, Y., Shaw, T.I., Silveira, A.B., Qu, C., et al. (2019). Histone H3.3 K27M Accelerates Spontaneous Brainstem Glioma and Drives Restricted Changes in Bivalent Gene Expression. Cancer Cell *35*, 140-155.e7. https://doi.org/10.1016/j.ccell.2018.11.015.

Lau, L.W., Cua, R., Keough, M.B., Haylock-Jacobs, S., and Yong, V.W. (2013). Pathophysiology of the brain extracellular matrix: a new target for remyelination. Nat. Rev. Neurosci. *14*, 722–729. https://doi.org/10.1038/nrn3550.

Laywell, E.D., Rakic, P., Kukekov, V.G., Holland, E.C., and Steindler, D.A. (2000). Identification of a multipotent astrocytic stem cell in the immature and adult mouse brain. Proc. Natl. Acad. Sci. U. S. A. *97*, 13883–13888. .

Lazow, M.A., Leach, J.L., Trout, A.T., Breneman, J.C., Fouladi, M., and Fuller, C. (2022). Extraneural Metastases of Diffuse Midline Glioma, H3 K27M-Mutant at Diagnosis: Case Report, Review of the Literature, and Identifying Targetable Alterations. J. Pediatr. Hematol. Oncol. *44*, e597. https://doi.org/10.1097/MPH.0000000000002189.

Lei, Q., Jeong, Y., Misra, K., Li, S., Zelman, A.K., Epstein, D.J., and Matise, M.P. (2006). Wnt Signaling Inhibitors Regulate the Transcriptional Response to Morphogenetic Shh-Gli Signaling in the Neural Tube. Dev. Cell *11*, 325–337. https://doi.org/10.1016/j.devcel.2006.06.013.

Levison, S.W., Chuang, C., Abramson, B.J., and Goldman, J.E. (1993). The migrational patterns and developmental fates of glial precursors in the rat subventricular zone are temporally regulated. Development *119*, 611–622. https://doi.org/10.1242/dev.119.3.611.

Lewis, P.W., Müller, M.M., Koletsky, M.S., Cordero, F., Lin, S., Banaszynski, L.A., Garcia, B.A., Muir, T.W., Becher, O.J., and Allis, C.D. (2013). Inhibition of PRC2 Activity by a Gain-of-Function H3 Mutation Found in Pediatric Glioblastoma. Science *340*, 857–861. https://doi.org/10.1126/science.1232245.

Li, X.-N. (2022). Defining the cell of origin for diffuse midline gliomas. Nat. Genet. *54*, 1770–1771. https://doi.org/10.1038/s41588-022-01231-8.

Li, L., Ying, J., Li, H., Zhang, Y., Shu, X., Fan, Y., Tan, J., Cao, Y., Tsao, S.W., Srivastava, G., et al. (2012). The human cadherin 11 is a pro-apoptotic tumor suppressor modulating cell stemness through Wnt/β-catenin signaling and silenced in common carcinomas. Oncogene *31*, 3901–3912. https://doi.org/10.1038/onc.2011.541.

Liao, Y., Luo, Z., Deng, Y., Zhang, F., Rao, R., Wang, J., Xu, L., Kumar, S.S., Sengupta, S., DeWire-Schottmiller, M., et al. (2021). OLIG2 maintenance is not essential for diffuse intrinsic pontine glioma cell line growth but regulates tumor phenotypes. Neuro-Oncol. *23*, 1183–1196. https://doi.org/10.1093/neuonc/noab016.

Lieberman, N.A.P., DeGolier, K., Kovar, H.M., Davis, A., Hoglund, V., Stevens, J., Winter, C., Deutsch, G., Furlan, S.N., Vitanza, N.A., et al. (2019). Characterization of the immune microenvironment of diffuse intrinsic pontine glioma: implications for development of immunotherapy. Neuro-Oncol. *21*, 83–94. https://doi.org/10.1093/neuonc/noy145.

Lin, S., and Bergles, D.E. (2004). Synaptic signaling between GABAergic interneurons and oligodendrocyte precursor cells in the hippocampus. Nat. Neurosci. *7*, 24–32. https://doi.org/10.1038/nn1162.

Lin, C., Wang, N., and Xu, C. (2023). Glioma-associated microglia/macrophages (GAMs) in glioblastoma: Immune function in the tumor microenvironment and implications for immunotherapy. Front. Immunol. *14*. .

Lin, G.L., Nagaraja, S., Filbin, M.G., Suvà, M.L., Vogel, H., and Monje, M. (2018). Non-inflammatory tumor microenvironment of diffuse intrinsic pontine glioma. Acta Neuropathol. Commun. *6*, 51. https://doi.org/10.1186/s40478-018-0553-x.

Liu, I., Jiang, L., Samuelsson, E.R., Marco Salas, S., Beck, A., Hack, O.A., Jeong, D., Shaw, M.L., Englinger, B., LaBelle, J., et al. (2022a). The landscape of tumor cell states and spatial organization in H3-K27M mutant diffuse midline glioma across age and location. Nat. Genet. *54*, 1881–1894. https://doi.org/10.1038/s41588-022-01236-3.

Liu, I., Jiang, L., Samuelsson, E.R., Marco Salas, S., Beck, A., Hack, O.A., Jeong, D., Shaw, M.L., Englinger, B., LaBelle, J., et al. (2022b). The landscape of tumor cell states and spatial organization in H3-K27M mutant diffuse midline glioma across age and location. Nat. Genet. *54*, 1881–1894. https://doi.org/10.1038/s41588-022-01236-3.

Lobon-Iglesias, M.J., Giraud, G., Castel, D., Philippe, C., Debily, M.A., Briandet, C., Fouyssac, F., De Carli, E., Dufour, C., Valteau-Couanet, D., et al. (2018a). Diffuse intrinsic pontine gliomas (DIPG) at recurrence: is there a window to test new therapies in some patients? J. Neurooncol. *137*, 111–118. https://doi.org/10.1007/s11060-017-2702-7.

Lobon-Iglesias, M.-J., Santa-Maria Lopez, V., Puerta Roldan, P., Candela-Cantó, S., Ramos-Albiac, M., Gomez-Chiari, M., Puget, S., Bolle, S., Goumnerova, L., Kieran, M.W., et al. (2018b). Tumor dissemination through surgical tracts in

diffuse intrinsic pontine glioma. J. Neurosurg. Pediatr. *22*, 678–683. https://doi.org/10.3171/2018.6.PEDS17658.

Louis, D.N., Perry, A., Reifenberger, G., von Deimling, A., Figarella-Branger, D., Cavenee, W.K., Ohgaki, H., Wiestler, O.D., Kleihues, P., and Ellison, D.W. (2016). The 2016 World Health Organization Classification of Tumors of the Central Nervous System: a summary. Acta Neuropathol. (Berl.) *131*, 803–820. https://doi.org/10.1007/s00401-016-1545-1.

Louis, D.N., Giannini, C., Capper, D., Paulus, W., Figarella-Branger, D., Lopes, M.B., Batchelor, T.T., Cairncross, J.G., van den Bent, M., Wick, W., et al. (2018). cIMPACT-NOW update 2: diagnostic clarifications for diffuse midline glioma, H3 K27M-mutant and diffuse astrocytoma/anaplastic astrocytoma, IDH-mutant. Acta Neuropathol. (Berl.) *135*, 639–642. https://doi.org/10.1007/s00401-018-1826-y.

Louis, D.N., Perry, A., Wesseling, P., Brat, D.J., Cree, I.A., Figarella-Branger, D., Hawkins, C., Ng, H.K., Pfister, S.M., Reifenberger, G., et al. (2021). The 2021 WHO Classification of Tumors of the Central Nervous System: a summary. Neuro-Oncol. *23*, 1231–1251. https://doi.org/10.1093/neuonc/noab106.

Lovén, J., Hoke, H.A., Lin, C.Y., Lau, A., Orlando, D.A., Vakoc, C.R., Bradner, J.E., Lee, T.I., and Young, R.A. (2013). Selective Inhibition of Tumor Oncogenes by Disruption of Super-Enhancers. Cell *153*, 320–334. https://doi.org/10.1016/j.cell.2013.03.036.

Loveson, K., and Fillmore, H. (2018). Intersection of Brain Development and Paediatric Diffuse Midline Gliomas: Potential Role of Microenvironment in Tumour Growth. Brain Sci. *8*, 200. https://doi.org/10.3390/brainsci8110200.

Lun, M., Lok, E., Gautam, S., Wu, E., and Wong, E.T. (2011). The natural history of extracranial metastasis from glioblastoma multiforme. J. Neurooncol. *105*, 261–273. https://doi.org/10.1007/s11060-011-0575-8.

Mackay, A., Burford, A., Carvalho, D., Izquierdo, E., Fazal-Salom, J., Taylor, K.R., Bjerke, L., Clarke, M., Vinci, M., Nandhabalan, M., et al. (2017). Integrated Molecular Meta-Analysis of 1,000 Pediatric High-Grade and Diffuse Intrinsic Pontine Glioma. Cancer Cell *32*, 520-537.e5. https://doi.org/10.1016/j.ccell.2017.08.017.

Manukjan, N., Ahmed, Z., Fulton, D., Blankesteijn, W.M., and Foulquier, S. (2020). A Systematic Review of WNT Signaling in Endothelial Cell Oligodendrocyte Interactions: Potential Relevance to Cerebral Small Vessel Disease. Cells *9*, 1545. https://doi.org/10.3390/cells9061545.

Martínez-Cerdeño, V., and Noctor, S.C. (2018). Neural Progenitor Cell Terminology. Front. Neuroanat. *12*, 104. https://doi.org/10.3389/fnana.2018.00104.

Massagué, J., and Obenauf, A.C. (2016). Metastatic Colonization. Nature *529*, 298–306. https://doi.org/10.1038/nature17038.

Masui, K., Suzuki, S.O., Torisu, R., Goldman, J.E., Canoll, P., and Iwaki, T. (2010). Glial progenitors in the brainstem give rise to malignant gliomas by platelet-derived growth factor stimulation. Glia *58*, 1050–1065. https://doi.org/10.1002/glia.20986.

Meel, M.H., Schaper, S.A., Kaspers, G.J.L., and Hulleman, E. (2018). Signaling pathways and mesenchymal transition in pediatric high-grade glioma. Cell. Mol. Life Sci. *75*, 871–887. https://doi.org/10.1007/s00018-017-2714-7.

Mellema, C. SIOPE DIPG/DMG Registry Protocol.

Mendez, F.M., Núñez, F.J., Garcia-Fabiani, M.B., Haase, S., Carney, S., Gauss, J.C., Becher, O.J., Lowenstein, P.R., and Castro, M.G. (2020). Epigenetic reprogramming and chromatin accessibility in pediatric diffuse intrinsic pontine gliomas: a neural developmental disease. Neuro-Oncol. *22*, 195–206. https://doi.org/10.1093/neuonc/noz218.

Mikheeva, S.A., Mikheev, A.M., Petit, A., Beyer, R., Oxford, R.G., Khorasani, L., Maxwell, J.-P., Glackin, C.A., Wakimoto, H., González-Herrero, I., et al. (2010). TWIST1 promotes invasion through mesenchymal change in human glioblastoma. Mol. Cancer *9*, 194. https://doi.org/10.1186/1476-4598-9-194.

Miller, F.D., and Gauthier, A.S. (2007). Timing Is Everything: Making Neurons versus Glia in the Developing Cortex.

Neuron *54*, 357–369. https://doi.org/10.1016/j.neuron.2007.04.019.

Milner, R., Edwards, G., Streuli, C., and ffrench-Constant, C. (1996). A Role in Migration for the αvβ1 Integrin Expressed on Oligodendrocyte Precursors. J. Neurosci. *16*, 7240–7252. https://doi.org/10.1523/JNEUROSCI.16-22-07240.1996.

Misuraca, K.L., Hu, G., Barton, K.L., Chung, A., and Becher, O.J. (2016). A Novel Mouse Model of Diffuse Intrinsic Pontine Glioma Initiated in Pax3-Expressing Cells. Neoplasia *18*, 60–70. https://doi.org/10.1016/j.neo.2015.12.002.

Miyajima, M., Tabata, H., and Nakajima, K. (2023). Migratory mode transition of astrocyte progenitors in the cerebral cortex: an intrinsic or extrinsic cell process? Neural Regen. Res. *19*, 471–472. https://doi.org/10.4103/1673-5374.380886.

Miyata, T., Kawaguchi, A., Saito, K., Kawano, M., Muto, T., and Ogawa, M. (2004). Asymmetric production of surface-dividing and non-surface-dividing cortical progenitor cells. Dev. Camb. Engl. *131*, 3133–3145. https://doi.org/10.1242/dev.01173.

Mizuguchi, R., Kriks, S., Cordes, R., Gossler, A., Ma, Q., and Goulding, M. (2006). Ascl1 and Gsh1/2 control inhibitory and excitatory cell fate in spinal sensory interneurons. Nat. Neurosci. *9*, 770–778. https://doi.org/10.1038/nn1706.

Mohiuddin, S., Maraka, S., Usman Baig, M., Gupta, S., Muzzafar, T., Valyi-Nagy, T., Lindsay, H., Moody, K., Razvi, S., Paulino, A., et al. (2021). Case series of diffuse extraneural metastasis in H3F3A mutant high-grade gliomas: Clinical, molecular phenotype and literature review. J. Clin. Neurosci. *89*, 405–411. https://doi.org/10.1016/j.jocn.2021.05.033.

Monje, M., Mitra, S.S., Freret, M.E., Raveh, T.B., Kim, J., Masek, M., Attema, J.L., Li, G., Haddix, T., Edwards, M.S.B., et al. (2011). Hedgehog-responsive candidate cell of origin for diffuse intrinsic pontine glioma. Proc. Natl. Acad. Sci. *108*, 4453–4458. https://doi.org/10.1073/pnas.1101657108.

Motamed, S., Del Borgo, M.P., Zhou, K., Kulkarni, K., Crack, P.J., Merson, T.D., Aguilar, M.-I., Finkelstein, D.I., and Forsythe, J.S. (2019). Migration and Differentiation of Neural Stem Cells Diverted From the Subventricular Zone by an Injectable Self-Assembling β-Peptide Hydrogel. Front. Bioeng. Biotechnol. *7*, 315. https://doi.org/10.3389/fbioe.2019.00315.

Muraguchi, T., Tanaka, S., Yamada, D., Tamase, A., Nakada, M., Nakamura, H., Hoshii, T., Ooshio, T., Tadokoro, Y., Naka, K., et al. (2011). NKX2.2 Suppresses Self-Renewal of Glioma-Initiating Cells. Cancer Res. *71*, 1135–1145. https://doi.org/10.1158/0008-5472.CAN-10-2304.

Nadarajah, B., and Parnavelas, J.G. (2002). Modes of neuronal migration in the developing cerebral cortex. Nat. Rev. Neurosci. *3*, 423–432. https://doi.org/10.1038/nrn845.

Nadarajah, B., Brunstrom, J.E., Grutzendler, J., Wong, R.O.L., and Pearlman, A.L. (2001). Two modes of radial migration in early development of the cerebral cortex. Nat. Neurosci. *4*, 143–150. https://doi.org/10.1038/83967.

Nagaraja, S., Vitanza, N.A., Woo, P.J., Taylor, K.R., Liu, F., Zhang, L., Li, M., Meng, W., Ponnuswami, A., Sun, W., et al. (2017). Transcriptional Dependencies in Diffuse Intrinsic Pontine Glioma. Cancer Cell *31*, 635-652.e6. https://doi.org/10.1016/j.ccell.2017.03.011.

Nagaraja, S., Quezada, M.A., Gillespie, S.M., Arzt, M., Lennon, J.J., Woo, P.J., Hovestadt, V., Kambhampati, M., Filbin, M.G., Suva, M.L., et al. (2019). Histone Variant and Cell Context Determine H3K27M Reprogramming of the Enhancer Landscape and Oncogenic State. Mol. Cell *76*, 965-980.e12. https://doi.org/10.1016/j.molcel.2019.08.030.

Nave, K.-A., and Werner, H.B. (2014). Myelination of the Nervous System: Mechanisms and Functions. Annu. Rev. Cell Dev. Biol. *30*, 503–533. https://doi.org/10.1146/annurev-cellbio-100913-013101.

Niehaus, A., Stegmüller, J., Diers-Fenger, M., and Trotter, J. (1999). Cell-Surface Glycoprotein of Oligodendrocyte Progenitors Involved in Migration. J. Neurosci. *19*, 4948–4961. https://doi.org/10.1523/JNEUROSCI.19-12-04948.1999.

Nikbakht, H., Panditharatna, E., Mikael, L.G., Li, R., Gayden, T., Osmond, M., Ho, C.-Y., Kambhampati, M., Hwang, E.I.,

Faury, D., et al. (2016). Spatial and temporal homogeneity of driver mutations in diffuse intrinsic pontine glioma. Nat. Commun. *7*, 11185. https://doi.org/10.1038/ncomms11185.

Noctor, S.C., Martínez-Cerdeño, V., Ivic, L., and Kriegstein, A.R. (2004). Cortical neurons arise in symmetric and asymmetric division zones and migrate through specific phases. Nat. Neurosci. *7*, 136–144. https://doi.org/10.1038/nn1172.

Oliveros, J.C. (2007). Venny. An interactive tool for comparing lists with Venn's diagrams.

Ono, K., Kagawa, T., Tsumori, T., Yokota, S., and Yasui, Y. (2001). Morphological Changes and Cellular Dynamics of Oligodendrocyte Lineage Cells in the Developing Vertebrate Central Nervous System. Dev. Neurosci. *23*, 346–355. https://doi.org/10.1159/000048718.

Osanai, Y., Yamazaki, R., Shinohara, Y., and Ohno, N. (2022). Heterogeneity and regulation of oligodendrocyte morphology. Front. Cell Dev. Biol. *10*, 1030486. https://doi.org/10.3389/fcell.2022.1030486.

Owen, L.A., Kowalewski, A.A., and Lessnick, S.L. (2008). EWS/FLI Mediates Transcriptional Repression via NKX2.2 during Oncogenic Transformation in Ewing's Sarcoma. PLoS ONE *3*, e1965. https://doi.org/10.1371/journal.pone.0001965.

Pachocki, C.J., and Hol, E.M. (2022). Current perspectives on diffuse midline glioma and a different role for the immune microenvironment compared to glioblastoma. J. Neuroinflammation *19*, 276. https://doi.org/10.1186/s12974-022-02630-8.

Pasqualini, C., Kozaki, T., Bruschi, M., Nguyen, T.H.H., Minard-Colin, V., Castel, D., Grill, J., and Ginhoux, F. (2020). Modeling the Interaction between the Microenvironment and Tumor Cells in Brain Tumors. Neuron *108*, 1025–1044. https://doi.org/10.1016/j.neuron.2020.09.018.

Pathania, M., De Jay, N., Maestro, N., Harutyunyan, A.S., Nitarska, J., Pahlavan, P., Henderson, S., Mikael, L.G., Richard-Londt, A., Zhang, Y., et al. (2017). H3.3K27M cooperates with Trp53 loss and PDGFRA gain in mouse embryonic neural progenitor cells to induce invasive high-grade gliomas. Cancer Cell *32*, 684-700.e9. https://doi.org/10.1016/j.ccell.2017.09.014.

Paugh, B.S., Qu, C., Jones, C., Liu, Z., Adamowicz-Brice, M., Zhang, J., Bax, D.A., Coyle, B., Barrow, J., Hargrave, D., et al. (2010). Integrated Molecular Genetic Profiling of Pediatric High-Grade Gliomas Reveals Key Differences With the Adult Disease. J. Clin. Oncol. *28*, 3061–3068. https://doi.org/10.1200/JCO.2009.26.7252.

Peretz, Y., Eren, N., Kohl, A., Hen, G., Yaniv, K., Weisinger, K., Cinnamon, Y., and Sela-Donenfeld, D. (2016). A new role of hindbrain boundaries as pools of neural stem/progenitor cells regulated by Sox2. BMC Biol. *14*, 57. https://doi.org/10.1186/s12915-016-0277-y.

Pfister, S.M., Reyes-Múgica, M., Chan, J.K.C., Hasle, H., Lazar, A.J., Rossi, S., Ferrari, A., Jarzembowski, J.A., Pritchard-Jones, K., Hill, D.A., et al. (2022). A Summary of the Inaugural WHO Classification of Pediatric Tumors: Transitioning from the Optical into the Molecular Era. Cancer Discov. *12*, 331–355. https://doi.org/10.1158/2159-8290.CD-21-1094.

Porter, D.D.L., Henry, S.N., Ahmed, S., Rizzo, A.L., Makhlouf, R., Gregg, C., and Morton, P.D. (2022). Neuroblast migration along cellular substrates in the developing porcine brain. Stem Cell Rep. *17*, 2097–2110. https://doi.org/10.1016/j.stemcr.2022.07.015.

Pu, W., Qiu, J., Riggins, G.J., and Parat, M.-O. (2020). Matrix protease production, epithelial-to-mesenchymal transition marker expression and invasion of glioblastoma cells in response to osmotic or hydrostatic pressure. Sci. Rep. *10*, 2634. https://doi.org/10.1038/s41598-020-59462-w.

Puget, S., Beccaria, K., Blauwblomme, T., Roujeau, T., James, S., Grill, J., Zerah, M., Varlet, P., and Sainte-Rose, C. (2015). Biopsy in a series of 130 pediatric diffuse intrinsic Pontine gliomas. Childs Nerv. Syst. *31*, 1773–1780. https://doi.org/10.1007/s00381-015-2832-1.

Qi, Y., Cai, J., Wu, Y., Wu, R., Lee, J., Fu, H., Rao, M., Sussel, L., Rubenstein, J., and Qiu, M. (2001). Control of oligodendrocyte differentiation by the Nkx2.2 homeodomain transcription factor. Development *128*, 2723–2733. https://doi.org/10.1242/dev.128.14.2723.

Qin, E.Y., Cooper, D.D., Abbott, K.L., Lennon, J., Nagaraja, S., Mackay, A., Jones, C., Vogel, H., Jackson, P.K., and Monje, M. (2017). Neural Precursor-Derived Pleiotrophin Mediates Subventricular Zone Invasion by Glioma. Cell *170*, 845-859.e19. https://doi.org/10.1016/j.cell.2017.07.016.

Rahman, R., Janowski, M., Killick-Cole, C.L., Singleton, W.G.B., Campbell, E., Walczak, P., Khatua, S., Faltings, L., Symons, M., Schneider, J.R., et al. (2023). Childhood Brain Tumors: A Review of Strategies to Translate CNS Drug Delivery to Clinical Trials. Cancers *15*, 857. https://doi.org/10.3390/cancers15030857.

Redwine, J.M., Blinder, K.L., and Armstrong, R.C. (1997). In situ expression of fibroblast growth factor receptors by oligodendrocyte progenitors and oligodendrocytes in adult mouse central nervous system. J. Neurosci. Res. *50*, 229–237. https://doi.org/10.1002/(SICI)1097-4547(19971015)50:2<229::AID-JNR11>3.0.CO;2-3.

Richardson, W.D., Pringle, N., Mosley, M.J., Westermark, B., and Dubois-Dalcg, M. (1988). A role for platelet-derived growth factor in normal gliogenesis in the central nervous system. Cell *53*, 309–319. https://doi.org/10.1016/0092-8674(88)90392-3.

Richardson, W.D., Young, K.M., Tripathi, R.B., and McKenzie, I. (2011). NG2-glia as multipotent neural stem cells – fact or fantasy? Neuron *70*, 661–673. https://doi.org/10.1016/j.neuron.2011.05.013.

Robinson, S., Tani, M., Strieter, R.M., Ransohoff, R.M., and Miller, R.H. (1998). The Chemokine Growth-Regulated Oncogene-α Promotes Spinal Cord Oligodendrocyte Precursor Proliferation. J. Neurosci. *18*, 10457–10463. https://doi.org/10.1523/JNEUROSCI.18-24-10457.1998.

Roujeau, T., Machado, G., Garnett, M.R., Miquel, C., Puget, S., Geoerger, B., Grill, J., Boddaert, N., Di Rocco, F., Zerah, M., et al. (2007). Stereotactic biopsy of diffuse pontine lesions in children. J. Neurosurg. Pediatr. *107*, 1–4. https://doi.org/10.3171/PED-07/07/001.

Ryall, S., Zapotocky, M., Fukuoka, K., Nobre, L., Guerreiro Stucklin, A., Bennett, J., Siddaway, R., Li, C., Pajovic, S., Arnoldo, A., et al. (2020a). Integrated Molecular and Clinical Analysis of 1,000 Pediatric Low-Grade Gliomas. Cancer Cell *37*, 569-583.e5. https://doi.org/10.1016/j.ccell.2020.03.011.

Ryall, S., Tabori, U., and Hawkins, C. (2020b). Pediatric low-grade glioma in the era of molecular diagnostics. Acta Neuropathol. Commun. *8*, 30. https://doi.org/10.1186/s40478-020-00902-z.

Sanders, L.M., Cheney, A., Seninge, L., van den Bout, A., Chen, M., Beale, H.C., Kephart, E.T., Pfeil, J., Learned, K., Lyle, A.G., et al. (2020). Identification of a differentiation stall in epithelial mesenchymal transition in histone H3–mutant diffuse midline glioma. GigaScience *9*, giaa136. https://doi.org/10.1093/gigascience/giaa136.

Schmittgen, T.D., and Livak, K.J. (2008). Analyzing real-time PCR data by the comparative C_T method. Nat. Protoc. *3*, 1101–1108. https://doi.org/10.1038/nprot.2008.73.

Schnädelbach, O., Blaschuk, O.W., Symonds, M., Gour, B.J., Doherty, P., and Fawcett, J.W. (2000). N-cadherin influences migration of oligodendrocytes on astrocyte monolayers. Mol. Cell. Neurosci. *15*, 288–302. https://doi.org/10.1006/mcne.1999.0819.

Schroeder, K.M., Hoeman, C.M., and Becher, O.J. (2014). Children are not just little adults: recent advances in understanding of diffuse intrinsic pontine glioma biology. Pediatr. Res. *75*, 205–209. https://doi.org/10.1038/pr.2013.194.

Schwartzentruber, J., Korshunov, A., Liu, X.-Y., Jones, D.T.W., Pfaff, E., Jacob, K., Sturm, D., Fontebasso, A.M., Quang, D.-A.K., Tönjes, M., et al. (2012). Driver mutations in histone H3.3 and chromatin remodelling genes in paediatric glioblastoma. Nature *482*, 226–231. https://doi.org/10.1038/nature10833.

Seano, G., and Jain, R.K. (2020). Vessel co-option in glioblastoma: emerging insights and opportunities. Angiogenesis

23, 9–16. https://doi.org/10.1007/s10456-019-09691-z.

Semple, B.D., Blomgren, K., Gimlin, K., Ferriero, D.M., and Noble-Haeusslein, L.J. (2013). Brain development in rodents and humans: Identifying benchmarks of maturation and vulnerability to injury across species. Prog. Neurobiol. *106–107*, 1–16. https://doi.org/10.1016/j.pneurobio.2013.04.001.

Seo, J.H., Maki, T., Maeda, M., Miyamoto, N., Liang, A.C., Hayakawa, K., Pham, L.-D.D., Suwa, F., Taguchi, A., Matsuyama, T., et al. (2014). Oligodendrocyte Precursor Cells Support Blood-Brain Barrier Integrity via TGF-β Signaling. PLoS ONE *9*, e103174. https://doi.org/10.1371/journal.pone.0103174.

Sethi, R., Allen, J., Donahue, B., Karajannis, M., Gardner, S., Wisoff, J., Kunnakkat, S., Mathew, J., Zagzag, D., Newman, K., et al. (2011). Prospective neuraxis MRI surveillance reveals a high risk of leptomeningeal dissemination in diffuse intrinsic pontine glioma. J. Neurooncol. *102*, 121–127. https://doi.org/10.1007/s11060-010-0301-y.

Shih, A.H., and Holland, E.C. (2006). Platelet-derived growth factor (PDGF) and glial tumorigenesis. Cancer Lett. *232*, 139–147. https://doi.org/10.1016/j.canlet.2005.02.002.

Silbereis, J.C., Pochareddy, S., Zhu, Y., Li, M., and Sestan, N. (2016). The Cellular and Molecular Landscapes of the Developing Human Central Nervous System. Neuron *89*, 248–268. https://doi.org/10.1016/j.neuron.2015.12.008.

Singh, N., Siebzehnrubl, F.A., and Martinez-Garay, I. (2023). Transcriptional control of embryonic and adult neural progenitor activity. Front. Neurosci. *17*. .

Sitbon, D., Podsypanina, K., Yadav, T., and Almouzni, G. (2017). Shaping Chromatin in the Nucleus: The Bricks and the Architects. Cold Spring Harb. Symp. Quant. Biol. *82*, 1–14. https://doi.org/10.1101/sqb.2017.82.033753.

Smith, A. (2006). A glossary for stem-cell biology. Nature *441*, 1060–1060. https://doi.org/10.1038/nature04954.

Snaidero, N., Möbius, W., Czopka, T., Hekking, L.H.P., Mathisen, C., Verkleij, D., Goebbels, S., Edgar, J., Merkler, D., Lyons, D.A., et al. (2014). Myelin Membrane Wrapping of CNS Axons by PI(3,4,5)P3-Dependent Polarized Growth at the Inner Tongue. Cell *156*, 277–290. https://doi.org/10.1016/j.cell.2013.11.044.

Somjen, G.G. (1988). Nervenkitt: Notes on the history of the concept of neuroglia. Glia *1*, 2–9. https://doi.org/10.1002/glia.440010103.

Sorrells, S.F., Paredes, M.F., Cebrian-Silla, A., Sandoval, K., Qi, D., Kelley, K.W., James, D., Mayer, S., Chang, J., Auguste, K.I., et al. (2018). Human hippocampal neurogenesis drops sharply in children to undetectable levels in adults. Nature *555*, 377–381. https://doi.org/10.1038/nature25975.

Soula, C., Danesin, C., Kan, P., Grob, M., Poncet, C., and Cochard, P. (2001). Distinct sites of origin of oligodendrocytes and somatic motoneurons in the chick spinal cord: oligodendrocytes arise from Nkx2.2-expressing progenitors by a Shh-dependent mechanism. Development *128*, 1369–1379. https://doi.org/10.1242/dev.128.8.1369.

Spitz, F., and Furlong, E.E.M. (2012). Transcription factors: from enhancer binding to developmental control. Nat. Rev. Genet. *13*, 613–626. https://doi.org/10.1038/nrg3207.

Stafford, J.M., Lee, C.-H., Voigt, P., Descostes, N., Saldaña-Meyer, R., Yu, J.-R., Leroy, G., Oksuz, O., Chapman, J.R., Suarez, F., et al. (2018). Multiple modes of PRC2 inhibition elicit global chromatin alterations in H3K27M pediatric glioma. Sci. Adv. *4*, eaau5935. https://doi.org/10.1126/sciadv.aau5935.

Steliarova-Foucher, E., Colombet, M., Ries, L.A.G., Moreno, F., Dolya, A., Bray, F., Hesseling, P., Shin, H.Y., Stiller, C.A., Bouzbid, S., et al. (2017). International incidence of childhood cancer, 2001–10: a population-based registry study. Lancet Oncol. *18*, 719–731. https://doi.org/10.1016/S1470-2045(17)30186-9.

Stephens, S., Tollesson, G., Robertson, T., and Campbell, R. (2019). Diffuse midline glioma metastasis to the peritoneal cavity via ventriculo-peritoneal shunt: Case report and review of literature. J. Clin. Neurosci. *67*, 288–293. https://doi.org/10.1016/j.jocn.2019.06.043.

Stroud, H., Otero, S., Desvoyes, B., Ramírez-Parra, E., Jacobsen, S.E., and Gutierrez, C. (2012). Genome-wide analysis of histone H3.1 and H3.3 variants in Arabidopsis thaliana. Proc. Natl. Acad. Sci. U. S. A. *109*, 5370–5375. https://doi.org/10.1073/pnas.1203145109.

Studer, M., Lumsden, A., Ariza-McNaughton, L., and Bradleyt, A. (1996). Altered segmental identity and abnormal migration of motor neurons in mice lacking ffoxb-. *384*. .

Su, Y., Wang, X., Yang, Y., Chen, L., Xia, W., Hoi, K.K., Li, H., Wang, Q., Yu, G., Chen, X., et al. (2023). Astrocyte endfoot formation controls the termination of oligodendrocyte precursor cell perivascular migration during development. Neuron *111*, 190-201.e8. https://doi.org/10.1016/j.neuron.2022.10.032.

Sun, X., and Yu, Q. (2015). Intra-tumor heterogeneity of cancer cells and its implications for cancer treatment. Acta Pharmacol. Sin. *36*, 1219–1227. https://doi.org/10.1038/aps.2015.92.

Sun, Q., Xu, R., Xu, H., Wang, G., Shen, X., and Jiang, H. (2017). Extracranial metastases of high-grade glioma: the clinical characteristics and mechanism. World J. Surg. Oncol. *15*, 181. https://doi.org/10.1186/s12957-017-1249-6.

Sun, T., Dong, H., Wu, L., Kane, M., Rowitch, D.H., and Stiles, C.D. (2003). Cross-Repressive Interaction of the Olig2 and Nkx2.2 Transcription Factors in Developing Neural Tube Associated with Formation of a Specific Physical Complex. J. Neurosci. *23*, 9547–9556. https://doi.org/10.1523/JNEUROSCI.23-29-09547.2003.

Sun, Y., Nadal-Vicens, M., Misono, S., Lin, M.Z., Zubiaga, A., Hua, X., Fan, G., and Greenberg, M.E. (2001). Neurogenin Promotes Neurogenesis and Inhibits Glial Differentiation by Independent Mechanisms. Cell *104*, 365–376. https://doi.org/10.1016/S0092-8674(01)00224-0.

Sun, Y., Yan, K., Wang, Y., Xu, C., Wang, D., Zhou, W., Guo, S., Han, Y., Tang, L., Shao, Y., et al. (2022). Context-dependent tumor-suppressive BMP signaling in diffuse intrinsic pontine glioma regulates stemness through epigenetic regulation of CXXC5. Nat. Cancer *3*, 1105–1122. https://doi.org/10.1038/s43018-022-00408-8.

Sussel, L., Kalamaras, J., Hartigan-O'Connor, D.J., Meneses, J.J., Pedersen, R.A., Rubenstein, J.L.R., and German, M.S. (1998). Mice lacking the homeodomain transcription factor Nkx2.2 have diabetes due to arrested differentiation of pancreatic β cells. Development *125*, 2213–2221. https://doi.org/10.1242/dev.125.12.2213.

Sutherland, K.D., and Visvader, J.E. (2015). Cellular Mechanisms Underlying Intertumoral Heterogeneity. Trends Cancer *1*, 15–23. https://doi.org/10.1016/j.trecan.2015.07.003.

Szenker, E., Ray-Gallet, D., and Almouzni, G. (2011). The double face of the histone variant H3.3. Cell Res. *21*, 421–434. https://doi.org/10.1038/cr.2011.14.

Tabata, H., Sasaki, M., Agetsuma, M., Sano, H., Hirota, Y., Miyajima, M., Hayashi, K., Honda, T., Nishikawa, M., Inaguma, Y., et al. (2022). Erratic and blood vessel-guided migration of astrocyte progenitors in the cerebral cortex. Nat. Commun. *13*, 6571. https://doi.org/10.1038/s41467-022-34184-x.

Tagami, H., Ray-Gallet, D., Almouzni, G., and Nakatani, Y. (2004). Histone H3.1 and H3.3 Complexes Mediate Nucleosome Assembly Pathways Dependent or Independent of DNA Synthesis. Cell *116*, 51–61. https://doi.org/10.1016/S0092-8674(03)01064-X.

Tanabe, S., and Yamashita, T. (2020). Function of Lymphocytes in Oligodendrocyte Development. The Neuroscientist *26*, 74–86. https://doi.org/10.1177/1073858419834221.

Taniuchi, K., Furihata, M., Naganuma, S., and Saibara, T. (2018). ARHGEF4 predicts poor prognosis and promotes cell invasion by influencing ERK1/2 and GSK-3α/β signaling in pancreatic cancer. Int. J. Oncol. *53*, 2224–2240. https://doi.org/10.3892/ijo.2018.4549.

Tauziède-Espariat, A., Siegfried, A., Uro-Coste, E., Nicaise, Y., Castel, D., Sevely, A., Gambart, M., Boetto, S., Hasty, L., Métais, A., et al. (2022). Disseminated diffuse midline gliomas, H3K27-altered mimicking diffuse leptomeningeal glioneuronal tumors: a diagnostical challenge! Acta Neuropathol. Commun. *10*, 119. https://doi.org/10.1186/s40478-022-01419-3.

Taverna, E., Götz, M., and Huttner, W.B. (2014). The Cell Biology of Neurogenesis: Toward an Understanding of the Development and Evolution of the Neocortex. Annu. Rev. Cell Dev. Biol. *30*, 465–502. https://doi.org/10.1146/annurev-cellbio-101011-155801.

Taylor, K.R., and Monje, M. (2022). Invasive glioma cells: The malignant pioneers that follow the current. Cell *185*, 2846–2848. https://doi.org/10.1016/j.cell.2022.06.033.

Taylor, K.R., Mackay, A., Truffaux, N., Butterfield, Y.S., Morozova, O., Philippe, C., Castel, D., Grasso, C.S., Vinci, M., Carvalho, D., et al. (2014a). Recurrent activating ACVR1 mutations in diffuse intrinsic pontine glioma. Nat. Genet. *46*, 457–461. https://doi.org/10.1038/ng.2925.

Taylor, K.R., Vinci, M., Bullock, A.N., and Jones, C. (2014b). ACVR1 mutations in DIPG: lessons learned from FOP. Cancer Res. *74*, 4565–4570. https://doi.org/10.1158/0008-5472.CAN-14-1298.

Tekki-Kessaris, N., Woodruff, R., Hall, A.C., Gaffield, W., Kimura, S., Stiles, C.D., Rowitch, D.H., and Richardson, W.D. (2001). Hedgehog-dependent oligodendrocyte lineage specification in the telencephalon. Development *128*, 2545–2554. https://doi.org/10.1242/dev.128.13.2545.

Tian, Y., Yin, H., Deng, X., Tang, B., Ren, X., and Jiang, T. (2018). CXCL12 induces migration of oligodendrocyte precursor cells through the CXCR4-activated MEK/ERK and PI3K/AKT pathways. Mol. Med. Rep. *18*, 4374–4380. https://doi.org/10.3892/mmr.2018.9444.

Tiane, A., Schepers, M., Rombaut, B., Hupperts, R., Prickaerts, J., Hellings, N., van den Hove, D., and Vanmierlo, T. (2019). From OPC to Oligodendrocyte: An Epigenetic Journey. Cells *8*, 1236. https://doi.org/10.3390/cells8101236.

Tomita, Y., Shimazu, Y., Somasundaram, A., Tanaka, Y., Takata, N., Ishi, Y., Gadd, S., Hashizume, R., Angione, A., Pinero, G., et al. (2022). A novel mouse model of diffuse midline glioma initiated in neonatal oligodendrocyte progenitor cells highlights cell-of-origin dependent effects of H3K27M. Glia *70*, 1681–1698. https://doi.org/10.1002/glia.24189.

Trainor, P.A., and Krumlauf, R. (2000). Patterning the cranial neural crest: Hinbrain segmentation and hox gene plasticity. Nat. Rev. Neurosci. *1*, 116–124. https://doi.org/10.1038/35039056.

Tsai, H.-H., Frost, E., To, V., Robinson, S., ffrench-Constant, C., Geertman, R., Ransohoff, R.M., and Miller, R.H. (2002). The Chemokine Receptor CXCR2 Controls Positioning of Oligodendrocyte Precursors in Developing Spinal Cord by Arresting Their Migration. Cell *110*, 373–383. https://doi.org/10.1016/S0092-8674(02)00838-3.

Tsai, H.-H., Tessier-Lavigne, M., and Miller, R.H. (2003). Netrin 1 mediates spinal cord oligodendrocyte precursor dispersal. Dev. Camb. Engl. *130*, 2095–2105. https://doi.org/10.1242/dev.00424.

Tsai, H.-H., Niu, J., Munji, R., Davalos, D., Chang, J., Zhang, H., Tien, A.-C., Kuo, C.J., Chan, J.R., Daneman, R., et al. (2016). Oligodendrocyte precursors migrate along vasculature in the developing nervous system. Science *351*, 379–384. https://doi.org/10.1126/science.aad3839.

Tso, C.-L., Shintaku, P., Chen, J., Liu, Q., Liu, J., Chen, Z., Yoshimoto, K., Mischel, P.S., Cloughesy, T.F., Liau, L.M., et al. (2006). Primary Glioblastomas Express Mesenchymal Stem-Like Properties. Mol. Cancer Res. *4*, 607–619. https://doi.org/10.1158/1541-7786.MCR-06-0005.

Vallstedt, A., Klos, J.M., and Ericson, J. (2005). Multiple Dorsoventral Origins of Oligodendrocyte Generation in the Spinal Cord and Hindbrain. Neuron *45*, 55–67. https://doi.org/10.1016/j.neuron.2004.12.026.

Vanan, M.I., and Eisenstat, D.D. (2015). DIPG in children – what can we learn from the past? Neuro-Oncol. 237. https://doi.org/10.3389/fonc.2015.00237.

Varn, F.S., Johnson, K.C., Martinek, J., Huse, J.T., Nasrallah, M.P., Wesseling, P., Cooper, L.A.D., Malta, T.M., Wade, T.E., Sabedot, T.S., et al. (2022). Glioma progression is shaped by genetic evolution and microenvironment interactions. Cell *185*, 2184-2199.e16. https://doi.org/10.1016/j.cell.2022.04.038.

Veldhuijzen van Zanten, S.E., Jansen, M.H., Sanchez Aliaga, E., van Vuurden, D.G., Vandertop, W.P., and Kaspers, G.J.

(2015). A twenty-year review of diagnosing and treating children with diffuse intrinsic pontine glioma in The Netherlands. Expert Rev. Anticancer Ther. *15*, 157–164. https://doi.org/10.1586/14737140.2015.974563.

Venkataramani, V., Yang, Y., Schubert, M.C., Reyhan, E., Tetzlaff, S.K., Wißmann, N., Botz, M., Soyka, S.J., Beretta, C.A., Pramatarov, R.L., et al. (2022). Glioblastoma hijacks neuronal mechanisms for brain invasion. Cell *185*, 2899-2917.e31. https://doi.org/10.1016/j.cell.2022.06.054.

Venkatesh, H.S., Johung, T.B., Caretti, V., Noll, A., Tang, Y., Nagaraja, S., Gibson, E.M., Mount, C.W., Polepalli, J., Mitra, S.S., et al. (2015). Neuronal Activity Promotes Glioma Growth through Neuroligin-3 Secretion. Cell *161*, 803–816. https://doi.org/10.1016/j.cell.2015.04.012.

Venkatesh, H.S., Tam, L.T., Woo, P.J., Lennon, J., Nagaraja, S., Gillespie, S.M., Ni, J., Duveau, D.Y., Morris, P.J., Zhao, J.J., et al. (2017). Targeting neuronal activity-regulated neuroligin-3 dependency in high-grade glioma. Nature *549*, 533–537. https://doi.org/10.1038/nature24014.

Venkatesh, H.S., Morishita, W., Geraghty, A.C., Silverbush, D., Gillespie, S.M., Arzt, M., Tam, L.T., Espenel, C., Ponnuswami, A., Ni, L., et al. (2019). Electrical and synaptic integration of glioma into neural circuits. Nature *573*, 539–545. https://doi.org/10.1038/s41586-019-1563-y.

Vinci, M., Burford, A., Molinari, V., Kessler, K., Popov, S., Clarke, M., Taylor, K.R., Pemberton, H.N., Lord, C.J., Gutteridge, A., et al. (2018). Functional diversity and cooperativity between subclonal populations of pediatric glioblastoma and diffuse intrinsic pontine glioma cells. Nat. Med. *24*, 1204–1215. https://doi.org/10.1038/s41591-018-0086-7.

Visvader, J.E. (2011). Cells of origin in cancer. Nature *469*, 314–322. https://doi.org/10.1038/nature09781.

Vuong, H.G., Ngo, T.N.M., Le, H.T., Jea, A., Hrachova, M., Battiste, J., McNall-Knapp, R., and Dunn, I.F. (2022). Prognostic Implication of Patient Age in H3K27M-Mutant Midline Gliomas. Front. Oncol. *12*, 858148. https://doi.org/10.3389/fonc.2022.858148.

Wagner, S., Benesch, M., Berthold, F., Gnekow, A.K., Rutkowski, S., Sträter, R., Warmuth-Metz, M., Kortmann, R.-D., Pietsch, T., and Wolff, J.E.A. (2006). Secondary dissemination in children with high-grade malignant gliomas and diffuse intrinsic pontine gliomas. Br. J. Cancer *95*, 991–997. https://doi.org/10.1038/sj.bjc.6603402.

Wang, J., Huang, T.Y.-T., Hou, Y., Bartom, E., Lu, X., Shilatifard, A., Yue, F., and Saratsis, A. (2021). Epigenomic landscape and 3D genome structure in pediatric high-grade glioma. Sci. Adv. *7*, eabg4126. https://doi.org/10.1126/sciadv.abg4126.

Wang, Z., Xu, C., Diplas, B.H., Moure, C.J., Chen, C.-P.J., Chen, L.H., Du, C., Zhu, H., Greer, P.K., Zhang, L., et al. (2020). Targeting Mutant PPM1D Sensitizes Diffuse Intrinsic Pontine Glioma Cells to the PARP Inhibitor Olaparib. Mol. Cancer Res. *18*, 968–980. https://doi.org/10.1158/1541-7786.MCR-19-0507.

Warren, K.E. (2012). Diffuse intrinsic pontine glioma: poised for progress. Front. Oncol. *2*. https://doi.org/10.3389/fonc.2012.00205.

Watada, H., Scheel, D.W., Leung, J., and German, M.S. (2003). Distinct Gene Expression Programs Function in Progenitor and Mature Islet Cells *. J. Biol. Chem. *278*, 17130–17140. https://doi.org/10.1074/jbc.M213196200.

Wegner, M. (2008). A Matter of Identity: Transcriptional Control in Oligodendrocytes. J. Mol. Neurosci. *35*, 3–12. https://doi.org/10.1007/s12031-007-9008-8.

Weider, M., Starost, L.J., Groll, K., Küspert, M., Sock, E., Wedel, M., Fröb, F., Schmitt, C., Baroti, T., Hartwig, A.C., et al. (2018). Nfat/calcineurin signaling promotes oligodendrocyte differentiation and myelination by transcription factor network tuning. Nat. Commun. *9*, 899. https://doi.org/10.1038/s41467-018-03336-3.

Welch, D.R., and Hurst, D.R. (2019). Defining the Hallmarks of Metastasis. Cancer Res. *79*, 3011–3027. https://doi.org/10.1158/0008-5472.CAN-19-0458.

Weng, Q., Chen, Y., Wang, H., Xu, X., Yang, B., He, Q., Shou, W., Chen, Y., Higashi, Y., van den Berghe, V., et al. (2012).

Dual-mode Modulation of Smad Signaling by Smad-interacting Protein Sip1 is Required for Myelination in the CNS. Neuron *73*, 713–728. https://doi.org/10.1016/j.neuron.2011.12.021.

Werbrouck, C., Evangelista, C.C.S., Lobón-Iglesias, M.-J., Barret, E., Le Teuff, G., Merlevede, J., Brusini, R., Kergrohen, T., Mondini, M., Bolle, S., et al. (2019). TP53 Pathway Alterations Drive Radioresistance in Diffuse Intrinsic Pontine Gliomas (DIPG). Clin. Cancer Res. *25*, 6788–6800. https://doi.org/10.1158/1078-0432.CCR-19-0126.

Wesseling, P., and Capper, D. (2018). WHO 2016 Classification of gliomas. Neuropathol. Appl. Neurobiol. *44*, 139–150. https://doi.org/10.1111/nan.12432.

WHO Classification of Tumours Editorial Board (2021). World Health Organization Classification of Tumours of the Central Nervous System.

Whyte, W.A., Orlando, D.A., Hnisz, D., Abraham, B.J., Lin, C.Y., Kagey, M.H., Rahl, P.B., Lee, T.I., and Young, R.A. (2013). Master Transcription Factors and Mediator Establish Super-Enhancers at Key Cell Identity Genes. Cell *153*, 307–319. https://doi.org/10.1016/j.cell.2013.03.035.

Winkler, F., Venkatesh, H.S., Amit, M., Batchelor, T., Demir, I.E., Deneen, B., Gutmann, D.H., Hervey-Jumper, S., Kuner, T., Mabbott, D., et al. (2023). Cancer neuroscience: State of the field, emerging directions. Cell *186*, 1689–1707. https://doi.org/10.1016/j.cell.2023.02.002.

Wu, G., Diaz, A.K., Paugh, B.S., Rankin, S.L., Ju, B., Li, Y., Zhu, X., Qu, C., Chen, X., Zhang, J., et al. (2014). The genomic landscape of diffuse intrinsic pontine glioma and pediatric non-brainstem high-grade glioma. Nat. Genet. *46*, 444–450. https://doi.org/10.1038/ng.2938.

Wu et al. (2012). Somatic histone H3 alterations in pediatric diffuse intrinsic pontine gliomas and non-brainstem glioblastomas. Nat. Genet. *44*, 251–253. https://doi.org/10.1038/ng.1102.

Xia, S., Lal, B., Tung, B., Wang, S., Goodwin, C.R., and Laterra, J. (2015). Tumor microenvironment tenascin-C promotes glioblastoma invasion and negatively regulates tumor proliferation. Neuro-Oncol. *18*, 507–517. https://doi.org/10.1093/neuonc/nov171.

Xiao, Y., Petrucco, L., Hoodless, L.J., Portugues, R., and Czopka, T. (2022). Oligodendrocyte precursor cells sculpt the visual system by regulating axonal remodeling. Nat. Neurosci. *25*, 280–284. https://doi.org/10.1038/s41593-022-01023-7.

Xu, C., Liu, H., Pirozzi, C.J., Chen, L.H., Greer, P.K., Diplas, B.H., Zhang, L., Waitkus, M.S., He, Y., and Yan, H. (2021). TP53 wild-type/PPM1D mutant diffuse intrinsic pontine gliomas are sensitive to a MDM2 antagonist. Acta Neuropathol. Commun. *9*, 178. https://doi.org/10.1186/s40478-021-01270-y.

Xu, X., Hou, Y., Long, N., Jiang, L., Yan, Z., Xu, Y., Lv, Y., Xiang, X., Yang, H., Liu, J., et al. (2023). TPPP3 promote epithelial-mesenchymal transition via Snail1 in glioblastoma. Sci. Rep. *13*, 17960. https://doi.org/10.1038/s41598-023-45233-w.

Yan, H., and Rivkees, S.A. (2002). Hepatocyte growth factor stimulates the proliferation and migration of oligodendrocyte precursor cells. J. Neurosci. Res. *69*, 597–606. https://doi.org/10.1002/jnr.10323.

Yang, Y., Schubert, M.C., Kuner, T., Wick, W., Winkler, F., and Venkataramani, V. (2022). Brain Tumor Networks in Diffuse Glioma. Neurotherapeutics *19*, 1832–1843. https://doi.org/10.1007/s13311-022-01320-w.

Yi, C., Verkhratsky, A., and Niu, J. (2023). Pathological potential of oligodendrocyte precursor cells: terra incognita. Trends Neurosci. *46*, 581–596. https://doi.org/10.1016/j.tins.2023.04.003.

Yu, H.-G., Nam, J.-O., Miller, N.L.G., Tanjoni, I., Walsh, C., Shi, L., Kim, L., Chen, X.-L., Tomar, A., Lim, S.-T., et al. (2011). p190RhoGEF (Rgnef) promotes colon carcinoma tumor progression via interaction with focal adhesion kinase. Cancer Res. *71*, 360–370. https://doi.org/10.1158/0008-5472.CAN-10-2894.

Yung, W.K.A., Tepper, S.J., and Young, D.F. (1983). Diffuse bone marrow metastasis by glioblastoma: Premortem

diagnosis by peroxidase-antiperoxidase staining for glial fibrillary acidic protein. Ann. Neurol. *14*, 581–585. https://doi.org/10.1002/ana.410140514.

Zadeh, G., and Aldape, K. (2014). ACVR1 mutations and the genomic landscape of pediatric diffuse glioma. Nat. Genet. *46*, 421–422. https://doi.org/10.1038/ng.2970.

Zhang, X., and Zhang, Z. (2019). Oncohistone Mutations in Diffuse Intrinsic Pontine Glioma. Trends Cancer *5*, 799–808. https://doi.org/10.1016/j.trecan.2019.10.009.

Zhang, C., Huang, H., Chen, Z., Zhang, Z., Lu, W., and Qiu, M. (2020). The transcription factor NKX2-2 regulates oligodendrocyte differentiation through domain-specific interactions with transcriptional corepressors. J. Biol. Chem. *295*, 1879–1888. https://doi.org/10.1074/jbc.RA119.011163.

Zhang, J., Wu, G., Miller, C.P., Tatevossian, R.G., Dalton, J.D., Tang, B., Orisme, W., Punchihewa, C., Parker, M., Qaddoumi, I., et al. (2013). Whole-genome sequencing identifies genetic alterations in pediatric low-grade gliomas. Nat. Genet. *45*, 602–612. https://doi.org/10.1038/ng.2611.

Zhang, L., Chen, L.H., Wan, H., Yang, R., Wang, Z., Feng, J., Yang, S., Jones, S., Wang, S., Zhou, W., et al. (2014). Exome sequencing identifies somatic gain-of-function *PPM1D* mutations in brainstem gliomas. Nat. Genet. *46*, 726–730. https://doi.org/10.1038/ng.2995.

Zhang, L., He, X., Liu, L., Jiang, M., Zhao, C., Wang, H., He, D., Zheng, T., Zhou, X., Hassan, A., et al. (2016). Hdac3 Interaction with p300 Histone Acetyltransferase Regulates the Oligodendrocyte and Astrocyte Lineage Fate Switch. Dev. Cell *36*, 316–330. https://doi.org/10.1016/j.devcel.2016.01.002.

Zheng, L., Gong, J., Yu, T., Zou, Y., Zhang, M., Nie, L., Chen, X., Yue, Q., Liu, Y., Mao, Q., et al. (2022). Diffuse Midline Gliomas With Histone H3 K27M Mutation in Adults and Children: A Retrospective Series of 164 Cases. Am. J. Surg. Pathol. *46*, 863. https://doi.org/10.1097/PAS.0000000000001897.

Zhou, B., Zhu, Z., Ransom, B.R., and Tong, X. (2021). Oligodendrocyte lineage cells and depression. Mol. Psychiatry *26*, 103–117. https://doi.org/10.1038/s41380-020-00930-0.

Zhou, Q., Choi, G., and Anderson, D.J. (2001). The bHLH Transcription Factor Olig2 Promotes Oligodendrocyte Differentiation in Collaboration with Nkx2.2. Neuron *31*, 791–807. https://doi.org/10.1016/S0896-6273(01)00414-7.

Zhou, Y., Song, H., and Ming, G. (2023). Genetics of human brain development. Nat. Rev. Genet. 1–20. https://doi.org/10.1038/s41576-023-00626-5.

Zhu, Q., Zhao, X., Zheng, K., Li, H., Huang, H., Zhang, Z., Mastracci, T., Wegner, M., Chen, Y., Sussel, L., et al. (2014a). Genetic evidence that *Nkx2.2* and *Pdgfra* are major determinants of the timing of oligodendrocyte differentiation in the developing CNS. Development *141*, 548–555. https://doi.org/10.1242/dev.095323.

Zhu, Q., Zhao, X., Zheng, K., Li, H., Huang, H., Zhang, Z., Mastracci, T., Wegner, M., Chen, Y., Sussel, L., et al. (2014b). Genetic evidence that *Nkx2.2* and *Pdgfra* are major determinants of the timing of oligodendrocyte differentiation in the developing CNS. Development *141*, 548–555. https://doi.org/10.1242/dev.095323.